DISPERSION IN OSCILLATORY FLOWS

by

J.W.Stairmand,

University College

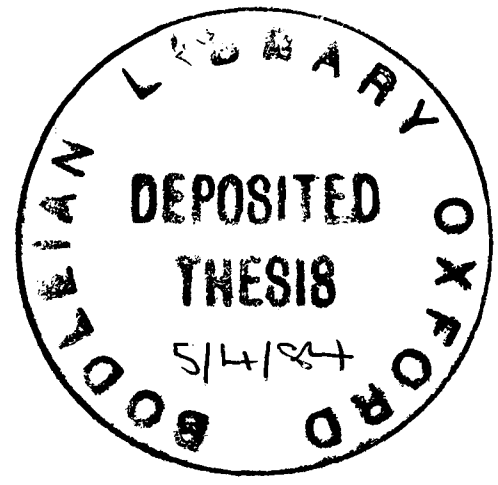

A Thesis submitted for the degree of

Doctor of Philosophy,

at the University of Oxford,

Department of Engineering Science.

August 1983.

ABSTRACT

DISPERSION IN OSCILLATORY FLOWS

J.W.Stairmand

University College

Trinity Term 1983

The enhanced axial mixing which is caused by dispersion in oscillatory flows in some mass transfer devices may limit the reactor performance. This effect has provided the motivation for the present study in which oscillatory flow dispersion in a flat channel of large aspect ratio is investigated. The rate of spreading of a uniform slug of some passive tracer has been predicted using numerical and analytical techniques and the results have been verified experimentally.

The numerical approach has used a finite difference time-marching method to obtain predictions for the channel concentrations. From the results, the dispersion coefficient (D) has been evaluated for Strouhal numbers of 0.01→0.2 and for mean Reynolds numbers of 0.4→200 at Schmidt numbers (Sc) $O(10^3)$. It has been concluded that under these conditions D varies as stroke squared. Unless the flow is not quasi-steady (i.e. if pulsatile Reynolds number $\alpha'^2 < O(1)$) D is only a weak function of frequency. These predictions for the dispersion coefficient have been in excellent agreement with those of Watson (256). It has also been concluded from the numerical study that the phase of the velocity sinusoid at the instant of injection has a critical effect upon the form of the concentration evolution.

An approximate analytical technique has been developed in which weighted mean cross-channel concentrations are defined. The wall concentration is expressed approximately using a Fourier series. This procedure leads to ordinary differential equations for the axial moments. When the axial variance of mean concentration and the dispersion coefficient were computed in this way for quasi-steady flows good agreement was obtained with the numerical work.

Simple opto-electronic gauges have been developed to measure mean cross-channel concentrations. The sensors have been used to obtain experimental data for the dispersion coefficient of a furrowed channel mass transfer device using slug stimulus techniques. Experimental investigations of dispersion in oscillatory flows in a flat channel using these gauges has produced values for D which are in agreement with the theoretical predictions for quasi-steady flows.

CONTENTS

NOTATION AND GLOSSARY

Throughout this work the symbols listed below have been used as consistently as possible. Deviations from these notations are described close to the relevant usage.

DIMENSIONLESS GROUPS

Pe → A steady flow Peclet number = Re Sc.

Po → An oscillatory flow Peclet number = α'^2 Sc.

Re → A Reynolds number for steady flow or for average forward flow when the velocity is oscillatory in time. The oscillatory flow value of Re is defined by the relation α^2 = Re St, where St and α^2 are defined as below.

Sc → A Schmidt number = $\frac{\nu}{\kappa}$.

St → A Strouhal number = $\frac{h}{2s}$ = ωh / $2U_{peak}$.

Sh → A Sherwood number.

α^2 → A pulsatile Reynolds number (= Re St) based on f.

$$\alpha^2 = \frac{fh^2}{4\nu}.$$

α'^2 → A pulsatile Reynolds number based on ω.

$$\alpha'^2 = \frac{\omega h^2}{4\nu}.$$

DIMENSIONAL VARIABLES

co-ordinates

r → the radial co-ordinate in a cylindrical duct.

x → the axial co-ordinate (length direction).

y → the tranverse co-ordinate (height direction).

z → the lateral co-ordinate (breadth direction).

t → time.

X → $x - \int U \, dt$.

experimental parameters

a → radius of a circular duct.

c_0 → the base concentration of the injected solution.

f → the pump frequency in Hz.

L → the mixing length of the concentration distribution.

s → the pump half-stroke in m.

h → the channel height in m.

Q → the mean volume flow rate in $m^3 s^{-1}$.

v → the gauge voltage produced by dye of concentration c.

V_a → the gauge voltage when air lies between sensors.

V_w → the gauge voltage when water lies between sensors.

W → a normalized voltage ($= V / V_w$).

x_u → the initial half-length of a slug of contaminant.

x_l → the total length of the channel

Ψ → partial fraction of a distillation component.

ω → the pump frequency in rads s^{-1}.

<u>fluid properties</u>

D → the dispersion (enhanced axial diffusion) coefficient.

k_p → the partition coefficient.

κ → the molecular diffusivity (diffusion coefficient) in m^2s^{-1}.

ρ → the fluid density in Kg m^{-3}.

$\Delta\rho$ → the difference in density between solvent and slug.

ν → the kinematic viscosity in m^2s^{-1}.

u → the dimensional channel velocity.

U → the dimensional bulk flow velocity.

<u>theoretical notations</u>

$C^n_{i,j}$ → the concentration at the i^{th} axial mesh point, the j^{th} transverse mesh point and the n^{th} time point.

Δt → the time between successive calculations in the time marching method.

Δx → the mesh step size in the axial direction.

Δy → the mesh step size in the transverse direction.

ϵ_1 → the noise in concentration due to a machine rounding error.

ϵ_2 → the noise transmitted to a calculated concentration by the finite difference scheme

$g_{(\theta)}$ → function defined by Taylor; see chapter 1.

L → length of channel in which large axial concentration changes occur.

m → an integer representing the transverse weighting factor.

M → the rheological flow-behaviour index.

n → the number of time steps per pump cycle.

→ in chapter 3, n represents the axial weighting factor.

$n_{0.25}$ → the number of cycles taken for the amplitude of the secondary oscillations in variance to reach $\frac{1}{4}$ amplitude of the primary oscillations.

$n_{0.50}$ → the number of cycles taken for the amplitude of the secondary oscillations in variance to reach $\frac{1}{2}$ amplitude of the primary oscillations.

$\hat{n}$ → the number of cycles taken for the amplitude of the secondary oscillations in variance to reach a certain fraction (g) of the amplitude of the primary

oscillations.

N → the smallest value of n leading to a stable simulation.

T_L → the Lagrangian integral time scale.

u^* → the friction velocity.

$\langle uc \rangle$ → the mean value of uc over the channel cross-section.

%5 → the ratio (expressed as a percentage) of the amplitudes of the secondary and primary variance oscillations after 5 cycles.

DIMENSIONLESS VARIABLES

β → $\hat{U}\ \frac{2}{\omega h}$, a dimensionless velocity.

γ → $4\ \frac{\kappa\pi^2}{\omega h^2}$, a dimensionless diffusivity.

R_∞ → the value of $\frac{\partial}{\partial t}(\sigma^2)$ averaged over a cycle as $t \to \infty$.

λ → $\frac{r}{a}$.

τ → ωt in oscillatory flow (a dimensionless time).

τ → $\frac{1}{4}\ \frac{\kappa t}{h^2}$ in steady flow (a dimensionless time).

χ → $x\ \frac{2}{h}$.

χ_0 → $x_0\ \frac{2}{h}$.

χ_1 → $x_1\ \frac{2}{h}$

ψ → $y\ \frac{2}{h}$.

$\bar{C}_m$ → $\int_0^1 c\ \psi^m\ d\psi$.

I_m^n → $\int_{-\infty}^{+\infty} \bar{C}_m\ \chi^n\ d\chi$.

I_n → $\left[\frac{h}{2}\right]^n\ I_0^n$.

J_m^n → I_m^n evaluated at $\tau = 0$

σ^2 → the axial variance of $\bar{C}_m$ about the centre of the slug.

σ'^2 → the temporal variance of $\bar{C}$ at a particular value of x.

v → alternative dimensionless variance = $\sigma^2\ \frac{h^2}{4s^2}$.

$\bar{X}$ → distance of the centre of mass of the slug from $\chi = 0$.

GLOSSARY

Aspect Ratio; this is a dimensionless number, the value of which describes the shape of some object. Throughout this work, the term will be understood to decribe the shape of the cross-section of a rectangular channel and will be defined as $\frac{b}{h}$.

Backmixing; see under "dispersion".

Breakthrough Curve refers to the plot of mean cross channel concentration (as measured at a particular downstream site) against time. Since this reading effectively monitors the movement of a slug of dye past gauges located at that axial position, it is termed the breakthrough or elution curve.

Contaminant is a general term refering to the tracer fluid.

Dispersion (sometimes refered to as backmixing) is a heat or mass transfer process by which an axial transport of some tracer occurs, usually as a result of the interaction of convection and diffusion. The process may also occur by the influence of vorticity effectively producing transverse "diffusion".

Dispersion Coefficient is a parameter analagous to the diffusion coefficient and gives the effective diffusivity for the convectively enhanced axial spreading of mean cross-channel concentration.

Elution Curve see "breakthrough curve".

Gaussian A concentration distribution is said to be Gaussian when the instantaneous axial concentration profile (refered to axes moving at the bulk speed) takes the form $c \alpha e^{-x^2}$.

Kurtosis is a statistical parameter and represents the peakedness of a set of data. All Gaussian curves have an absolute kurtosis of three and because of this a relative kurtosis is frequently defined to be

relative kurtosis = absolute kurtosis - 3.

Mixing Length is defined to be the distance between the two points along the channel where $\bar{C}$ is 10% of its maximum value down the channel at that instant. This parameter therefore gives an impression of the slug length.

Plug flow is said to occur when the velocity does not vary over the channel cross-section.

Ramp Slug (see slug); this term indicates that in the region of the channel in which the tracer has been introduced, the concencentration is uniform over the channel cross-section but falls off linearly with axial distance from the slug centre.

Slug is a general reference to the region occupied by the tracer. Initially this is a given distance of channel and on increasing time it lengthens in accord with the spread of the tracer.

Two Dimensional Assumption; see appendix 2.

Transitional; this term will be used in two very different ways to describe changes in the velocity profile. Depending on the context, "transitional" may refer to the change from laminar to turblent flow or to the change from a parabolic to a plug velocity profile. (see chapter 2 for more details of the latter phenomenon).

Uniform Slug; this term indicates that in the region of the channel

in which the tracer has been introduced, the concentration is constant over a limited region.

Velocity Profile is the shape of a plot of axial velocity against cross-channel co-ordinate. The velocity profile therefore indicates the distribution of velocities over a channel cross-section.

Chapter 1

INTRODUCTION AND LITERATURE SURVEY.

1.1 Introduction.

1.2 Aims and Applicability of the Current Work.

CHAPTER 1

INTRODUCTION

1.1 INTRODUCTION

The phenomenon of mass dispersion has been the subject of much investigation since Taylor (223) formulated the classical analysis of this phenomenon in 1953. Dispersion or "back-mixing" is a transport process by which an initial non-uniformity in temperature or concentration is spread out through a moving fluid by the interaction of convection and diffusion at a rate which is frequently orders of magnitude greater than would be achieved by diffusion alone. This fundamental process is applicable to circumstances as diverse as the spreading of pollutants in canals, rivers, estuaries and tides, the movement and breakup of clouds, the mixing of reactants in packed and fluidized beds, chromatography experiments, the mixing of gases in the airways of the lungs, the dispersion of chemicals in the blood stream and the movement of enzymes in the water-conducting capillaries of plants.

The motivation for the present study has been the importance of dispersion in limiting the efficiency of high-performance mass transfer devices such as dialysers and oxygenators. The versions of these reactors which are being developed by Bellhouse et al (267, 268) consist of a furrowed channel with permeable membrane walls through which gases or liquids may be transfered to or from a laminar flow of blood which passes through the device. In the case of the oxygenator, de-oxygenated blood flows into the channel and is pulsed over the furrows where vortices are consequently continually formed and ejected, leading to high efficiency transfer of oxygen (see Sobey (220) and Stephanoff, Sobey and Bellhouse (223)). In this way, the oxygen content at outlet from the channel can be made very high. The transfer efficiency cannot reach 100% however, since axial dispersion will provide a limit by effectively contaminating the oxygenated blood at outlet with the de-oxygenated blood from the inlet. For the case of a furrowed channel, the very feature which promotes the desirable transfer of oxygen in a direction transverse to the flow, may also lead to an undesirable enhancement in a direction along the axis of the channel. Sobey (221) (and others) have set out procedures by which the effect that axial dispersion has upon the transfer efficiency of a dialyser may be quantified, once the dispersion coefficient is known. The purpose of this work is to study the dispersion process in a flat channel carrying a laminar oscillatory flow and to obtain a set of predictions describing how the dispersion coefficient depends upon the frequency and tidal volume of the oscillations. Although it is not expected that the dispersion coefficients calculated for the flat channel will be the same as those that describe furrowed channel dispersion, some of mechanisms for the latter will be revealed by studying the simpler case. In one respect at least it

is anticipated that the mechanism for dispersive transfer in a furrowed channel will differ from that in a flat channel. In the case of oscillatory flow in a flat channel, when the diffusion coefficient is zero there will be no overall dispersive spreading. However this is not true of a furrowed channel in which a net spreading will be observed on account of the irreversible nature of the flows. The mechanism by which the enhanced spreading occurs in oscillatory flows down a flat channel is described in appendix 1.

1.2 AIMS AND APPLICABILITY OF THE CURRENT WORK

A method which is frequently used to determine the mass transfer characteristics of a reactor is the introduction into the channel of a slug stimulus of some detectable tracer (see Danckwerts (71)). This involves the injection of some substance into the stream and the subsequent observation of how quickly it spreads out. One may then evaluate various parameters (given by Danckwerts), the values of which will summarize the effect of dispersion upon the transfer processes taking place. The problem arising from the initial condition of such a uniform slug, bounded by an impermeable flat channel bearing an oscillatory laminar flow, is the major interest in the current investigation. In particular, the evaluation of the dispersion coefficient associated with this process is the principle goal. A knowledge of the response of the steady state dispersion coefficient to changes in the flows will provide the most useful information to the designer of a device in which axial dispersion may be a limiting effect.

The main part of this investigation is a numerical study by finite difference techniques of the uniform slug initial condition. The axial moments of mean cross-channel concentration have been evaluated and the behaviour of the centre of mass, variance, skewness and kurtosis with time has been investigated for a range of Strouhal and Reynolds numbers. The Schmidt number is assumed to be of order 10^3 making the analysis applicable to dispersion in liquid rather than gaseous systems. Mean forward-flow Reynolds numbers are chosen in the range 0.4→200 and Strouhal numbers in the range 0.01→0.2. The velocity profile is therefore not necessarily quasi-steady. Typically, the numerical simulations have been continued for times such that

$$t\,\frac{4\kappa}{h^2} = O(0.1).$$

Experiments have been carried out at a Schmidt number of 2000 and the dispersion coefficient has been evaluated for combined steady and oscillatory flow in a furrowed channel as well as purely oscillatory flow in a uniform channel. Strouhal numbers were in the range 0.01→0.05 and the pulsatile Reynolds numbers were such that the velocity profile remained approximately quasi-steady. Typically the duration of the experiments was such that

$$t\,\frac{4\kappa}{h^2} > O(0.1), \text{ but less than } 1.$$

These ranges of Reynolds and Strouhal numbers are typical of those found in mass transfer devices for medical uses in which sustained turbulent flows may not be imposed on account of the possible ensuing damage to the channel fluid. The Schmidt numbers also are typical of those arising from the diffusion of elements in liquids such as blood. The steady state performance of a device is generally of interest, so that the early stages of the tendency of

a dispersing system towards its steady state are not really critical. It has therefore been useful that the experiments and the numerical work should have been extended for long enough times for the nature of the steady state behaviour to be determined or extrapolated reliably.

Chapter 2

VELOCITY PROFILE IN LAMINAR OSCILLATORY FLOW.

2.1 Introduction.

2.2 Mathematical treatment.

2.3 Physical interpretation of the velocity profile.

CHAPTER 2

VELOCITY PROFILE IN LAMINAR OSCILLATORY FLOW

2.1 INTRODUCTION

The distribution of velocity over the channel cross-section will be seen to be a critical factor in determining the extent and nature of axial dispersion. This is of course to be expected since the large enhancement of axial mass transfer in an oscillatory flow is entirely due to the variation of velocity across the channel (see appendix 1). An oscillatory velocity can be regarded as arising from the imposition of an oscillatory driving pressure down the channel, or due to the imposition of a sinusoidal volume flow rate. Using the analysis of, for example, Moore (286), it will be shown that these two unsteady quantities, although related, are not necessarily in phase. The phase angle (θ), and the way that the velocity varies over the channel cross-section are governed by the dominant force by which the moving fluid creates an adverse pressure gradient. In this chapter the oscillatory velocity profile in a flat channel will be derived and the solution interpreted physically.

2.2 MATHEMATICAL TREATMENT

We seek an exact and explicit solution for the velocity profile in an infinitely wide flat channel carrying fully-developed laminar incompressible flow at a volume flow rate which is sinusoidal in time.

$$\frac{\partial u}{\partial t} = - \frac{1}{\rho} \frac{\partial p}{\partial x} + \nu \frac{\partial^2 u}{\partial y^2}. \qquad (2\text{-}1)$$

We shall require the boundary conditions that the flow is symmetrical about the line $\psi = 0$, and that at $\psi = \pm 1$, $u = 0$. We assume a sinusoidal pressure gradient in time such that

$$- \frac{1}{\rho} \frac{\partial p}{\partial x} = RE\{ \gamma e^{i(\theta+\tau)} \}. \qquad (2\text{-}2)$$

and suppose that in sympathy to this oscillatory driving pressure, the channel velocity is of the form

$$u_{(\tau,\psi)} = RE\{u_0 e^{i\tau}\}, \qquad (2\text{-}3)$$

where u_0 is a complex number and a function of ψ.

As in the analysis described by Moore, we substitute (2-2) and (2-3) into (2-1), and solve the resulting ordinary differential equation to give

$$u = RE\left\{ e^{i(\tau+\theta)} \frac{\gamma}{i\omega} \left(1 - \cosh\left[\frac{h\psi}{2}\sqrt{\frac{i\omega}{\nu}}\right] \operatorname{sech}\left[\frac{h}{2}\sqrt{\frac{i\omega}{\nu}}\right] \right) \right\}. \qquad (2\text{-}4)$$

This formulation expresses the velocity as a function of the magnitude of the pressure oscillations (γ). It would be more convenient to relate the velocity to the pump parameters. This may be achieved by writing the instantaneous volume flow rate per unit width (q) as

$$q = \omega sh \sin[\tau]. \qquad (2\text{-}5)$$

Integration of (2-4) over the channel height (ψ = -1 → 1) yields an alternative expression for q which may be equated to (2-5) giving a value for θ and expressing γ in terms of s and ω. Hence we obtain

$$u = \frac{1}{\beta} \text{IM}\left[e^{i(\tau+\theta)} \left(1 - \cosh[\psi\alpha"]\text{sech}[\alpha"] \right) \right] \qquad (2\text{-}6)$$

$$\text{where } \alpha" = \frac{h}{2}\sqrt{\frac{\omega i}{\nu}} = \alpha'\sqrt{i}, \qquad (2\text{-}7)$$

$$\beta = \frac{1}{\omega s}\left| 1 - \frac{1}{\alpha"}\tanh[\alpha"] \right|, \qquad (2\text{-}8)$$

$$\text{and} \quad \theta = -\text{ARG}\left[1 - \frac{1}{\alpha"}\tanh[\alpha"] \right]. \qquad (2\text{-}9)$$

2.3 PHYSICAL INTERPRETATION OF THE VELOCITY PROFILE

α is known as the Womersley parameter or pulsatile Reynolds number and gives the ratio between the viscous and inertial forces acting on the channel fluid at a particular frequency. Values of α less than order unity imply that the fluid motion is dominated by its viscosity. In this case the flow profile represents a quasi-steady form of the solution to the steady flow problem in that the velocity varies parabolically with ψ and the velocity at any point on the cross-section varies sinusoidally with time. Values of α greater than order unity imply that the fluid motion is dominated by inertial effects; that is, the pressure drop is mainly due to the force needed to continually change the momentum of the mass of fluid within the channel. In this case, the variation of velocity with ψ, is confined to a thin boundary layer adjacent to the channel walls. This profile is of the plug-flow type. At intermeduate α^2 ($\doteq$5) the profile does not closely resemble either extreme. Figure 2.1 shows the velocity profile within the channel at various points in the cycle, for various values of α.

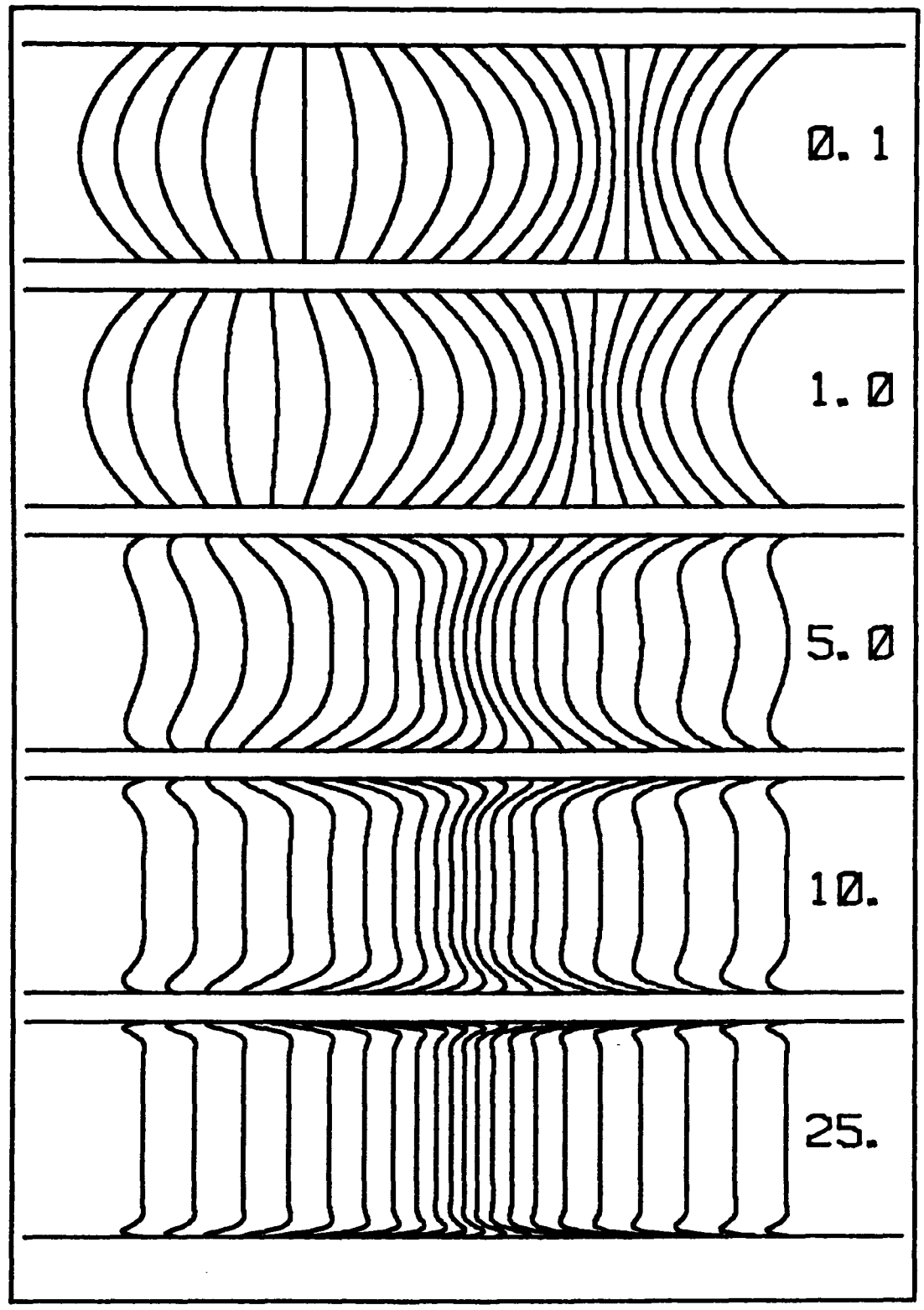

The velocity profile in a flat channel for α' equal to 0.1, 1.0, 5.0, 10.0, 25.0. The profiles are plotted at 20 degree intervals in the cycle for one cycle.

Figure 2.1

The value of θ, the phase lag between the pressure and velocity sinusoids also reflects the change in nature of the flow as α is increased. In the limit of small α, the velocity and pressure are in phase, whereas the limiting value of θ as $\alpha \to \infty$ is 90°. A plot showing the variation of θ with $LOG_{10}[\alpha]$ is shown in figure 2.2.

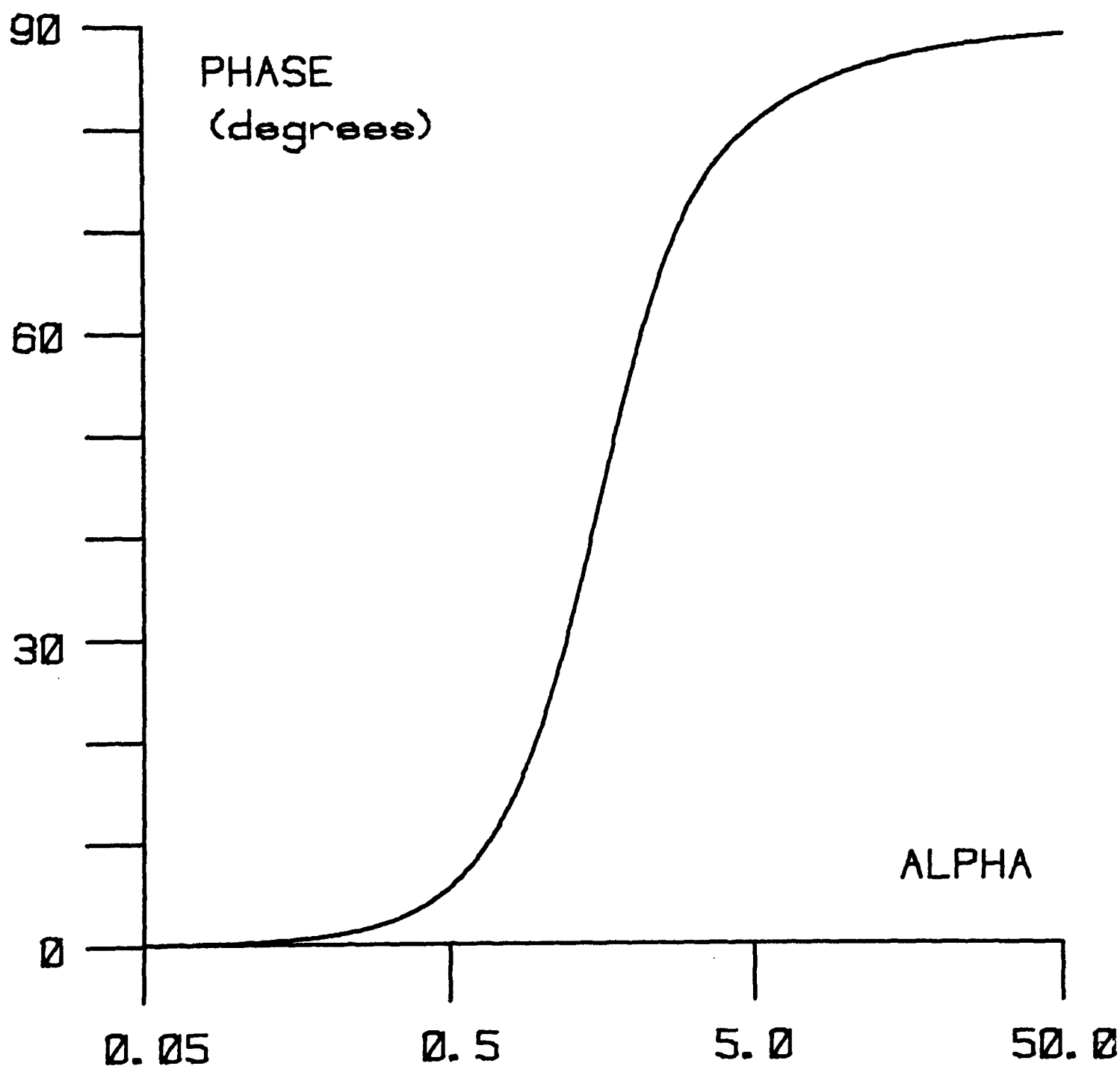

A plot showing the alpha (α) variation of the angle by which the pressure sinusoid leads the bulk velocity sinusoid for oscillatory flow in a uniform flat channel.

Figure 2.2

For values of α less than about 2, the difference between the parabolic extreme and the actual profile is barely discernible, although the value of θ does show some marked deviation from the 0° limit. As α is increased above 2 however, the profile does indeed become more blunt, and for part of the cycle, the maximum velocity occurs not on the centre-line, but at a point near the wall. Inside of this point, the velocity varies little with ψ, but outside of the point there can be seen a thin boundary layer of high shear. The magnitude of the velocity gradient $\left|\frac{\partial u}{\partial \psi}\right|$ at the wall, when raised to the $\frac{1}{3}$ power and averaged over a period varies approximately linearly with frequency (and therefore with α^2) (see figure 2.3). Further conclusions arising from this method of analysis are given by Moore (286) who derives the mean square velocity over a cycle and describes how to evaluate the velocity distribution due to a general pressure pulse in time.

An alternative and novel approach to this analysis, is to seek a series solution (in ψ) to the Navier-Stokes equations. Thus we may write

$$u = \sin(\tau)\sum_{i=0}^{\infty} a_i \psi^{2i} + \cos(\tau)\sum_{i=0}^{\infty} b_i \psi^{2i}. \qquad (2\text{-}10)$$

Substituting this formulation into (2-1) and equating powers of ψ which are in phase yields the recurrence relations for the set of a and b coefficients

$$b_{i+2} = - a_i \frac{\alpha}{(i+2)} \frac{2}{(i+1)}, \qquad (2\text{-}11)$$

$$a_{i+2} = + b_i \frac{\alpha}{(i+2)} \frac{2}{(i+1)}, \qquad (2\text{-}12)$$

where $i \geq 2$.

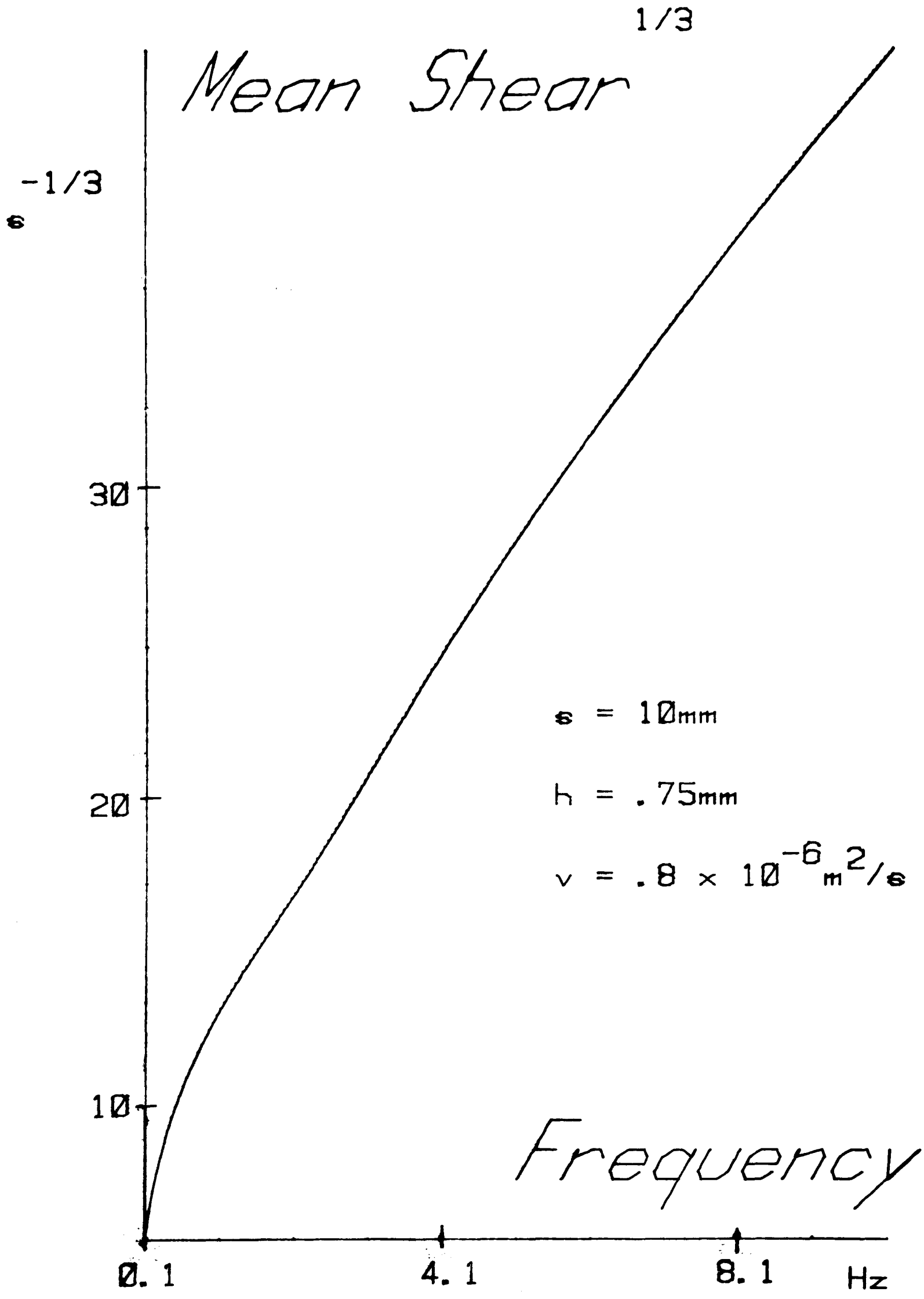

A plot showing the frequency variation of the wall shear stress to the power $\frac{1}{3}$ averaged over the forward flow part of a cycle of oscillatory flow in a flat channel.

Figure 2.3

This set of equations enables one to specify the series as a function of a_0, a_1, b_0 and b_1. To calculate these starting parameters we use the boundary condition that the wall velocity is zero for all time and then set the phase and amplitude of the bulk flow sinusoid to that delivered by the pump. This gives the following four equations

$$0 = \sum_{i=0}^{\infty} a_i, \tag{2-13}$$

$$0 = \sum_{i=0}^{\infty} b_i, \tag{2-14}$$

$$\omega s = \sum_{i=0}^{\infty} \frac{1}{2i+1} a_i, \tag{2-15}$$

$$0 = \sum_{i=0}^{\infty} \frac{1}{2i+1} b_i, \tag{2-16}$$

This formulation describes the transition from parabolic to plug-type in an interesting light. The small α limit is indicated by the series only including terms in ψ^0 and ψ^2; i.e. a parabolic profile. As α is increased through the transition regime, more and more terms need to be included in the series for an accurate representation which correctly follows the large velocity gradients which occur near the wall. This alternative expression for the velocity profile will be used in the theoretical work described in chapter 3.

The velocity profile for oscillatory flow in a circular channel follows substantially the same trends. A similar analysis of the velocity distribution in a circular pipe was carried out by, for example, Peacock and Stairmand (275). The results were used to calibrate heated thin film probes, and good agreement was obtained with the theory, justifying the velocity solution and the use of the probes in oscillatory flows. The main algebraic difference between the two analyses is that in the pipe flow solution, the

hyperbolic functions (cosh, sech, tanh) of the flat channel case are replaced by Bessel functions (J_0, J_1) which are somewhat more cumbersome to evaluate numerically. For this reason, the case of flat channel dispersion is more amenable to a numerical study than pipe flow dispersion, although essentially the same methods may be used in solving these problems.

Chapter 3

THE METHOD OF MOMENTS APPROACH TO DISPERSION.

3.1 Introduction.

3.2 Analytical treatment by the method of moments.

- 3.2.1 Background.
- 3.2.2 Transversely weighted moments for small frequency flows.
- 3.2.3 Treatment of the case of Womersley parameter of order unity.
- 3.2.4 Extension to smaller times.

CHAPTER 3

THE METHOD OF MOMENTS APPROACH TO DISPERSION

3.1 INTRODUCTION

A very concise way of summing up the dispersive behaviour of a system is provided by the method of moments which also has the advantage of yielding a reasonably tractable mathematical analysis. In this chapter, the method of moments will be described and a simplified approximate solution will be set out for the concentration moments in oscillatory flow. The analysis will be used to provide a description of the effects of stroke and frequency upon the dispersion coefficient and to show some features of the time evolution of the first three moments.

Taylor (233) presented the first analytical description of dispersion from the slug stimulus starting condition. The Taylor model supposed that the variation in concentration over the channel cross-section was very small; after neglecting axial diffusion and setting up axes moving with the bulk fluid velocity, this yields a straight-forward solution for the dispersion coefficient. In a later analysis (237) Taylor wrote $\frac{\partial c}{\partial x}$ = constant and obtained an

analysis which was subject to a less stringent asymptotic behaviour in time. The approach which Taylor had devised was adapted by Bowden (36) to the oscillatory flow case, assuming a concentration evolution of the form :

$$C = \bar{C} + P_{(\psi)}\cos(\tau) + Q_{(\psi)}\sin(\tau).$$

Holley, Harleman and Fischer (121) have used a similar extension of Taylor's approach and have applied their work to the determination of the steady-state dispersion coefficient in estuarine flows. These authors recognised the important dependence of the dispersion process upon the dimensionless group Po, where

$$Po = \frac{\omega h^2}{4K}.$$

For small values of Po, they concluded that the dispersion process was essentially quasi-steady, whereas the dependence of the dispersion coefficient (D) upon Po was relatively insignificant for $Po > O(1)$.

Aris (5) developed the method of moments approach to dispersion problems and went on to apply (10) the technique to oscillatory flow problems. He concluded from his results that for a combined steady and oscillatory flow, the contribution of the oscillations to the dispersion coefficient was only rarely greater than $\frac{1}{128}$ of the total. To describe the method of moments let us define the mean cross-channel concentration $\bar{C}$ as

$$\bar{C} = \frac{1}{h}\int_{-h/2}^{h/2} c\, dy \qquad (3\text{-}1)$$

If we now take weighted axial moments about this mean concentration by integrating over the whole channel length, then we may define the n^{th} axial moment as

$$I_n = \int_{-\infty}^{\infty} \chi^n \bar{C}\, d\chi, \qquad (3\text{-}2)$$

where n = 0,1,2 etc.

These functions of time are useful since the value of I_0 is proportional to the total amount of contaminant within the channel. The ratio of the first and zeroth moments gives the axial distance $\bar{X}$ of the centre of gravity of the contaminant from the origin,

$$\bar{X} = I_1 / I_0. \qquad (3\text{-}3)$$

$\bar{X}$ quantifies the extent to which the convective effects are shifting the slug. The diffusion of the contaminant does not in fact affect the value of $\bar{X}$ for an initially laterally uniform slug. This can be appreciated by considering that diffusion is in origin a random process at the molecular level, the contaminant molecules being just tagged versions of the channel fluid molecules. The spreading out of the slug is simply due to the migration of these tagged molecules into sparcely populated areas...a process which exhibits a certain isotropy in that for any particular molecule no one direction is prefered for this self-diffusion. Thus, at a given location, for any molecule which migrates 'a' units to the left, there will on average be another which has moved 'a' units to the right therefore cancelling out any possible effect on $\bar{X}$. Also, since there is initially a uniform distribution of contaminant molecules over any cross-section, the ensemble velocity of the contaminant molecules is equal to the bulk flow velocity in the duct. For a uniform slug which intially lies symmetrically about the origin, the value of $\bar{X}$ is therefore given by the time integral of the bulk velocity within the channel,

$$\bar{X}_{(t)} = \int_0^t \frac{1}{h} \int_{-h/2}^{h/2} u_{(y,t')} \, dy \, dt' . \qquad (3\text{-}4)$$

The zeroth moment then is independent of convective and diffusive effects, whilst the first moment is influenced only by convection. The second moment is the first one which will give some indication of the diffusion-convection interaction. We may define σ^2 to be the variance of mean cross-channel concentration about the instantaneous centre of gravity, where

$$\sigma^2 = \left[I_2 \; / \; I_0 \right] - \bar{X}^2 . \qquad (3\text{-}5)$$

The time derivative of σ^2 gives the rate of spreading of the slug. This will of course include possible large peaks which are due to the slug being continually deformed and reformed by the velocity oscillations. This is a feature of this form of presentation since all the moments plots may reveal large oscillations upon a time asymptoting function, the peaks being due to the oscillatory convection rather than a permament spreading. The summary of the dispersion process in terms of $\bar{C}$ thus yields some results which are merely artefacts of this averaging procedure (see chapters 4, 5 and 8). However, when the rate of increase of the variance is averaged over a cycle, one obtains a true measure of the rate of dilution of the slug fluid. If, in the limit of large time, this parameter tends to a value R_∞, then we may define the dispersion coefficient (D) to be $\frac{1}{2}R_\infty$ and this will represent the effective longitudinal diffusivity. This single parameter is perhaps the most important one describing the longitudinal dispersion process since its value indicates the rate of permament spreading.

The first three moments thus give an insight into the dispersion process. The moment I_3 can be related to the skewness of the mean cross-channel concentration, whilst the kurtosis (or "peakedness") of the distribution is dependent upon I_4. These higher moments which are not often considered can yield further information about the spreading process. Aris's original moment approach was to integrate the dispersion equation axially and to then define axial concentration moments. These moments were functions of τ and ψ and obeyed partial differential equations in these variables. These equations were then solved in a series form.

3.2 ANALYTICAL TREATMENT BY THE METHOD OF MOMENTS

3.2.1 Background

The method that will be described here, is an approximate description of the time evolution of dispersion in an oscillatory flow of small Womersley parameter at large times. The method can be extended to arbitrary accuracy by including more terms in a truncated series representation for the wall concentration; this may however lead to rather unwieldy algebra. The method is original, but similar in concept to the analysis of Aris (5) which is in principle exact. The main advantage of this novel treatment is that it is only necessary to solve ordinary differential equations in time (τ), since the complex ψ-dependence of the moments is approximated by a truncated Fourier series. The Aris analysis on the other hand yields partial differential equations in τ and ψ which are less easy to solve, especially for the case of oscillatory flow.

The equation describing two-dimensional dispersion is

$$\omega \frac{\partial c}{\partial \tau} = - \frac{2}{h} u \frac{\partial c}{\partial \chi} + \frac{4\kappa}{h^2} \left[\frac{\partial^2 c}{\partial \chi^2} + \frac{\partial^2 c}{\partial \psi^2} \right], \qquad (3\text{-}6)$$

where c is the dimensionless concentration at any point in the channel. The boundary conditions are numbered in square brackets and are -

$$c \to 0 \text{ as } \chi \to \pm\infty \text{ , for all } \psi, \tau \qquad [3\text{-}1],$$

$$\frac{\partial c}{\partial \psi} = 0 \text{ at } \psi = \pm 1 \text{ , for all } \chi, \tau \qquad [3\text{-}2].$$

The initial conditions ($\tau = 0$) to be imposed are -

$$c = 1 \text{ for } |\chi| < \chi_0 \text{ , for all } \psi \qquad [3\text{-}3],$$

$$c = 0 \text{ for } |\chi| > \chi_0 \text{ , for all } \psi \qquad [3\text{-}4].$$

Condition [3-1] expresses the fact that the dye does not get washed right out of the channel and condition [3-2] imposes the zero wall flux condition...i.e. the walls are impermeable. The initial condition is the familiar slug stimulus with the slug dimensionless half length being χ_0. Since the initial distribution is symmetrical about the line $\psi = 0$, we may add an extra boundary condition which is applicable when the velocity profile is also symmetrical about the $\psi = 0$ line,

$$c_{(\psi)} = c_{(-\psi)} \qquad [3\text{-}5].$$

Integrating equation (3-6) with respect to ψ, over the channel, integrating by parts and applying boundary conditions [3-2] and [3-5] then gives us

$$\omega \frac{\partial}{\partial \tau}(\bar{c}) = - \frac{2}{h} \frac{\partial}{\partial \chi} \langle cu \rangle + \frac{4\kappa}{h^2} \frac{\partial^2}{\partial \chi^2}(\bar{c}). \qquad (3\text{-}7)$$

where $\langle cu \rangle$ denotes the average of cu over the channel

cross-section.

Noting that boundary condition [3-1] effectively states that the defining integral for I_n^0 exists, we proceed to multiply both sides of (3-7) by χ^n (where n is an integer ≥ 0), and integrate over χ from $\chi = -\infty$ to $\chi = \infty$. When we integrate by parts and apply boundary condition [3-2] we get

$$\omega \frac{\partial}{\partial \tau}(I_n) = 2 \frac{n}{h} \int_{-\infty}^{\infty} \langle cu \rangle \chi^{n-1} d\chi + \frac{4\kappa}{h^2} n(n-1) I_{n-2}. \qquad (3\text{-}8)$$

Note that the last term of this equation is due to axial diffusion alone and that this term only operates for $n \geq 2$. It therefore follows that the axial diffusive behaviour should not affect the position of the centre of the slug which is a parameter dependent only upon the first two moments n=0 and n=1. The difficulty in proceeding is that $\langle cu \rangle$ is not known.

3.2.2 Transversely Weighted Moments For Small Frequency Flows

If we take the new step of extending our definition of the mean cross-channel concentration, then we may continue with the analysis given above. Let us initially restrict attention to the case of small Womersley parameter (see chapter 2) in which case the velocity is given by

$$u = \hat{u} (1 - \psi^2) \sin\{\tau\}. \qquad (3\text{-}9)$$

We may now define the m^{th} transversely weighted moment of concentration as

$$\bar{c}_m = \frac{1}{2} \int_{-1}^{+1} (\psi^m c) \, d\psi. \qquad (3\text{-}10)$$

Now, since the concentration is symmetrically distributed about the line $\psi = 0$, (boundary condition [3-5]) then for odd values of m we may write

$$\bar{C}_m = 0. \tag{3-11}$$

We may also define the n^{th} axial moment of the m^{th} transverse moment of concentration as

$$I_n^m = \int_{-\infty}^{\infty} \chi^n \bar{C}_m \, d\chi. \tag{3-12}$$

This novel procedure expresses the problem in a rather different light, since if we multiply both sides of (3-6) by ψ^m, where m is even, substitute in for u from (3-9) and integrate transversely over the channel, using the boundary conditions and the definition (3-10) we obtain,

$$\omega \frac{\partial}{\partial \tau}(\bar{C}_m) = -\hat{u}\,\frac{2}{h}\,\frac{\partial}{\partial \chi}\left[\bar{C}_m - \bar{C}_{m+2}\right] + \frac{4\kappa}{h^2}\left[m(m-1)\bar{C}_{m-2} - mc_w + \frac{\partial^2}{\partial \chi^2}(\bar{C}_m)\right], \tag{3-13}$$

where $c_w = c|_{\psi=1}$ = wall concentration.

We may now multiply both sides of (3-13) by χ^n, integrate axially over $|\chi| = -\infty \to \infty$, so that using the boundary conditions and the definitions of (7) we may obtain

$$\omega \frac{\partial}{\partial \tau}(I_n^m) = n\hat{u}\frac{2}{h}\left(I_{n-1}^m - I_{n-1}^{m+2} \right)\sin(\tau) + \frac{4\kappa}{h^2}\left[n(n-1)I_{n-2}^m + m(m-1)I_n^{m-2} - m\int_{-\infty}^{\infty} \chi^n c_w \, d\chi\right]. \tag{3-14}$$

The problem now, is to find an expression for c_w, the wall concentration, as some function of time or as a function of $\bar{C}_m$ for some m. A general formulation of this is use the series expression,

$$c_w = \sum_{i=0}^{\infty} d_{2i}\,\bar{C}_{2i}. \tag{3-15}$$

The most simple approximation to this is to write

$$c_w = \bar{C}_0. \tag{3-16}$$

This expression does not however account for some important features of the dispersion equation (this will be discussed further in section 3.2.4), so let us take the first two terms of the series given by equation (3-15).

i.e. $$c_w = d_0\bar{C}_0 + d_2\bar{C}_2. \tag{3-17}$$

We may evaluate the 'd' coefficients by expressing the transverse concentration distribution as a Fourier series.

$$c = a_0 + \sum_{i=1}^{\infty} a_i \cos\{\pi i \psi\}. \qquad (3\text{-}18)$$

This formulation incorporates boundary conditions [3-2] and [3-5]. We may now evaluate expressions for $\bar{C}_0$ and $\bar{C}_2$ by multiplying both sides of (3-18) by ψ^m for m=0, 2, and integrating over the channel using integrataion by parts. This yields the following pair of equations

$$\bar{C}_0 = a_0 \quad \text{and} \quad \bar{C}_2 = \frac{1}{3}a_0 - \frac{2}{\pi^2}a_2. \qquad (3\text{-}19)$$

These solve to give

$$a_0 = \bar{C}_0. \qquad (3\text{-}20)$$

$$a_2 = \frac{1}{3}\bar{C}_0 - \frac{\pi^2}{2}\bar{C}_2. \qquad (3\text{-}21)$$

On substituting ψ=1 into the truncated form of (3-18), we get

$$c_w = a_0 - a_2. \qquad (3\text{-}22)$$

Hence from (3-20), (3-21) and (3-22) we obtain

$$c_w = (1 - \frac{\pi^2}{6})\bar{C}_0 + \frac{\pi^2}{2}\bar{C}_2. \qquad (3\text{-}23)$$

This expresses c_w in terms of the first two transversely weighted moments. By substituting this expression into equation (3-14), we have a 'family' of equations for each combination of n and m. This set of ordinary diferential equations may be solved for any I_m^n. Let us now review how one should calculate the dispersion coefficient which is given by the mean value of

$$\frac{\partial}{\partial\tau}(\sigma^2) = \frac{\partial}{\partial\tau}\left[\{I_2^0/I_0^0\} - \{I_1^0/I_0^0\}^2 \right]. \qquad (3\text{-}24)$$

The equation for I_2^0 requires us to evaluate I_1^2, I_1^0 and I_0^0.
The equation for I_1^2 requires us to evaluate I_0^4, I_0^2 and I_0^0.
The equation for I_1^0 requires us to evaluate I_0^2 and I_0^0.
The equation for I_0^4 requires us to evaluate I_0^2 and I_0^0.
The equation for I_0^2 requires us to evaluate I_0^0.

The procedure for calculating the dispersion coefficient will therefore be to work up the above table using equation (3-14). Let us now define the initial values of the moments as

$$J_n^m = I_n^m \Big|_{\tau=0}. \tag{3-25}$$

Applying the initial conditions specified in [3-3] and [3-4] we obtain

$$J_1^m = 0, \text{ due to the initial symmetry about } \chi = 0. \tag{3-26}$$

Writing m = 0,n = 0 in equation (3-14) gives us

$$\omega \frac{\partial}{\partial \tau}(I_0^0) = 0 \tag{3-27}$$

so we conclude that

$$I_0^0 = J_0^0 \text{ for all } \tau. \tag{3-28}$$

This result expresses the fact the total amount of contaminant within the channel remains unchanged. This result would not have been obtained if we had chosen the more difficult boundary condition of constant wall concentration rather than zero wall concentration gradient. Writing m=2, n=0 in equation (3-14) gives

$$\omega \frac{\partial}{\partial \tau}(I_0^2) = \frac{8K}{h^2}\left[I_0^0 - d_0 I_0^0 - d_2 I_0^2 \right]. \tag{3-29}$$

On substituting in the values of d_0 and d_2 and applying the boundary conditions, we arrive at the expression

$$I_0^2 = \frac{1}{3} J_0^0 . \tag{3-30}$$

Similarly the expression for I_0^4 may be solved to yield

$$I_0^4 = \frac{1}{5} J_0^0 . \tag{3-31}$$

Thus the cross-weighted moments of zero axial weight are all independent of time and may be expressed generally as

$$I_0^m = \frac{1}{m+1} J_0^0 . \tag{3-32}$$

Applying these equations for the case m=0, n=1 we get

$$I_1^0 = J_0^0 \left[1 - \cos\{\tau\}\right] \frac{4}{3\omega h}\hat{u}. \tag{3-33}$$

and hence $\bar{x}$ is given by

$$\bar{x} = s \left[1 - \cos(\tau) \right]. \qquad (3\text{-}34)$$

Thus the centre of the slug of contaminant moves with the bulk fluid velocity. This equation agrees exactly with the predictions of the numerical routines which will be presented in chapter 5. The time derivative of the variance is expressed in terms of the moments by (3-24). Let us first evaluate

$$\frac{\partial}{\partial \tau} \left[I^2_0 \; / \; I^0_0 \right].$$

Solving for m=2, n=1 gives us

$$I^2_1 = \zeta \sin(\tau) + \eta \cos(\tau) - \Xi e^{-\tau} + \frac{2}{9} \beta J^0_0, \qquad (3\text{-}35)$$

where $\zeta = - J^0_0 \frac{4}{45} \frac{\beta\gamma}{1+\gamma^2}$

$$\eta = - J^0_0 \frac{2}{45} \beta \frac{3+5\gamma}{1+\gamma^2},$$

$$\Xi = + J^0_0 \frac{2}{45} \beta \frac{5\gamma-2}{1+\gamma^2},$$

and where β is a dimensionless velocity and γ is a dimensionless diffusivity (see the notation list for definitions).

We have now evaluated I^2_1, I^0_1 and I^0_0 and we therefore proceed to determine $\partial_t(\sigma^2)$, using

$$\frac{\partial}{\partial t}(I^0_2) = \frac{4}{\omega h} \hat{u} \; (I^0_1 - I^2_1) \sin(t) + \frac{8\kappa}{\omega h^2} I^0_0. \qquad (3\text{-}36)$$

Thus the expression for σ^2 can be easily obtained by integrating (3-36) with respect to time (see appendix 4). Plots of $\left[\sigma^2 - \sigma^2 \big|_{\tau=0} \right] St^{-2}$ versus $\frac{\tau}{2\pi}$ obtained in this way are plotted out in figures 3.1→3.6 for the following conditions

(1) Re = 10.0 St = 0.01

(2) Re = 100.0 St = 0.02

(3) Re = 10.0 St = 0.02

(4) Re = 2.5 St = 0.02

(5) Re = 2.5 St = 0.05

(6) Re = 0.4 St = 0.40

The results are compared with the numerical predictions of chapter 5 on the same plots. The analytical predictions assume a parabolic velocity profile whereas the actual profile (which was used in the numerical study) is likely to be somewhat different from this; it is likely therefore that the dispersion coefficient (mean slope of the plots) will be under-estimated by the analytical work. This is indeed the case and constitutes the main difference between the two predictions. The time evolution of the two sets of curves follows almost exactly the same course and agreement between the approximate theory and the exact numerical results is very good.

The value of $\frac{\partial \sigma^2}{\partial t}$ can be obtained easily by averaging the final expression for $\partial_t(\sigma^2)$ over a cycle and setting the exponential terms to zero as the large time limit. This procedure gives

$$\frac{4}{\omega h^2} R_\infty = \frac{2}{45} \frac{\gamma\beta^2}{1+\gamma^2} + \frac{\gamma}{\pi^2}. \qquad (3\text{-}37)$$

In dimensional terms this becomes

$$D = \kappa \left[1 + \frac{2\pi^2}{45} \frac{\beta^2}{1+\gamma^2} \right]. \qquad (3\text{-}38)$$

Note that the parameter β is independent of frequency and directly proportional to stroke. The low frequency prediction for the dispersion coefficient given above therefore predicts that the dispersion coefficient is not a strong function of frequency for $Sc=O(10^3)$ but is proportional to stroke squared. The first of these properties is a little surprising but we should be careful how we interpret this. In choosing the quasi-steady low frequency Poiseuille-type velocity profile we ignored one mechanism by which the frequency may affect the dispersion coefficient. In chapter 2

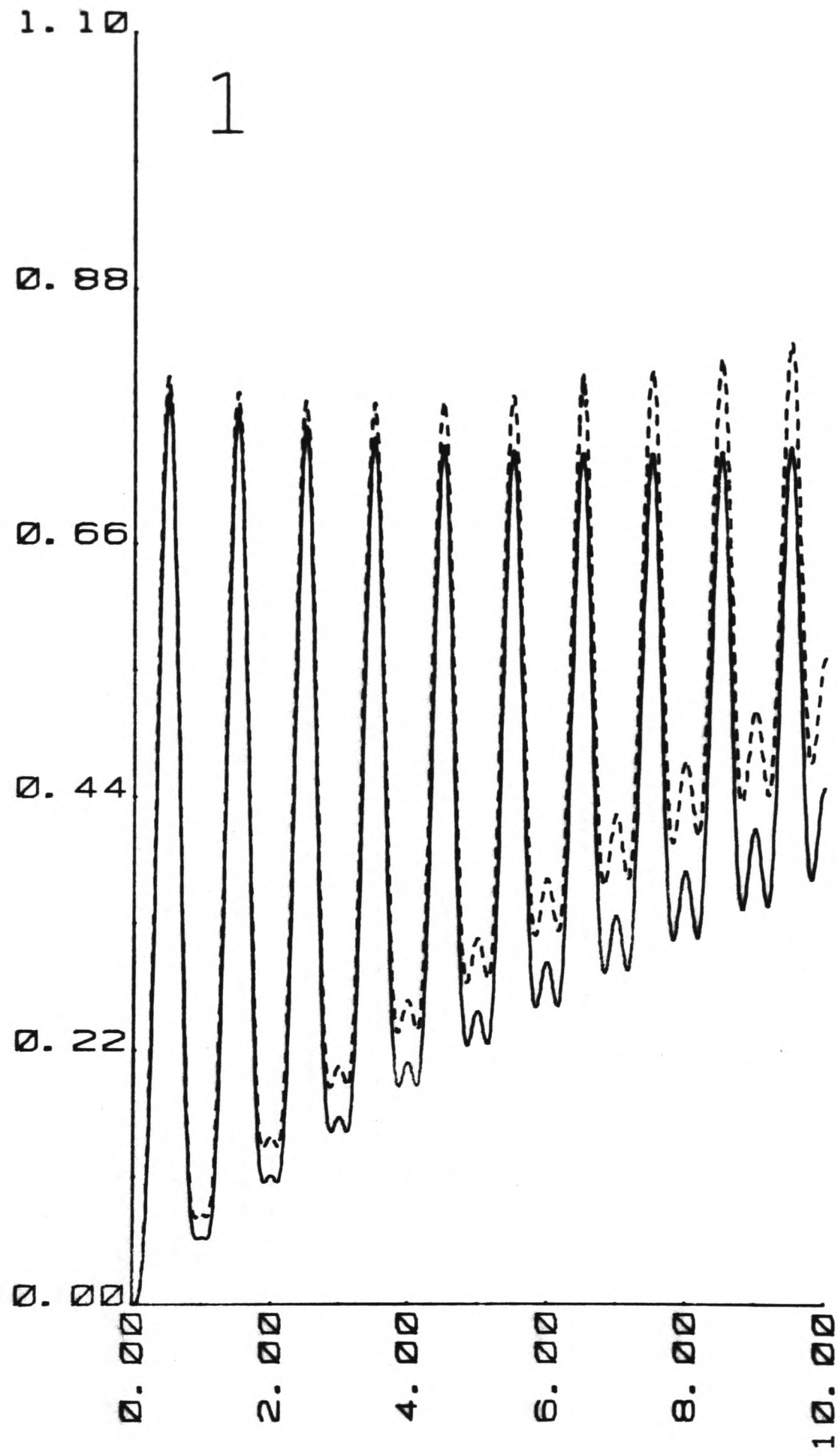

- - numerical

——— analytical

Plot of $[\sigma^2-\sigma^2|_{\tau=0}]$ St^2 versus $\frac{\tau}{2\pi}$

Figure 3.1

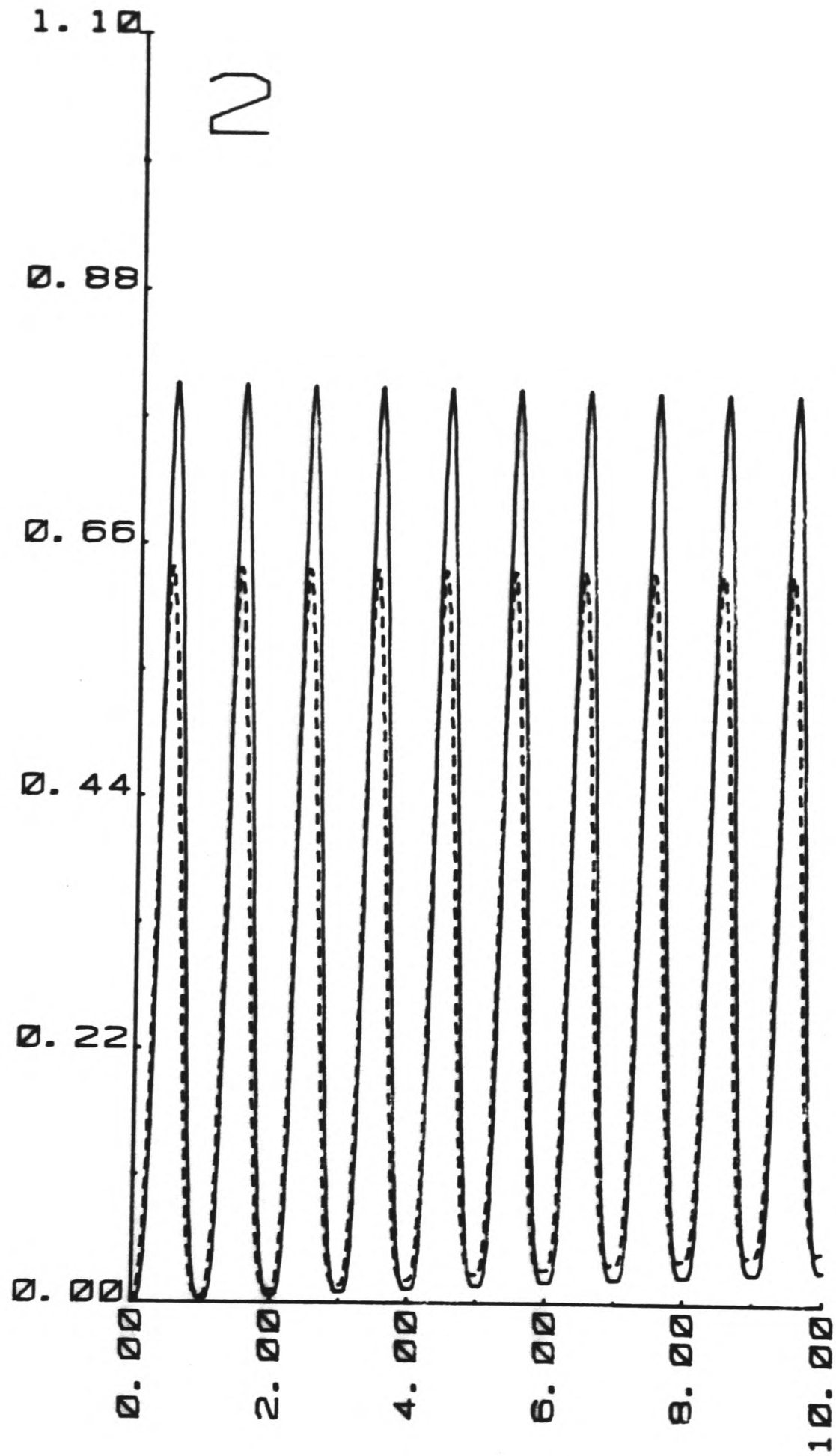

- - numerical

——— analytical

Plot of $[\sigma^2-\sigma^2|_{\tau=0}]$ St^2 versus $\frac{\tau}{2\pi}$

Figure 3.2

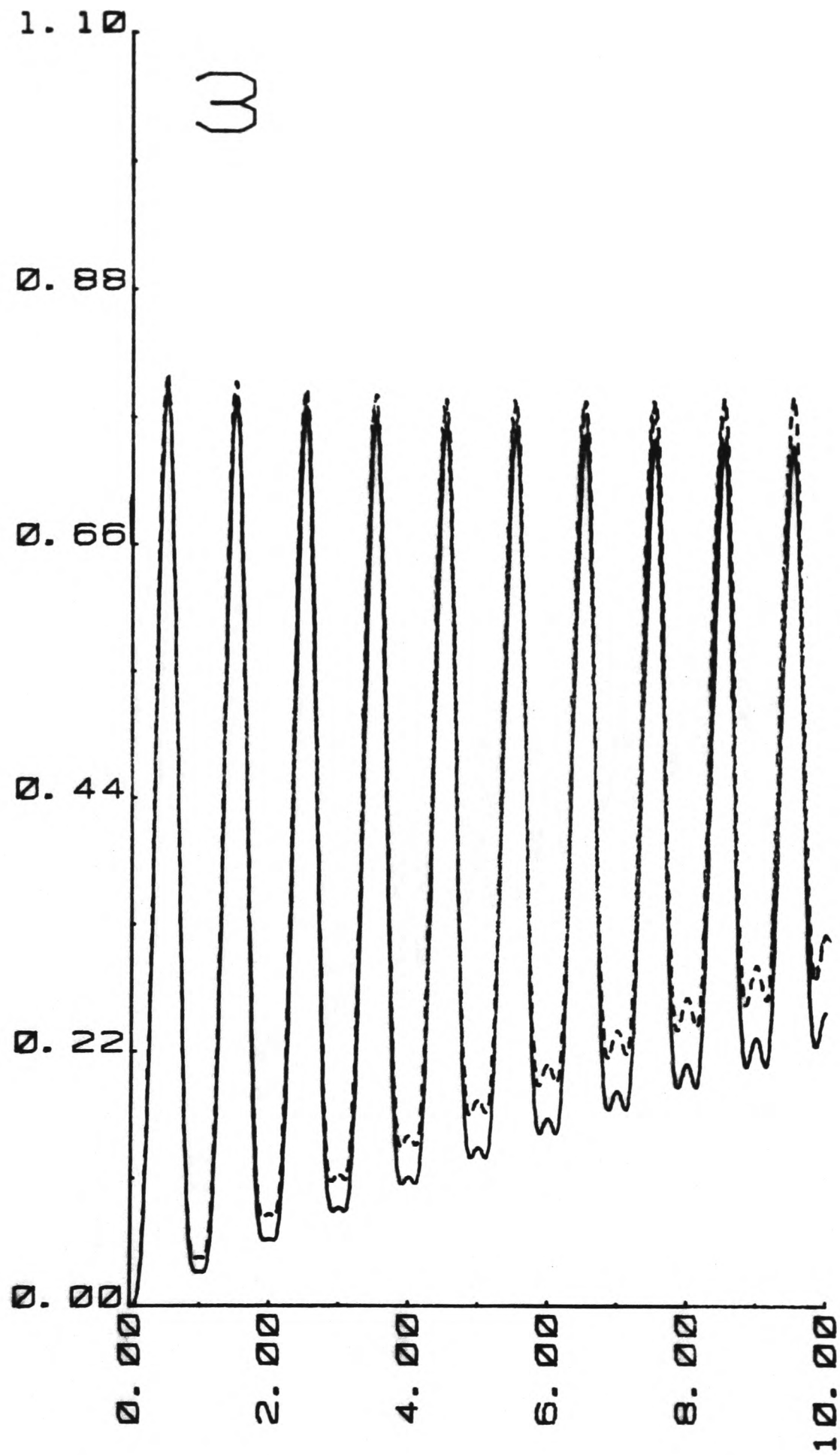

- - numerical

——— analytical

Plot of $[\sigma^2-\sigma^2|_{\tau=0}]$ St^2 versus $\frac{\tau}{2\pi}$

Figure 3.3

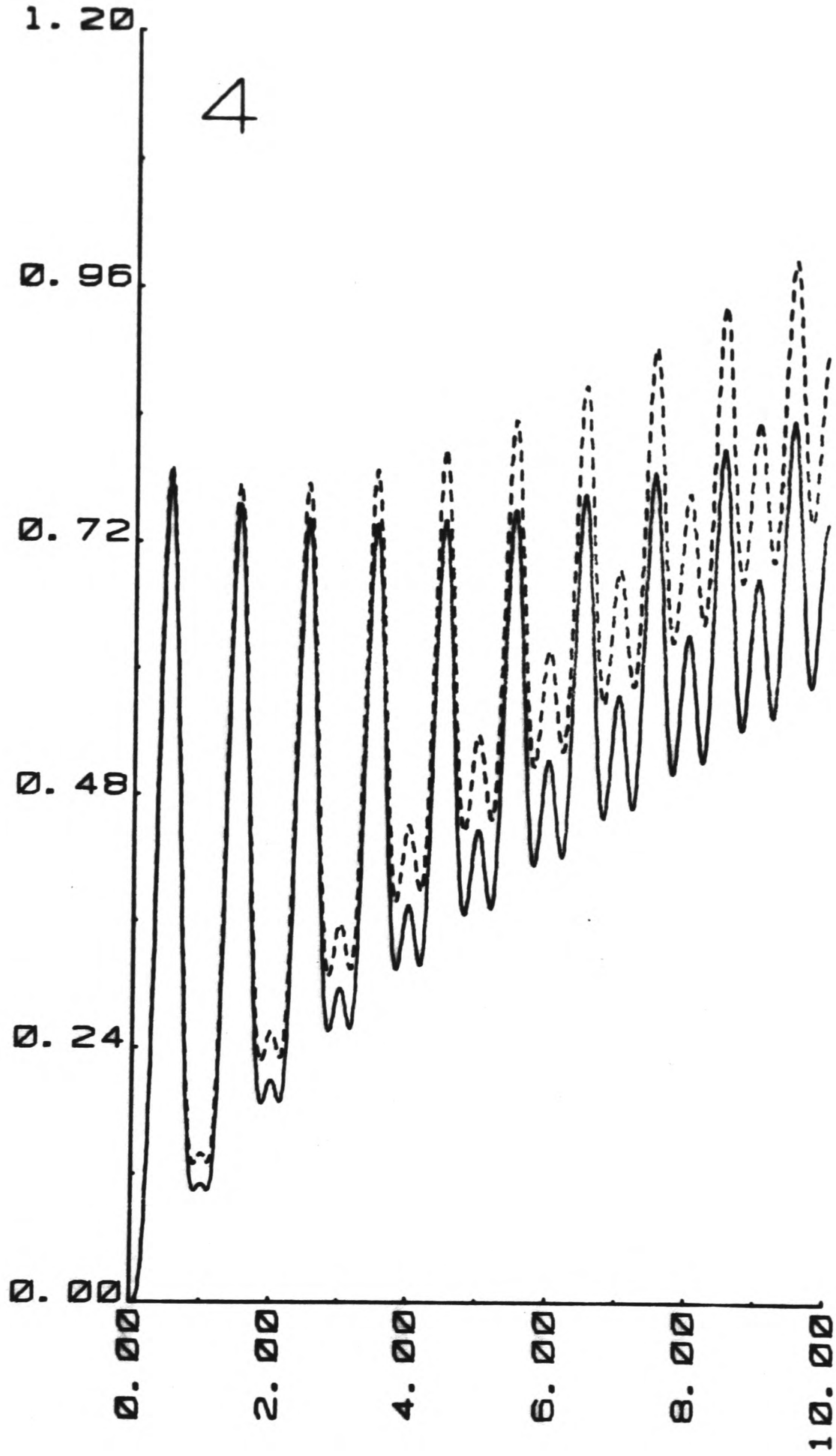

- - numerical

——— analytical

Plot of $[\sigma^2-\sigma^2|_{\tau=0}]\ St^2$ versus $\frac{\tau}{2\pi}$

Figure 3.4

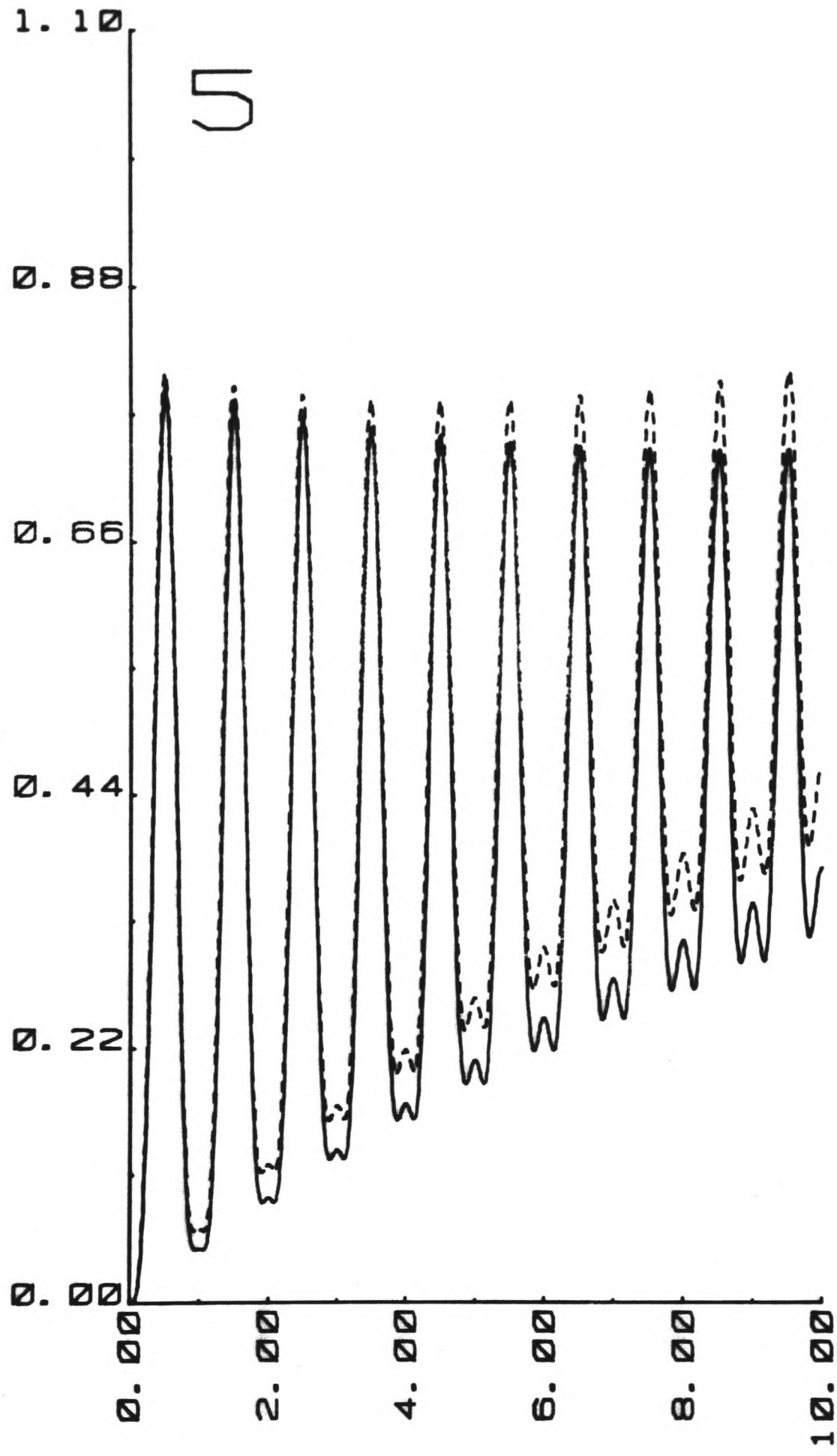

- - numerical

——— analytical

Plot of $[\sigma^2-\sigma^2|_{\tau=0}]\ St^2$ versus $\frac{\tau}{2\pi}$

Figure 3.5

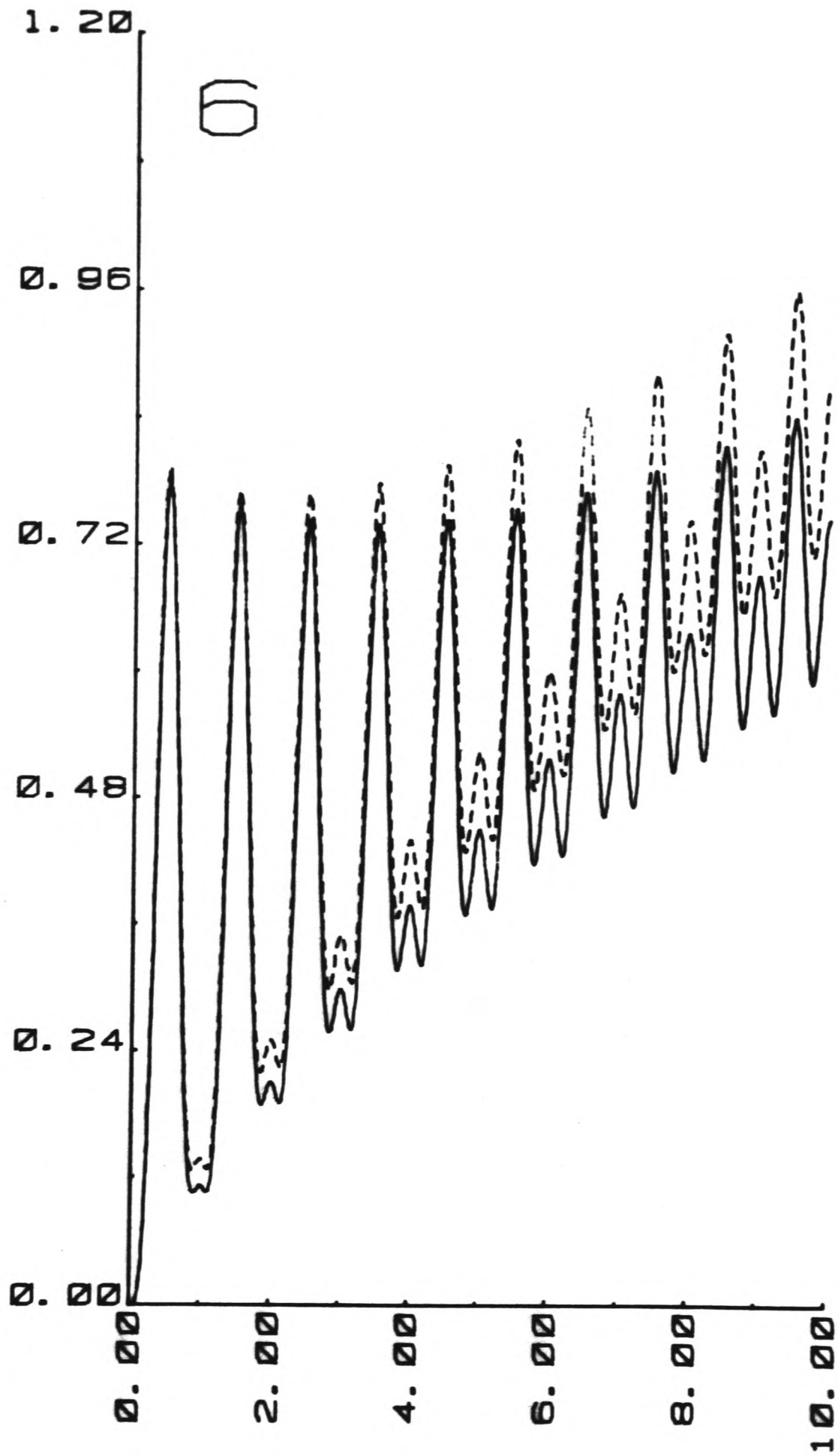

- - numerical

——— analytical

Plot of $[\sigma^2-\sigma^2|_{\tau=0}]\ St^2$ versus $\frac{t}{2\tau}$

Figure 3.6

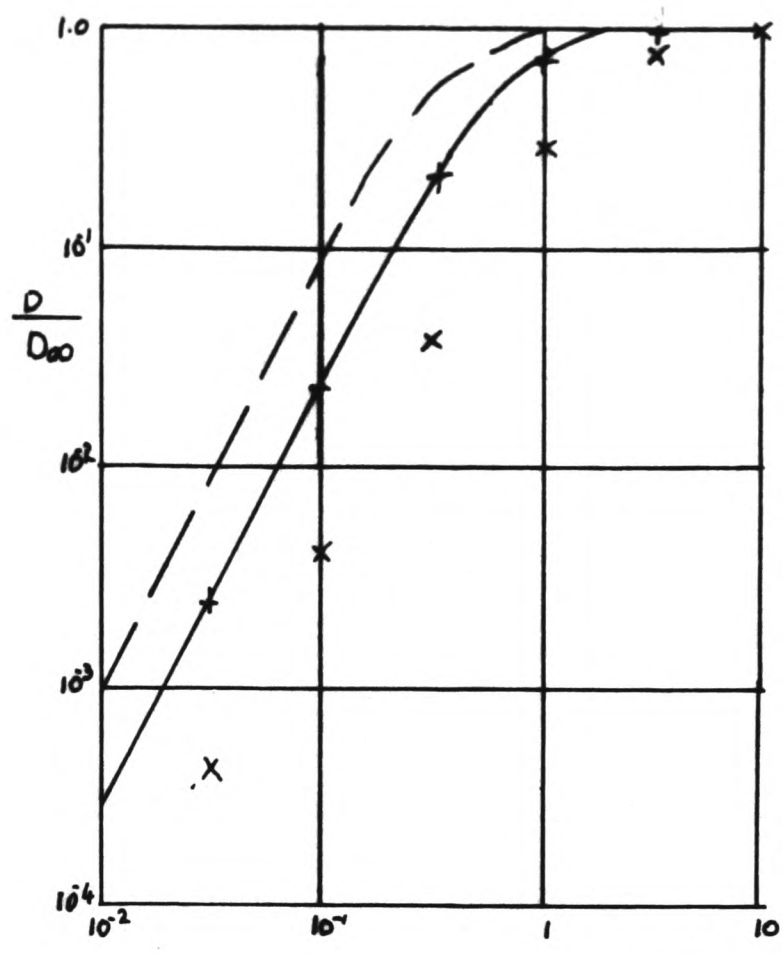

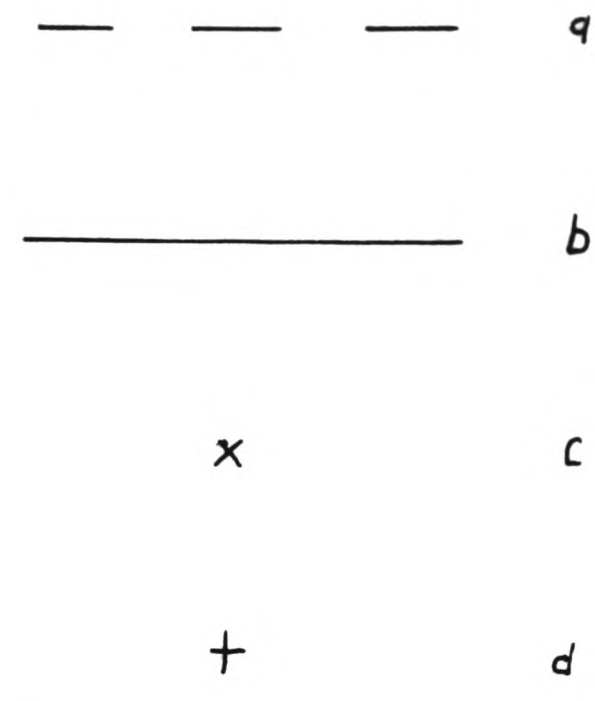

$$D_\infty = \lim_{P_o \to \infty} D$$

(a) tube flow after Holley, Harlemann and Fischer (121)

(b) uniform shear flow after Holley, Harlemann and Fischer (121)

(c) flat channel flow using modified moments analysis with a two-term expression for the wall concentration and assuming a quasi-steady velocity profile

(d) uniform shear flow using the first term of the series derived by Holley, Harleman and Fischer (121).

Dependence of dispersion coefficient upon P_o.

Figure 3.1

the frequency dependence of the shape of the velocity profile was described and it was concluded that on increasing the frequency, the flow profile tended closer and closer to the plug limit. This tendency, which the above analysis has ignored, will certainly mean that $\frac{\partial D}{\partial f} > 0$ and not zero. At Schmidt numbers (Sc) of order unity, the frequency dependence is much stronger since the concentration evolution approaches a quasi-steady development. If we define D_∞ as the limit of D as $Po \to \infty$, then we may plot out D/D_∞ against Po. This curve is shown in figure 3.7 and the analytical results are compared with the predictions of Holley, Harlemann and Fischer (121). The low Po limit behaviour of both analyses indicates that $D \propto Po^2$ but that as Po attains values greater than O(1), this effect disappears and D becomes independent of Po.

3.2.3 Treatment Of The Case Of Womersley Parameter Of Order Unity

In the analysis of the velocity profile given in chapter 2, it was pointed out that the velocity could be given by a Taylor series in ψ. The limit of small α^2 truncates this series to include just the first two terms (in ψ^0 and ψ^2), and increasing α^2 necessitates the inclusion of more terms. The analysis set out in section 3.2.2 requires that we should express the velocity profile as such a series. It is therefore possible to extend the range of frequencies to which this approach is applicable by using a general quartic velocity profile. The coefficients in this quartic expression may be evaluated using the analysis given in chapter 2. The algebra is more involved in this case since the equations for I_m^n are more intimately coupled. Nevertheless, the analysis is basically the same and the results are not greatly different. The quartic expression was investigated by writing down a general form

for the velocity profile as

$$u = \sin\{\tau\} \left[a_0 + a_1\psi^2 + a_2\psi^4 \right] + \cos\{\tau\} \left[b_0 + b_1\psi^2 + b_2\psi^4 \right]. \quad (3\text{-}39)$$

This formulation was used in the moments equation and the moments evaluated as in section 3.2.2. The equation for I_2^0 now requires us to solve for I_1^0, I_1^2, I_1^4 and I_0^0, whereas the parabolic profile did not necessitate the calculation of the third of these. Once the solution had been obtained in terms of the 'a' and 'b' coefficients, a number of frequencies were chosen for which the quartic profile was an accurate representation. For each value of α^2, the coefficients in the quartic expression for the velocity profile were evaluated and from these the dispersion coefficient was deduced. As in the parabolic profile case, the value of I_0^m was found to equal $\frac{1}{m+1} J_0^0$ for m even, and $\bar{X}$ was found to be given by the time integral of the bulk flow velocity. Plots of the dispersion coefficient (calculated using these methods) against Strouhal number and Reynolds number on logarithmic axes are shown and described in chapter 5. From these plots, for both profiles, the dispersion coefficient can be seen to vary as stroke squared (or as St^{-2}). The parabolic profile incorrectly predicts no change of D with frequency, whereas the quartic expression reveals that D increases slightly with frequency.

Naturally, the values obtained for D using this procedure are only accurate for values of α^2 less than perhaps O(1). To extend this approach to higher frequencies it is necessary to use more and more terms in the expression for the velocity profile and hence to incur a stronger coupling between the moments equations. The amount of work necessary to follow dispersion in plug-type velocity

profiles increases vastly with a^2. This is also a feature of the numerical analysis (see chapter 4) of this phenomenon in which one needs a very fine mesh near the wall in order to follow the large transverse gradients in velocity and concentration there.

3.2.4 Extension To Smaller Times

The analysis given above is approximate even for the case of small frequency since it was necessary to truncate the Fourier series expression for c_w. This meant that we could express c_w as a function of $\bar{C}_0$ and $\bar{C}_2$, whereas for an exact representation it would be necessary to relate $\bar{C}$ to a series in $\bar{C}_m$ for $m = 0 \rightarrow \infty$. The error we incur by using a two term representation for the wall concentration rather than a three term expression is interesting. Using the two term expression as above we found that the prediction for σ^2 contained an exponentially decaying term, the decay constant being γ. When we use a more complex formulation for c_w

$$c_w = \bar{C}_0\left[\, 1 - \frac{5}{6}\pi^2 + \frac{7}{90}\pi^4 \,\right] + \bar{C}_2\left[\, \frac{5}{2}\pi^2 - \frac{1}{3}\pi^4 \,\right] + \bar{C}_4\frac{1}{6}\pi^4, \qquad (3\text{-}40)$$

we find that the the steady state values of σ^2 are negligibly different from those predicted by a two term expression. The new feature picked out by this more cumbersome approach is that the solutions for the time evolution of σ^2 contain exponential terms with decay constants of γ and 4γ. Since this new exponential term has a larger decay constant, it describes an extra feature of the evolution which is only significant for small times.

Chapter 4

PROCEDURE FOR SOLVING THE DISPERSION EQUATION NUMERICALLY.

CHAPTER 4

PROCEDURE FOR SOLVING THE DISPERSION EQUATION NUMERICALLY

4.1 INTRODUCTION

The complexity of the dispersion equation, especially in an oscillatory flow in which the velocity profile is not of a simple analytical form, requires either a numerical approach or the use of some asymptotic analysis. It has been the purpose of the work described in this chapter to predict the channel concentrations resulting from an initial uniform slug stimulus. The numerical methods which have been implemented in order to study oscillatory flow dispersion may be readily applied to any two dimensional mass transfer problem in which the velocity field may be calculated with relative ease. The application of the numerical methods to the problem of mass transfer in an entry length will be described in section 4.6. Details of how to adapt the information about the channel concentrations to give a useful summary of the transfer processes are described in section 4.7.6.

4.2 FINITE DIFFERENCING OF THE DISPERSION EQUATION

The flat channel dispersion equation in dimensional form is

$$\frac{\partial c}{\partial t} = -u_{(y,t)} \frac{\partial c}{\partial x} + \kappa \left[\frac{\partial^2 c}{\partial x^2} + \frac{\partial^2 c}{\partial y^2} \right]. \qquad (4\text{-}1)$$

The boundary conditions that will be applied to this equation are described in chapter 3 by equations [3-1] → [3-5]. The earliest description of a method for studying such a dispersion problem numerically was due to King (134) and later implemented by Allen (2). In this scheme in one sets up an array of particles and uses a random walk technique to follow the spreading. Holley, Harlemann and Fischer (121) described an approximate approach based not upon equation (4-1) but upon what they believed to be the underlying transport process. This scheme involved dividing the flow area into a number of stream tubes each of which was considered to contain fluid moving at the same velocity. Each step of the simulation consisted of a period of pure convection followed by a lateral diffusion. The method used by Ananthakrishnan, Gill and Barduhn (4) has most in common with the approach which has been used in the present study. These authors solved the finite difference form of (4-1) using an implicit formulation. We shall solve the problem by an explicit finite difference scheme which has been described in general terms by Roach (187). Let us use a space and time centred scheme to rewrite the differential terms as

$$\frac{\partial c}{\partial t} \rightarrow \frac{1}{2\Delta t} \left[c^{n+1}_{i,j} - c^{n-1}_{i,j} \right], \qquad (4\text{-}2)$$

$$\frac{\partial c}{\partial x} \rightarrow \frac{1}{2\Delta x} \left[c^{n}_{i+1,j} - c^{n}_{i-1,j} \right], \qquad (4\text{-}3)$$

$$\frac{\partial^2 c}{\partial y^2} \rightarrow \left[\frac{1}{\Delta y} \right]^2 \left[c^{n}_{i,j+1} + c^{n}_{i,j-1} - 2c^{n}_{i,j} \right], \qquad (4\text{-}4)$$

$$\frac{\partial^2 C}{\partial x^2} \rightarrow \left[\frac{1}{\Delta x}\right]^2 \left\{ C^n_{i+1,j} + C^n_{i-1,j} - 2C^n_{i,j} \right\}. \qquad (4\text{-}5)$$

In this formulation we have denoted the concentration at time point number 'n', axial position number 'i' and lateral position number 'j' as $C^n_{i,j}$. It is assumed at this stage that the x,y and t meshes are all uniform; in section 4.3 the difference analogue of the $\frac{\partial^2 C}{\partial y^2}$ term is written for the case of a mesh which is not uniform in the y-direction. The transformations given by equations (4-2) to (4-5) may be used to express equation (4-1) in a difference form. The resulting scheme is unconditionally unstable, but we may use the Dufort-Frankel transformation to express $C^n_{i,j}$ as the average of the values at the succeeding and preceding times, obtaining a scheme of excellent stability and good accuracy. We therefore write

$$C^n_{i,j} \rightarrow \frac{1}{2} \left\{ C^{n+1}_{i,j} + C^{n-1}_{i,j} \right\}. \qquad (4\text{-}6)$$

This scheme expresses the concentration at time 'n+1' and position i,j in terms of the concentrations at previous times. This is the basis for the time marching method which has been used to produce values of concentration in the channel for the first thirty or so cycles of oscillation. Further details of the Dufort-Frankel approach may be found in Roache (187).

4.3 FINITE DIFFERENCE MESH

A finite difference scheme requires the spatial and/or temporal domains which are physically continuous to be split up into discrete points. The time mesh which has been used, contains a uniform step (size Δt), there being at least 100 steps per cycle and more than this when stability requirements are critical. Typically, simulations have modelled 20-30 cycles of the pump. The

mesh in the axial (x) direction is also uniform with there being about 6 steps in the slug half-length, and the mesh being made long enough to prevent the diluted contaminant being washed out of the ends during the simulation. The mesh in the transverse (y) direction is somewhat different in that the step size is non-uniform. This is necessary since the concentration gradients close to the walls of the channel may be large. In order to follow the wall concentrations accurately, but avoid using a vast number of steps over the channel cross-section, it is logical to use a mesh which is fine at the walls and coarse near to the centre-line. This has been achieved using two methods:

1/ A scheme using two overlapping meshes ...a uniformly fine mesh of small extent which is confined to the walls, and a coarse mesh which fills the rest of the space with a uniform grid. This line distribution is illustrated in figure 4.1.

2/ A scheme in which one mesh occupies the entire domain, with lines which converge to a limit at the wall. The step size in this scheme varies as ψ^2. This line distribution is illustrated in figure 4.2. Scheme 1 has the advantage of being very stable and it is also fairly easy to install. The computer time which is used when this scheme is implemented is less than that which scheme 2 would use if an equal number of steps were imposed. Scheme 2, however is better when a very small step size is required near the wall. There is therefore a trade-off between accuracy and restricting computer time. Both meshes have been used, the dispersion work being done with scheme 1, and the mass transfer in an entry region utilizing scheme 2.

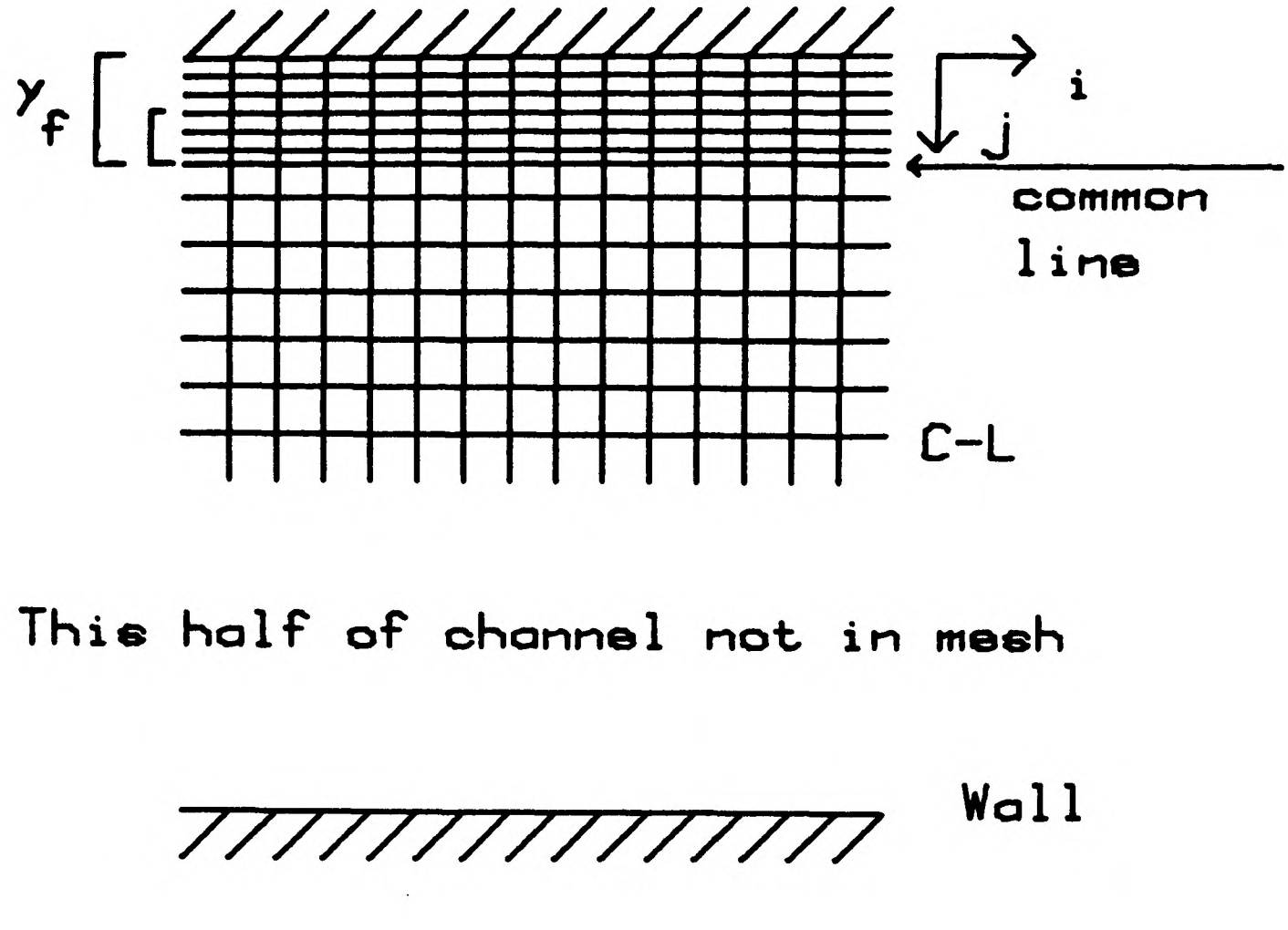

An illustration of the two-level finite difference scheme mesh.

Figure 4.1

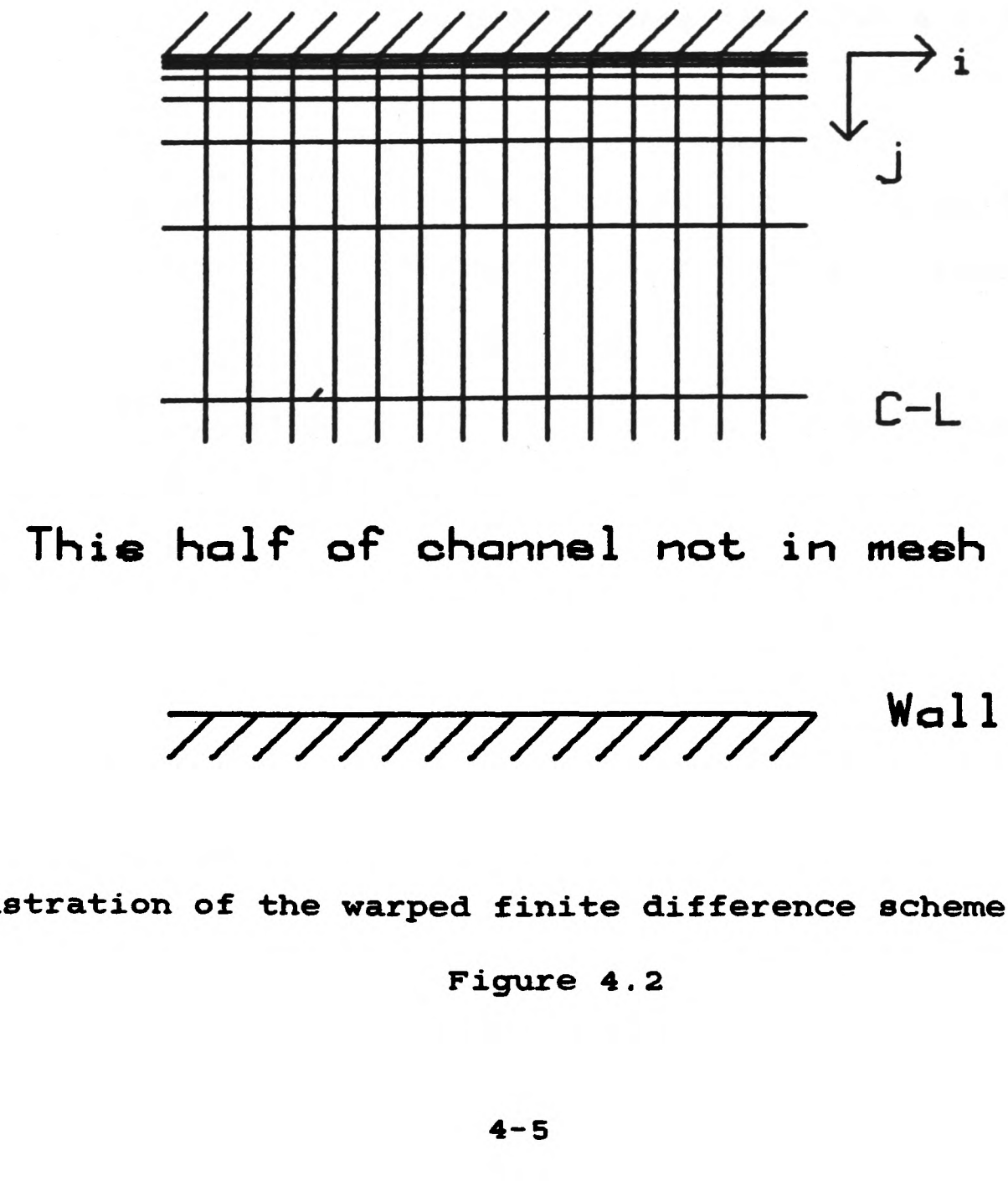

An illustration of the warped finite difference scheme mesh.

Figure 4.2

Both of the non-uniform meshes which have been implemented require a modification to be made to equation (4-4). In the case of mesh 1, the grids are interleaved such that the total distance y_f occupied by the fine mesh is equal to twice the distance (Δy_c) between the coarse mesh lines. Equation (4-4) is now applied directly, using the fine or coarse value of Δy, depending upon the siting of the point where the concentration is being calculated. The points which lie at the junction of the two meshes (arrowed in figure 4.1) are, however, treated differently. The careful overlapping of the meshes produces the property that there is a line of points in the fine mesh which is a distance Δy_c from the line of common points; let the value of j associated with these points be k. We therefore replace equation (4-4) with

$$\frac{\partial^2 c}{\partial y^2} \rightarrow \left[\frac{1}{\Delta y}\right]^2 \left\{ C^n_{i,j+1} + C^n_{i,k} - 2C^n_{i,j} \right\}, \qquad (4\text{-}4')$$

and set Δy equal to Δy_c when determining the concentrations along the line of common points.

When a completely non-uniform distribution of grid-lines, such as that exemplified by mesh 2, is used, it is necessary to change the form of equation (4-4) somewhat. The step sizes in the directions of increasing and decreasing j are denoted by Δ and δ respectively. By writing out the Taylor series in y for the concentrations at points i,j-1,n and i,j+1,n and then eliminating the term in $\frac{\partial c}{\partial y}$ we obtain

$$\frac{\partial^2 c}{\partial y^2} \rightarrow \frac{2}{\delta+\Delta}\left[\frac{1}{\Delta}(C^n_{i,j+1} - C^n_{i,j}) + \frac{1}{\delta}(C^n_{i,j-1} - C^n_{i,j})\right] \qquad (4\text{-}4")$$

Equation (4-4") does of course reduce to (4-4) when Δ equals δ.

Typically between 10 and 20 steps have been used in the y-mesh, although for very accurate contour plotting, as many as 40-50 steps have been set up. For cases in which the concentration and velocity distributions have been symmetrical about the channel centre-line, only half of the channel has been studied; this effectively allows one to halve the time taken to complete a simulation.

4.4 BOUNDARY CONDITIONS

Figure 4.3 illustrates the way in which the scheme proceeds to calculate new concentrations in the temporal domain, with the shaded rectangles indicating the sites where it is necessary to know the concentration in order to progress through one time step of the method for a particular (i,j).

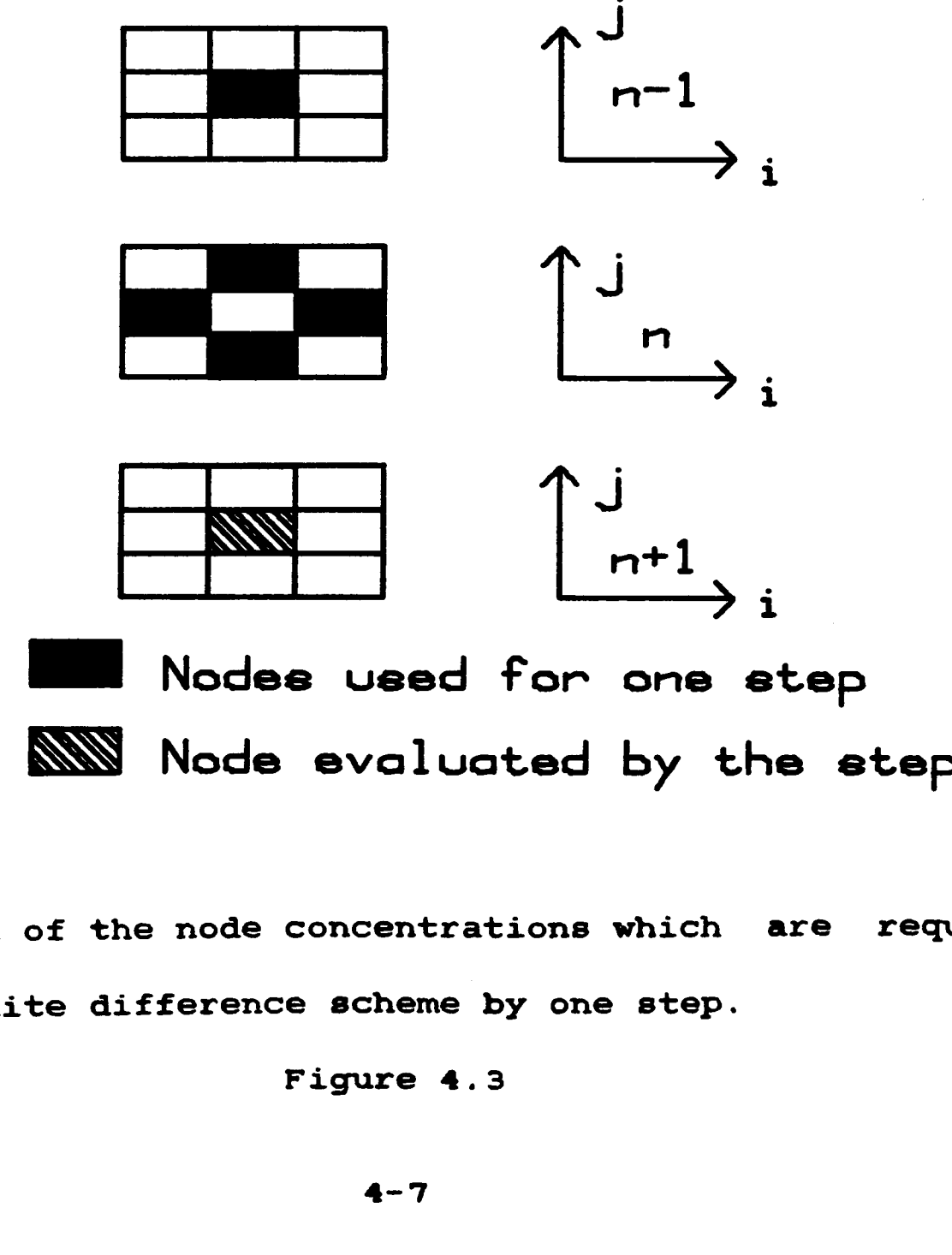

An illustration of the node concentrations which are required to advance the finite difference scheme by one step.

Figure 4.3

The procedure is straightforward for cases in which none of the shaded rectangles shown in figure 4.3 lies outside of the spatial or temporal meshes. When this condition is not satisfied, we need to apply the boundary conditions. When a point lies outside the axial space mesh, we apply boundary condition [3-1], by forcing the concentration at the end points of the mesh to be zero. If significant amounts of contaminant reach the axial ends of the mesh then the simulation must be stopped. The boundary conditions associated with the transverse limits of the mesh are somewhat different in character. We require (condition [3-2]) that the lateral concentration gradient $\frac{\partial c}{\partial y}$ is zero at the wall (impermeable wall condition) and that it is also zero on the channel centre-line (symmetry condition). If j=1 is the line of the wall then we write

$$C^{n}_{i,0} = C^{n}_{i,2}, \qquad (4\text{-}7)$$

and use a similar form for the centre-line condition. This expression may then be used in equation (4-6) when j=1.

The temporal mesh also poses some problems. The initial values are given by boundary conditions [3-3,3-4] and this specifies the channel concentrations at n=0. The Dufort-Frankel scheme, however, requires the concentrations at times n and n-1 in order to calculate the concentrations at time n+1. The initial condition only gives the value for one of these levels, so to get around this difficulty two methods have been tried out. The first method uses a two-timestep difference scheme for the first calculation and switches to the Dufort-Frankel approach once the requisite two time level concentrations have been calculated. The second method simply supposes that the concentrations at time levels n=0 and n=1 are the same. This method gave the same results

as the first and was easier to implement so it was used for most of the calculations.

4.5 TRANSPORTIVE PROPERTY

It is desirable (but not necessary) that a finite difference scheme possesses the transportive property. Let us consider the simple differencing scheme given above. It will be shown in the next section that it is the convective term which imposes the most severe stability restrictions. This term is also responsible for the violation of the transportive requirement. Consider the extreme of no diffusion and a steady velocity in the positive x-direction. On physical grounds we would not expect the concentration at a particular point to be in any way dependent upon the values downstream. It can be seen that in writing the $u \frac{\partial c}{\partial x}$ term as a centred difference, we have violated this property. This is not an insurmountable problem however, since we may choose to express the convective term as

$$u \frac{\partial c}{\partial x} \rightarrow u \frac{1}{\Delta x} \left[c^{n}_{i,j} - c^{n}_{i-1,j} \right]. \qquad (4\text{-}8)$$

This is termed upwind differencing since only the upwind properties of the convected species may affect the value at a particular point. In the case of an oscillatory velocity, we would use the above backward differencing formulation when the flow was in the positive sense, and change to a forward difference approach when the velocity reversed. In this way the transportive requirement would be met, but there would be a price to pay. The centred difference scheme is accurate to $O(\Delta x^2)$ whereas the scheme described above is only accurate to $O(\Delta x)$. For a sufficiently fine mesh size, the centred difference scheme would meet the

transportive requirement approximately and would be more accurate and quicker to implement and execute than the corresponding forward/backward difference scheme. There are thus two conflicting goals which we should aim for when choosing a differencing scheme to represent the convective components. On the one hand we are seeking a scheme which is accurate to $O(\Delta x^2)$, and on the other we do not wish to badly violate the transportive property. Both of these ideals may be realized in a scheme which considers not just the neighbouring points, but takes the concentration at two points on each side of the central node. This results in

$$\frac{\partial c}{\partial x} \rightarrow \frac{1}{2\Delta x}\left\{ C^{n}_{i-2,j} - 4C^{n}_{i-1,j} + 3C^{n}_{i,j} \right\}, \text{ for } u>0. \qquad (4\text{-}9)$$

The advantage of this scheme is that the transportive requirement is met, and the accuracy is $O(\Delta x^2)$. For negative u, there is a similar formulation which also posseses these properties. This scheme may be regarded as an upwind weighted differencing. More complex and more accurate approaches may be devised by writing out the Taylor series for the concentrations at as many neighbouring nodes as one wishes to use in the scheme, and then solving the truncated equations to yield an expression for the particular concentration derivative being sought. The disadvantage in using such schemes is the greatly increased execution time and in addition, the stability of the simulation may be impaired. These considerations may effectively make some of the more primitive schemes preferable in practice.

4.6 STABILITY REQUIREMENTS

The most stringent requirement upon the range of flows which can be reproduced by the numerical work is the necessity that the differencing scheme should produce solutions that are stable. It is inevitable that due to machine rounding errors, the concentrations that are calculcated will not be exact, hence it is very necessary that such small errors should not be amplified so as to produce a divergence from the correct solution. The Dufort-Frankel scheme can be made stable by using a sufficiently small time step; this however increases the run-time of the simulation so it is necessary to set up some stability criterion which enables the numerical work to be carried out with a temporal step size which is just sufficient to produce a converging solution. The complex forms of stability analysis (see Roache (187)) such as those due to Hirt or Von Neumann are not easily adapted to this dispersion equation, in which the flow field is two dimensional and unsteady. The approach which was taken in solving this problem was the use of a discrete perturbation method; this may not under all circumstances produce a rigid threshold for N (the number of steps per cycle), but it has been found to be useful and infallible for predicting a 'safe' time step size which is reasonably close to the limit. Consider the case of a uniform transverse mesh in which there is a small perturbation error ϵ_1 upon a single node concentration at any of the rectangles illustrated in figure 4.3. This error upon the correct solution will be transmitted to the concentration being calculated ($C^{n+1}_{i,j}$) in the form of an error ϵ_2. For stability we require that $|\epsilon_2 / \epsilon_1|$ is less than unity, otherwise the magnitude of the error will grow. To analyze this case we consider the perturbation to lie at each of

the following node points in turn:

1/ i-1, j, n 2/ i+1, j, n 3/ i, j, n-1

4/ i, j-1, n 5/ i, j+1, n.

A strength of the difference scheme is that for four of these points, the error is unconditionally damped out. The exception to this is direction 1 which may be the cause of instablility under some circumstances. The discrete perturbation analysis stability criterion for a space and time-centred Dufort-Frankel scheme is

$$N > \frac{1}{f}\left[\frac{u}{\Delta x} - \frac{2\kappa}{\Delta y^2}\right], \qquad (4\text{-}10)$$

In order that the system should be stable for all time, we choose the worst values for u and Δy. In both these cases, this entails consideration of the values close to the channel centre-line. Observation of contour plots for which the stability criterion has been deliberately violated, has indicated that it is at this position that instabilities generallly set in.

When we apply the stability criterion to the upwind scheme to which the Dufort-Frankel time average has only been applied to the diffusive terms, we find that it is still along direction 1 that the instabilites progress, but that the criterion for convergence is more severe by a factor of 2:

$$N > \frac{2}{f}\left[\frac{u}{\Delta x} - \frac{\kappa}{\Delta x^2} - \frac{\kappa}{\Delta y^2}\right]. \qquad (4\text{-}11)$$

However, when the convective term is time-averaged as well, the stability criterion is found to be identical to that of the space-centred non-transportive method.

The smallness of the diffusivity (κ) for this problem means that the Dufort-Frankel scheme is not unconditionally stable as it might be in a heat transfer or momentum transfer problem in which the diffusivity term would be at least 4 orders of magnitude larger and hence enable a much coarser time mesh to be used. In addition, the smallness of the diffusivity causes problems of accuracy since the convective effect is, on the short term, by far the dominant mechanism governing changes in concentration at a point. The smaller diffusive effect, by acting very gradually, produces a relatively insignificant change when considered over one time step. Unless good accuracy is achieved, the true dispersive behaviour may be masked by small noise spikes.

4.7 IMPOSITION OF DIFFERENT BOUNDARY CONDITIONS

The boundary conditions set out in chapter 3 equations [3-1] → [3-5] describe the dispersion of a uniform slug of contaminant in a channel with impermeable walls. For this case, a two-tiered y-mesh was used as described in section (4.2). In the dispersion study, the main departure from these conditions was to set up a different initial condition which modelled a ramp slug. Thus equations [3-3] and [3-4] are replaced by

$$\text{for} \quad |\chi| > \chi_0 \quad \text{and} \quad t = 0, \quad c = 0$$

$$\text{for} \quad |\chi| < \chi_0 \quad \text{and} \quad t = 0, \quad c = 1 - \left|\frac{\chi}{\chi_0}\right|. \qquad (4\text{-}12)$$

Another variation dispensed with the impermeable wall condition and supposed that both upper and lower walls were held at some constant concentration. This of course makes it unecessary to calculate the wall (j=1) concentrations, so the outer extreme of the y-mesh is no longer a special case.

The flexibility of the set of numerical routines was such that it was quite easy to adapt the dispersion work to the study of mass transfer in an entry length. This problem is being studied experimentally (273) and the purpose of the numerical approach was to provide some theoretical guide-lines for this work. The boundary conditions are entirely different and are reproduced below:

$$c = 0 \quad \text{at } \chi = 0,\ \chi_1, \qquad \text{for all } \psi,\ \tau. \qquad [4\text{-}1]$$

$$c = -1 \text{ at } \psi = 1, \qquad \text{for all } \chi,\ \tau. \qquad [4\text{-}2]$$

$$c = 1 \text{ at } \psi = -1, \qquad \text{for all } \chi,\ \tau. \qquad [4\text{-}3]$$

$$c = -\psi \quad \text{at } \tau = 0 \qquad \text{for all } \psi, \text{ and } 0 < \chi < \chi_1 \qquad [4\text{-}4]$$

Condition [4-1] sets up an entry length at the origin of the χ axis and at a position further downstream ($\chi = \chi_1$). Conditions [4-2] and [4-3] model the diffusion of some species from one channel wall through the moving channel fluid into the opposite wall. The initial condition specified by equation [4-4] is the steady state concentration distribution that would be achieved by diffusion acting in the absence of any convective effects. In addition, the initial condition of zero concentration throughout the channel was also set up. The principal difficulty with this problem is that to obtain values for the wall transfer rate, it is necessary to evaluate the concentration gradient at $\psi = \pm 1$. The gradients at the wall tend to be rather large so it is essential to use a transverse mesh with a very fine edge resolution. This was accomplished by using the warped mesh described in section (4.2). In this study, it was assumed that the velocity profile was not a function of the axial co-ordinate χ. The justification for this

assumption is that the velocity entry length is much shorter than that for mass transfer; it may be, however, that some errors will be incurred at positions very close to the channel entrance due to neglect of the developing velocity. In a more detailed study, it may be possible to overcome this deficiency by using an exact velocity distribution although this would involve the use of an even more cumbersome expression for the profile than that calculated in chapter 2.

4.8 PRESENTATION OF NUMERICAL RESULTS

4.8.1 Introduction

The method used to solve the problem of dispersion predicts values of the concentrations in the channel for a large number of positions and times. Having formulated the routines to produce this information, the next problem is how to present the results. It seems that there are two methods. The first approach is to define a single parameter which summarises the extent and nature of the mass transfer processes taking place. The second method is to obtain a very detailed set of graphs and plots which give one an intuition for the mechanisms by which the transfer is affected. It has been the aim of this study to present results using both these approaches. The following sub-sections give details of the way in which the results were processed; the results of the numerical work are presented and discussed in chapter 5.

4.8.2 Method Of Moments And The Dispersion Coefficient

The usefulness of the method of moments as a means of summarising the dispersive behaviour has been described in chapter 3. In order to evaluate the moments of concentration, it is a straightforward matter to evaluate the average of the node concentrations over the ψ-direction at a particular axial position and time in order to calculate the mean cross-channel concentration. Having been multiplied by an axial weighting factor, these values are then integrated over the channel length. In this way the values of I_n have been calculated for n = 0 to 4 (see chapter 3 for further details), and from these parameters, the position of the centre of mass of the contaminant, the variance, the skewness and the kurtosis were all calculated. These parameters were evaluated at 100 uniformly spaced points in each cycle and this enabled the behaviour of the various moments with time to be observed. In order to evaluate $\frac{\partial \sigma^2}{\partial t}$, a time centred difference scheme was imposed upon the successive values of the variance σ^2.

To calculate the time-averaged dispersion coefficient, using an analytical approach, one should evaluate the mean of $\frac{\partial \sigma^2}{\partial t}$ over one cycle. This is, however, an exceedingly inaccurate approach when applied to the numerically derived variances. For most cases, the variance plots are dominated by the large spikes arising from the continual transient excursions of the slug from its central position; the gradual increase in the level of the variance due to true dilution only occurs gradually. When one evaluates the time derivative of such a function, the diffusive effect is initially imperceptible or at best swamped by noise, and this renders an accurate calculation of the dispersion coefficient impossible. In

order to avoid these difficulties, the variance was averaged over a cycle, usually providing 30 values for the mean variance at successive time intervals equal to the pump period. By operating a time centred differencing scheme on consecutive values, the time dependence of the dispersion coefficient was determined.

4.8.3 Simulation Of Experimental Dispersion Results

Experimental studies of dispersion have, almost without exception, been dedicated to presenting results as values of the mean cross-channel concentration measured at a particular axial position for some value(s) of time. The experimental procedure described in chapter 6 will also present results in this form, so it was considered to be useful to adapt the numerical work to provide a theoretical prediction for the concentrations that would be measured experimentally under ideal conditions. The method used to evaluate $\bar{C}$ was the same as that described in section (4.8.2). These values of $\bar{C}$ were calculated at a number of axial positions in the channel corresponding to the locations of the dye sensing gauges. For 100 uniformly distributed times in each period, the value of $\bar{C}$ was calculated and the results for a particular value of χ were plotted out against time, thus giving a prediction for the gauge readings.

4.8.4 Axial Distribution Of Mean Cross-Channel Concentration

The approach here was the same as that described in section (4.8.2), except that $\bar{C}$ was evaluated along each transverse mesh line and the resulting $\bar{C}$ versus χ data was plotted out for certain times. The experimental predictions were different in that they took the form of plots of $\bar{C}$ versus τ for certain values of χ.

4.8.5 Numerical Flow Visualization By Contour Plotting

The methods of presenting results which have been described above, entail the evaluation of the mean cross-channel concentration. This averaging process provides a summary of the system but also smothers much useful information. The ultimate ideal for presenting results is the plotting out of lines within the channel, representing contours of equal concentration. This of course is also quite cumbersome and does not readily lend itself to a concise and comprehensive description. The advantage that contour plotting does have is that by observing a number of such plots one can build up a good intuition as to how the contaminant spreading is taking place.

The numerical work provides predictions for concentrations at a number of points in the channel. In order to convert this information to a contoured description, a linear interpolation was carried out between neighbouring points to determine where a particular contour would cross the mesh lines. Once these cross-over points were known, they could be joined up using straight lines and a simple geometrical algorithm. The particular contours plotted have been separated by a linear or a logarithmic interval.

These methods of presenting the dispersion data may be regarded as three extremes of summarisation. The most condensed form is the moments analysis in which spatial integration is carried out in two dimensions (χ and ψ). The integration smothers some of the information leading to a concise but limited conclusion. The summary of the behaviour of the system in terms of the asymptotic dispersion coefficient is a further extreme in which

temporal variations are covered up as well. The process of integrating the concentration over the y-direction alone (so as to calculate $\bar{C}$) is not such a severe condensation of the process, but information is still lost. The shortcomings of the whole concept of working in terms of mean cross-channel concentrations, a method which has been central to most theoretical analyses, has been pointed out by Smith (219), the criticism being that the integration introduces various effects which are merely artefacts of this averaging process. The particular case that Smith draws attention to is the behaviour of the skewness in a steady flow, although the large peaks in the variance, skewness and kurtosis plots (see chapter 5) are also manifestations of this. In section 8.3 a novel treatment is proposed by which mean concentrations may be expressed without incurring this shortcoming.

4.8.6 Treatment Of Data For Entry Length Mass Transfer

The main purpose of the entry length study was to provide predictions of the Sherwood number for various flow conditions that would be imposed experimentally. Here the Sherwood number is the ratio of the wall mass transfer rate (averaged over time and axial distance) to the rate that would be achieved by diffusion alone. The results were therefore treated by using a forward differencing scheme to evaluate $\frac{\partial c}{\partial y}$ at the wall for all axial positions. The value of $\frac{\partial c}{\partial y}$ at the wall, when averaged over all the axial positions and normalized in terms of the convectionless value $(\frac{2}{h})$, yielded the Sherwood number. This was plotted out against time for a number of strokes, frequencies and steady flows. In this way, one could obtain a prediction for the reading which would be taken experimentally. One could also observe the time evolution of this

parameter....something which could not be discerned experimentally.

The results of the numerical method of treating oscillatory flow dispersion which has been described in this chapter are presented in chapter 5.

Chapter 5

RESULTS OF NUMERICAL ANALYSIS OF MASS TRANSFER.

5.1 Introduction.

5.2 Evolution of the axial moments of concentration.
- 5.2.1 Introduction.
- 5.2.1 Discussion of plots of X versus time.
- 5.2.3 Discussion of plots of variance versus time.
- 5.2.4 Discussion of the rate of growth of the variance plots.
- 5.2.5 Time dependence of the dispersion coefficient.
- 5.2.6 Observations of the time evolution of the skewness plots.
- 5.2.7 Observations of the time evolution of the kurtosis plots.
- 5.2.8 Effect of starting from a ramp slug.
- 5.2.9 Effect of slug size on the moments plots.
- 5.2.10 Effect of using permeable walls.
- 5.2.11 Effect of changing the Schmidt number.
- 5.2.12 Effect of changing the velocity phase.
- 5.2.13 Summary of the time evolution of the moments plots.

5.3 Plots of mean cross-channel concentration.
- 5.3.1 Introduction.
- 5.3.2 Breakthrough curve measured initially inside slug.
- 5.3.3 Breakthrough curve measured initially inside deformed slug.
- 5.3.4 Breakthrough curve measured initially outside deformed slug.

5.4 Contour plots of lines of equal concentration.

CHAPTER 5

RESULTS OF NUMERICAL ANALYSIS OF MASS TRANSFER

5.1 INTRODUCTION

The numerical approach described in chapter 4 has been used to simulate the evolution of the dispersion process for six Strouhal numbers in the range 0.01 → 0.2 and ten Reynolds numbers in the range 0.4 → 200.0. The routines have been implemented on two separate systems (VAX 11/780 and PDP 1134) using different versions of Fortran and identical results have been obtained. The numerical dispersion study has been in the main directed towards calculating the time evolution of the axial moments plots since concise and comprehensive results are easiest to present using this method.

5.2 EVOLUTION OF THE AXIAL MOMENTS OF CONCENTRATION

5.2.1 Introduction

In this study, the following values of the experimental parameters have been imposed

h = 1mm, x_0 = 2.5mm, uniform slug, impermeable walls

$\nu = 1 \times 10^{-6}\ m^2 s^{-1}$, $\kappa = 1 \times 10^{-9}\ m^2 s^{-1}$.

The initial bulk velocity in the channel has been taken to be zero ($\phi = 0$). It will be demonstrated that this condition affects the transient behaviour of the moments plots critically. The concentration distribution which evolves as a result of this zero initial velocity condition is in a sense asymmetrical, since the slug always lies to the same side of the origin. The symmetrical case corresponds to the zero initial acceleration ($\phi = \frac{\pi}{2}$) condition in which the bulk fluid velocity is initially at its maximum and the slug is bowed out to equal distances either side of the starting point during the course of one period.

The first five moments ($I_0 \rightarrow I_4$) have been computed and the values of the functions have been used to calculate $\bar{X}$, σ^2, $\frac{\partial \sigma^2}{\partial t}$, the skewness Sk and the kurtosis Ku. The skewness and kurtosis are here defined as

$$Sk = \int_{-\infty}^{+\infty} \bar{C} \, (x - \bar{X})^3 \, dx \; / \; \sigma^3, \qquad (5\text{-}1)$$

and

$$Ku = \int_{-\infty}^{+\infty} \bar{C} \, (x - \bar{X})^4 \, dx \; / \; \sigma^4. \qquad (5\text{-}2)$$

It should be noted that for a Gaussian curve Sk = 0 and Ku = 3, so we would expect the computed moments to approach these values for large time, since the mean cross-channel concentration eventually becomes a Gaussian function of distance along the channel.

5.2.2 Discussion Of Plots Of $\bar{X}$ Versus Time

In chapter 3 a moments analysis was used to show that the effective position of the centre of a slug of contaminant moved with the bulk fluid velocity. A comparison of the numerical and analytical predictions for the $\bar{X}$ versus time plot if shown in

figure 5.1. The value of $\bar{X}$ was never negative, since the slug centre was always positioned to the same side of the origin. The effect of changing ϕ (the phase of the initial velocity) has been studied and it was observed that any change will cause a downward shift of the plot shown in figure 5.1. The shift will reach a maximum when the phase angle is π, the curve lying entirely below the time axis. When $\phi = \frac{\pi}{2}$ or $\frac{3\pi}{2}$, the curve is centred on the x-axis. When the simulation had been run for a time large enough for significant amounts of contaminant to be washed out of the edges of the mesh, the $\bar{X}$ plot would show noticeable deviation from the predicted behaviour and this was used as an indication that the results being produced by the numerical scheme were no longer reliable. The behaviour of $\bar{X}$ with time is well known but the agreement with theoretical predictions has been used as an indication that the velocity profile and concentrations were being calculated correctly.

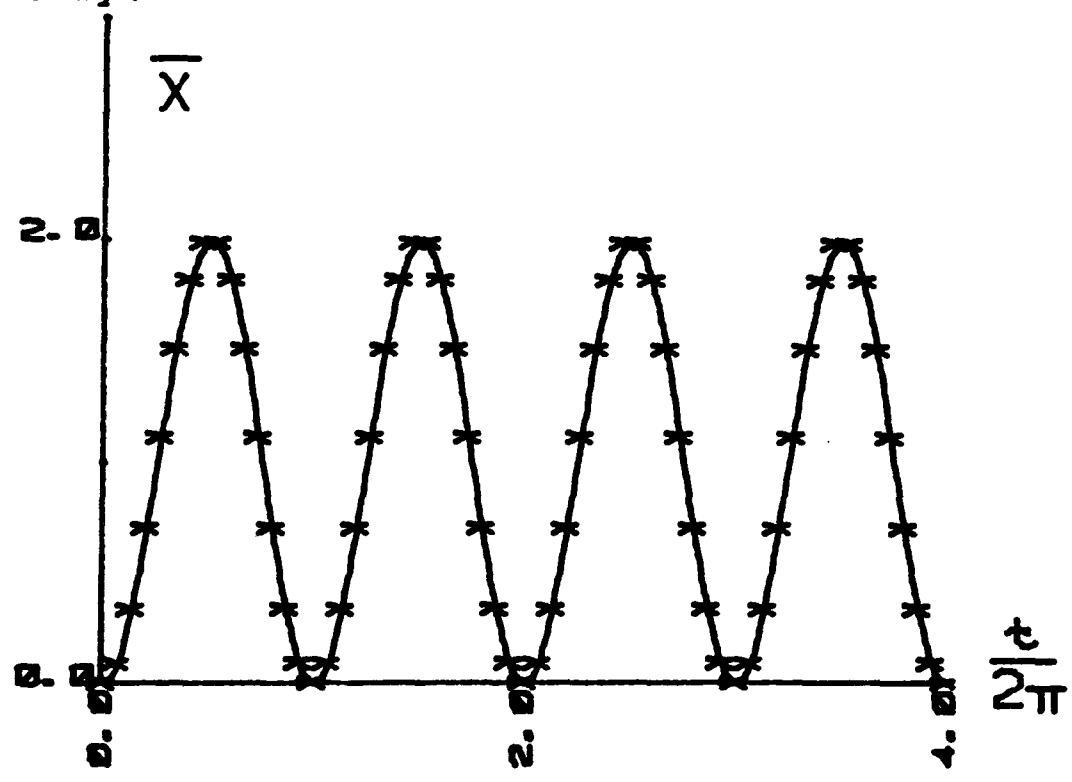

Numerical (solid line) and analytical (crosses) predictions for the plot of $\bar{X}$ versus $\frac{\tau}{2\pi}$. The amplitude of the oscillations is 2s and the period is equal to that of the pump.

Figure 5.1

5.2.3 Discussion Of Plots Of Variance Versus Time

Examples of the variance versus time plots are shown in figure 5.2 for six conditions

(1) Re = 10. $St = 1 \times 10^{-2}$

(2) Re = 100. $St = 2 \times 10^{-2}$

(3) Re = 10. $St = 2 \times 10^{-2}$

(4) Re = 2.5 $St = 2 \times 10^{-2}$

(5) Re = 2.5 $St = 5 \times 10^{-2}$

(6) Re = 0.4 St = 0.125

These predictions are compared with the approximate analytical values in chapter 3. The plots generally take the form of large oscillations superimposed upon a much less significant linear rise with time. The amplitude and the frequency of the oscillatory component of the variance plots can be seen to vary with time. The amplitude of the oscillations decays with time to a finite value. The frequency of the oscillations is initially equal to that of the pump, but as the simulation progresses, a secondary oscillation 180 degrees out of phase with the primary grows until the two sets of peaks appear to be an oscillation of frequency 2f. The plots of concentration variance for dispersion in an oscillatory flow produced by Smith (216) also show this trend, but the effect was not discussed in detail.

Let us consider the amplitude of the oscillations of the variance plots during the first period. At $\tau = 0$, the slug is completely undisturbed but the variance is not zero. In fact the

initial variance is $\frac{1}{3} x_0^2$. If we define the height of the first peak on the variance plot as the vertical distance 'a' between the top of the first peak and the level of the linear rise then we may plot the ratio of 'a' to the initial variance on a 3-D logarithmic plot against Reynolds number and Strouhal number. This ratio is determined by convective effects alone since it is the velocity shear which leads to the peaks on the variance plot. Note that the effect of diffusion will be small during the first cycle and by measuring the distance of the peak from the linear (dispersive) rise we are subtracting off the small diffusive contribution to the variance. Plotting out this graph† in figure 5.3 using the numerical predictions gives a form which we may explain using intuitive arguements. The dominant feature is the behaviour as s^2. This is expected since, for a given velocity profile (and therefore for a given frequency), the distance to which the slug is deformed is proportional to the stroke. On dimensional grounds we suppose that the variance is proportional to the slug deformation distance squared and this explains the stroke dependence. Thus the stroke and frequency affect the surface by quite distinct mechanisms. For

† Throughout this chapter a logarithmic three dimensional plot will be used to illustrate the dependence of a particular parameter (plotted on the z-axis) upon the Reynolds number and the Strouhal number (plotted on the base plane). This graph is drawn in the isometric system. To take a reading from the plot, firstly locate the Reynolds number and Strouhal number on the base plane. The z-value will be obtained by drawing a vertical line upward to the curve and measuring its length. The ends of each axis are labelled as the log (to base 10) of the quantity so that a value of "2" on the "Re" axis implies a Reynolds number of 100.

values of α^2 below the critical value of about 1, the frequency does not affect the velocity profile so lines of constant St show little variation of level for changes in Re. As one increases the frequency into the regime of transitional α^2, so the velocity profile will tend towards the plug form. The velocity will therefore cease to have such a large effect in bowing out the slug and the variance will be consequently reduced. Indeed, in the plug flow limit of infinite frequency, the velocity will only serve to shift the slug bodily down the channel and there will be no initial change in variance due to convective effects. This trend is also observed on the plot shown in figure 5.3 where the large frequency case of large St and large Re shows a very marked dip. In fact the line $\alpha = 1$ seems to separate the two regimes of frequency variation quite precisely.

As the dispersion process acts in smoothing out the slug, so the size of the peaks on the variance plots caused by a temporary convective bowing out of the contaminated fluid will become smaller. This is due to the gradual effect of diffusion in smoothing out the axial concentration non-uniformity.

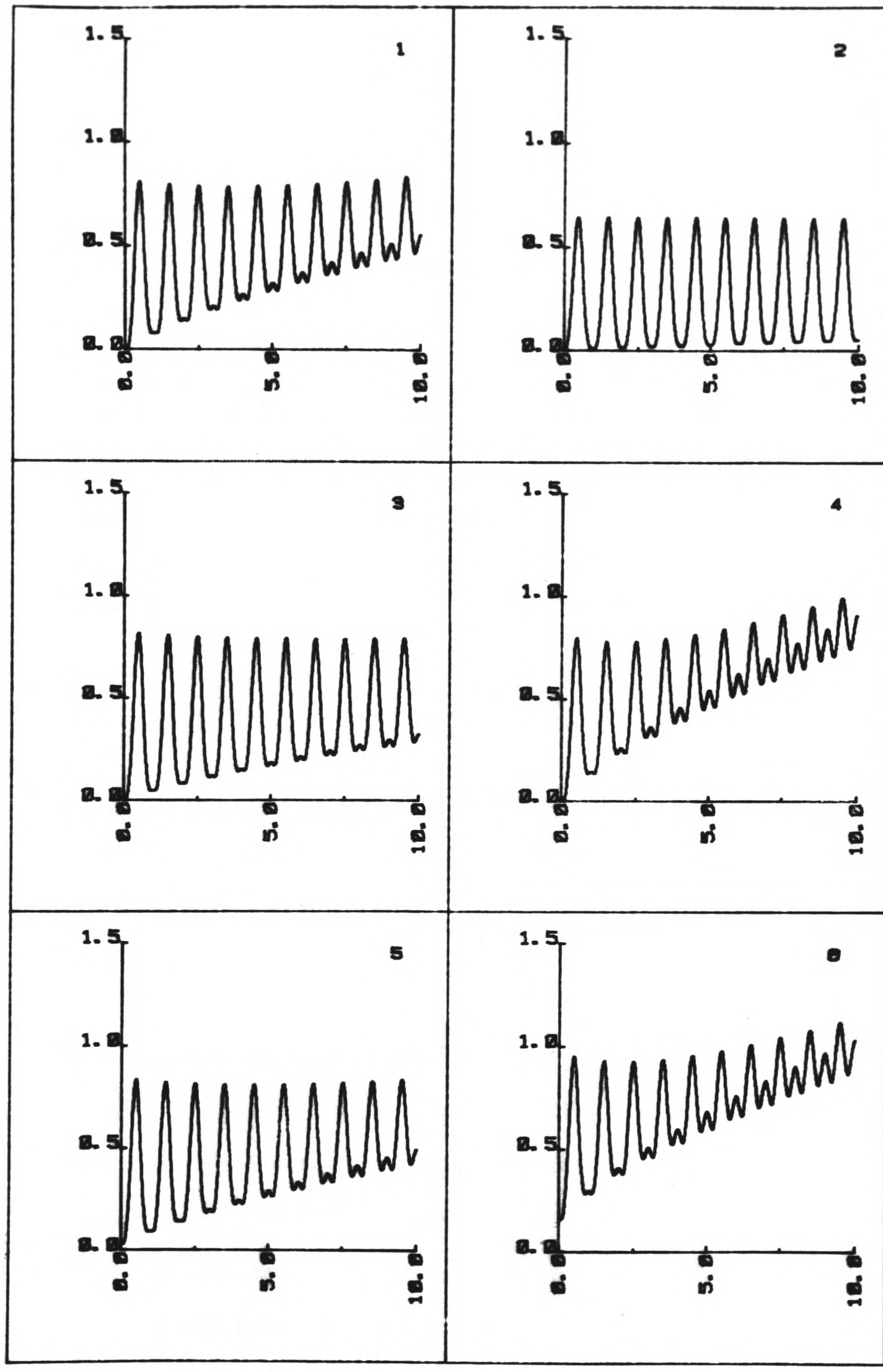

Plots of σ^2 St^2 against $\frac{\tau}{2\pi}$ (see text for conditions)

Figure 5.2

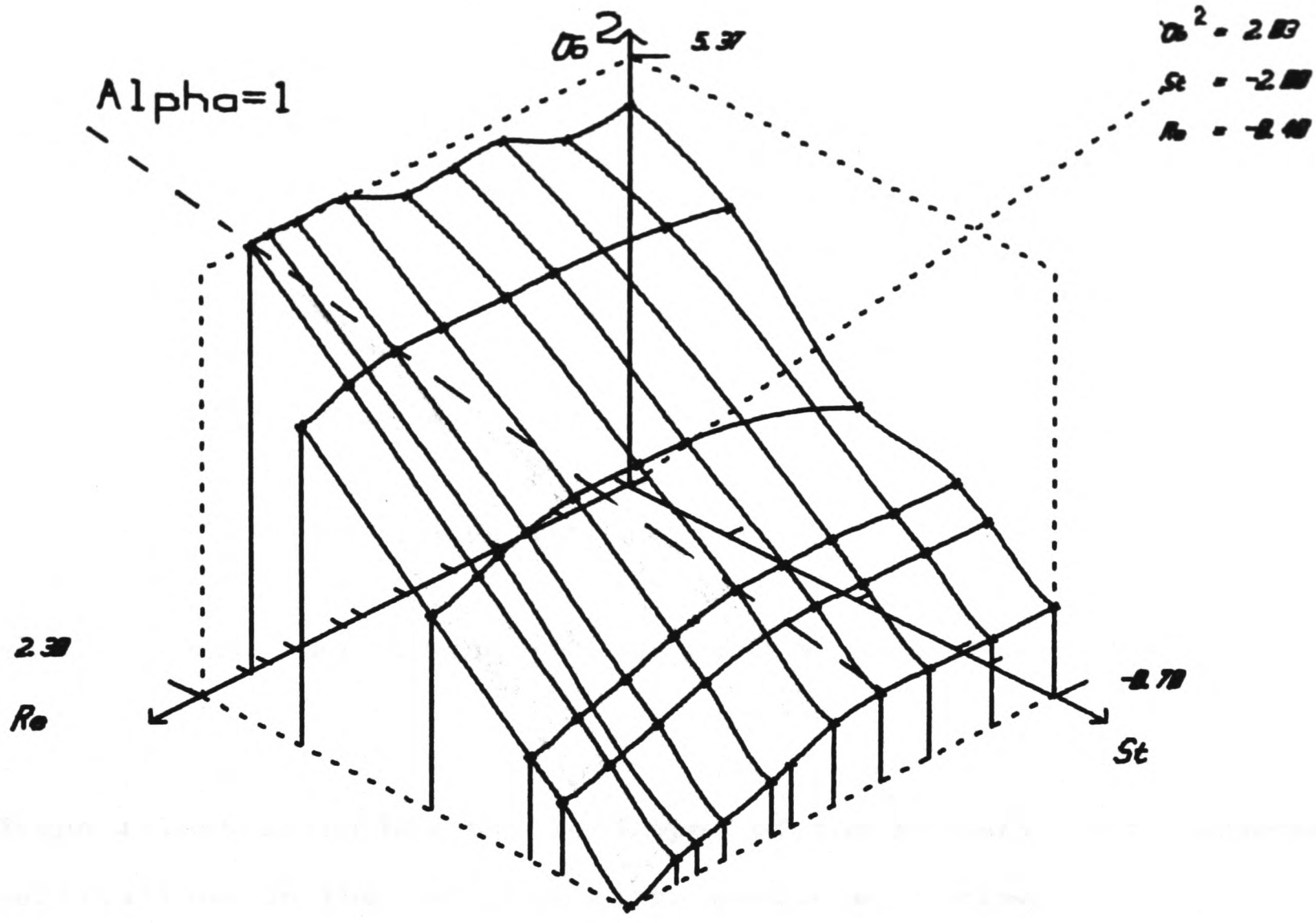

Three dimensional plot on logarithmic axes showing the dependence of the initial height of the variance peaks (in dimensionless form) on the Reynolds number and the Strouhal number

Figure 5.3

An unusual feature is exhibited by the form of the oscillations upon the variance-time graphs. The peaks which were initially observed, decayed with time to some steady height; these will be termed the primary oscillations. In addition to these oscillations, a second set of peaks, 180 degrees out of phase with the primary set, grew from zero amplitude until the two sets become indistinguishable from a single oscillation of double the frequency. The form of the envelopes of the two sets of peaks is sketched in figure 5.4.

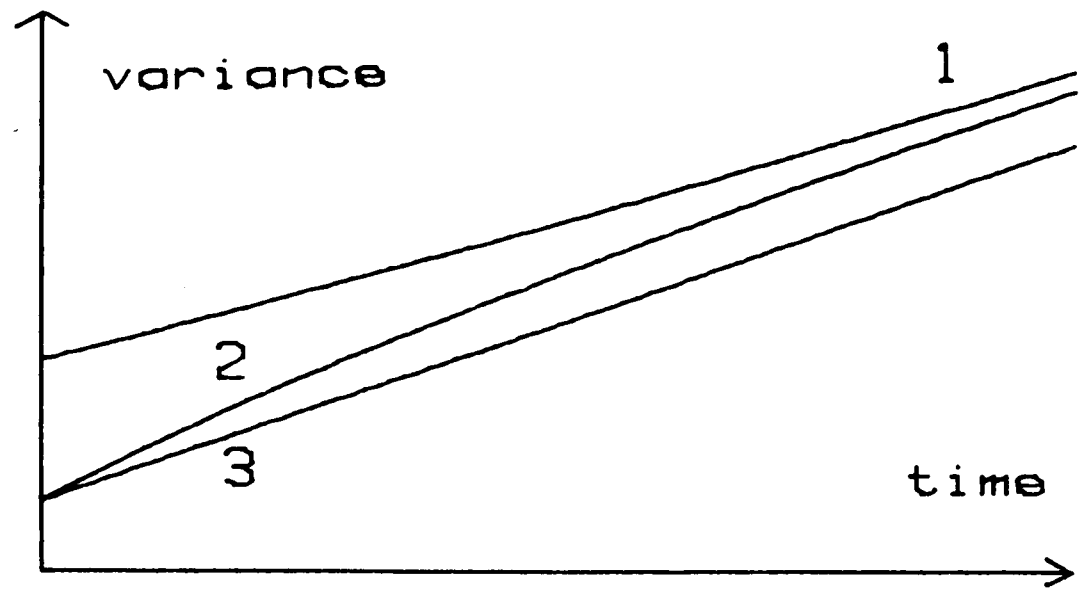

1) maximum of primary

2) maximum of secondary

3) minimum of primary and secondary

Graph illustrating how the envelopes of the primary and secondary oscillations on the variance plots evolve with time.

Figure 5.4

Let us consider the effect of the starting phase angle of the velocity upon these convectively created peaks. When the pump starts by delivering zero velocity at $\tau = 0$, in each cycle we would expect only a single peak upon the variance plot (see figure 5.16.6). This is because at $\tau=\pi$ in the cycle the slug is bowed out to its maximum extent and hence the variance exhibits a maximum. In the second half of the cycle the variance falls down to its initial level as the backward velocity pushes it up the channel gradually reversing the distorting effects of the shear in the first half. In fact there is also a small net increase in the variance over the course of a whole cycle due to diffusive effects spreading the slug out. Thus the oscillations upon the variance-time plots are of a frequency equal to that of the pump. Now let us compare this result with the one which would be observed

when the pump delivers its maximum velocity at $\tau = 0$ (i.e. the injection of the slug takes place $\frac{\pi}{2}$ later on in the period) (see figure 5.16.11). This is a circumstance which is not easily set up experimentally due to the difficulty in creating a slug of controlled size in a moving stream. Nevertheless, this is in a sense a more natural starting condition since the velocity now reverses at the $\tau=\frac{\pi}{2}$ point, pushes the slug back to its starting position at $\tau=\pi$, and for the final half of the cycle it bows the slug out onto the negative side of the origin. The "asymmetric" starting condition bows the slug out twice as far from the origin but only on one side of it.

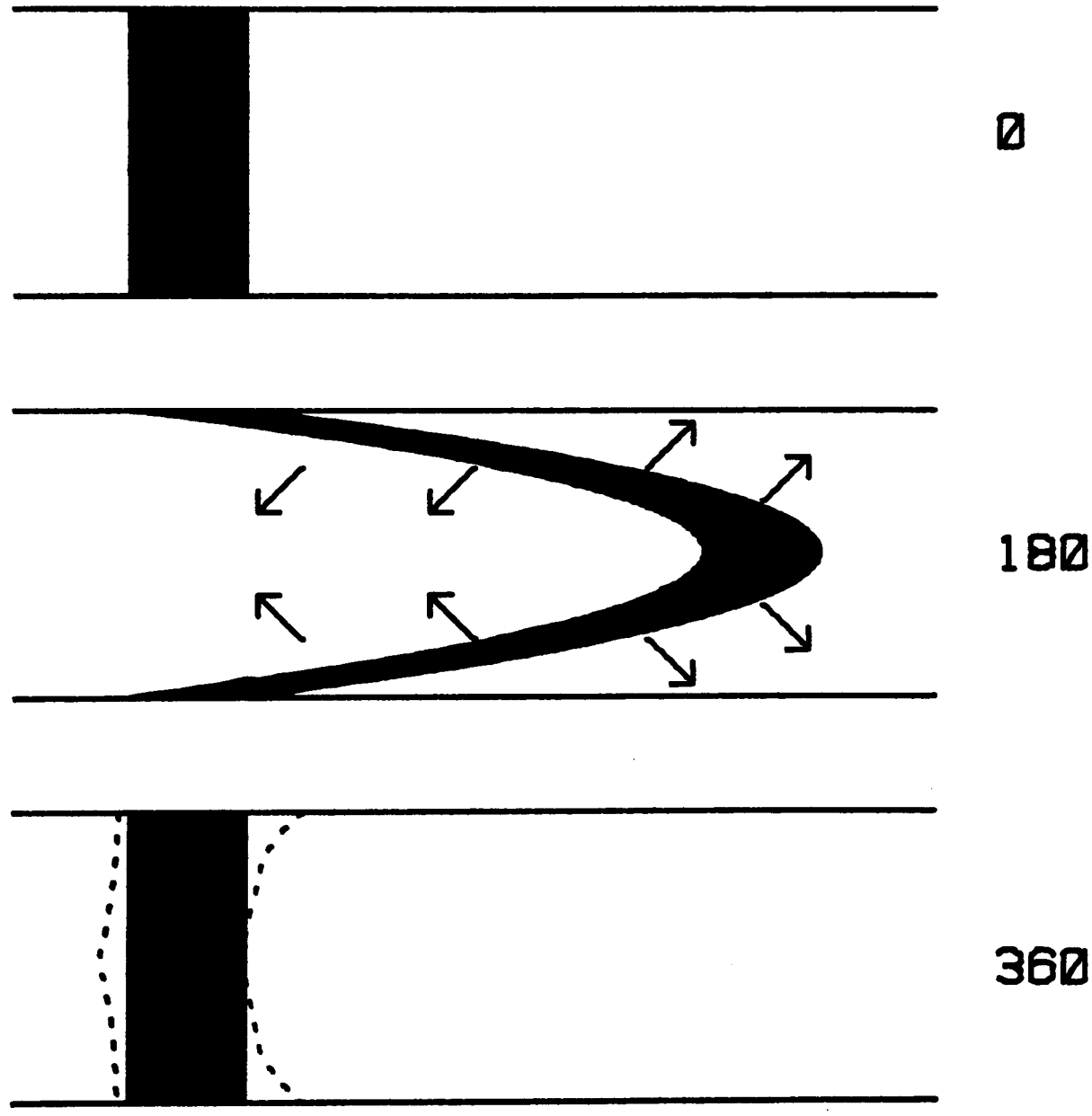

Exaggerated illustration of the slug form at the 0, 180, 360 degree positions in the dispersion evolution. The arrows illustrate the direction in which the local mass diffusion from the slug occurs.

Figure 5.5

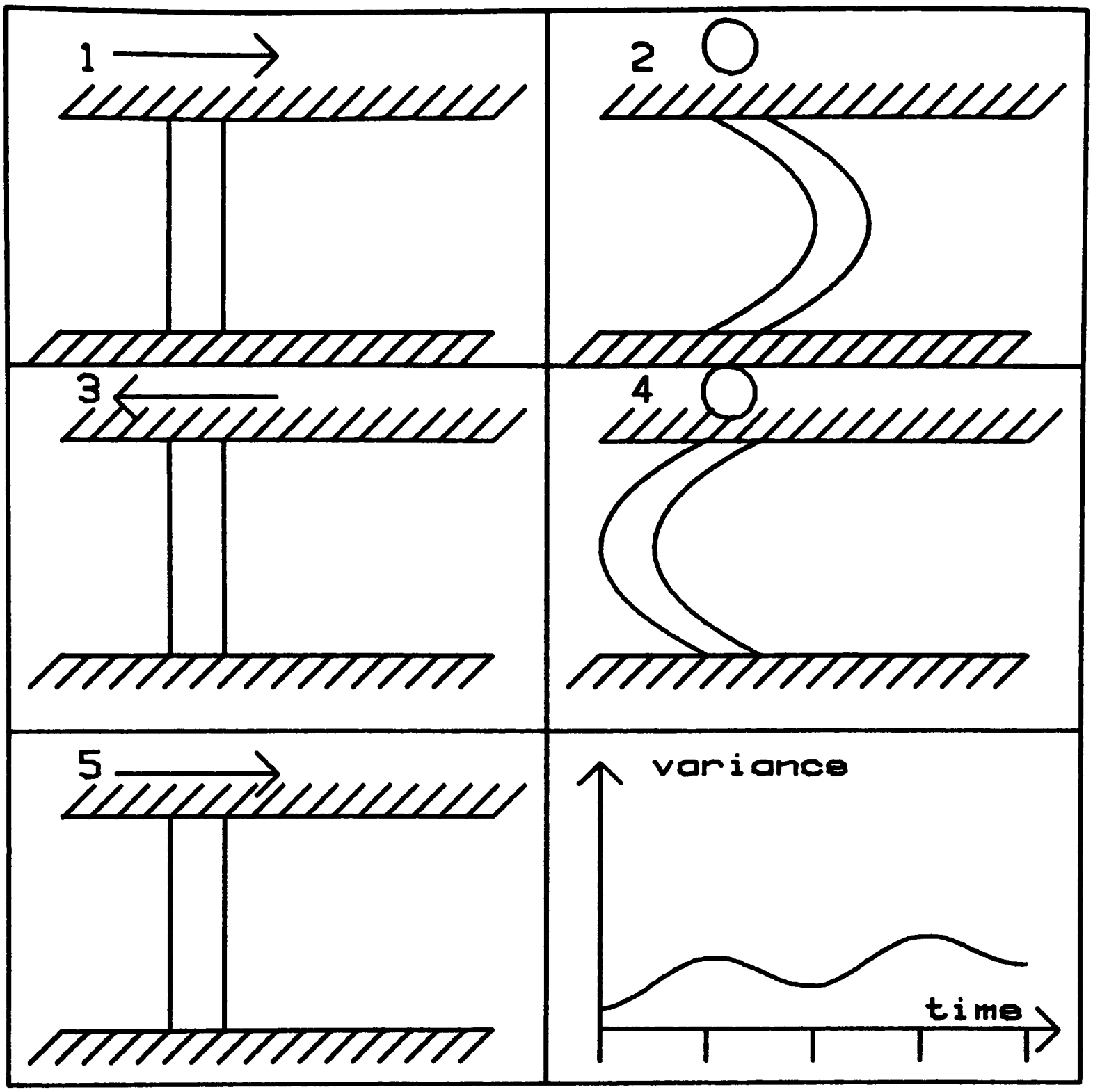

Illustration of the relation between the slug position and its variance during the first cycle when the bulk fluid velocity is a maximum at the instant of injection. The slug shape is sketched for the 0, 90, 180, 270 and 360 degree positions. The symbols above the curve indicate the direction of the instantaneous bulk velocity and the sixth curve shows the resulting variance versus time plot.

Figure 5.6

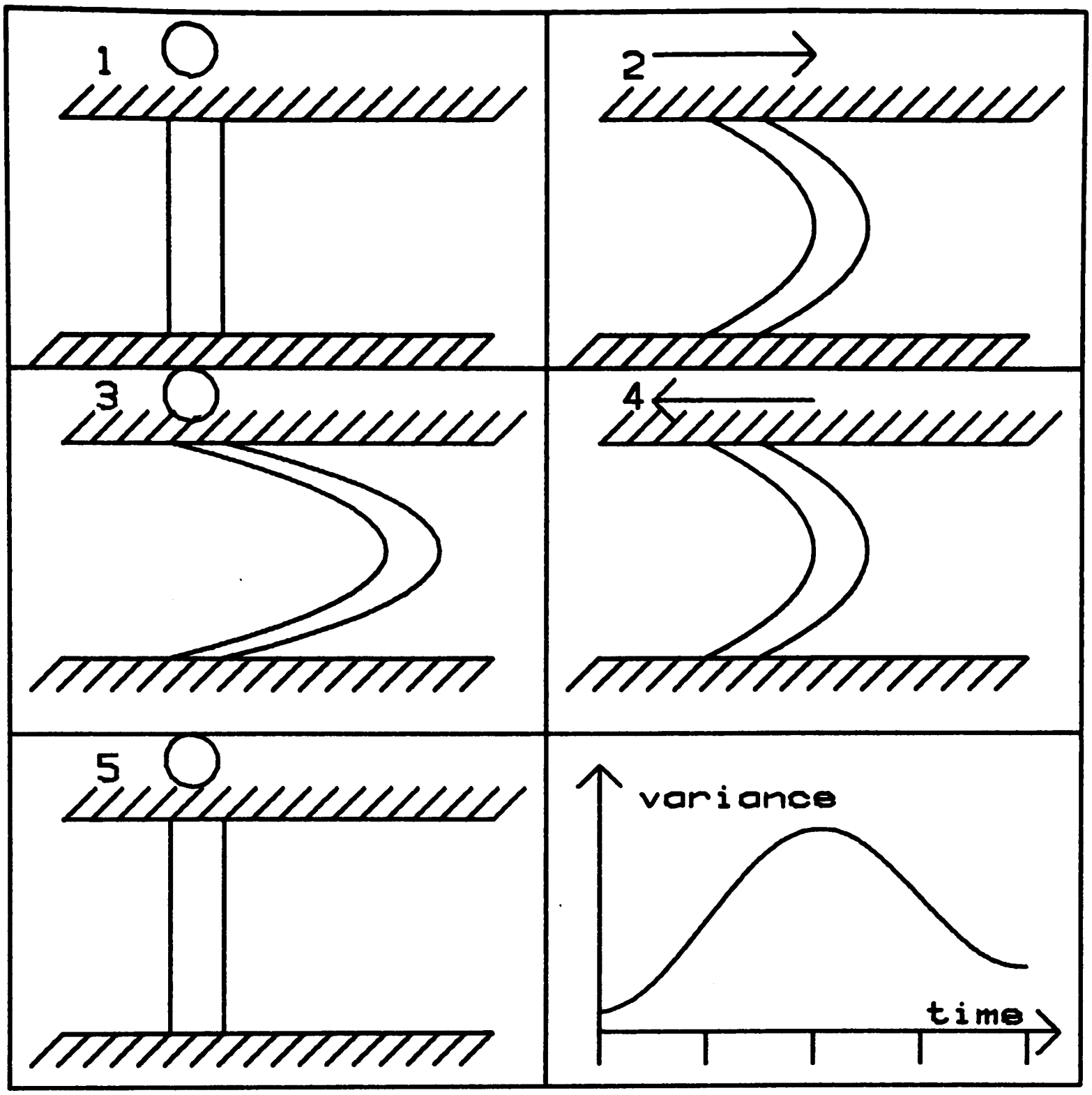

Illustration of the relation between the slug position and its variance during the first cycle when the bulk fluid velocity is zero at the instant of injection. The slug shape is sketched for the 0, 90, 180, 270 and 360 degree positions. The symbols above the curve indicate the direction of the instantaneous bulk velocity and the sixth curve shows the resulting variance versus time plot.

Figure 5.7

The peaks in axial variance of the concentration distribution within the channel therefore occur at twice the pump frequency because the slug is bowed out twice (once on each side of the origin) during each pump period. This prompts one to wonder if the variance plot shows different oscillations even in the limit of large time, depending upon the initial velocity phase angle. It would certainly be very surprising if this were the case since the effect of diffusion is to slowly smooth out concentration non-uniformities and to therefore gradually erode the effects of the concentration distribution at earlier times†. The only alternative to this explanation is that one of the forms tends towards the other for increasing time. The growth of these secondary peaks is caused by the asymmetrical spreading due to the slug centre only entering one half of the channel. If we consider the leading and trailing edges of the slug, then it is apparent that the diffusion of contaminant out of the leading edge must always imply movement towards the nearest wall. On the other hand, diffusion out of the concave back end of the bowed out slug leads to a drift of marked molecules towards the channel centre-line. This process will tend to change the shape of the dye slug so that at the end of the period it will not lie symmetrically about the origin, although its centre of gravity must lie on the origin for slugs which were initially transversely uniform. During the early stages of the dispersion, this effect will not drastically change the shape of the end-of-cycle concentration distribution, but as τ $\uparrow$

This was a feature of the dispersion process which Smith attempted to model in the delay-diffusion equation by supposing that the concentrations in the channel were determined by a fading "memory" of the earlier levels.

increases and the slug becomes more and more dilute and distorted, so the appearance of the concentration distribution resembles that which one might more readily associate with the zero fluid acceleration starting condition. At the end of each period the diluted slug tends to take on a paraboloidal shape when the flow is at rest; this is characteristic of the symmetrical starting condition. At this stage, the contaminant may be so dilute that during the course of a period, the movement of the slug of dye may be almost indiscernible by eye. Studies of the effect of varying the synchronization of the slug injection and the bulk velocity sinusoid have been investigated by Allen (2) (her figure 8). The observations described above were not detected in Allen's numerical study. It is possible that the reason for this is that the oscillatory Peclet number (α^2 Sc) was so small (i.e. the frequencies were small as they should be for the tidal simulation being considered) that the time taken for the system to reach the stage at which the primary and secondary oscillation amplitudes were equal, was less than one period. This would mean that the system had already stabilized before the first secondary peak had appeared.

Measurements taken from the numerically obtained variance plots have been used to 'empirically' describe the gradual growth of the secondary oscillation peaks. The results of this study are shown in table 5.1 which gives the number of cycles ($n_{0.25}$, $n_{0.5}$) taken for the amplitude of the secondary oscillations to reach $\frac{1}{4}$ and $\frac{1}{2}$ of the primary value at that time. The ratio (expressed as a percentage) of the secondary to primary amplitude (%5) during the fifth period is also shown.

Re	α^2	St	$n_{0.25}$	$n_{0.5}$	%5
0.4	0.004	0.010	0	0	c100
1.0	0.010	0.010	1	2	c100
2.5	0.025	0.010	3	5	55
5.0	0.050	0.010	5	8-9	24
10.0	0.100	0.010	10	17	9
25.0	0.250	0.010	>14	>14	3.5
50.0	0.500	0.010	>10	>10	1.3
>75.0	>0.750	0.010	>10	>10	c 0
0.4	0.008	0.020	0	1	c100
1.0	0.020	0.020	2	4	63
5.0	0.100	0.020	10	>10	10
10.0	0.200	0.020	>10	>10	3.5
>20.0	>0.400	0.020	>10	>10	c 0
0.4	0.020	0.050	1	3	76
0.5	0.025	0.050	2-3	5	63

continued overleaf

Re	α^2	St	$n_{0.25}$	$n_{0.5}$	%5
1.0	0.050	0.050	5	8→9	23
2.0	0.100	0.050	10	17	5.8
2.5	0.125	0.050	13	>17	4.5
5.0	0.250	0.050	>17	>17	3.7
>10.0	>0.500	0.050	>17	>17	c 0
0.4	0.04	0.100	4	7	32
1.0	0.10	0.100	10	>10	10
1.25	0.125	0.100	11→12	21	9.2
2.5	0.250	0.100	25	>25	c 0
>5.0	>0.500	0.100	>25	>25	c 0
0.4	0.05	0.125	5	9	24
1.0	0.125	0.125	>12	>12	5.4
2.5	0.3125	0.125	>12	>12	1.7
>5.0	>0.625	0.125	>12	>12	c 0
0.4	0.08	0.200	7	>10	16.6
1.0	0.20	0.200	>10	>10	5
>2.5	>0.50	0.200	>10	>10	c 0

Table 5.1

The results shown in table 5.1 indicate that the growth of the secondary oscillations obeys the following empirical equation:

$$\hat{n} = 0.4\ g\ \alpha^2\ Sc, \qquad (5\text{-}3)$$

where we define $\hat{n}$ as the number of cycles taken for the amplitude of the secondary oscillations to be a fraction g of the amplitude of the primary oscillations. The group $\alpha^2 Sc$ is an oscillatory Pelcet number (Po) and its importance to dispersion in oscillatory flows has been decribed by Holley, Harleman and Fischer (121). In essence Po determines the degree of quasi-steadiness of the concentration field.

5.2.4 Discussion Of The Rate Of Growth Of The Variance Plots

The time derivative of the variance plots described in section 5.2.3 tends to exaggerate the oscillations. For all Strouhal numbers less than 0.2, the oscillations upon the variance plots were larger than the linear rise over a cycle. However, for Strouhal numbers in the range $10^{-2} \rightarrow 0.2$, the oscillations on all the rate of growth of variance plots were consistently completely dominant, the linear rise term being barely detectable. As described in chapter 4, the dispersion coefficient may be calculated from the rate of growth of the variance plots. Figure 5.8 shows a 3-D plot of dispersion coefficient against Reynolds number and Strouhal number on logarithmic axes. Similar plots are displayed in figures 5.9, 5.10 and 5.11 showing the results obtained from the analytical predictions given in chapter 3. Watson (256) and Chatwin (155) have developed theoretical predictions for the dispersion coefficient of oscillatory flows in unform ducts. Their technique was to suppose that $\frac{\partial C}{\partial x}$=constant and

to then obtain an expression for $\overline{UC}$ in terms of $\bar{U},\bar{C}$. In figure 5.12 we show a 3-D plot of the Chatwin-Watson dispersion coefficient predictions which were calculated using a flat channel analysis given by Watson. All of the results shown on the 3-D plots are combined to form six 2-D plots in figure 5.13. These graphs show the variation of D with log(Re) for Strouhal numbers in the range 0.01→0.2. As was shown in chapter 3, the frequency dependence of the dispersion coefficient at the large Schmidt numbers which are applicable to this study, is mainly due to changes in the velocity profile. The data calculated from the analytical work in chapter 3 are reasonably accurate for low frequencies where the velocity profile is approximately parabolic in γ. For large frequencies the velocity profile is more plug-like and the dispersion coefficient is consequently much higher. This feature is not exhibited by the analytical results which are not applicable to this regime. The numerical points and those calculated using the Chatwin-Watson approach agree very well. All of the 3-D plots indicate that the dispersion coefficient varies predominantly as stroke squared, and that the frequency dependence is much less marked.

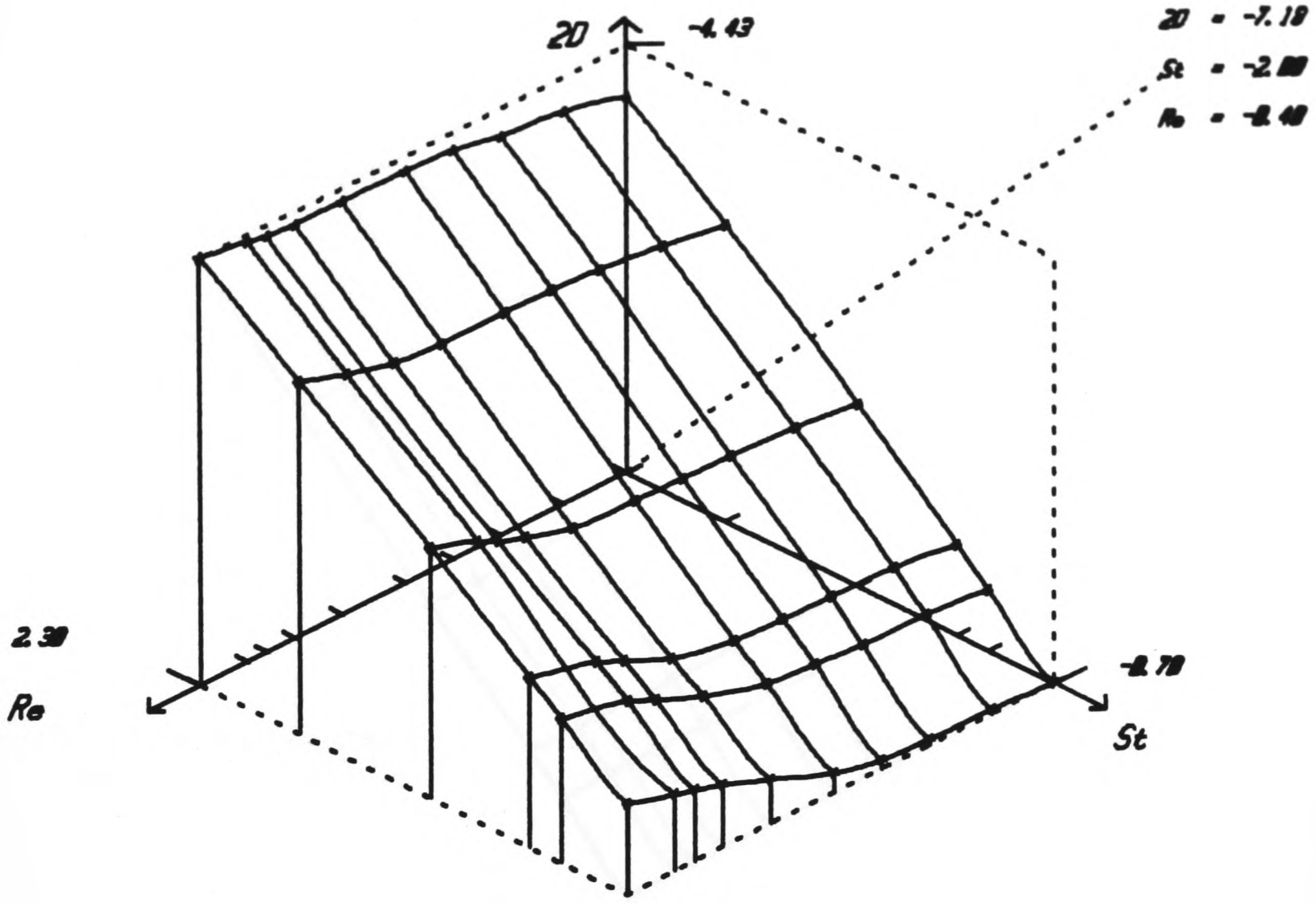

Three dimensional plot on logarithmic axes of the numerically predicted value of 2D against Reynolds number and Strouhal number for a Schmidt number of 10^3.

Figure 5.8

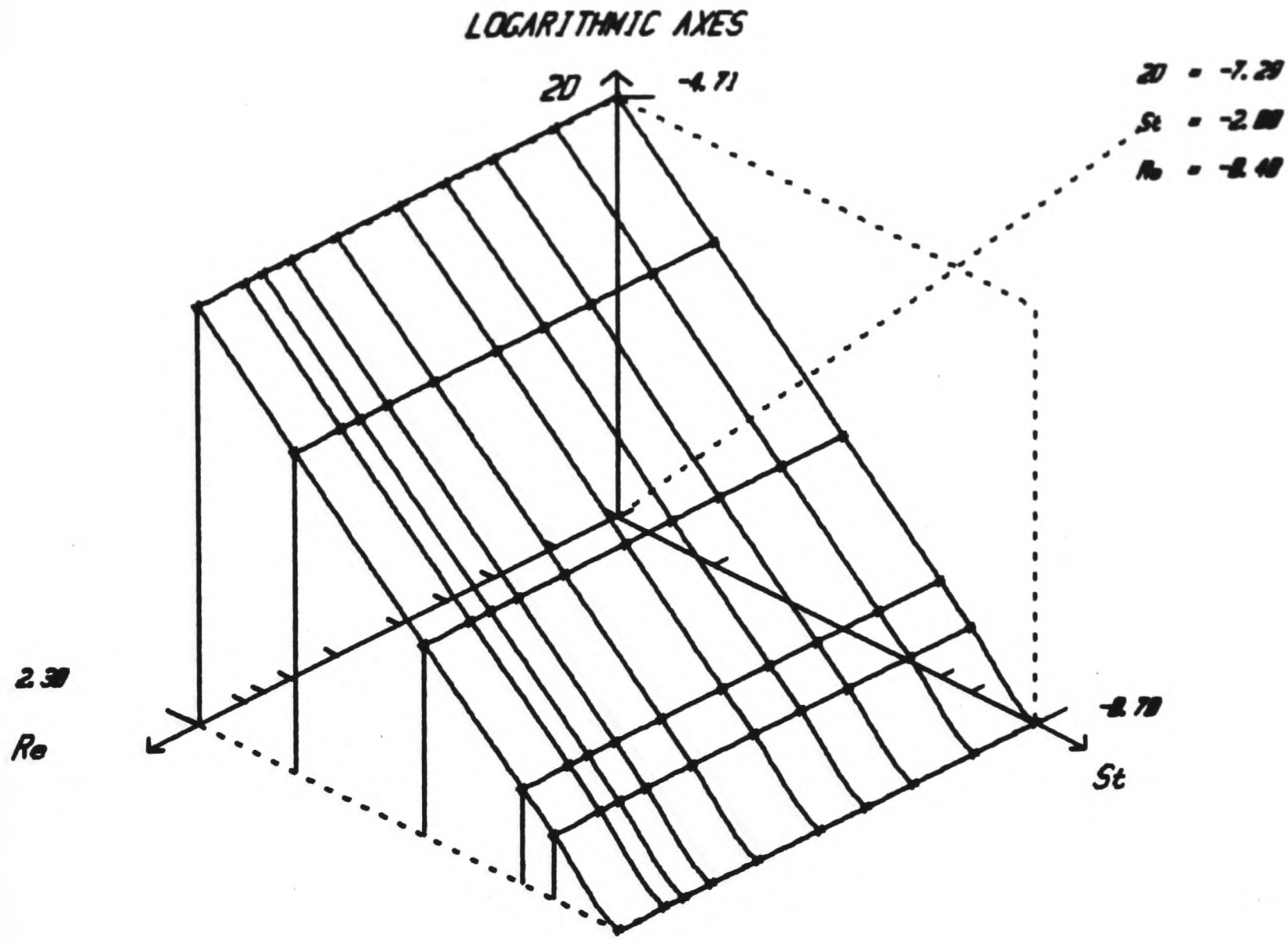

Three dimensional plot on logarithmic axes of 2D calculated using the methods described in chapter 3 (parabolic velocity profile and two term expression for the wall concentration) against Reynolds number and Strouhal number for a Schmidt number of 10^3.

Figure 5.9

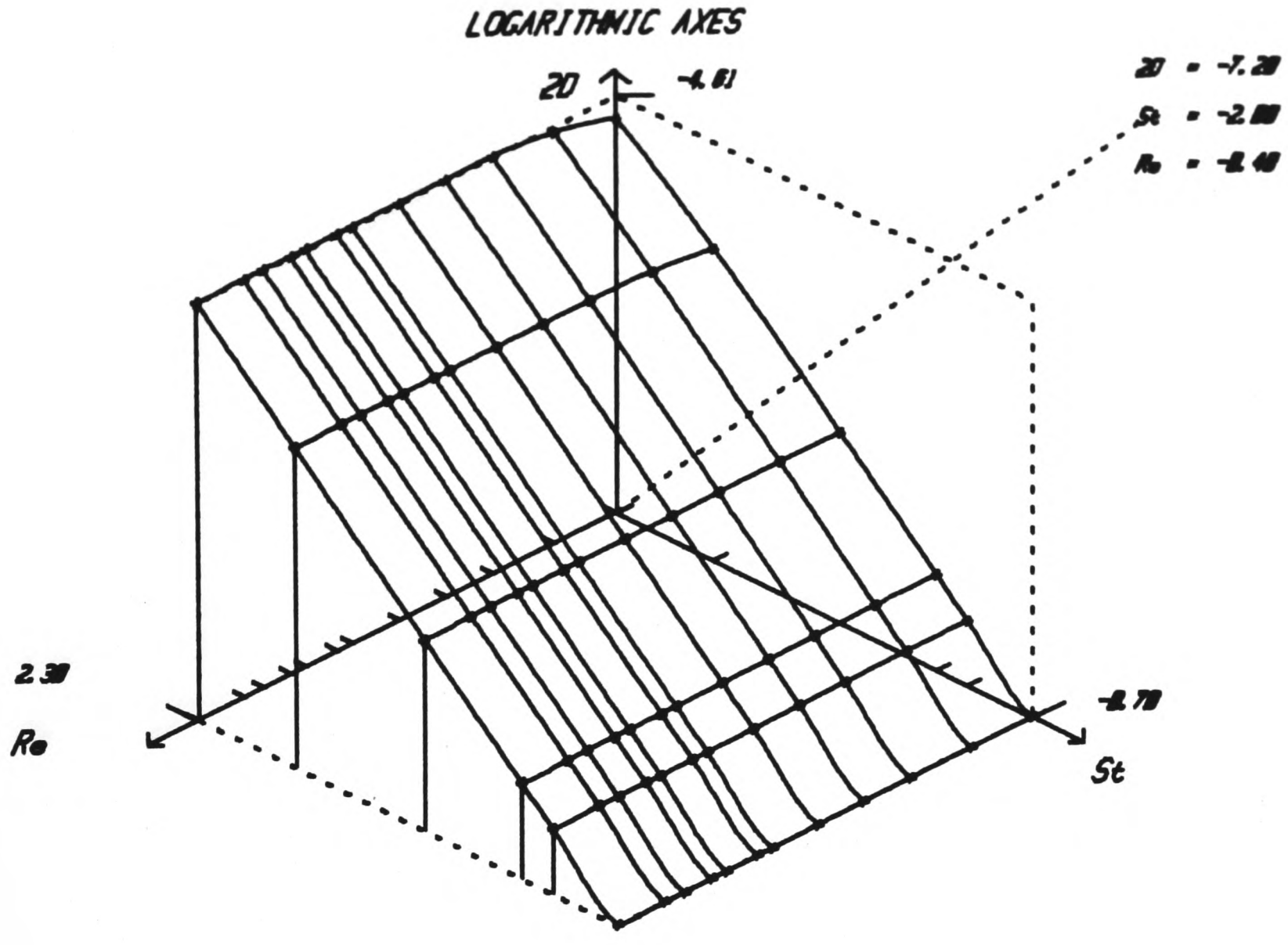

Three dimensional plot on logarithmic axes of 2D calculated using the methods described in chapter 3 (parabolic velocity profile and three term expression for the wall concentration) against Reynolds number and Strouhal number for a Schmidt number of 10^3.

Figure 5.10

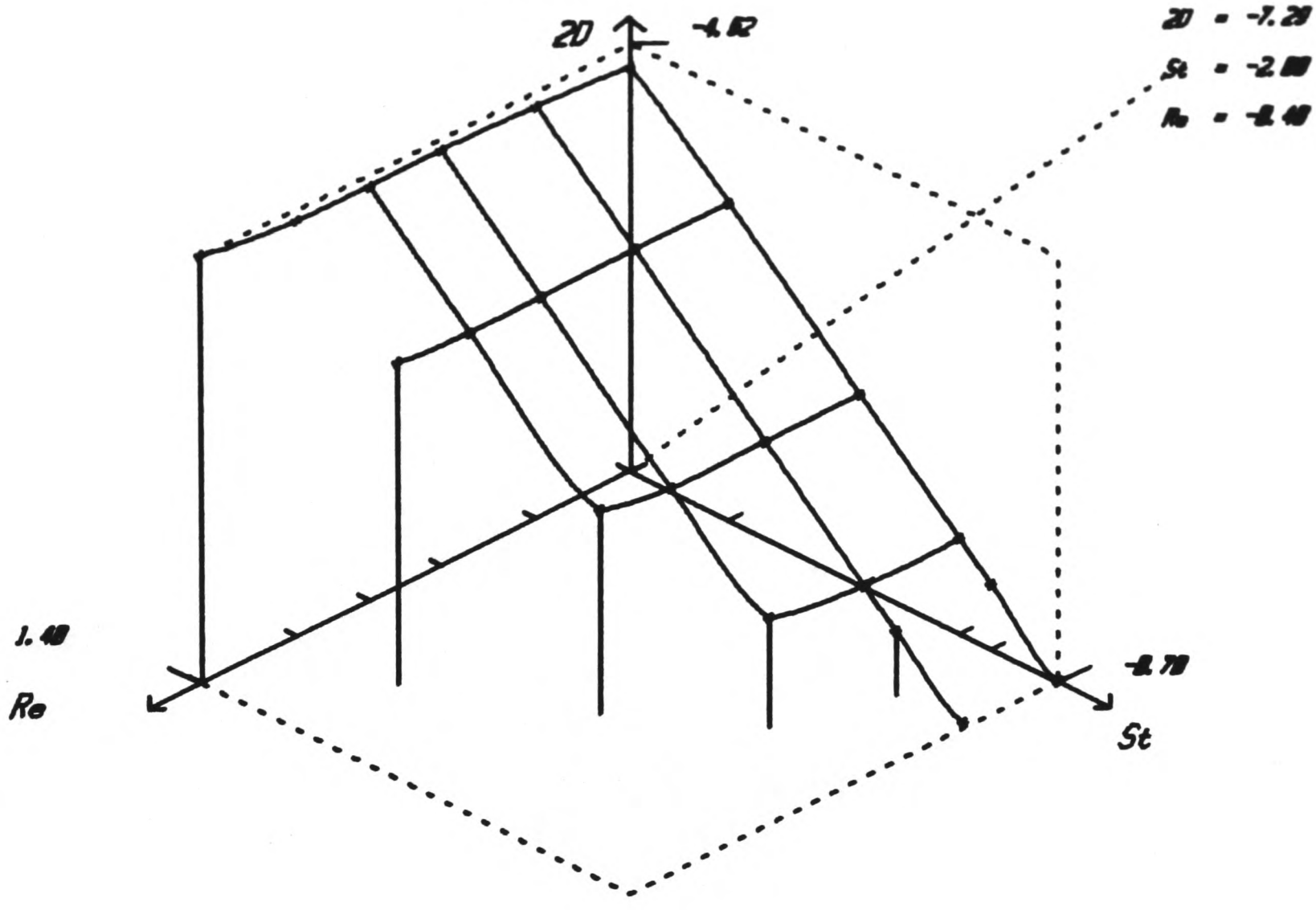

Three dimensional plot on logarithmic axes of 2D calculated using the methods described in chapter 3 (quartic velocity profile and two term expression for the wall concentration) against Reynolds number and Strouhal number for a Schmidt number of 10^3.

Figure 5.11

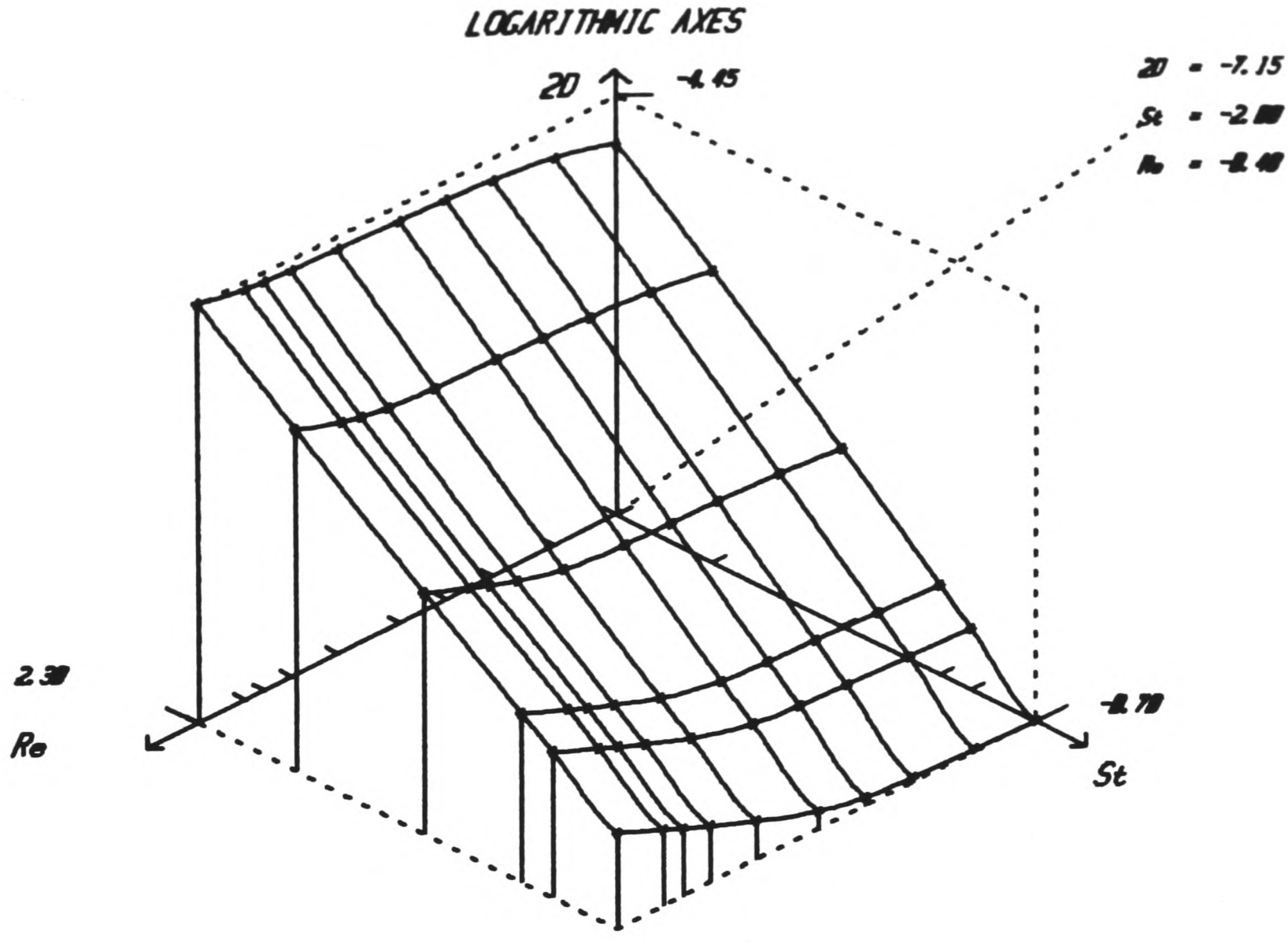

Three dimensional plot on logarithmic axes of 2D (based upon the theory of Watson (256)) against Reynolds number and Strouhal number for a Schmidt number of 10^3.

Figure 5.12

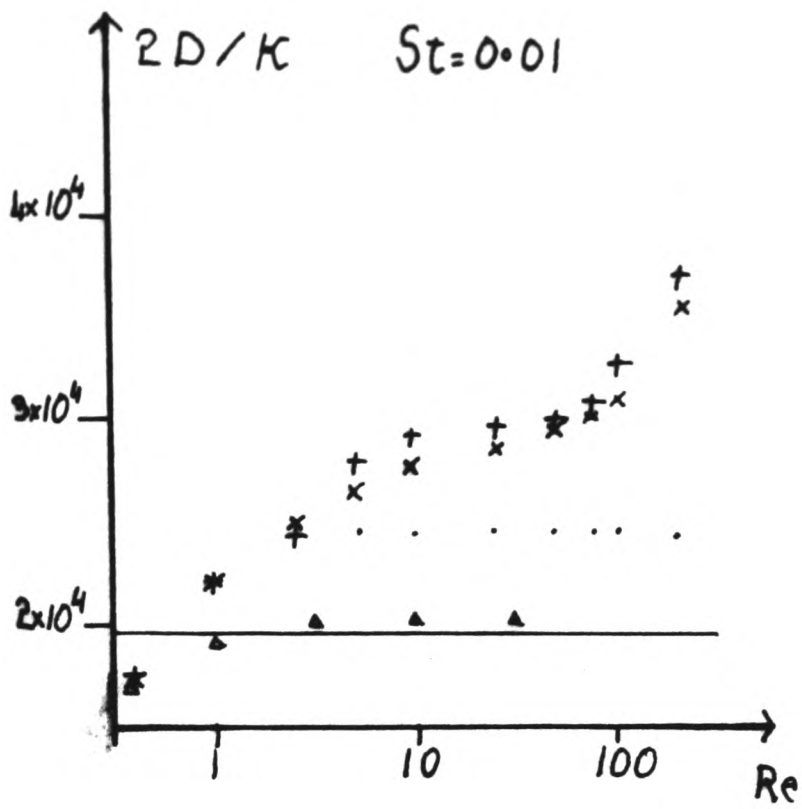

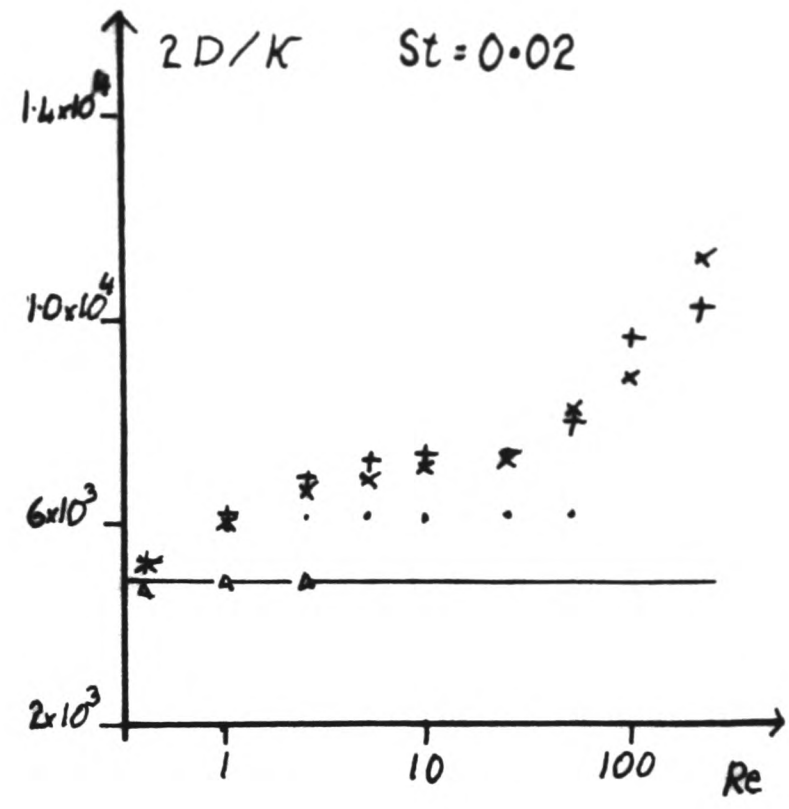

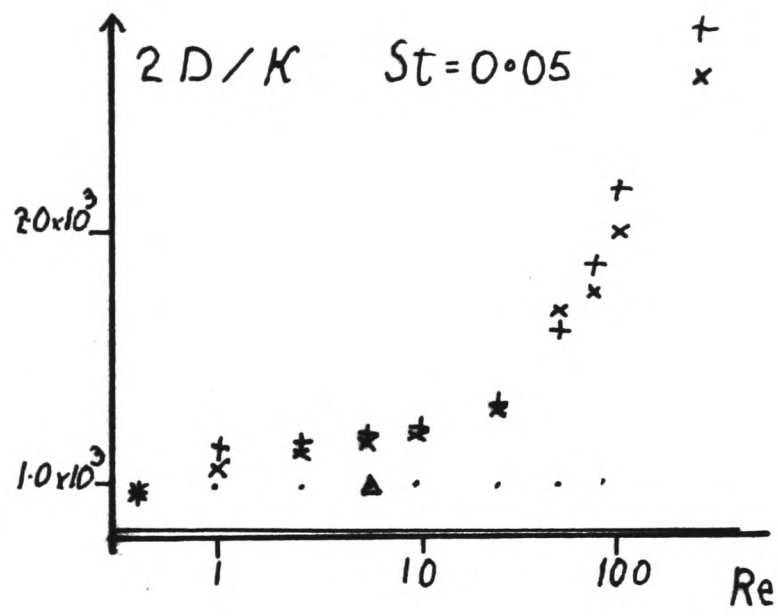

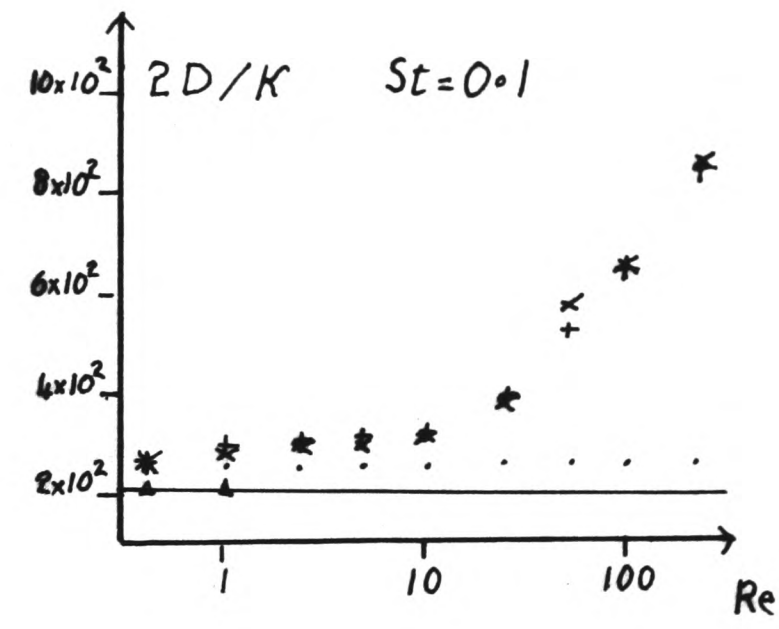

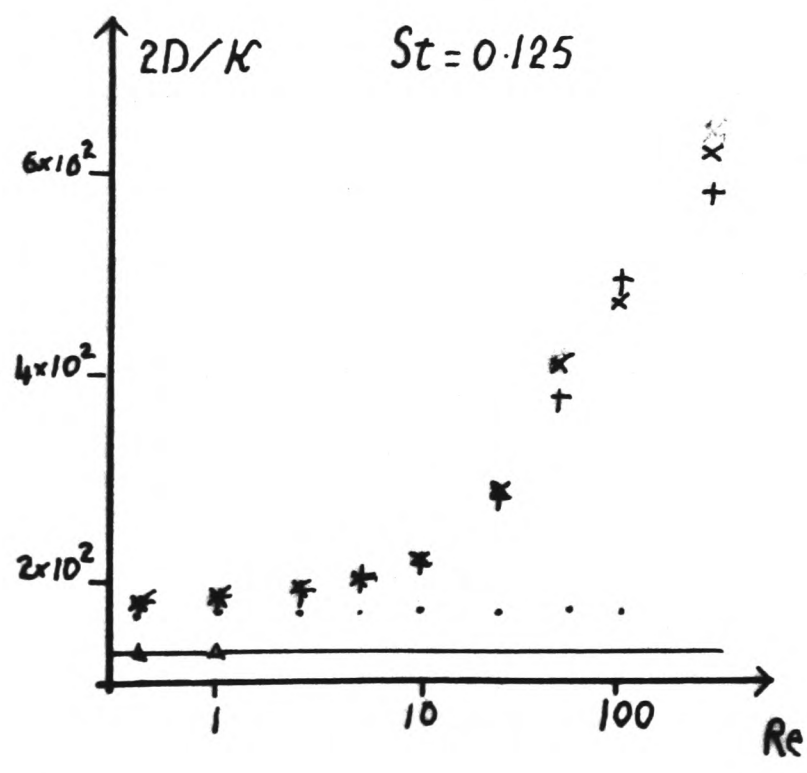

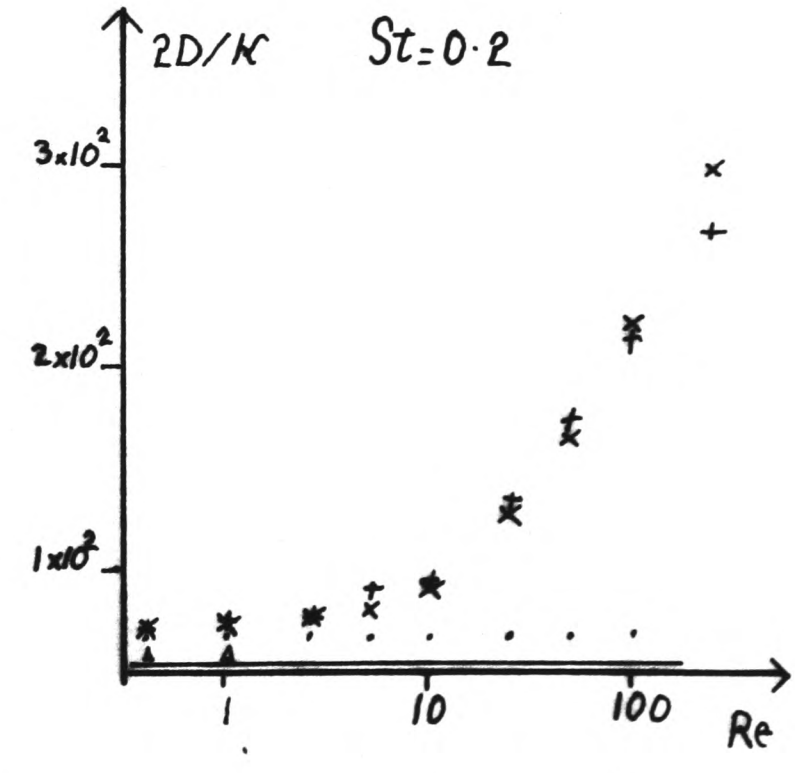

× Watson Analysis + Numerical — Parabolic Moment

Δ Quartic Moment . 3 Terms in Moment Series

Plot of 2D/κ against log(Re)

Figure 5.13

5.2.5 Time Dependence Of The Dispersion Coefficient

One striking feature of the plots of cycle-averaged $\frac{\partial \sigma^2}{\partial t}$ versus time has been the very constant level even through times much less than that formally required for the Taylor state to be developed. This implies that although the concentration distribution may not have reached the Gaussian stage, the rate of growth of the time averaged variance is relatively constant. Over a limited number of cycles, the shape of the dispersion coefficient versus time plot showed different behaviour. For values of α^2 greater than 10 (i.e for plug-type flow), D increased with time. For α^2 less than 10 but greater than 0.4, the level decreased with time; at α^2 approximately equal to 10, the mean growth rate of the variance was very constant but did form a weak maximum. For α^2 less than 0.4, a minimum in the D versus time plot was observed. This regime corresponds to a parabolic velocity profile.

5.2.6 Observations Of The Time Evolution Of The Skewness Plots

Examples of the skewness versus time plots are shown in figure 5.14 for the six variance conditions (see above). In the limit of large time, the skewness tends to zero and carries no oscillations although, transiently, quite large peaks may be seen on the plots. The envelope of the oscillations consists of a relatively sharp rise followed by a very gradual fall down to the time axis. The base level upon which these oscillations are superimposed also rises to a peak and then drifts down to touch the time axis, although this state is reached much more quickly than the peak level decay described above. Generally, the larger α^2, the more cycles are necessary for this description to be applicable. The shape of the peaks also evolves with time in a complex way.

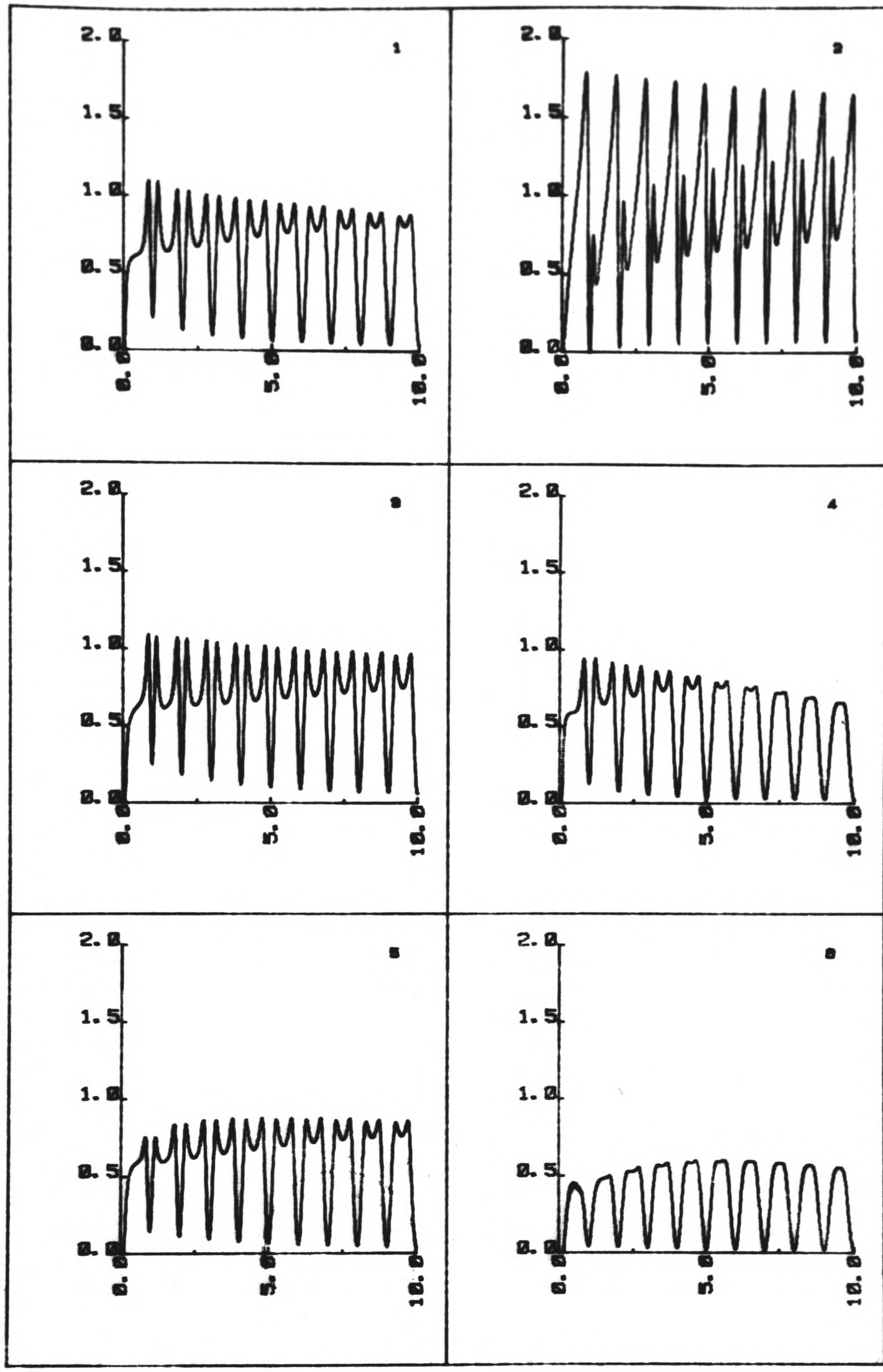

Plots of skewness against $\frac{\tau}{2\pi}$ (see text for conditions).

Figure 5.14

Initially the peaks consist of a fairly skewed dip within the peak which gradually becomes less deep and more symmetrical. The dips eventually disappear and the peaks consist of flat tops which become sharper with time.

5.2.7 Observations Of The Time Evolution Of The Kurtosis Plots

Examples of the kurtosis versus time plots are shown in figure 5.15 for the six variance conditions (see above). The kurtosis tends to a steady state value of 3 (i.e. the Gaussian level) and at this large time limit, it does not carry any oscillations. In evolving to this form however, very substantial fluctuations may occur. The behaviour may be summarized as comprising a base level which starts from some finite value (1.8 for a uniform slug) and gradually increases to the level Ku = 3. Upon this slowly changing evolution there occur large amplitude oscillations with a frequency which is initially equal to that of the pump. The amplitude of successive peaks increases quickly to a maximum before gradually decaying to zero. For some frequencies and strokes, the time taken for the oscillations to peak out is less than one period and so the apparent behaviour is that the amplitude decreases with time for all time. Not only does the size of the peaks on the kurtosis plots change; the shape of the shrinking peaks also evolves in an interesting way. The initially sharp peaks gradually broaden so that the impulsive spikes eventually take on a sinusoidal appearance. The speed with which this evolution takes place is greatest for small values of α^2. Associated with this apparent "squashing" of the kurtosis plot peaks, is the way in which the frequency of the oscillations becomes twice that of the pump. This is similar to the frequency increase on the variance plots. As the

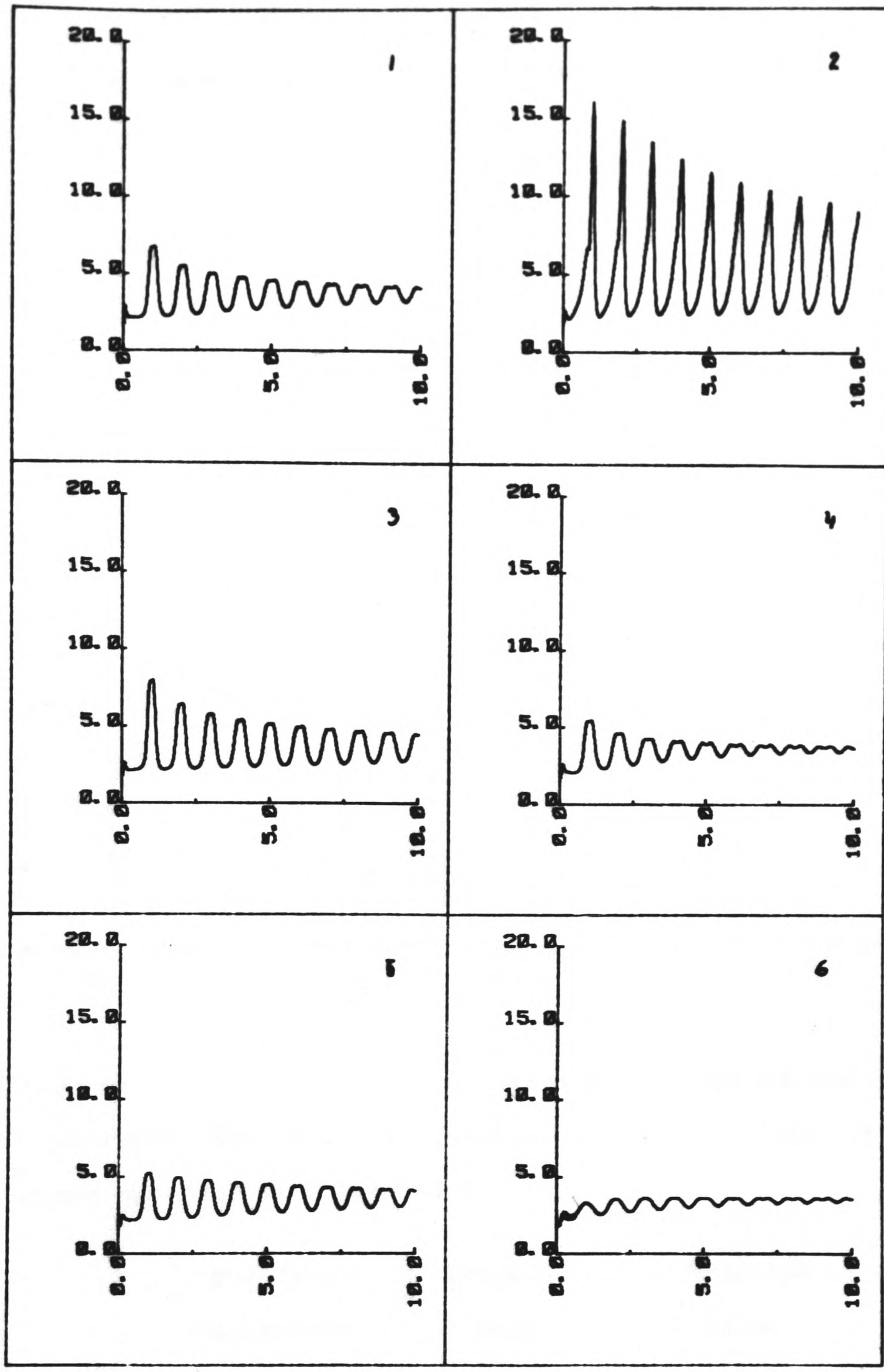

Plots of kurtosis against $\frac{\tau}{2\pi}$ (see text for conditions).

Figure 5.15

maximum level of the kurtosis peaks flattens due to the broadening, a dip occurs on this plateau. With succeeding periods, this trough becomes deeper and broader until eventually the oscillations consist of two equal amplitude sets of peaks which are 180 degrees out of phase i.e. the frequency has effectively doubled.

5.2.8 Effect Of Starting From A Ramp Slug†

The moments plots were observed to be very close to those of the uniform slug starting condition. The variance and $\bar{X}$ plots were virtually the same and the evolution and levels of the skewness and kurtosis were very similar. This latter observation does however seem to depend upon the values of the Reynolds and Strouhal numbers; further work will be necessary to describe this effect.

5.2.9 Effect Of Slug Size On The Moments Plots

The size of the slug does not noticeably affect the evolution

†

Refer to figures 5.16,5.17 and 5.18 which give predictions for the variance, skewness and kurtosis versus time plots at Re=0.4 and St=0.125 under the following conditions

Code	Modified Parameter	Default Value	Modified Value
6	none	default	default
7	Sc	1000	100
8	$\frac{x}{s}_0$	.625	1.25
9	slug shape	uniform	ramp
10	wall condition	$\frac{\partial c}{\partial \psi}=0$	c=0
11	starting angle	0	$\frac{\pi}{2}$

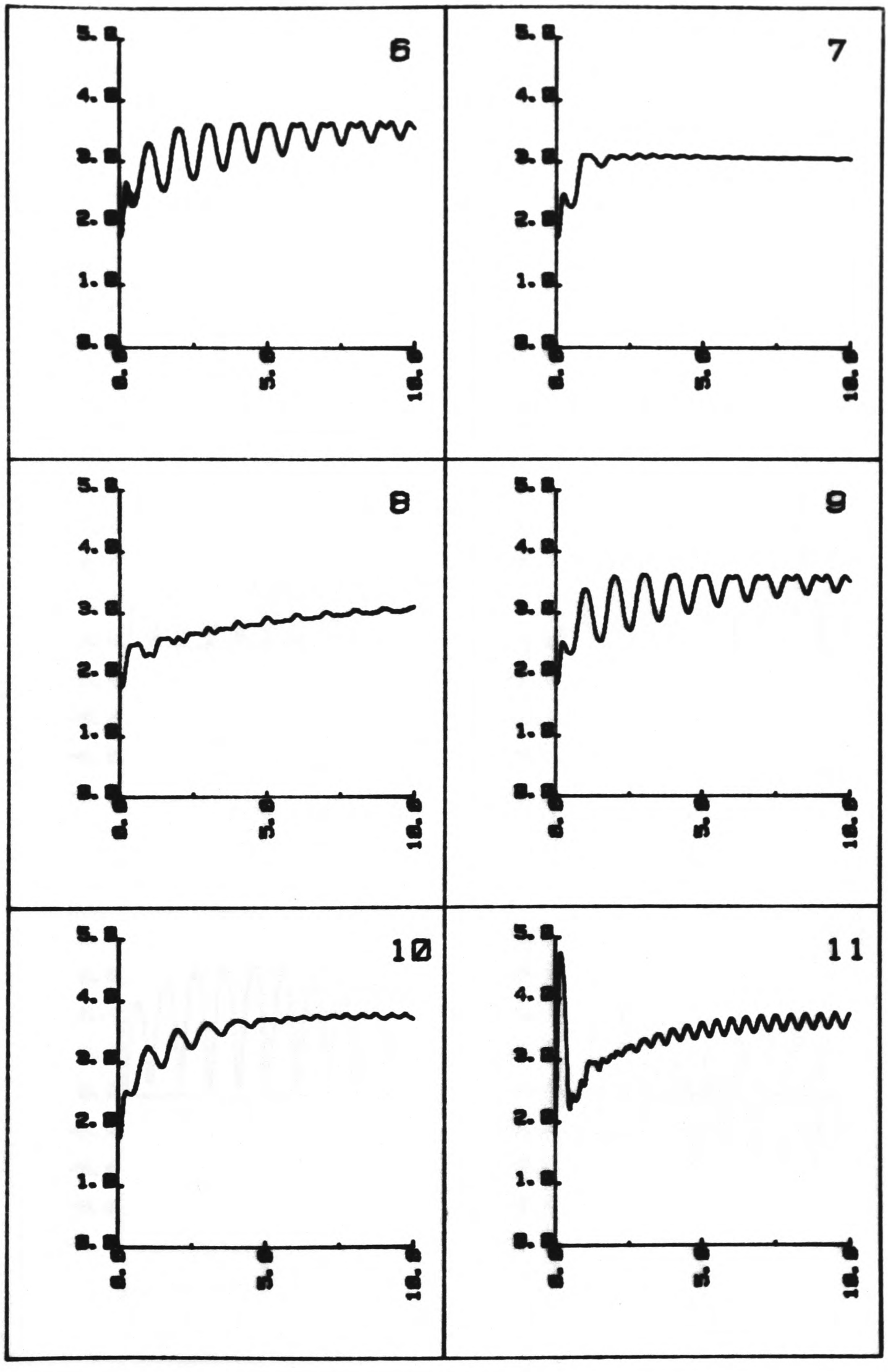

Plots of σ^2 St^2 against $\frac{\tau}{2\pi}$ (see text for conditions)

Figure 5.16

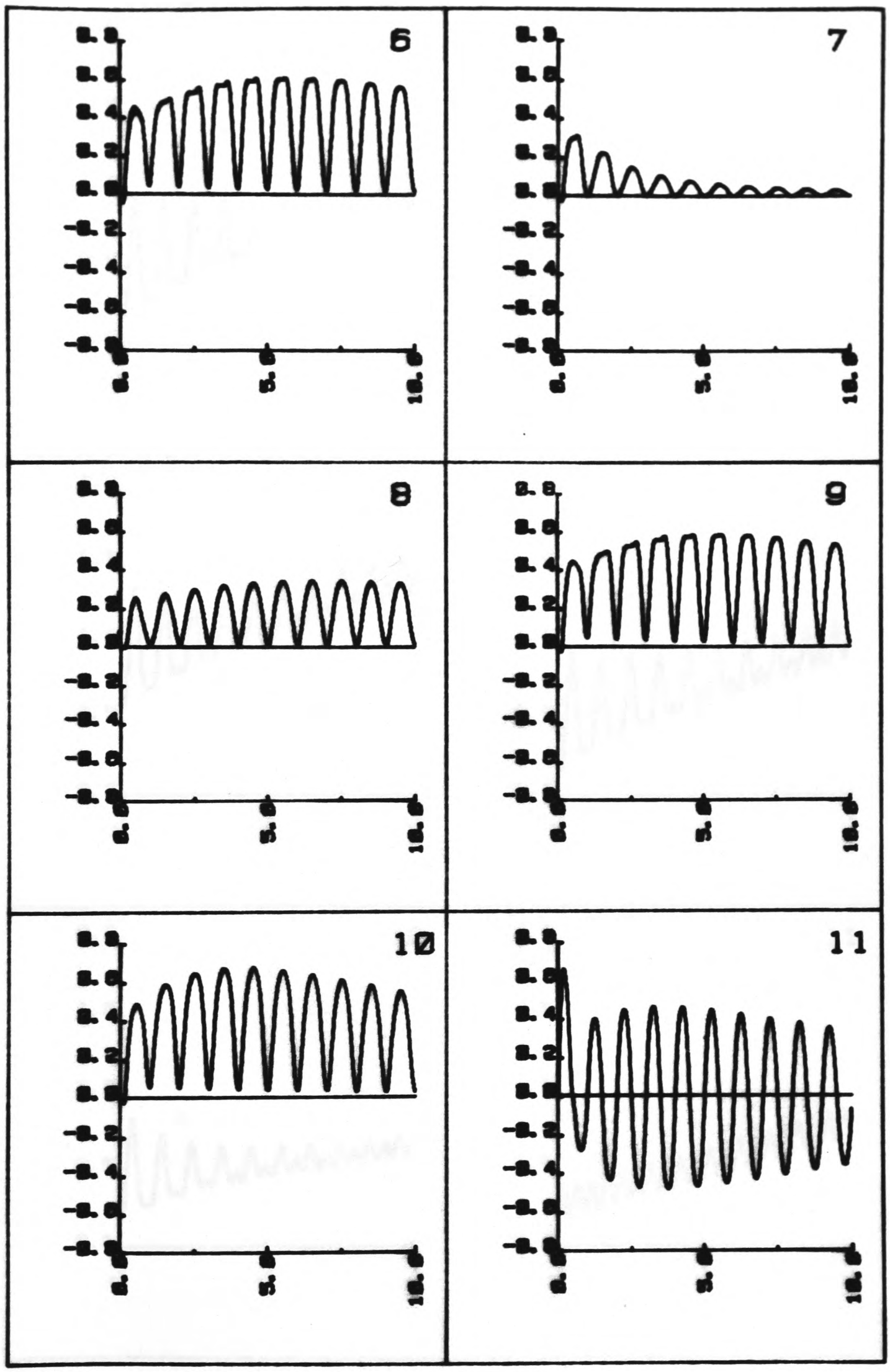

Plots of skewness against $\frac{T}{2\pi}$ (see text for conditions).

Figure 5.17

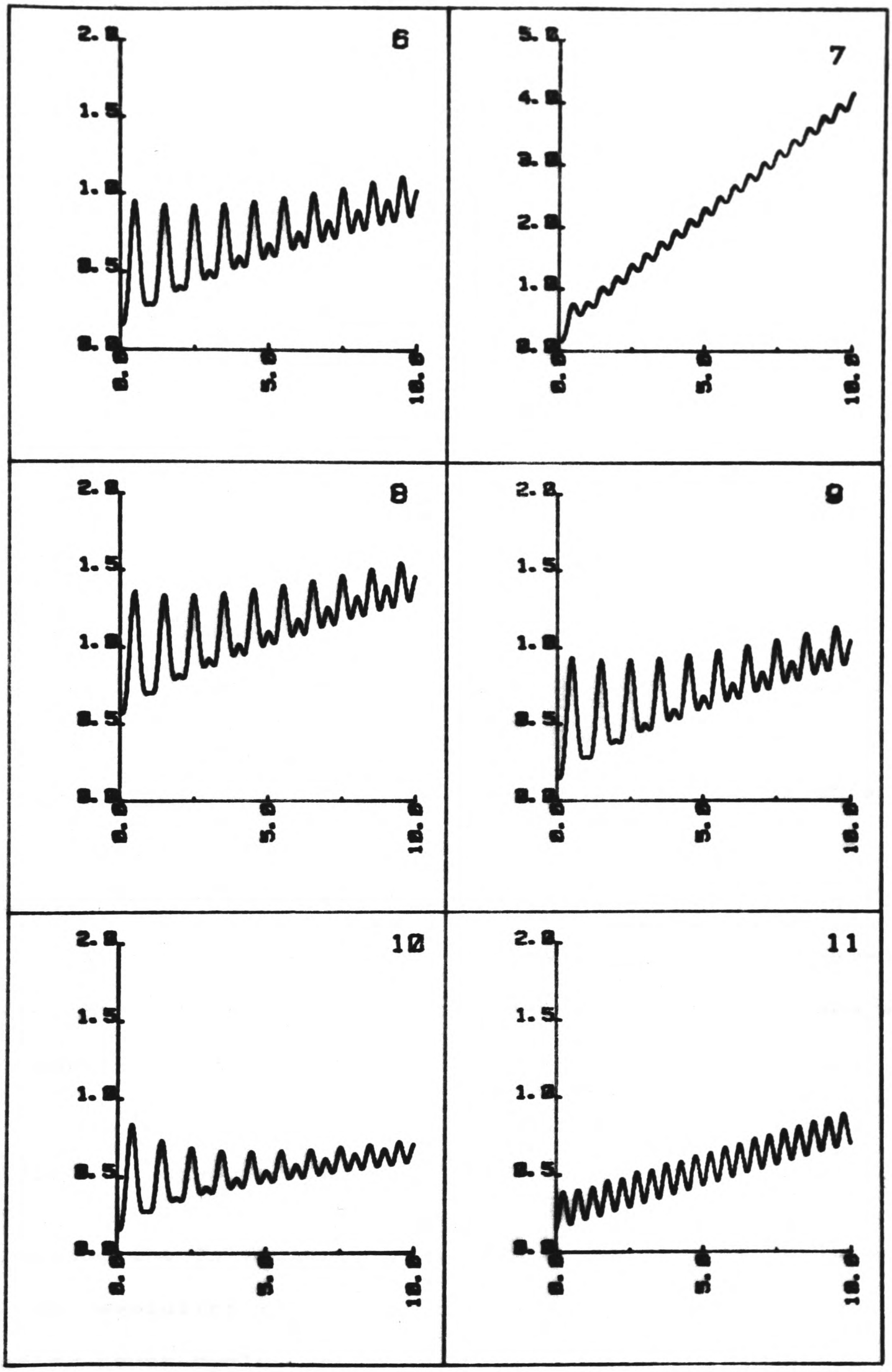

Plots of kurtosis against $\frac{\tau}{2\pi}$ (see text for conditions).

Figure 5.18

of the variance plots, implying that the dispersion coefficient evolved with time by precisely the same mechanism and that this evolution did not depend upon an axial diffusion process. If axial diffusion were important in determining when the Taylor asymptotic state was reached then the evolution of the dispersion coefficient would have been affected by a modification of the distance over which the axial diffusion mechanism would have to have acted. The kurtosis plots on the other hand, were observed to evolve more slowly when a larger slug was used and on both the skewness and the kurtosis plots, the convectively formed peaks were of a smaller amplitude.

5.2.10 Effect Of Using Permeable Walls

In this part of the investigations, the wall concentration was held at zero throughout the channel length, so we would expect the contaminant to gradually diffuse out through the channel walls. The variance plots were not greatly affected by the use of this new boundary condition. The time evolution of the plots was substantially unaltered except that the peaks decayed more quickly than for the impermeable wall case. The kurtosis and the skewness plots were not changed greatly although the kurtosis peaks were somewhat reduced in level.

5.2.11 Effect Of Changing The Schmidt Number

Increasing the diffusivity by an order of magnitude greatly altered the evolution of the moments plots. The steady state was reached after fewer cycles (this is in agreement with equation 5-3) but $\frac{D}{K}$ did not change appreciably (in agreement with Holley, Harlemann and Fischer (121) and chapter 3).

5.2.12 Effect Of Changing The Velocity Phase

By imposing the maximum bulk velocity to coincide with $\tau=0$, the evolution of the moments plots was greatly modified. The primary and secondary oscillations appeared for all $\tau>0$ and were of equal amplitude. The skewness attained negative values and the amplitude of the peaks of the kurtosis plots were reduced.

5.2.13 Summary Of The Time Evolution Of The Moments Plots

Owing to the large influence of the convective effects, all the moments plots carry quite large oscillations. For the higher moments, the amplitude of these oscillations decays with time. The frequency of the oscillations on the moments plots (I_n for $n > 1$) tends to become twice that of the pump. This behaviour, it is argued, is a manifestation of the somewhat asymmetrical initial conditions that were imposed and occurs since the system is tending to a (symmetrical) state with which the double-frequency components are associated. The number of cycles necessary for a particular stage of evolution of the moments plots to have been attained is determined by a paramater α^2 Sc. Since the steady flow Peclet number is given by the product of steady flow Reynolds number and Schmidt number, we may refer to this group as a pulsatile Peclet number since it is given by the product of a pulsatile Reynolds number and the Schmidt number. This pulsatile Peclet number is proportional to the ratio of the time for cross-sectional diffusive mixing to the period of the oscillations; in this study the number has typically been of order 10^3. For cases when this parameter is much less than unity, we would expect the dispersive behaviour to

be quasi-steady and therefore be described by the work of Bishoff (31). The present study has dealt with the more complex (and more common) case in which the velocity reverses direction long before the Taylor asymptotic state is reached.

5.3 PLOTS OF MEAN CROSS-CHANNEL CONCENTRATION

5.3.1 Introduction

In this section, plots of $\bar{C}$ versus t for a particular value of x are presented. The forms of these plots are described and the conditions under which the various forms are achieved are given. Since these graphs provide a numerical prediction of the gauge reading that may be obtained experimentally, the downstream distance of the cross-section over which one averages the concentration is refered to as the measurement position. Three distinct cases should be distinguished and these are determined by the remoteness of the measurement point relative to the slug length and the piston stroke.

5.3.2 Breakthrough Curve Measured Initially Inside Slug

For values of x so close to the injection point that $x_0 > x > -x_0$, we obtain a response similar to that shown in figure 5.20. The important feature of this plot is that the dimensionless concentration is initially unity. $\bar{C}$ decreases during the course of the first half-period as the slug is bowed out so that clean fluid moves along the centre-line of the channel and across the measurement domain. At the 180 degrees point in the first cycle, the slug reaches its maximum deformation and $\bar{C}$ is at its minimum. The second half of this first period returns the slug back to its

central position and the value of $\bar{C}$ approaches unity again. The peak value that is reattained at the start of the second period is somewhat less than that at the start of the first on account of the diffusive and dispersive effects which dilute the slug. The decay of the peaks continues over successive periods and the troughs rise in level so that the amplitude of the peaks decreases with time. This rise of the troughs occurs since the clean fluid which is washed in front of the measurement position at the 180 degrees point in the cycle does itself become contaminated due to the slug spreading. At large enough times the peaks and troughs tend to converge so that the oscillations on the $\bar{C}$ versus t plot become too small to be measured.

For very small strokes, it is possible that the slug is not bowed out far enough for clean fluid to pass across the measurement cross-section. This occurs when $x_0 > x > -x_0$, and $x_0+x > 2s$ (for oscillatory plug flow) or $x_0+x > 4s$ (for oscillatory parabolic flow). In this case, the oscillations are not detected until a significant amount of dispersion has occured. An example of a breakthrough curve in which this effect is apparent is shown in figure 5.19.

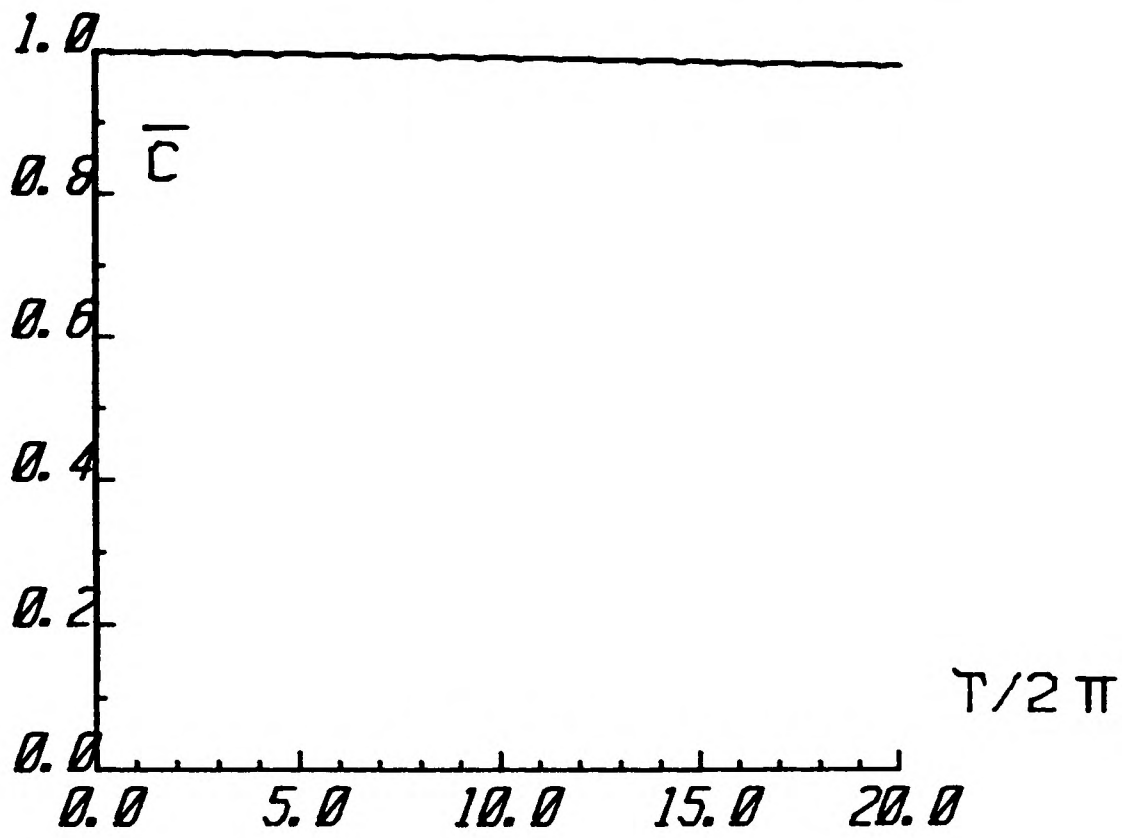

Breakthrough curve when the measurement point lies inside the undeformed slug and the stroke does not push clean water across the measurement site. $x/x_0 = -0.5$, Re = 10, St = 0.2, Sc = 10^3, x_0 = 10mm.

Figure 5.19

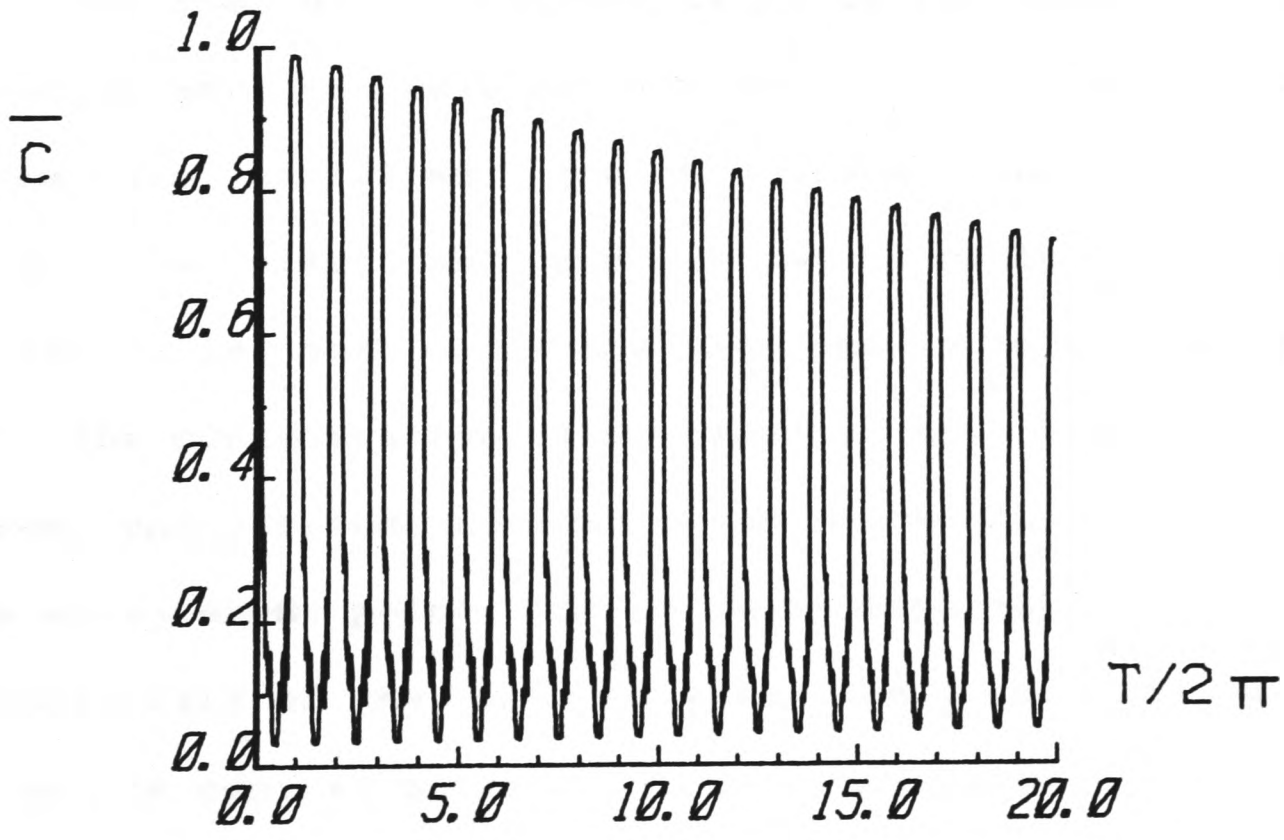

Breakthrough curve when the measurement point lies inside the undeformed slug. $x/x_0 = 0.0$, Re = 10, St = 0.05, Sc = 10^3.

Figure 5.20

Even when the stroke is not so small that this effect is not active over the whole of a cycle, it will still occur over the first fraction of the cycle as the slug (which at this stage is composed of contaminant of approximately uniform concentration) is moved past the measurement site producing little change in $\bar{C}$. This effect is a manifestation of the fact that in the early stages the concentrations in the slug are uniform axially, even in the deformed state.

5.3.3 Breakthrough Curve Measured Initially Inside Deformed Slug

For intermediate values of x, part of the slug lies in front of the measurement site for a part of each cycle. There are also times when the deformed slug does not occupy any of the measurement cross-section. For a perfect plug flow, this condition is achieved when $2s + x_0 > x > x_0$. In a parabolic flow, the centre-line portions of the slug are moved twice as far down the channel and the criterion may be relaxed to $4s + x_0 > x > x_0$. When these conditions are satisfied, the $\bar{C}$ versus time plots consist of a period at the start and end of each cycle in which the concentration is zero. As the slug passes across the section of interest, the concentration rises rapidly (see figure 5.21). If the large undistorted concentration on the centre-line is pushed past the measurement point, the concentration falls again until in the second half of the cycle it rises and drops again as the slug returns to its central position. It is thus possible for the peaks to occur twice during each cycle. Note that this is a quite distinct effect from the frequency doubling that was observed on the moments plots. As diffusion and dispersion act on the slug during this continual bowing out, so the peaks on the plot become

smaller and the troughs rise. In the case described above, in which two peaks may occur in each period, the overall spreading of the slug gradually masks the effect so that the two peaks appear to merge. After a long time has passed, the base level of the oscillating $\bar{C}$ values will start to decay towards zero very slowly as the remaining slug concentrations become more and more dilute.

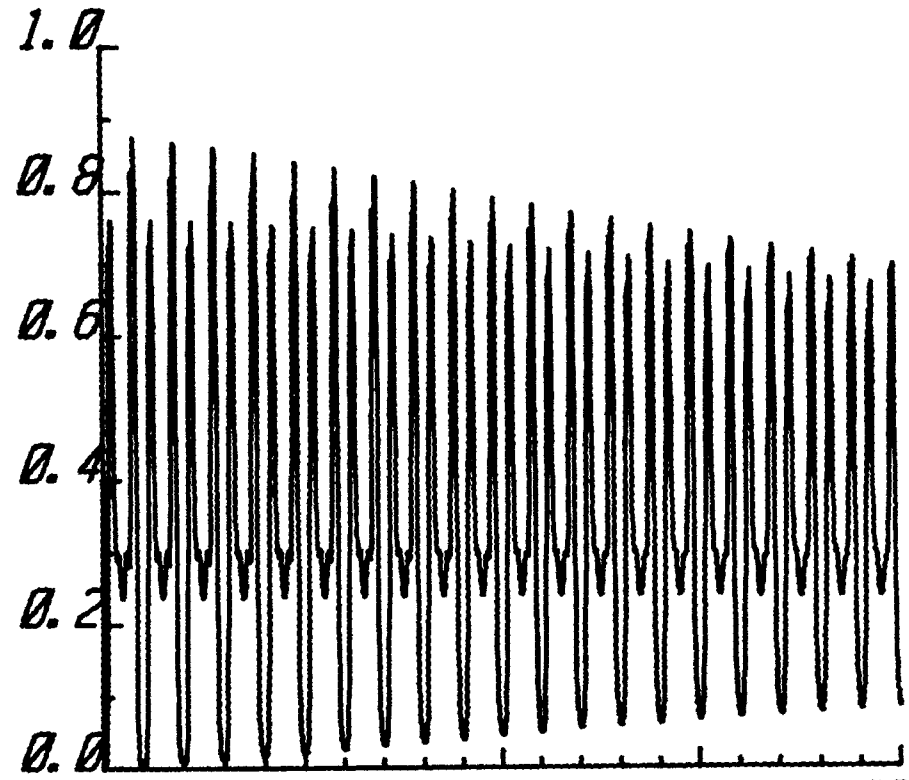

Breakthrough curve when the measurement point lies outside the undeformed slug but inside the deformed slug. $x/x_0 = 2$, Re = 10, St = 0.05, Sc = 10^3.

Figure 5.21

5.3.4 Breakthrough Curve Measured Initially Outside Deformed Slug

When the measurement position lies outside the region into which the slug is deformed, the mean cross-channel concentration is initially zero. In a plug flow, the condition for this regime to apply is that $x > 2s + x_0$ and in a parabolic flow, the condition

becomes $x > 4s + x_0$. Eventually, as the axial extent of the diluted slug increases, small concentration levels are washed over the measurement cross-section and small peaks grow about the 180 degree cycle positions on the time axis of the $\bar{C}$ verus t plots. After growing to a maximum, the amplitude of these peaks eventually decreases very slowly again on account of further dilution of the very greatly spread out slug. This evolution is shown in figure 5.22.

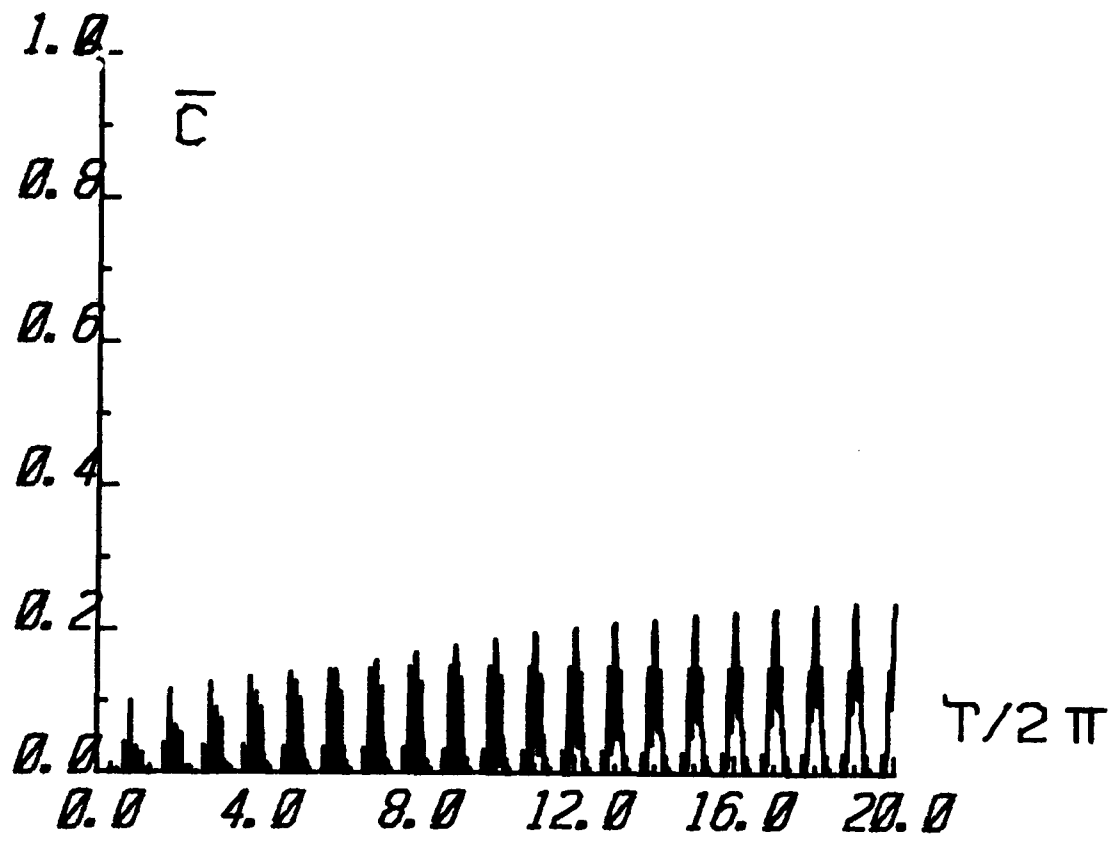

Breakthrough curve when the measurement point lies outside the deformed slug. $x/x_0 = -1.2$, $Re = 10$, $St = 0.05$, $Sc = 10^3$.

Figure 5.22

For the case of oscillatory parabolic flow we may consider the essential features of the three types of plots described above to be those given in table 5.2 . The regions of the channel in which the various different types of response are obtained are shown schematically in figure 5.23.

condition	$\bar{C}$ behaviour
$\|x\| < x_0$	initially unity: transient -ve peaks
$x_0 < x < x_0$ 4s	initially zero: transient +ve peaks
$x > x_0 + 4s$	initially zero: eventually small +ve peaks

Table 5.2

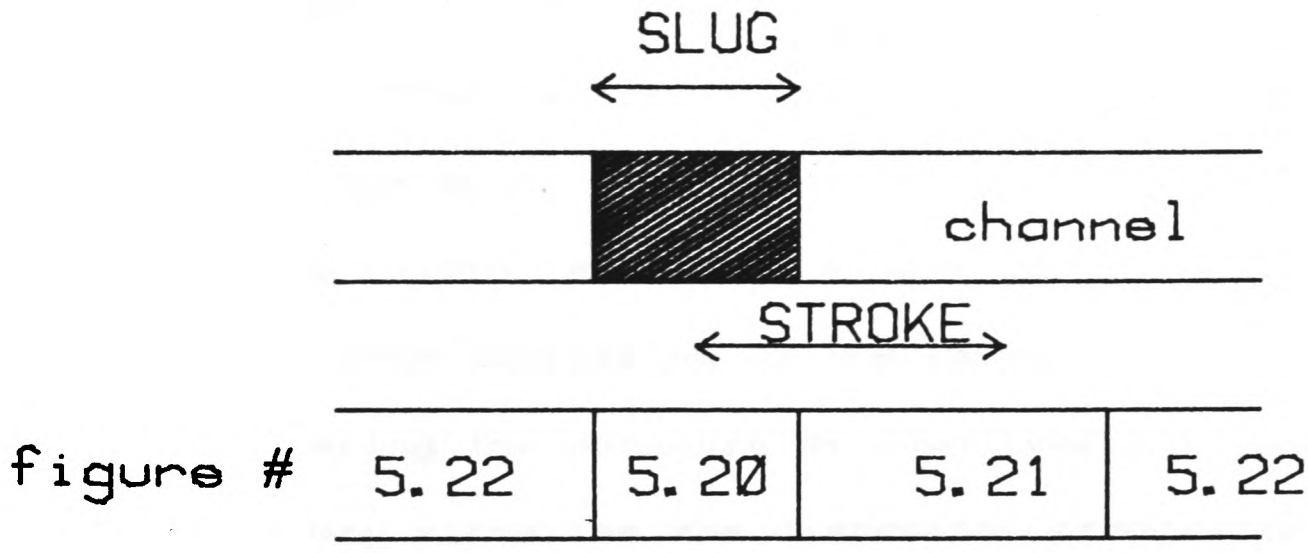

gauge mounting position

Diagram illustrating the axial channel positions to which figures 5.20, 5.21 and 5.22 apply in the case of parabolic flow.

Figure 5.23

5.4 CONTOUR PLOTS OF LINES OF EQUAL CONCENTRATION

A useful form of flow visualization has been provided by drawing out lines of equal concentration within the half-channel at a particular instant. An example of the results of this procedure is shown in figure 5.24. This shows concentrations at the 90, 180, 270 and 360 degree positions in the first three cycles at a Reynolds number of 10.0 and a Strouhal number of 0.1. The contours plotted represent dimensionless concentrations of 0.8, 0.6 and 0.4. The contours migrate up and down the channel as the reversing

velocity continually deforms and then reforms them. At the 180 degrees instant, the slug excursion down the channel has reached its limit and at this position, we notice that the centre-line and wall contours are, although shifted and deformed, still intact. However at cross-channel locations in between these two limits, some breakdown of the contours is discernible. Naturally as the slug becomes more and more dilute so the 0.8, 0.6 and finally the 0.4 contours disappear by apparently shrinking to a point on the centre-line. The speed with which this occurs is determined by the initial slug width and the time history of the dispersion coefficient. Some impression of the extent of the slug dilution is given by comparing the contours at identical positions in suceeding periods. We may visualize the dispersion process by imagining that for each contour line, there is an equation of motion within the channel. Let us postulate the form of the migration for a contour representing a small concentration. Initially the line is located close to the limits of the slug. As spreading proceeds, the contour migrates down the channel as the diluted tracer eventually contaminates the oscillating liquid. However, a time is reached when the concentration of this contour is no longer small compared to that of the remaining contaminant levels. Indeed the contour migrates back up the channel since the maximum instantaneous channel concentration always occurs near to the line $x = 0$ (or the convectively distorted version of it). The two contours to the left and right of this line gradually close in disappear to a point. In summary then, all contours migrate down the channel, reach a limit and then retreat back onto the origin where they disappear. This effect is entirely diffusive and is quite distinct from the transient large rates of movement of the contours due to the continual convective bowing.

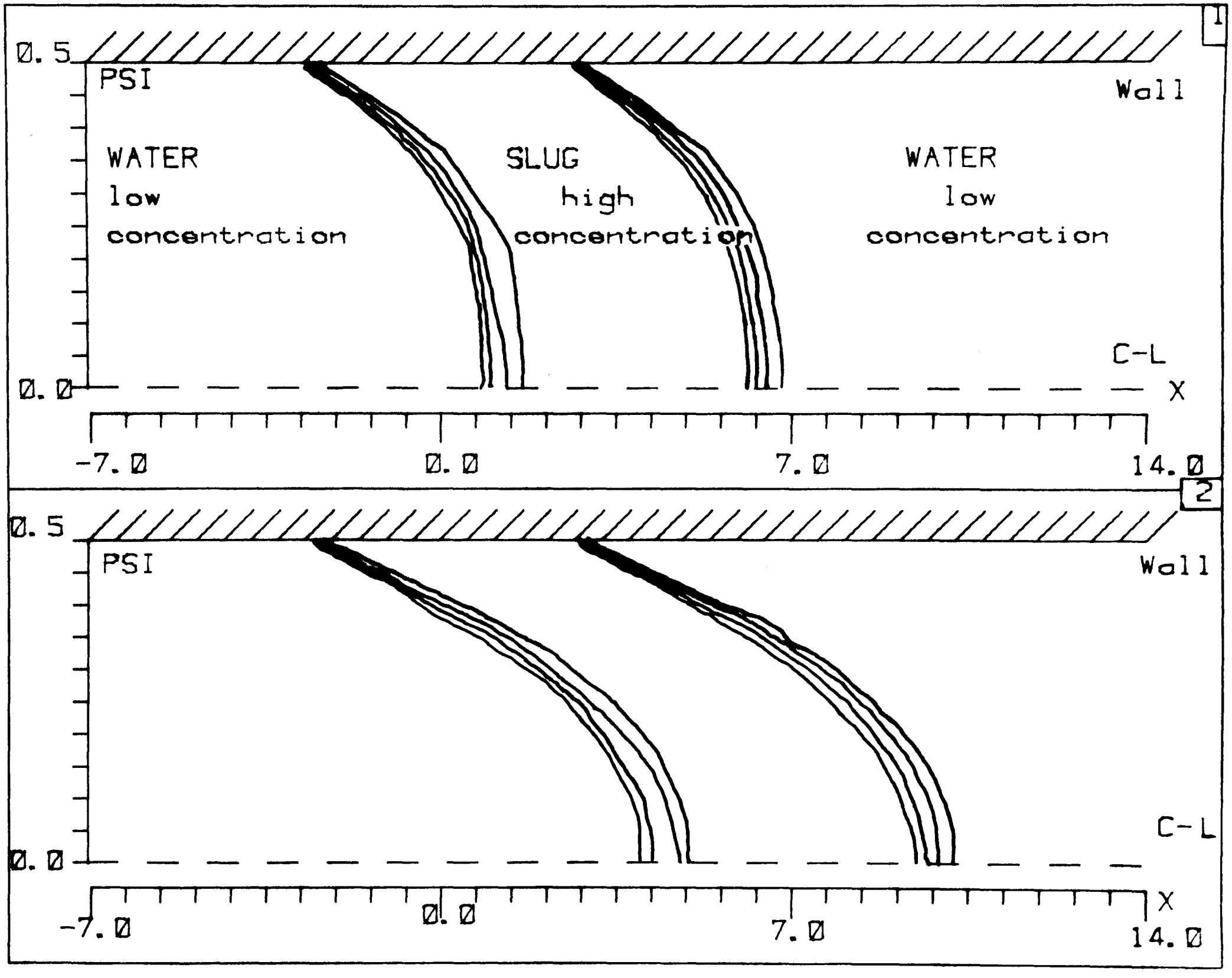
1
Ø.5
PSI
Wall
WATER
low
concentration
SLUG
high
concentration
WATER
low
concentration
C-L
Ø.Ø
X
-7.Ø
Ø.Ø
7.Ø
14.Ø
2
Ø.5
PSI
Wall
C-L
Ø.Ø
X
-7.Ø
Ø.Ø
7.Ø
14.Ø

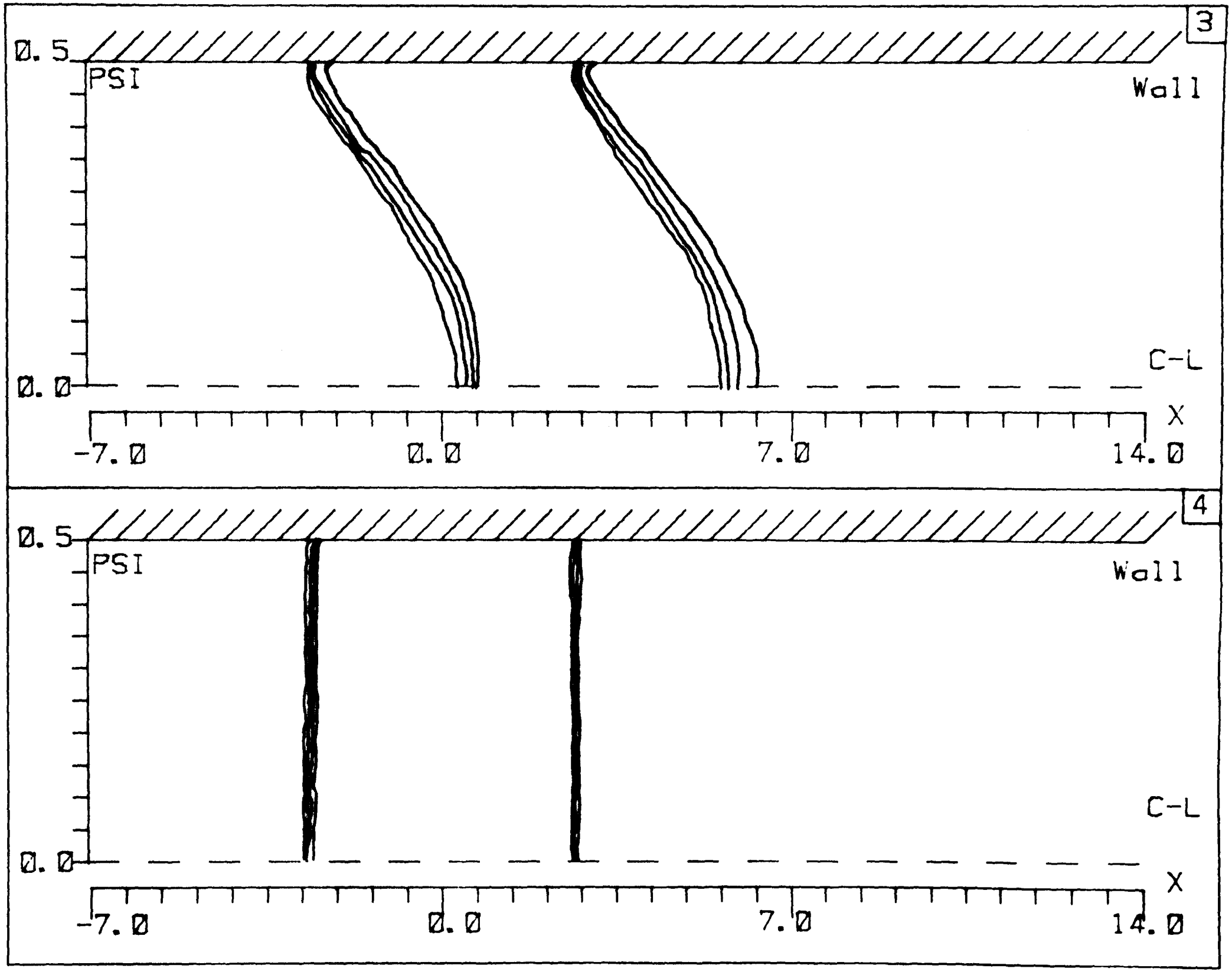
3
0.5
PSI
Wall
C-L
0.0
X
-7.0
0.0
7.0
14.0
4
0.5
PSI
Wall
C-L
0.0
X
-7.0
0.0
7.0
14.0

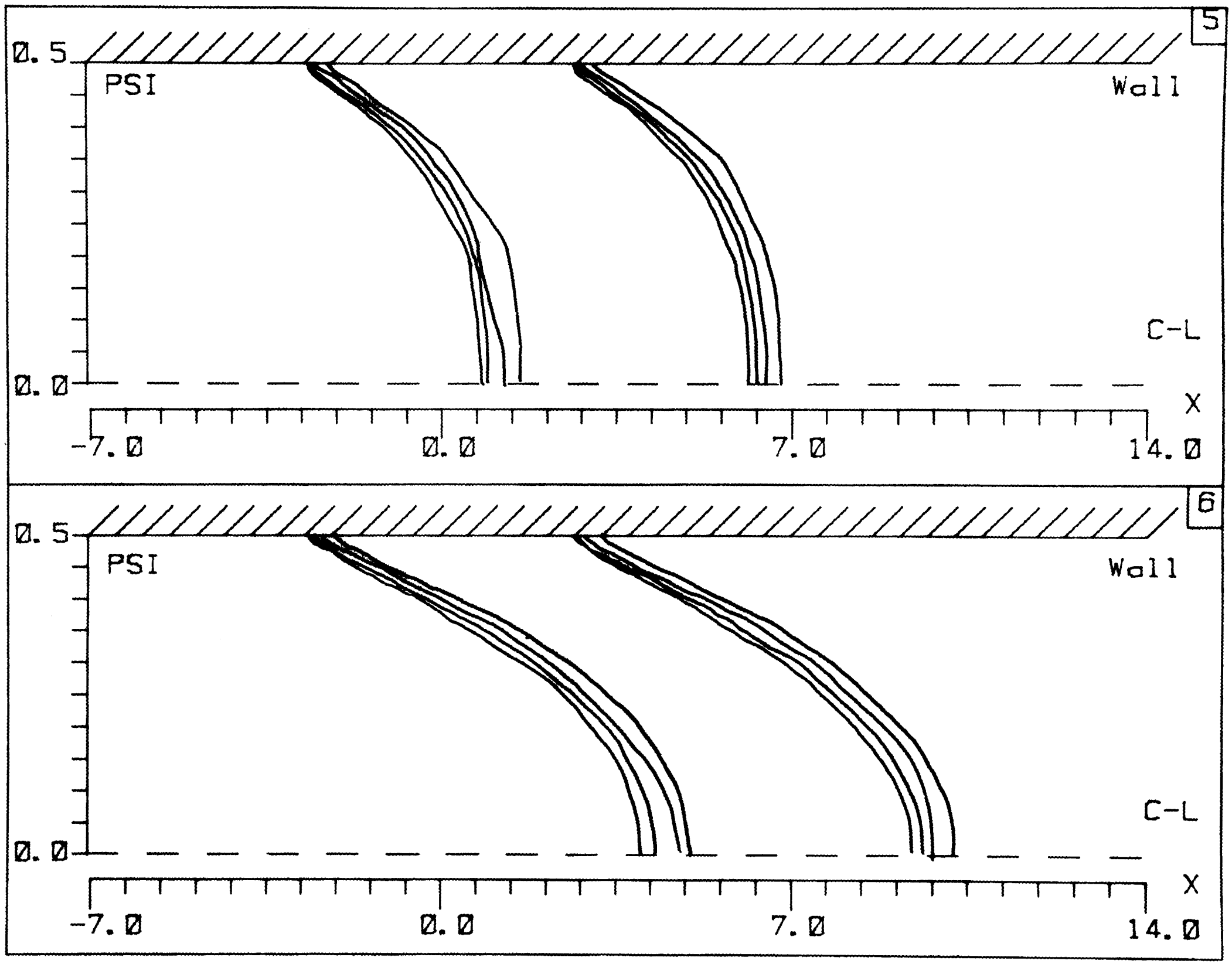
5
0.5
PSI
Wall
C-L
0.0
X
-7.0
0.0
7.0
14.0
6
0.5
PSI
Wall
C-L
0.0
X
-7.0
0.0
7.0
14.0

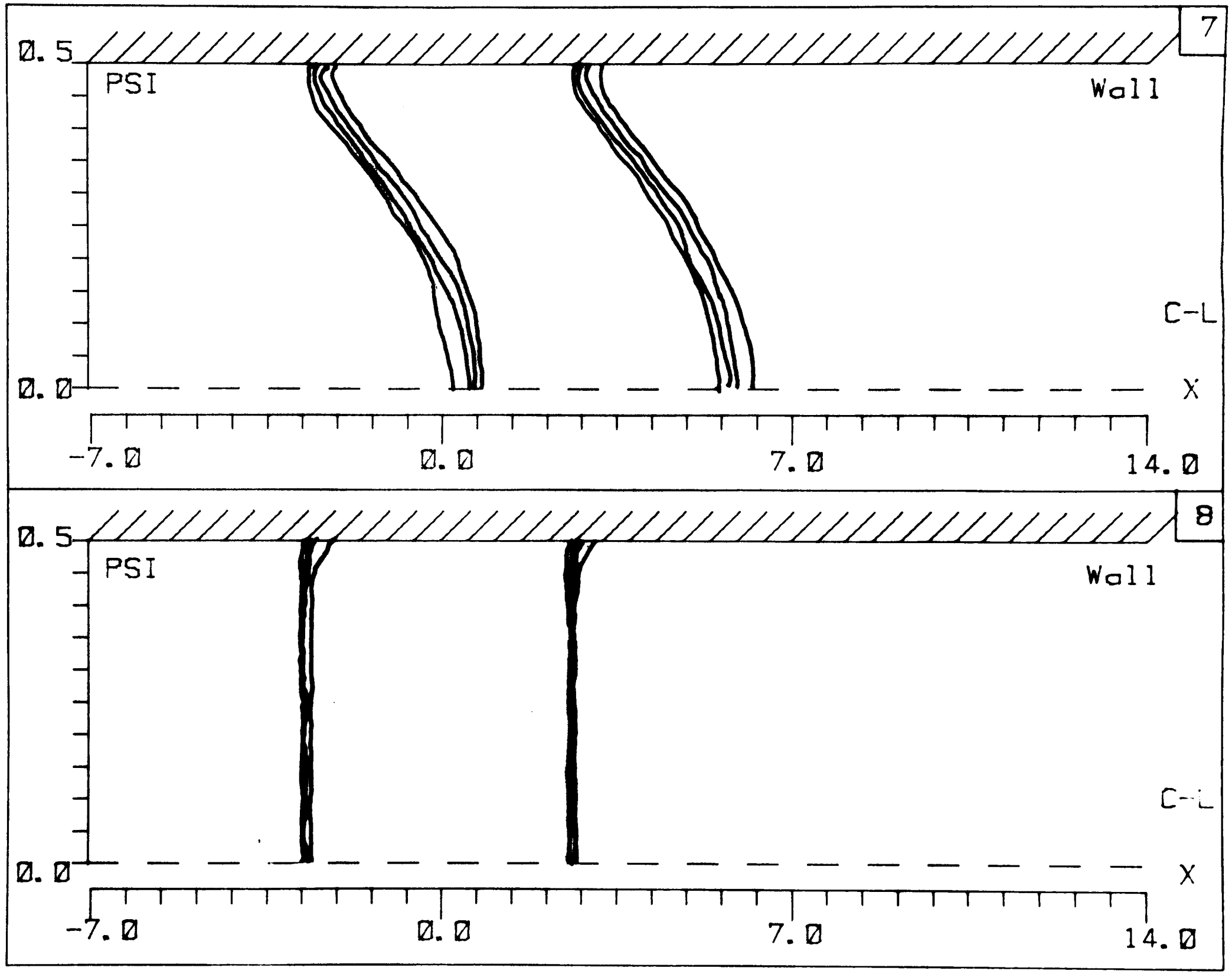
7
0.5
PSI
Wall
C-L
0.0
X
-7.0
0.0
7.0
14.0
8
0.5
PSI
Wall
C-L
0.0
X
-7.0
0.0
7.0
14.0

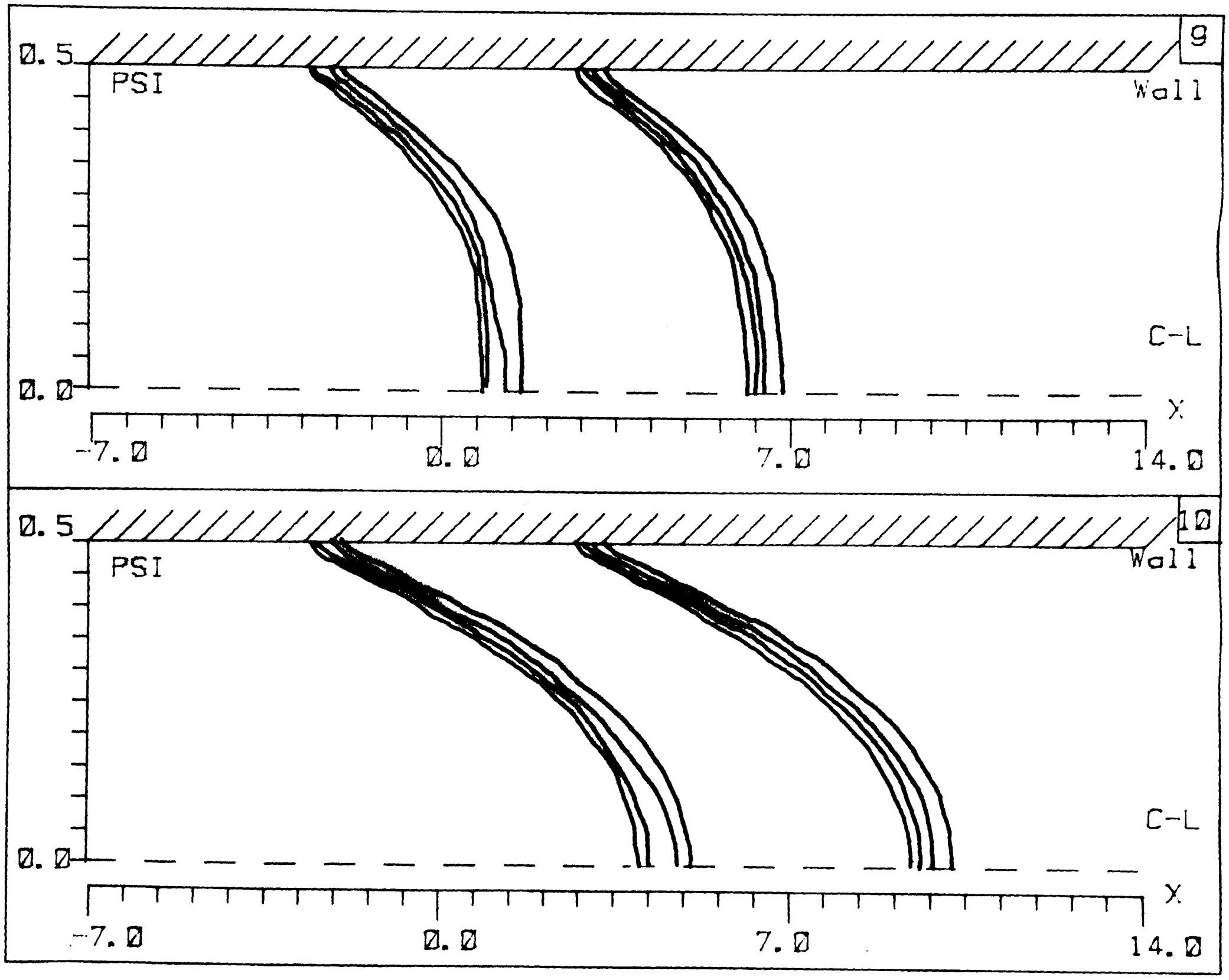
0.5
PSI
9
Wall
C-L
0.0
X
-7.0
0.0
7.0
14.0
0.5
PSI
10
Wall
C-L
0.0
X
-7.0
0.0
7.0
14.0

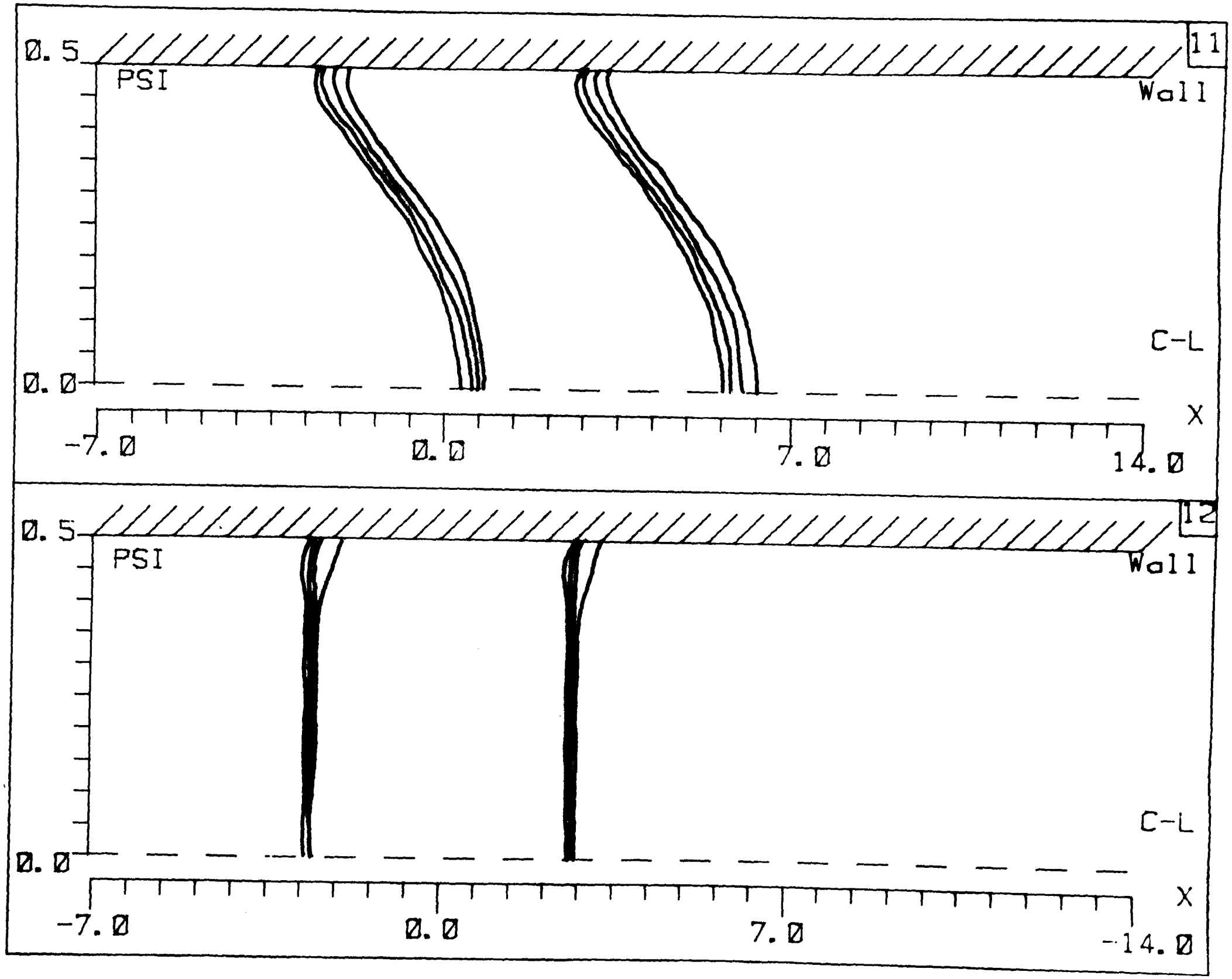
0.5
PSI
11
Wall
C-L
0.0
X
-7.0
0.0
7.0
14.0
0.5
PSI
12
Wall
C-L
0.0
X
-7.0
0.0
7.0
-14.0

Plots of contours of equal concentration at the 0, 90, 180, 270 degree positions of the first 3 cycles. The c = 0.2, 0.4, 0.6 contours are shown. The lines nearest to the slug centre represent the higher concentratons. Only half the channel cross-section is shown (i.e. $0 < \psi < 1$). Re = 10, St = 0.1, Sc = 10^3. Note that PSI = $\frac{\psi}{2}$.

Figure 5.24

In figure 5.25 contour plots are drawn showing the 0.5, 0.05, 5.0×10^{-3}, 5.0×10^{-4} contour lines at the start of the 7^{th} and 14^{th} periods. Note that the contour lines are no longer parallel to $\chi = 0$.

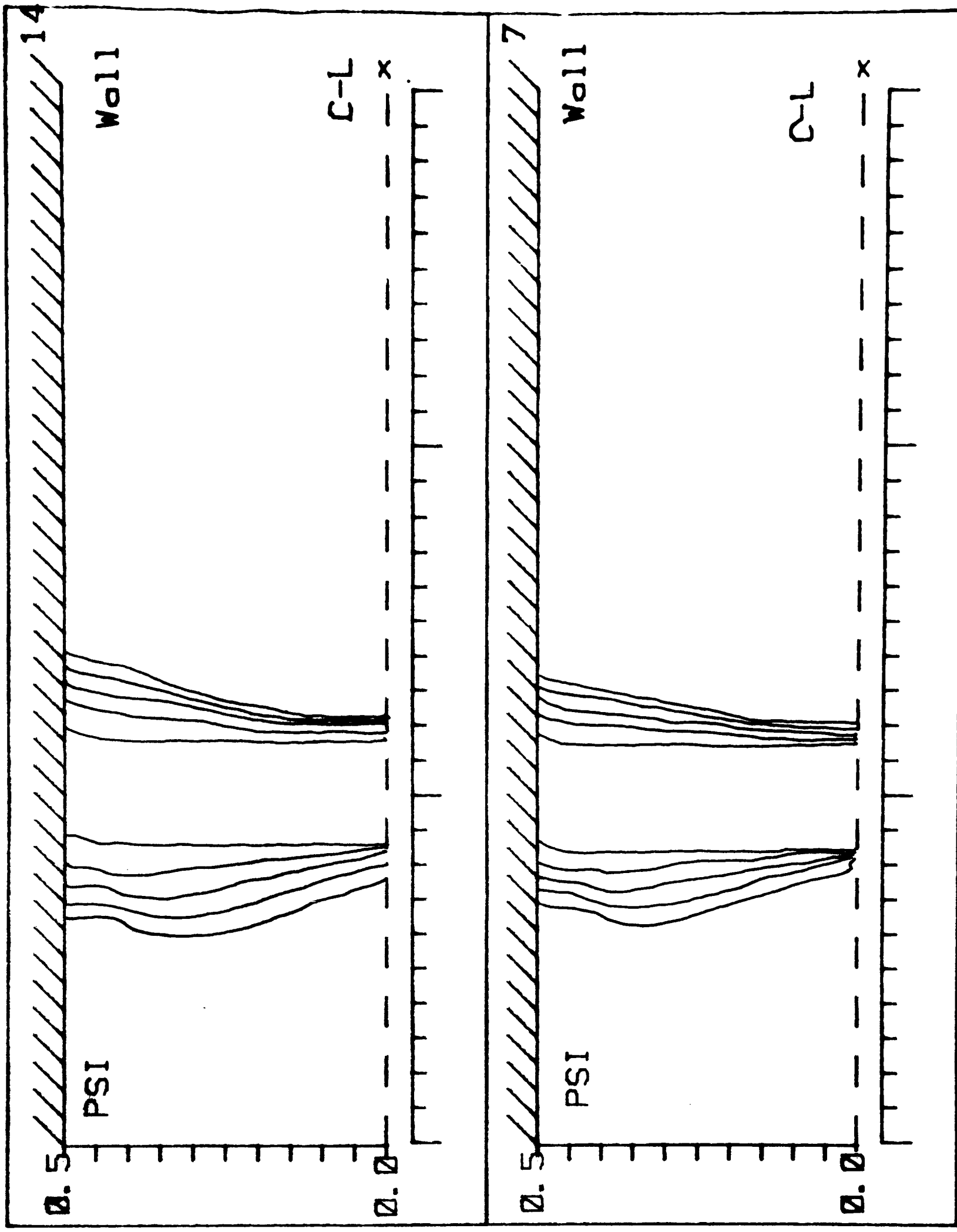

Plots of the 0.5, 0.05, 5.0×10^{-3}, 5.0×10^{-4} contour lines at the start of the 7^{th} and 14^{th} periods. Only half the channel cross-section is shown (i.e. $0 < \Psi < 1$). Re = 10, St = 0.1, $Sc = 10^3$.

Figure 5.25

Chapter 6

EXPERIMENTAL APPARATUS AND TECHNIQUES

6.1 Introduction.

6.2 Electrical system for the bias and interface circuits.

6.3 Gauge response to variations in concentration of common dyes.

6.4 Calibration of gauges in a flat channel.

6.5 Channel dimensions and construction.

6.6 Pumping arrangements.

6.7 Precautions taken to exclude air from the system.

6.8 Dye injection mechanism.

6.9 Location of opto-electronic gauges.

6.10 Density matching.

6.11 Sources of error in the dispersion experiments.
- 6.11.1 Slug malformation.
- 6.11.2 Dependence on diffusion coefficient.
- 6.11.3 Tendency towards asymptotic forms.

6.12 Summary of experimental procedure.

6.13 Investigations of a mass transfer device.

CHAPTER 6

EXPERIMENTAL APPARATUS AND TECHNIQUES

6.1 INTRODUCTION

The problem of dispersion in a flat channel carrying an oscillatory flow has been studied experimentally by continuously measuring the mean cross-channel concentration at a number of axial positions located along the centre-line of a rectangular duct for times of order 50 seconds. The concentrations have been measured optically by directing a beam of light across the channel and measuring its attenuation by the tracer dye. A similar method has been used in previous studies by Taylor (223), Caro (41) and many others.

Joshi, Kamm, Drazen and Slutsky (henceforth JKDS) (284) have recently reported experimental results obtained for dispersion in oscillatory gas flow. The Schmidt number (Sc) for their system is of order 1 so we would not expect their results to be similar to those obtained in the present study of liquid dispersion in which Sc is three orders of magnitude greater. The approach of JKDS was to shine an infra-red laser beam across a glass tube containing the

dispersing tracer. In this study a set of electronic sensors has been designed which have been made compatible with a high speed computer data-logging package. This approach is similar to that of Caro and of JKDS but has the advantage that the inexpensive circuitry (about £3 per gauge) makes it possible to obtain large amounts of data by the use of many sensors. The gauges have been anchored permamently to a set of positions on a channel; operation has therefore been simplified since movement of the gauges would have lead to a different calibration curve. The experiments reported by Reejsinghani, Gill and Barduhn (180) also employed light transmission studies to measure concentrations. Their experimental method, however, required one to stop the flow before a reading was taken. The gauges which have been used in the present study do not require such a procedure and are therefore a significant improvement.

The devices which have been used to achieve these gains consist of an infra-red light emitting diode (LED) and a matched phototransistor, the peak response being at a wavelength of about 900nm. These have been set up so that the LED directed a beam of light across the channel onto the sensitive face of a diametrically opposite phototransistor. This latter device has the property that, when suitably biased, it carries a conduction current proportional to the intensity of its illumination. When the space between the gauges is occupied by some light absorbing material, the beam is attenuated and the conduction current through the phototransistor decreases. Thus, by measuring the conduction current, one can predict the concentration of the light absorbing species.

6.2 ELECTRICAL SYSTEM FOR THE BIAS AND INTERFACE CIRCUITS

The manufacturer's specifications for the gauges are reproduced in table 6.1. The circuit required to drive the light source is standard and is shown in figure 6.1 and in figure 6.2. The LED is fed from a 5v source through a series resistance which acts as a current limit. The sensor circuit should impose a bias voltage of about 15v across the phototransistor; it is preferable for the bias to be approximately constant and independent of the conduction current of the device as this will produce a more linear response. The output voltage from this circuit (which is some function of the channel concentration) should vary between 0 and 5v since this is the range of the input to the data-logging system.

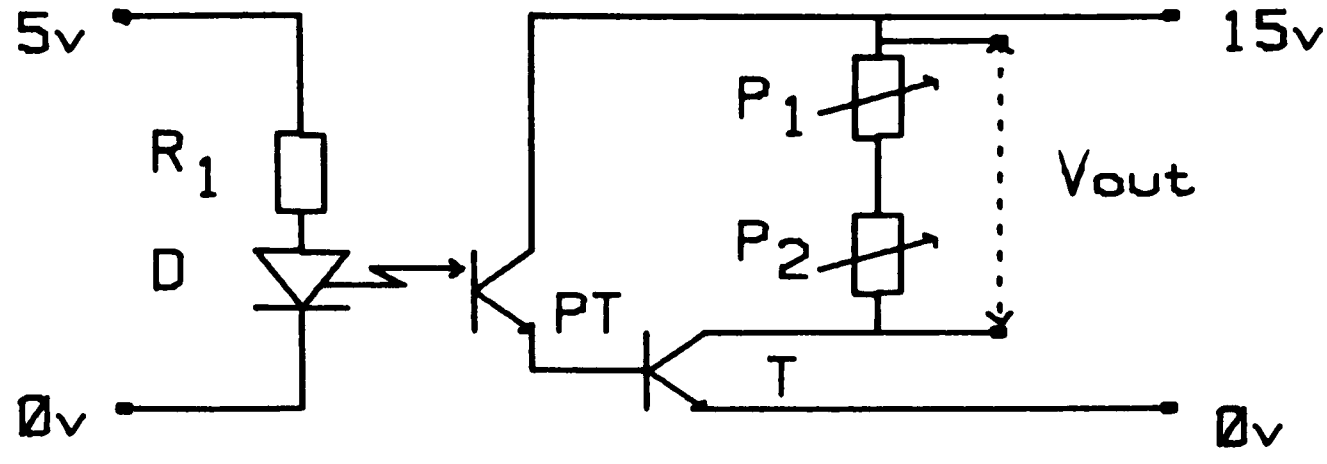

Electronic circuit I which was used to bias the opto-electronic concentration measuring devices. (For component values see tables 6.1, 6.2)

Figure 6.1

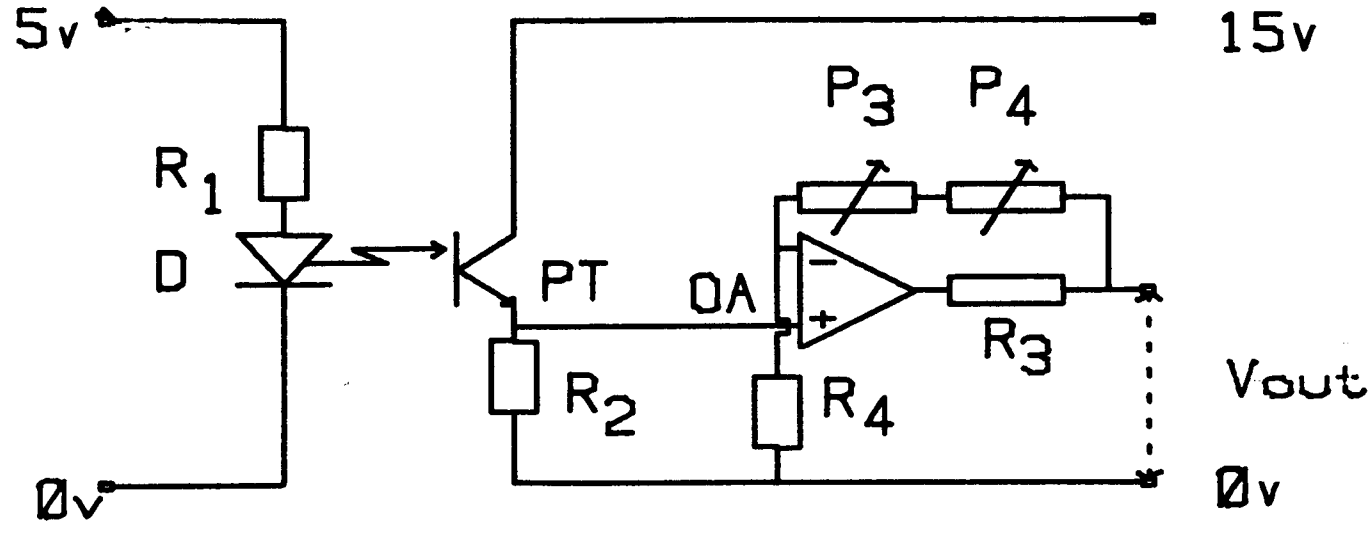

Electronic circuit II which was used to bias the opto-electronic concentration measuring devices. (For component values see tables 6.1, 6.2)

Figure 6.2

Light Emitting Diode

maximum forward current	= 150 mA,
rated voltage	= 5 v,
dissipated thermal power	= 225 mW,
typical voltage across diode	= 1.4 v,
radiated power at 100 mA	= 12 mW.

Phototransistor

rated current I_r	= 100 μA,
rated voltage at I_r	= 30 v,
capacitance at 1 MHz and 3v	= 30 pF.
conduction current at bias of 10 v and a light power of 10 mW cm^{-2}	= 10 μA.

Table 6.1: Device Specifications

Two designs of circuit have been built to bias the phototransistor. Circuit I (see figure 6.1) feeds the conduction current to ground through the base-emitter junction of a transistor (T), so pulling the necessary amplified current through the collector. This current is then passed through a simple potentiometer which is set to give the required output voltage. One shortcoming of this circuit is the possible temperature dependence of the current gain (h_{fe}) of the amplifying transistor. Circuit II (see figure 6.2) performs the same function as circuit I, but does not have this deficiency. The conduction current is

fed through a small resistance to ground. The resulting voltage across this resistor is amplified by OA, the gain of which is adjusted to give the desired output voltage range. The presence of the series resistance makes the bias across the phototransistor weakly dependent upon the conduction current but this coupling can be reduced to a value as small as required by using a small enough resistance and a larger gain on the amplifier.

Code	Value	Purpose
R_1	47Ω	resistor to limit current through LED.
T	BFY 51	transistor to amplify conduction current.
P_1	0-2.2kΩ	fine gain potentiometer to set output voltage.
P_2	0-10kΩ	coarse gain potentiometer to set output voltage.
R_2	12kΩ	resistor to convert conduction current to voltage.
R_3	51Ω	resistor to set bias of operational amplifier.
R_4	16Ω	resistor to set gain of operational amplifier.
OA	LM324N	operational amplifier to amplify signal voltage.
P_3	0-10kΩ	fine gain potentiometer to set output voltage.
P_4	0-470Ω	coarse gain potentiometer to set output voltage.

Table 6.2: Components Used in Electronic Circuits.

6.3 GAUGE RESPONSE TO VARIATIONS IN CONCENTRATION OF COMMON DYES

In order to determine the response of the gauges, a test cell was made up (see figure 6.3). A 4.5ml sample of the specimen dye was placed in a 5ml perspex test-tube of square cross-section and side 12.5mm. In order to eliminate the effects of radiation emitted by objects in the laboratory, the outside of the perspex cell was sprayed black. The holder provided a firm mounting for both the test tube and the electronic devices; this is important since a slight change in the separation of the gauges or in the direction of the beam may alter the response significantly.

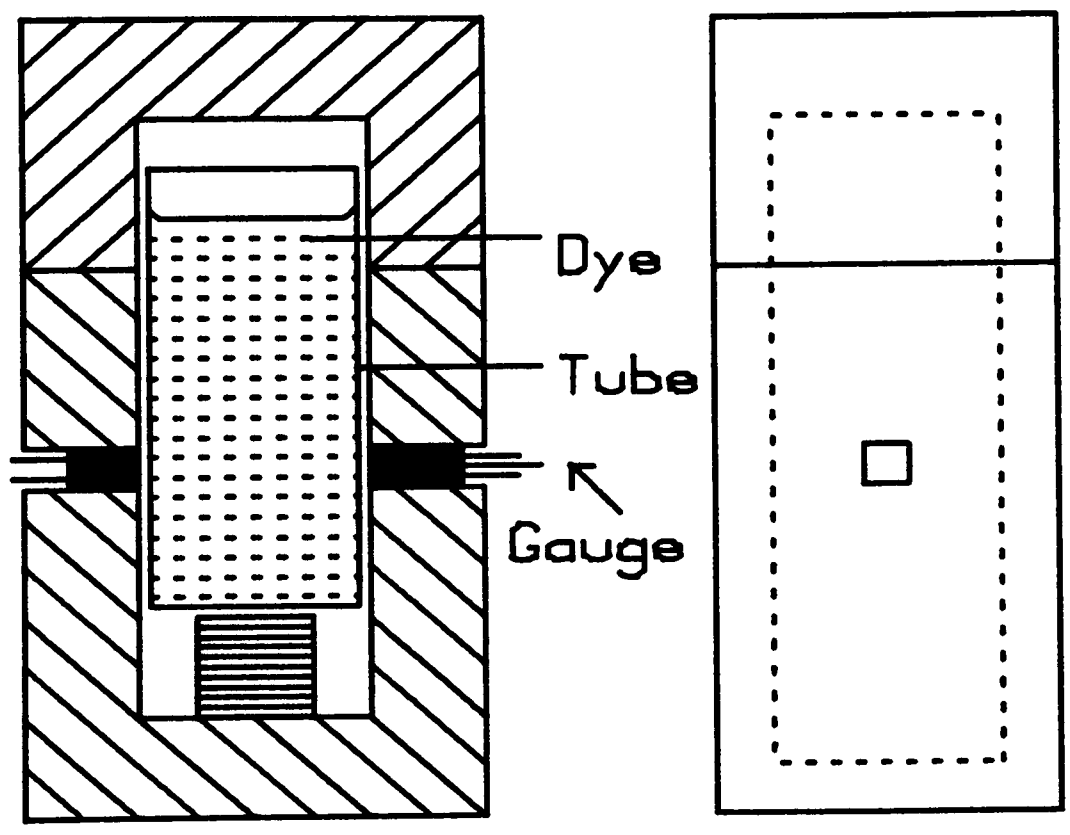

Diagram illustrating the device used to mount the gauges for the preliminary dye investigation.

Figure 6.3

For each dye a solution of concentration c_0 (usually O(1)M) was made up and from this stock a range of solutions which were successively weaker by a factor of 2 was obtained. These results were then plotted out as V_a-V against $\log_{10}(c / c_0)$ where V_a is the voltage produced by an empty tube, and V is the voltage produced by a dye of concentration c (see figure 6.4). Naturally, the more dilute a solution was, the more light passed through it. This created a larger conduction current through the phototransistor and hence a larger gauge voltage. The gradient of the plots obtained by this method (shown in figure 6.4) is therefore positive for all c. For a dye which absorbed the light effectively, one would expect V to be close to 0 volts for the most concentrated solutions. In fact only a few of the dyes which were tested produced sufficient light absorption for this to be observed. Duranol Blue and Duranol Brilliant Blue (ICI Organics) did, however, exhibit this result, a factor of 100 change in concentration producing approximately 5v full scale deflection on the voltmeter. Naturally, if one were to use a shorter optical path length then a smaller fraction of the light would be absorbed and it would be more difficult to find a dye which gave sufficient light attenuation.

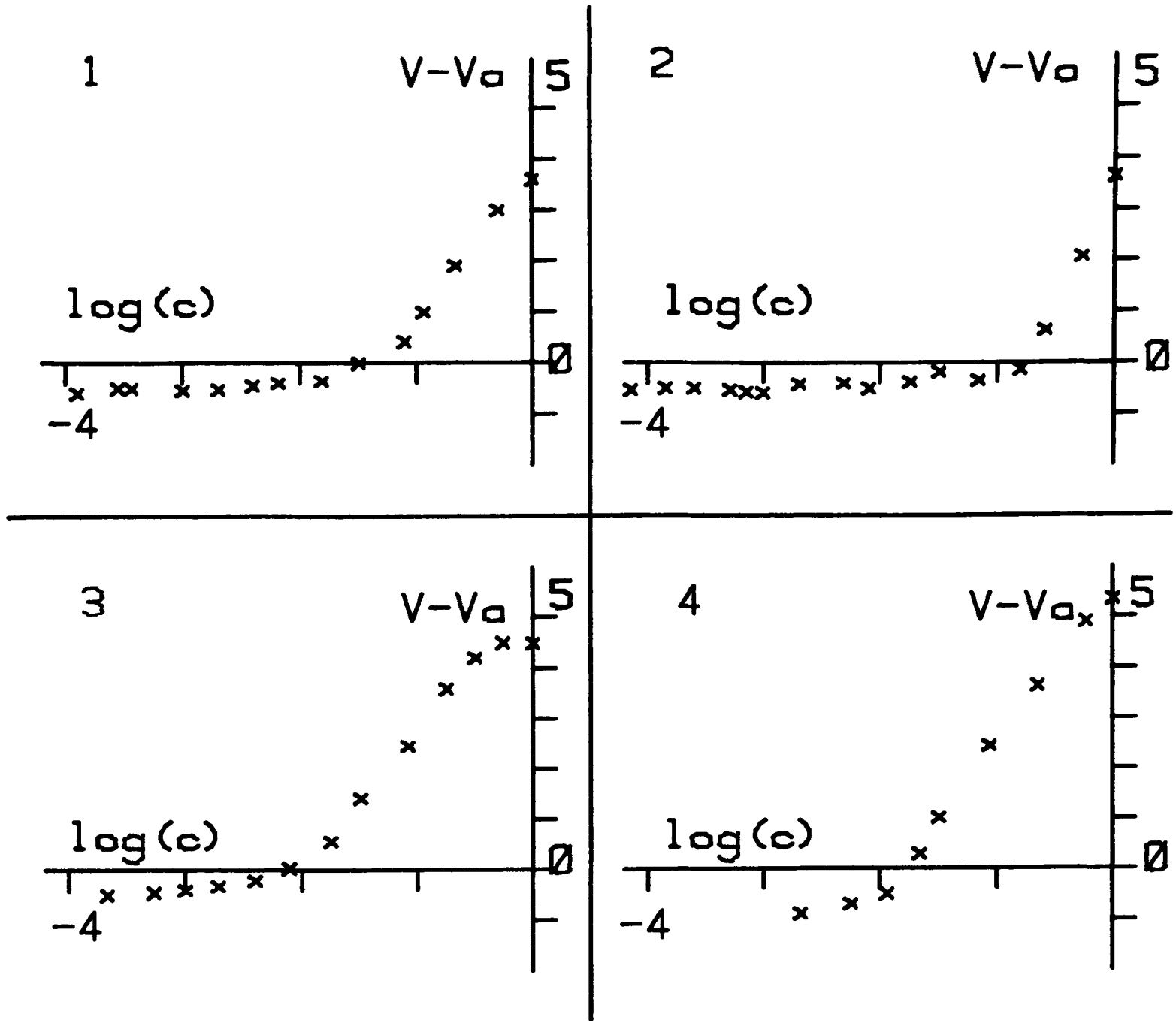

Plots of the V - V_a versus log to base 10 of concentration for four dyes

1/ Disulphine BLue V.

2/ Gentian Violet.

3/ Duranol Blue.

4/ Duranol Brilliant Blue.

Figure 6.4

6.4 CALIBRATION OF GAUGES IN A FLAT CHANNEL

In order to measure the dispersion of a contaminant in laminar oscillatory flow, a flat channel of height of 1mm and consisting of transparent perspex walls held in an aluminium frame was made up (see section 6.5). A number of the gauges described in section 6.2

were placed at various points along the channel length with the beam directed over the 1mm dimension. The dimensions of this apparatus are such that a much shorter optical path was used than had been realized in the commissioning cell. A survey was therefore carried out to collect a range of dyes which could be used to produce a good light absorption over this small distance. The dispersed dyes were the best for absorbing light, but it was considered to be desirable to also find a direct dye (i.e. a simple solution). Table 6.3 gives details of the results of this investigation.

Dye	Percentage absorption
Alizarin Cyanine Green	7.3
Azo Black	4.3
Azophloxine	0.04
Dispersol Blue	25.3
Dispersol Fast Scarlet	10.3
Dispersol Fast Yellow A300	23.2
Dispersol Fast Yellow G	37.2
Disulphine Blue V	1.9
Duranol Blue G	31.4
Duranol Brilliant Blue BN	18.9
Duranol Red X3B300	18.0
Methylene Blue	5.3
Trypan Blue	4.4

Table 6.3: absorption performance of a range of dyes.

In order to calibrate the gauges, the channel was filled with water and the voltages V_w were measured. A base solution of concentration c_o was made up and the resulting gauge voltages V measured. This solution was then diluted by a few percent and further readings were taken. This process was repeated until a twenty-fold dilution had been achieved. At each stage of this operation, care was taken to flush the channel through with the

solution under test, re-empty it and then refill. This ensured that the remnants of the previous solution which lingered between the plates did not dilute the incoming dye and cause errors in the local dye concentration. The voltages were read by a DEC AR11 data logging module and the data processed on a PDP 1134 minicomputer. Results are presented as a plot of dimensionless voltage W (V/V_w) versus dye concentration (see figures 6.5, 6.6, 6.7). This procedure has the advantage that even if the gain of the output potentiometer is changed by as much as a factor of 5, the calibration will still be accurate to within about 1% as long as a reading of V_w is taken prior to each experiment. The calibration data may be used to measure concentrations in two ways. One could construct a "look-up" table and then interpolate between data points. Alternatively, some reasonable calibration curve could be fitted to the data. The latter method has been used since its results are more compact and it gives a better insight into the behaviour of the gauges. Three curves have been fitted to the data

$$W = e^{-Bc} \qquad \text{[6-1].....exponential,}$$

$$W = \frac{1}{1+Ac} \qquad \text{[6-2],....hyperbola,}$$

$$W = A^{-Bc} \qquad \text{[6-3].....inverse power,}$$

where c is the normalized concentration and W is the normalized voltage. Each of these functions obeys the necessary conditions that $W \to 0$ as $c \to \infty$ and that $W = 1$ at $c = 0$. The parameters A and B have been found numerically using a least squares fit and the secant method to solve the resulting implicit equations. Examples of these fitted curves are shown in figures 6.5 and 6.6. The gauges performed in a very similar manner although the calibration

constants for each were slightly different. Figure 6.7 shows a plot of the voltage-concentration calibration curve for Duranol Blue for each of the gauges. The points are very self consistent, the typical distance (expressed as dimensionless volts) from a smooth curve being 0.02 and it can be seen that the exponential fit follows the data best. This is in agreement with the results and predictions of McLaughlin and Rushton (274) who set out a numerical model of the absorption of light by a solution of spherical particles and concluded that a plot of light intensity versus concentration was exponential. The fact that the calibration equation is an exponential is useful since this means that the gauges do indeed measure the mean cross-channel concentration whatever the particular distribution of concentration over the cross-section happens to be (see appendix 3).

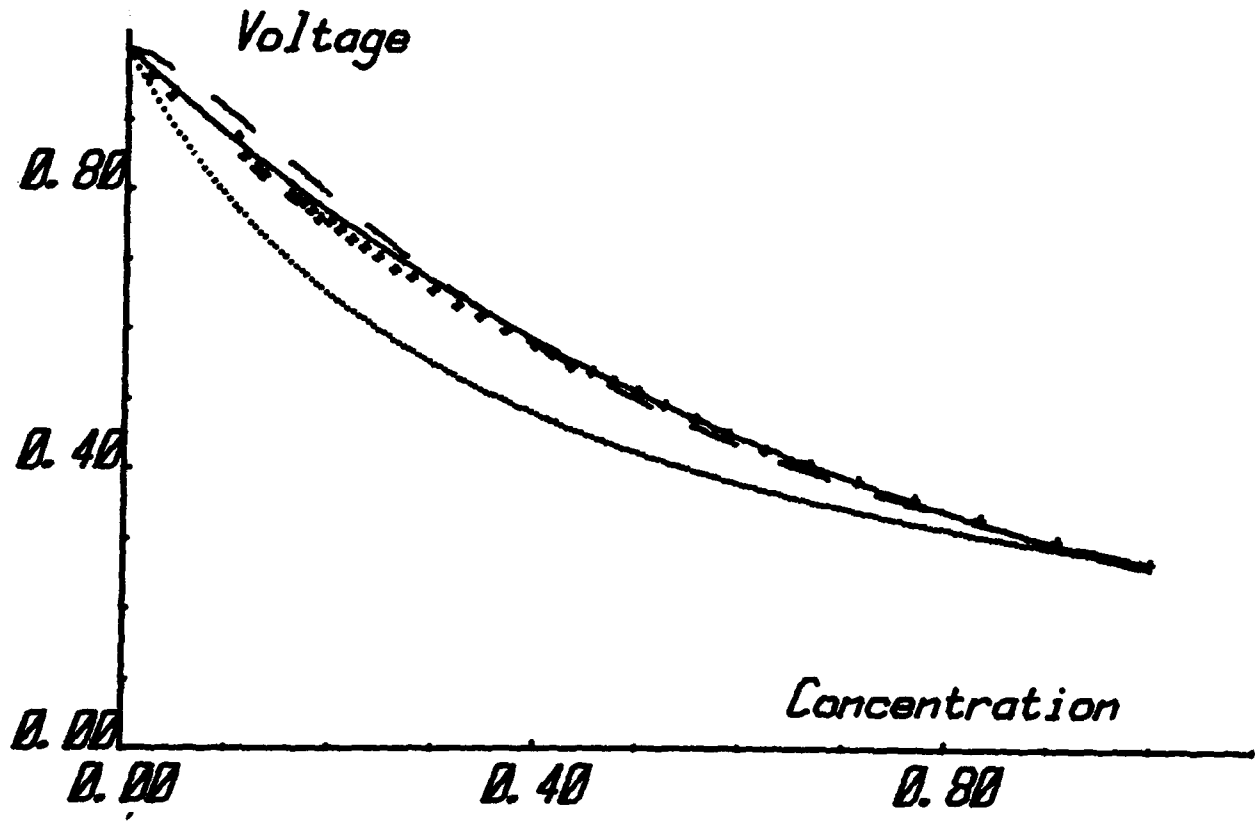

Duranol blue dimensionless calibration plot of voltage versus concentration. The crosses show the experimental points, the solid line is the best fit exponential, the dashed line is the best fit power law and the dotted line is the best fit hyperbola.

Figure 6.5

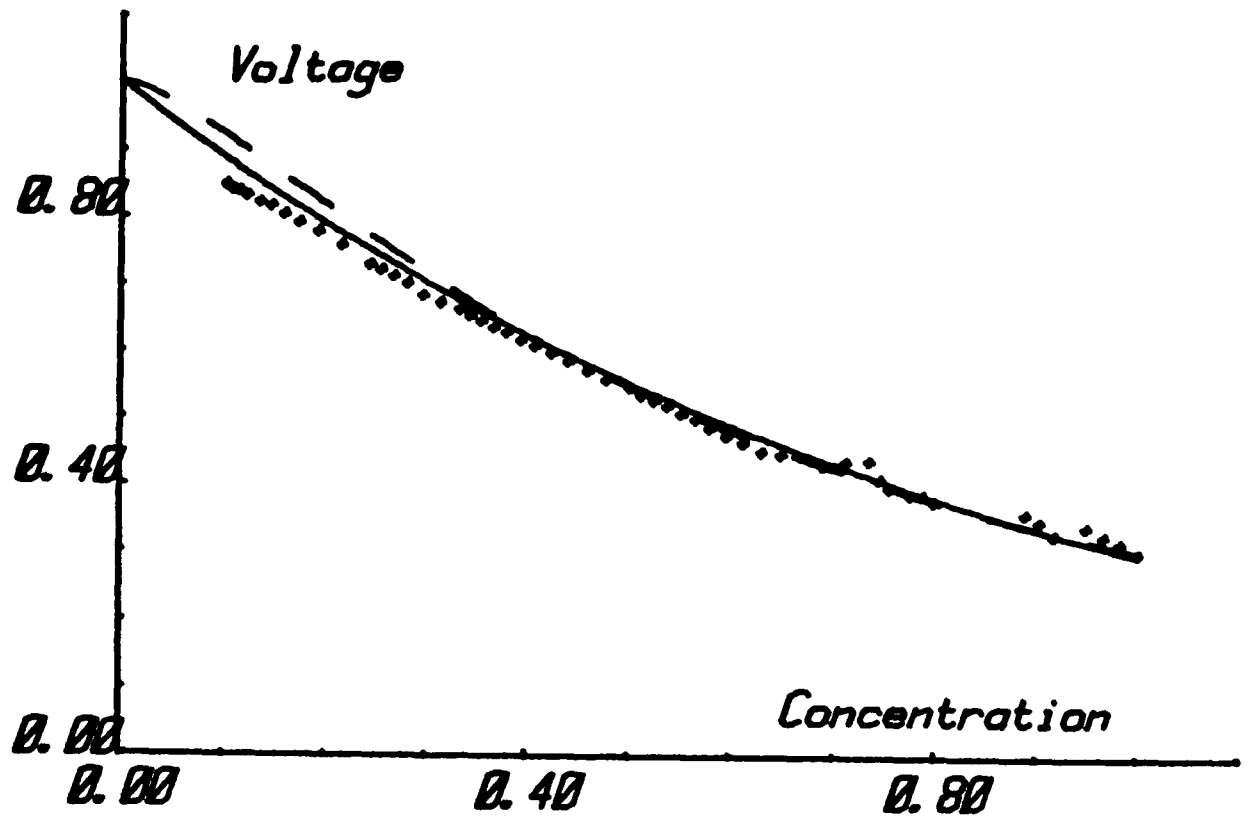

Calibration points (for Alizarin Cyanine Green dye) on a plot of dimensionless voltage versus dimensionless concentration. Best fits of exponential (continuous line) and power law (dashed line) curves are also shown.

Figure 6.6

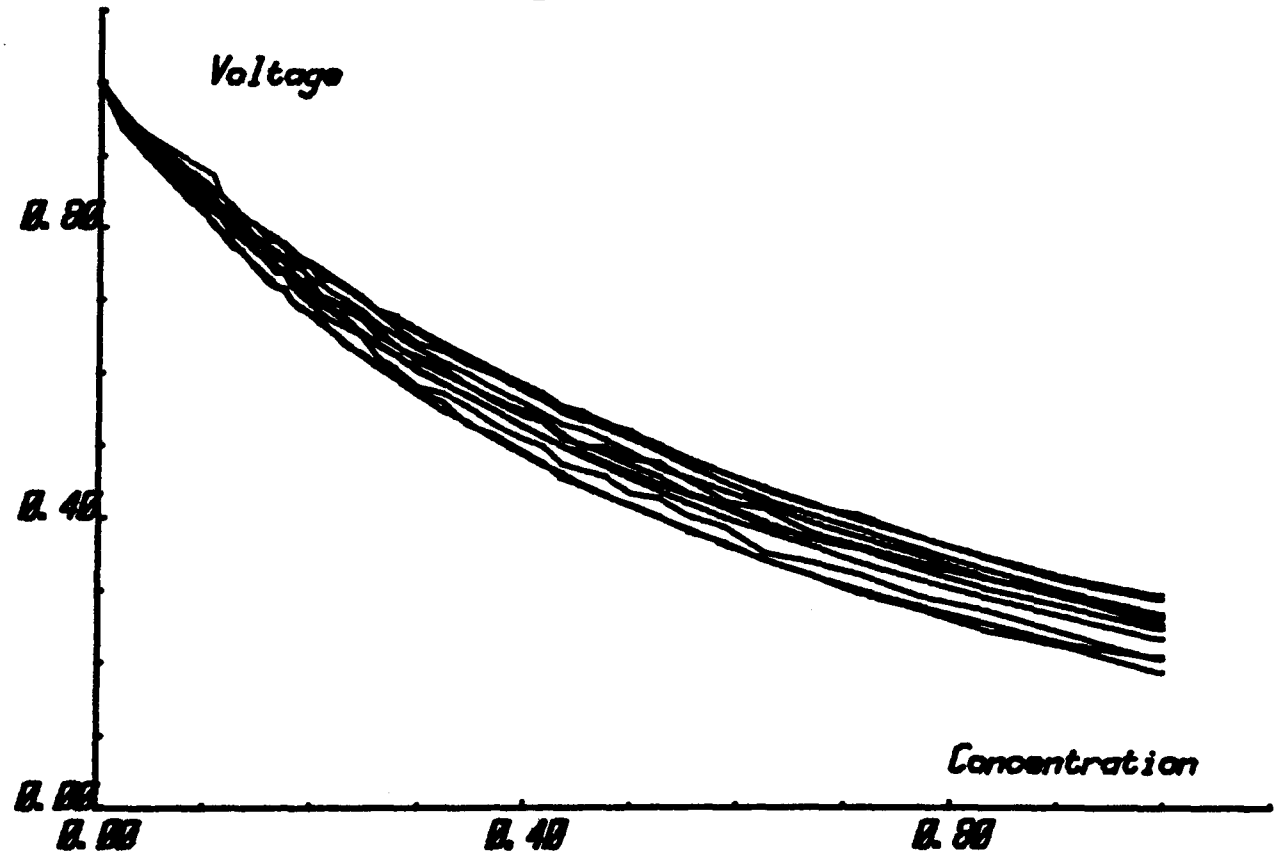

Calibration plot (for Duranol Blue dye) of dimensionless voltage versus dimensionless concentration showing data from all the calibrated gauges. Straight lines connect the data points obtained from a particular gauge.

Figure 6.7

6.5 CHANNEL DIMENSIONS AND CONSTRUCTION

A flat channel having a height of 1mm and a breadth of 90mm has been made up. This cross-section was chosen so that an aspect ratio of roughly 100 could be achieved, while at the same time a cross-sectional area ($90mm^2$) could be used which was not so large or so small as to make pumping difficult. The channel length (2.5m) has been made rather large for two reasons. Firstly, use of a long channel ensures that entry length effects are unlikely to be significant, and secondly it is possible that this apparatus may be used to measure dispersion in a furrowed channel; this would involve much larger dispersion coefficients and necessitate use of a long channel to contain the rapidly spreading dye.

The working section of the channel is bounded by sections of .75m length. We may use the theoretical predictions of Mohanty and Asthana (287) to demonstrate that entry length effects should not be significant with this length of settling section. If we assume that the hydraulic diameter of the channel is 2h, then Mohanty and Asthana predict that, at a distance x downstream of entry, the centre-line velocity will have attained at least 99% of its fully developed value if

$$0.15 < \frac{x}{2hRe} = 1.875 \quad (6\text{-}1)$$

for Re = 200, h = 1 x 10^{-3}m, x = .75m. We may thus regard the flow as being fully developed.

The structure consists of an aluminium alloy frame in three roughly equal lengths. A molded 'silcoset' seal was placed at the junction of each section and the whole was supported by raisable legs which were adjusted so as to produce a perfectly level path

for the fluid (see figure 6.8). Within this metal structure runs a rectangular hole with dimension 10mm x 100mm. Inside the gap of each section, an upper and a lower polished perspex insert were placed. These inserts left a 1mm x 90mm channel within the framework. The cross-section was uniform along the length of the device, but the use of the cheap and replaceable perspex sleeves may enable future investigations to study the effect of furrowed channels by simply making up a new set of inserts.

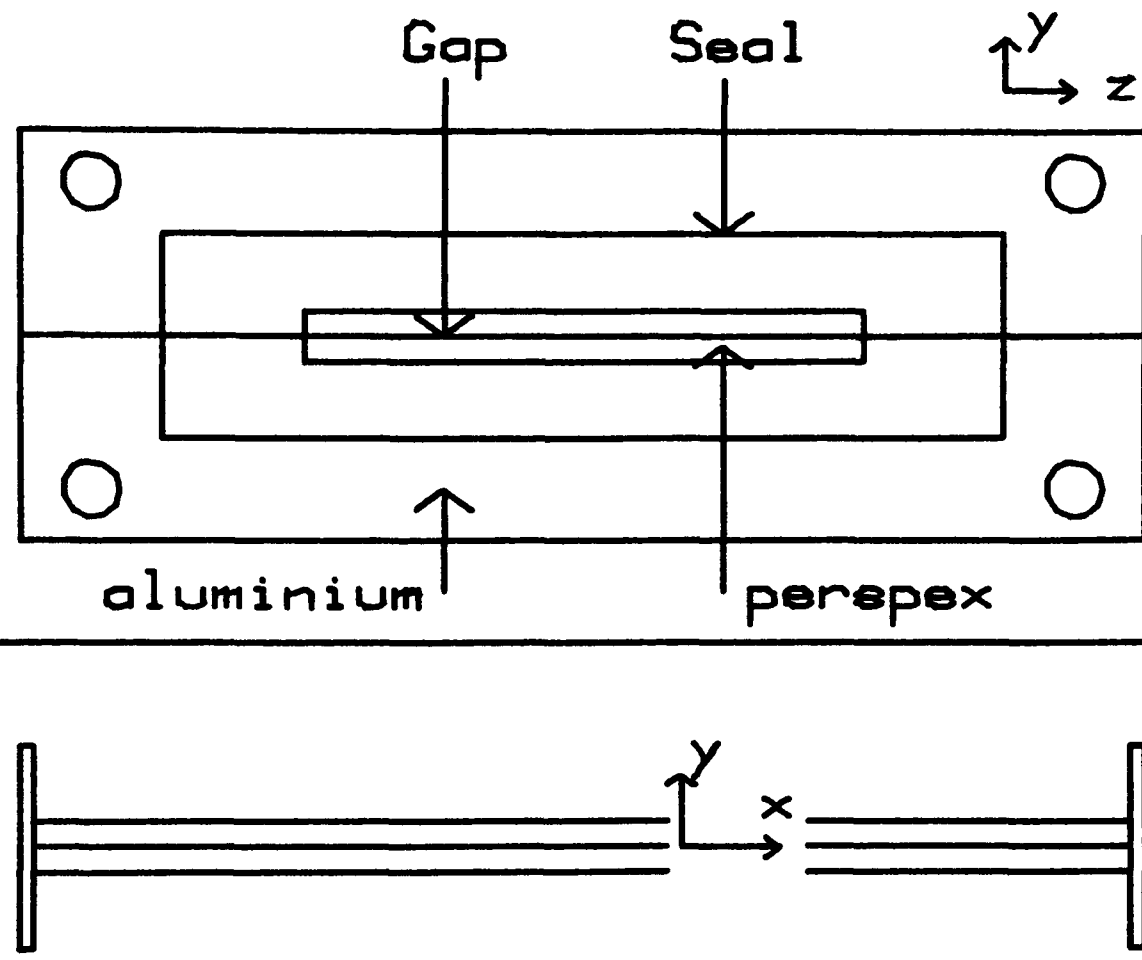

Diagram showing the end plates and one section of the channel.

Figure 6.8

At one end of the channel (henceforth referred to as the pump end) a pump was situated, capable of delivering channel half-strokes of up to 100mm at frequencies of up to 5Hz (see section 7.3). At this end of the channel, the rectangular cross-section was faired to one of circular form. A supply pipe of $\frac{1}{4}$ inch bore lead from in front of the piston to the water supply

enabling the channel to be filled easily. This line could be shut off using a "Saunders" $\frac{1}{4}$ inch "A-type" diaphragm valve. An air bleed was sited directly in front of the limit of movement of the pump piston head and a three way valve was also attached so that surfactant detergent or saline solutions could be injected into the channel (see figure 6.9). At the opposite end of the channel (henceforth referred to as the reservoir end) was a reservoir of dimensions 165x190x140 mm. This enabled a back pressure of up to about 140mm of water to be applied down the channel length.

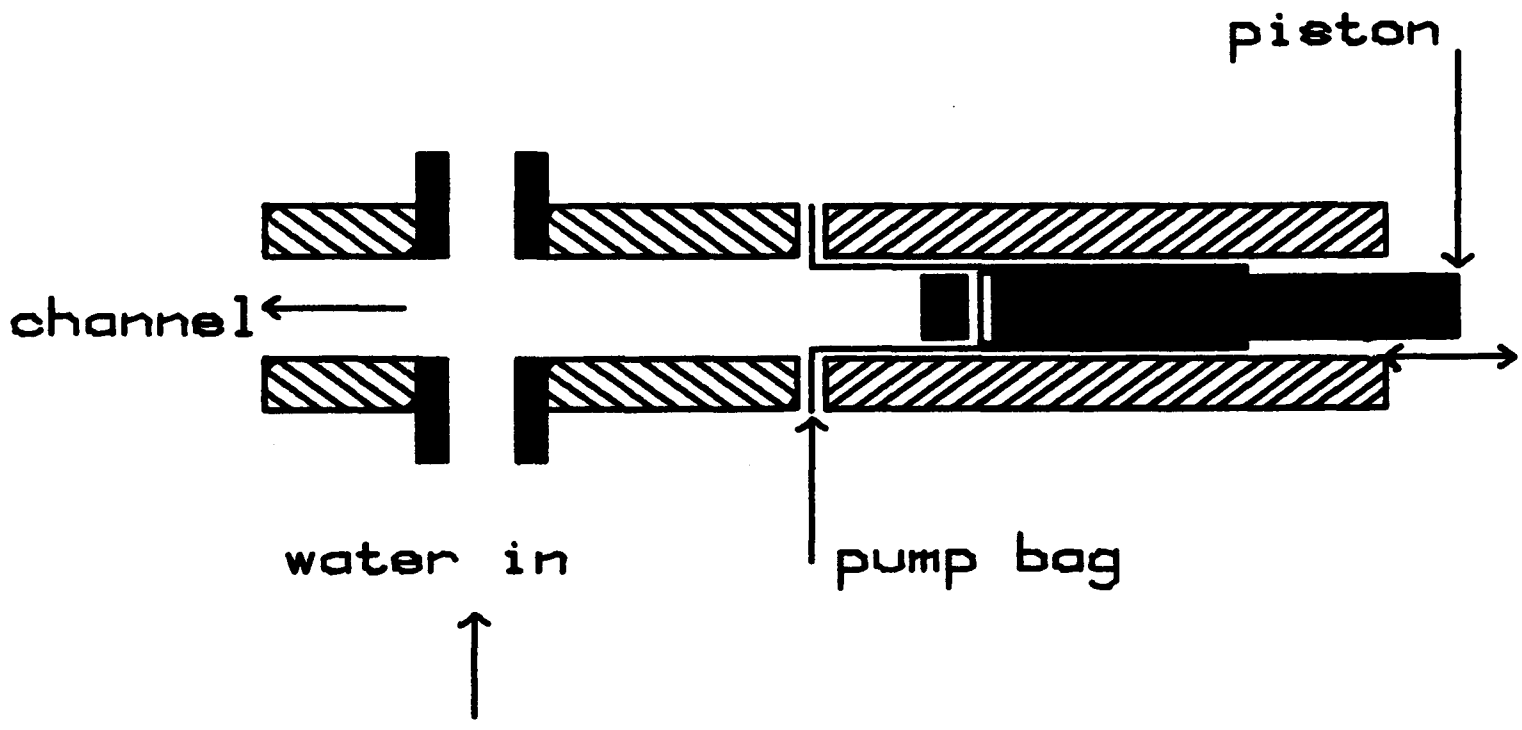

Diagram showing the pump bag and piston.

Figure 6.9

6.6 PUMPING ARRANGEMENTS

The pump which has been used to provide the oscillatory flows uses a simple crank shaft and flywheel mechanism. The crank arm may be moved up and down the flywheel to give a pump half stroke at the piston head of between 0 and 50mm. The frequency may be adjusted by a 'Parvalux' controller enabling frequencies of 0.3 up to 5Hz to be applied. The pump frequency was measured using a Hall effect switch which rotated with the motor shaft and activated a stationary sensor which it passed once every cycle. The time separation between successive signals was measured and in this way the period was determined. The stroke was measured by attaching an arm to the piston shaft. This arm was then connected to the plunger of a (solenoid) displacement transducer. A 5v bias was put across the windings so that a measurement of the peak to peak sweeper voltage enabled the stroke to be deduced.

It was considered to be important to not only log the opto-electronic gauge voltages, but to also sample the velocity in some way, so as to be sure of the time phase of the readings. This was achieved by feeding the displacement transducer voltages into the data-logger. Such a facility was useful since it meant that in addition to detecting the phase of the signals, one could also measure the pump stroke and frequency very accurately by analyzing the piston head position data.

The chief difficulty encountered in providing an oscillatory flow down the channel was the question of how to seal the piston head so that there was no leak of water past it. Initially, the simple approach of attaching a tight-fitting washer to the circular piston head was used. During the first hundred cycles, this

performed adequately, but as it was used more and more, the washer wore out and despite the use of grease to aid sealing, a very significant back flow developed. Frequent replacement of the washer was very tedious and ultimately of little avail. The second solution was to make a "biomer" rubber pump bag and screw this onto the piston head with a washer being included to prevent the bag from ripping. This makes back flow impossible but does require there to be a large head of water at the reservoir end. If this is not the case, then the pump bag will not inflate fully and will effectively result in one not obtaining the full stroke volume. A 140 mm head of water could be imposed by filling up the header tank at the reservoir end of the channel and simple calculations indicated that for the oscillatory flows which would be imposed, this pressure would exceed the pressure drop down the channel and therefore enable the pump bags to remain inflated. There are two further solutions to this problem which would have been used had the single pump bag method not been successful. One could have arranged to have a pump bag and piston at each end of the channel with a tie rod connecting the two mechanisms ensuring equal displacements. An alternative procedure would have been to use a metal bellows chamber at the pump end. The first of these approaches is somewhat impractical over a $2\frac{1}{2}$m long channel and the bellows method has the disadvantage that there is some uncertainty in the effective stroke one is imposing.

6.7 PRECAUTIONS TAKEN TO EXCLUDE AIR FROM THE SYSTEM

It is critical that when we are observing the dispersion of a contaminant within the system, there should be no small air bubbles in the channel. Such bubbles are undesirable since they may affect the velocity distribution if they are large enough and, more importantly, if a bubble moves in between a pair of the sensors, it will cause a significant amount of light absorption and lead to concentration readings which may be greatly in error. In order to exclude air from the system, water was flushed from the tap into the channel at the pump end and siphoned away at the reservoir. When small bubbles ceased to appear in the reservoir, the tap at the pump end was shut off and 10ml of a surfactant detergent (10g/litre Sodium Lauryl Sulphate) solution were injected into the channel. A slower flow was then sent into the channel and this dislodged all of the fine bubbles which had ahdered to the walls. The final step was to open up the bleed holes and remove the last air pockets that remained.

6.8 DYE INJECTION MECHANISM

In order to be able to introduce a slug of dye into the channel, a housing was attached half-way along the 2.5m long channel on its upper side. This device consisted of a hollow metal cylinder of 20mm diameter down the length of which a 1mm wide slot was milled. This cylinder was then inserted into a sleeving with a small radial clearance. The sleeving did not completely surround the inner cylinder but formed an arc around it. Circular end plates were attached to the inner cylinder making it possible to turn it within the sleeving. A 1mm diameter hole was drilled into

the centre of one of the end-plates and a three-way valve attached. Along the top of the sleeving four bleed holes (sealable using OBA bolts) were introduced. This mechanism enables one to introduce dye into the cylinder through the three-way tap, at the same time expelling the air through the bleed holes. When dye starts to seep out of the uppermost holes, then the cylinder is full so the tap is closed and the bleed holes are screwed shut (see figure 6.10).

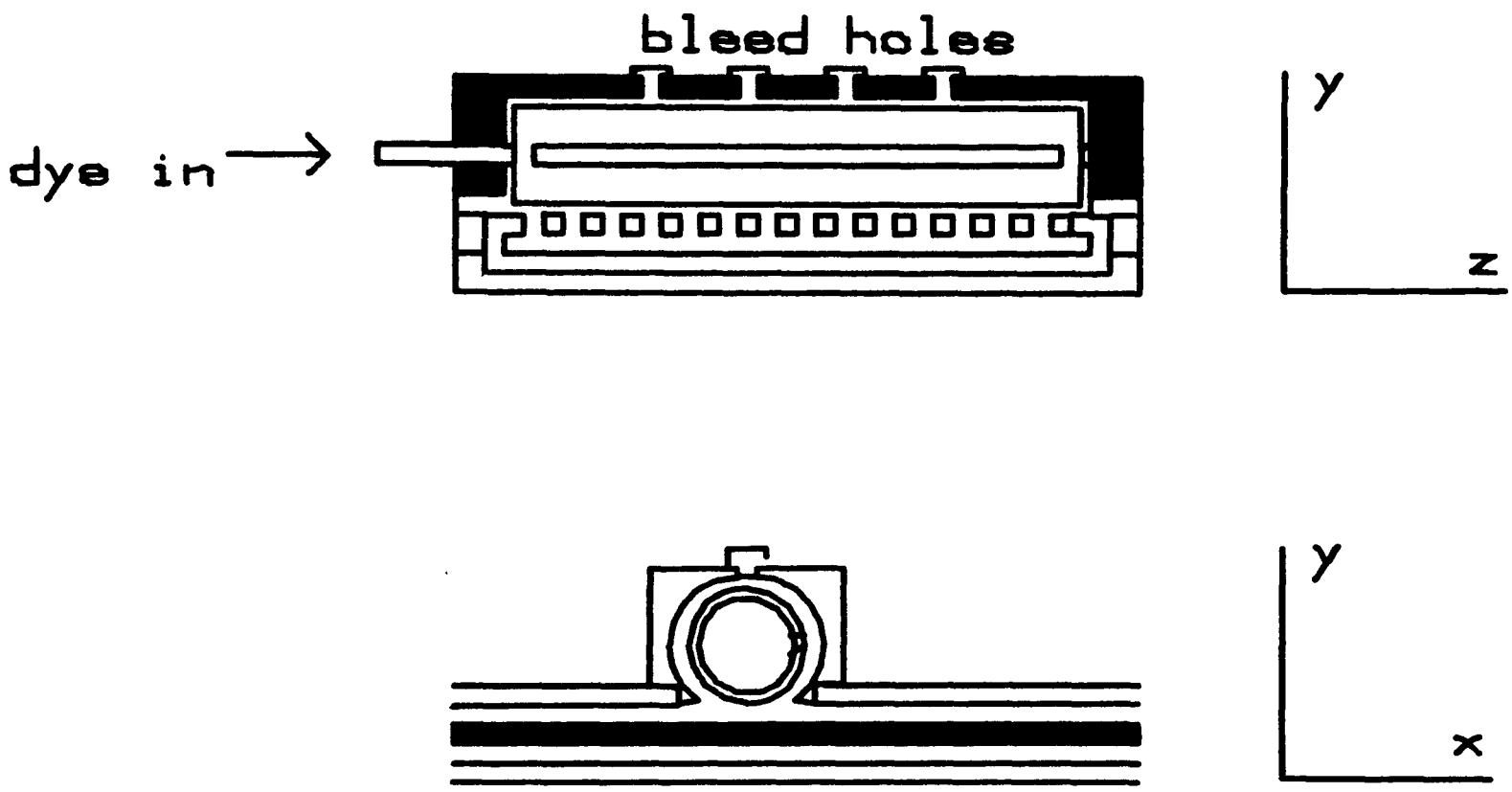

Illustration of the dye injection mechanism

Figure 6.10

At the axial position on the channel where the injection mechanism was to be sited, a rectangular slot was milled across the aluminium channel and six screw holes were drilled in the aluminium frame. A seal was placed on the underside of the injection housing which could then be screwed down onto the channel bed. The final stage in the construction of the device was to drill a series of closely separated 0.5mm diameter holes straight through the perspex

inserts across the entire 90mm width of the channel.

In order to inject a slug into the channel, the following operations were carried out. Firstly the inner cylinder was rotated in its housing until the slot was uppermost. The cylinder tap and the upper bleed holes were then opened and the dye stock was placed into the mechanism in the manner described above. The tap and bleed holes were then closed and a graduated syringe was filled with a quantity of the dye which was dependent upon how large a slug was to be introduced. When this syringe was attached to the tap, the latter was opened and the cylinder rotated so that the slot was aligned with the row of holes in the perspex inserts. By depressing the syringe piston, a controlled volume of dye could be introduced into the channel and the cylinder then rotated to prevent further leakage of the stock in the cylinder into the channel.

Injection of this extra volume of liquid into the system necessitates displacement of fluid elsewhere. The main way this is achieved is by slightly raising the level of the water at the reservoir end. This of course means that the injected slug does not lie symmetrically about the point of injection, but rather it is be displaced so that its leading edge lies just in front of the injection holes. The only problem that was encountered in the operation of this system was that when the reservoir was filled high, there was a tendency during the priming operation for water to seep into the mechanism by leakage in between the cylinder and its housing. This was prevented by packing the radial gap with grease and periodically renewing the seal when it failed. It is unrealistic to suppose that this injection scheme should produce a

perfectly uniform slug. The concentration variation across the y and the z directions is likely to be relatively small, but there was undoubtedly some variation with x, especially near the ends.

6.9 LOCATION OF THE OPTO-ELECTRONIC GAUGES

The gauge pairs which have been described in chapter 6 were mounted at various axial positions adjacent to the channel centre-line. For each component a housing was made up to hold it firmly in place. This consisted of a small block of aluminium 1 inch sqaure and $\frac{1}{4}$ inch deep. A hole was drilled straight through the centre of the face of this block and the opto-electronic device was cemented into the hole using an epoxy resin adhesive. The end of the gauge protruded 2mm beyond the base so that when the block was mounted in position over a specially drilled hole in the aluminium plate, the face of the device was flush with the perspex insert. The following gauge locations were chosen with distances being expressed in mm from the centre of the injection mechanism

±200, ±120, ±100, ±80, ±65, ±40, ±25

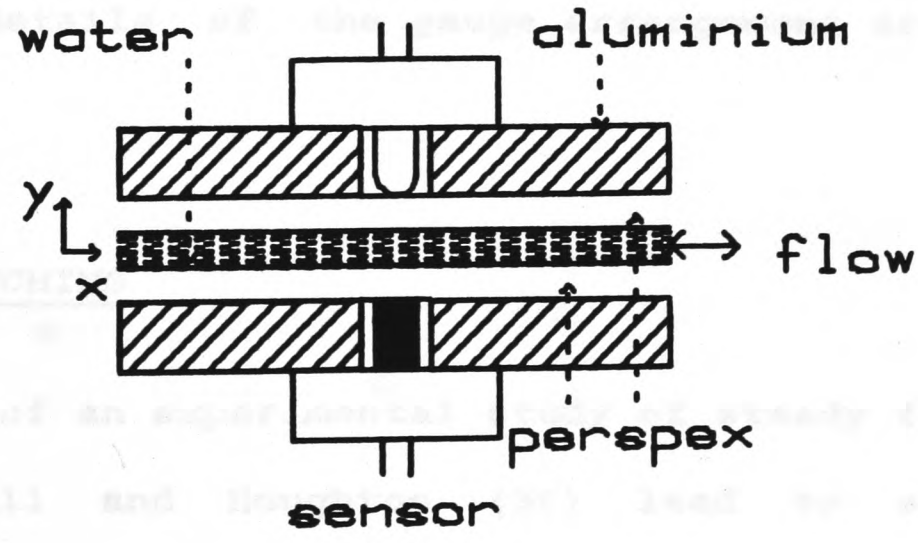

Diagram showing the gauge mounting assembly.

Figure 6.11

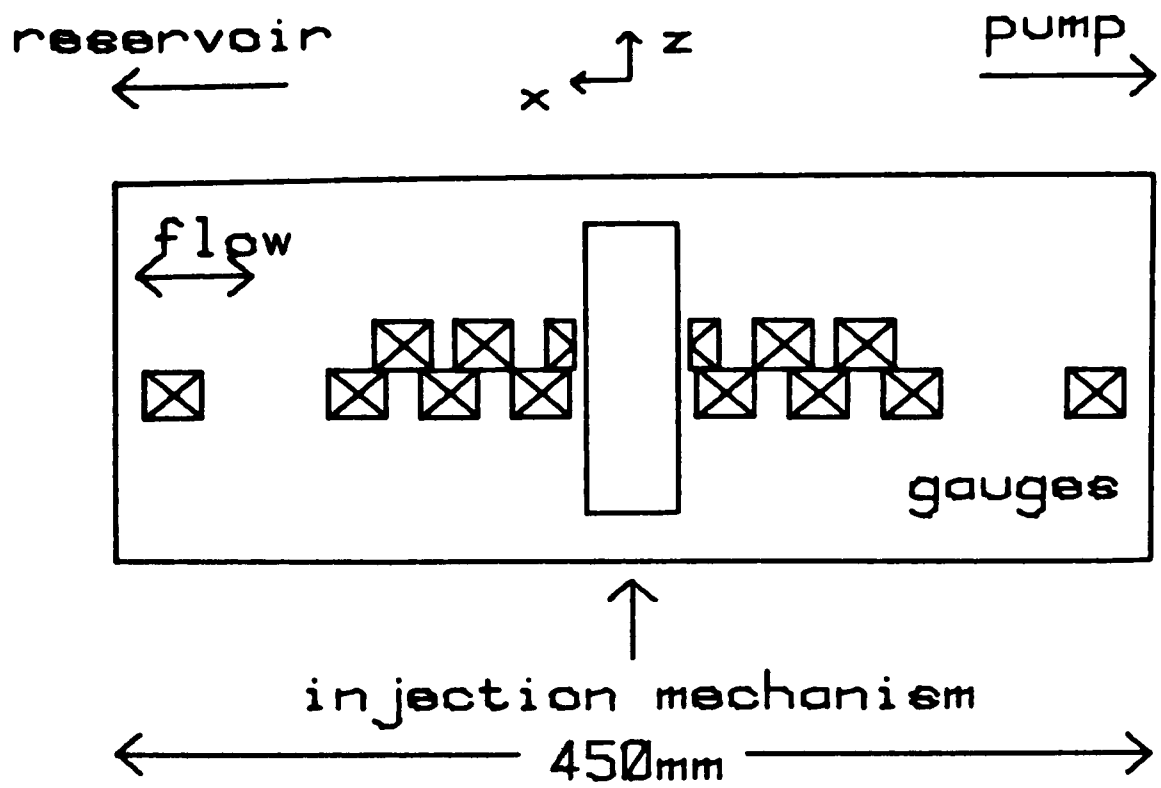

Diagram showing the gauge locations on the central section of the channel

Figure 6.12

There was a limit as to how small the distance of a particular gauge from the injection device could be made due to the finite width of the injection housing itself. The beams from the concentration sensors were not directed over the centre-line of the channel but were instead offset by 12.5mm to allow a closer gauge spacing. The details of the gauge arrangement are indicated in figure 6.12.

6.10 DENSITY MATCHING

The results of an experimental study of steady flow dispersion by Bournia, Coull and Houghton (35) lead to some misleading conclusions. Their data indicated that the dispersion coefficient predicted by the Taylor-Aris theory was too small for low Peclet numbers. A subsequent numerical and experimental study by Reejsinghani, Gill and Barduhn (181), however, showed that the BCH

experimental work was in error. The cause for the discrepancy was shown to be the influence of natural convective effects upon the dispersion process. Reejsinghani et al went on to state that the natural convection would be important if

$$\frac{\Delta\rho}{\rho} > 10^{-4} \quad (6\text{-}2)$$

where ρ is the density of the solvent and $\Delta\rho$ is the difference in density between the solvent and the solute. There is a potential for such effects to be critical in the dispersion experiments described in this study, since the specific gravity of a 50g/l Duranol Blue solution has been measured with a density bottle to be 1.0194. In order to minimize this effect, the specific gravity of the channel fluid has been matched to that of the dye solution. A saline solution of concentration 26.500g/l was made up and the difference between the specific gravity of this solution and that of the tracer was found to be about 2×10^{-5}. Before the dye was injected, 350ml of this saline solution were therefore flushed into the channel so that the contaminant was indeed neutrally buoyant. As an alternative assurance of this, we may evaluate the mass transfer Grashof number ($=\Delta\rho\ g\ h\ h^3\ /\ \rho\ \nu^2 = 2 \times 10^{-5}$) and use the results described by Holman (288). For the mean flow Reynolds numbers used in this study, the results of Holman also indicate that natural convection ought not to be a problem.

6.11 SOURCES OF ERROR IN THE DISPERSION EXPERIMENTS

6.11.1 Slug Malformation

Probably the main inadequacy of the experiments is the failure to inject a perfectly uniform slug. The slug is likely to be more dilute at the ends than at the centre. In addition there may be a small initial concentration gradient in both the z and the y-directions. The fact that the slug one creates is not identical to that modelled theoretically need not be a serious limitation if one aims to determine the dispersion coefficient alone. Direct comparisons of theoretical and experimental breakthrough curves are however, less likely to give good agreement since the form of such plots is determined to a large degree by the intial conditions.

6.11.2 Dependence On Diffusion Coefficient

Throughout the theoretical work, it has been assumed that the diffusion coefficient was independent of solute concentration. Perry (277) states that this assumption is valid for dilute solutions. However, Taylor's (233) steady flow determination of the diffusion coefficient from dispersion studies indicated that the diffusivity of potassium permanganate solution varied most for dilute solutions. It is possible though that this conclusion may be true only for a limited range of concentrations of that particular solvent.

If we wish to compare the experimental measurements of the dispersion coefficient with theoretical estimates, it will be necessary to know the value of the diffusion coefficient. Perry (277) describes an equation with which one may estimate K from a

knowledge of the molecular structure of the solvent. For the case of Duranol Blue, this yields $\kappa = 0.5 \times 10^{-9}\ m^2 s^{-1}$. It was felt that experimental determination of κ by the methods described by Taylor (233) would be unsatisfactory. If the 2-D aprroximation had been an important shortcoming, it would have affected the measured values of both diffusion and dispersion coefficients and the effect might not have been observed.

6.11.3 Tendency Towards The Asymptotic Forms

When calculating a dispersion coefficient from the experimental results we shall assume that the 2-D Taylor asymptotic stage has been reached but that sufficient time has not elapsed for the three-dimensional asymptotic description to be applicable. For this to be the case (see appendix 2), measurements should be made close to the centre-line and the experiment should be continued for times of order at least 30 seconds. It does not seem to be practical to investigate the Chatwin-Sullivan 3-D stage of the flat channel dispersion process since, by the time the dispersion behaviour conforms to this description, the channel concentrations would be so small that there would be a considerable difficulty in measuring them accurately.

We suppose that the impulsive starting of the pump does not greatly affect the results for the times of interest in this study (see Gill, Ananthakrishnan and Nunge (107)). Entry length effects are also expected to be small since the section of the channel in which the slug is moved is far from either end of the duct.

6.12 SUMMARY OF EXPERIMENTAL PROCEDURE

In order to measure the mean cross-channel concentrations with the apparatus described above, the following procedure was carried out. The channel was first filled with water and the air bubbles expelled using the methods described in section 6.7. The pump piston stroke and frequency were set using the position transducer and Hall effect switch described in section 6.6 and these results were then checked by feeding the transducer voltages into the data-logger and analysing the signal. In order to ensure that the pump phase was correct (see chapter 5) the flywheel was positioned so that the piston was at the extreme of its travel. The channel was next flushed with the density matched saline solution and the dye injection mechanism was primed. Finally, the dye was injected into the channel and the pump switched on. In between successive experiments, care was taken to completely flush the channel out with clean water. This was important if the sodium chloride solution was not to scale the channel. Also, this washed out the dye which might have otherwise affected the gauge readings in the next set of observations. The results obtained using these experimental methods are described in chapter 7.

6.13 INVESTIGATION OF A MASS TRANSFER DEVICE

A cell has been made up (see figure 6.13) which will hold the infra-red source and sensor in place. The beam produced by the LED is directed across a perspex tube with a bore of 1cm. This cell was then plugged onto the outlet pipe of a blood oxygenator which is being developed by Bellhouse et al (see the description of this device in chapter 1). This mass transfer reactor may be studied

empirically using an approach described by Danckwerts (71) in which a slug of some tracer is injected into the inlet stream and its concentration is measured at the outlet as a function of time. To accomplish this, the cell was initially calibrated using a technique similar to the one described in section 6.3. The oxygenator was set up to deliver water with a mean and an oscillatory component and the cell was then placed in the outlet stream. 60 ml of Duranol Blue (concentration $\frac{3}{50}$ g/l) was injected into the inlet of the device and the pumps were then turned on. The gauge response was followed by a chart recorder until the concentration reading had fallen back down to the water level. The results of this study are given in the next chapter.

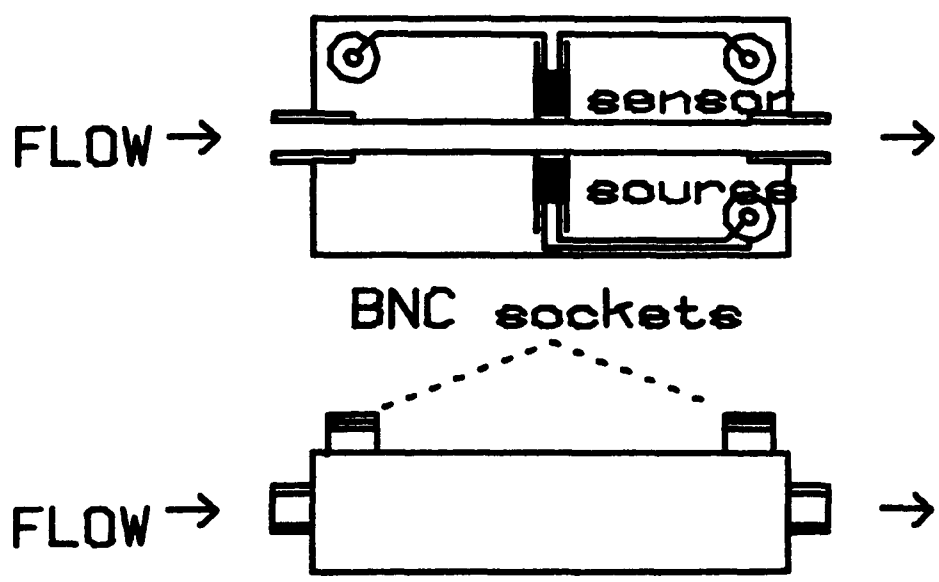

Diagram showing the in-line device used to measure the dispersive behaviour of a furrowed channel blood oxygenator or other continuous flow mass transfer device.

Figure 6.13

Chapter 7

EXPERIMENTAL DISPERSION RESULTS.

CHAPTER 7

EXPERIMENTAL DISPERSION RESULTS

7.1 INTRODUCTION

The results of the experiments described in chapter 6 are presented in this chapter. A description of the empirical observations of the dispersion process within a vortex mixing channel is set out and the dependence of the dispersion coefficient upon frequency and stroke is deduced. The experimental results obtained from the study of oscillatory flow dispersion in a flat channel are then presented. Neither of these two experimental results may be meaningfully compared to the work of Joshi, Kamm, Drazen and Slutsky (284). These authors have recently been pursuing an experimental study of dispersion in tubes bearing an oscillatory flow of gas. The Schmidt numbers characteristic of such a system are of order 1 so that the concentration evolution is approximately quasi-steady for pulsatile Reynolds numbers of order unity. The present studies, however, are far removed from this regime, the Schmidt number being 2000. The concentration evolution is therefore far from quasi-steady (see the results of, for example, Watson (256) or Holley, Harleman and Fischer (121)).

7.2 DISPERSION IN A FURROWED CHANNEL OXYGENATOR

The slug dispersion measurement scheme described in section 6.13 was used to investigate the dispersive behaviour of a furrowed-channel, permeable membrane† blood-oxygenator. Typical examples of the output produced by the gauges are shown in figure 7.1. Curves such as these have been obtained for six frequencies in the range 1→6 Hz, three strokes in the range 4→15 mm and three mean flow rates in the range 122→440 ml/min for various combinations of steady and oscillatory flows.

† Note that the channel walls were permeable to oxygen but impermeable to the dye and the solvent used was water, not blood.

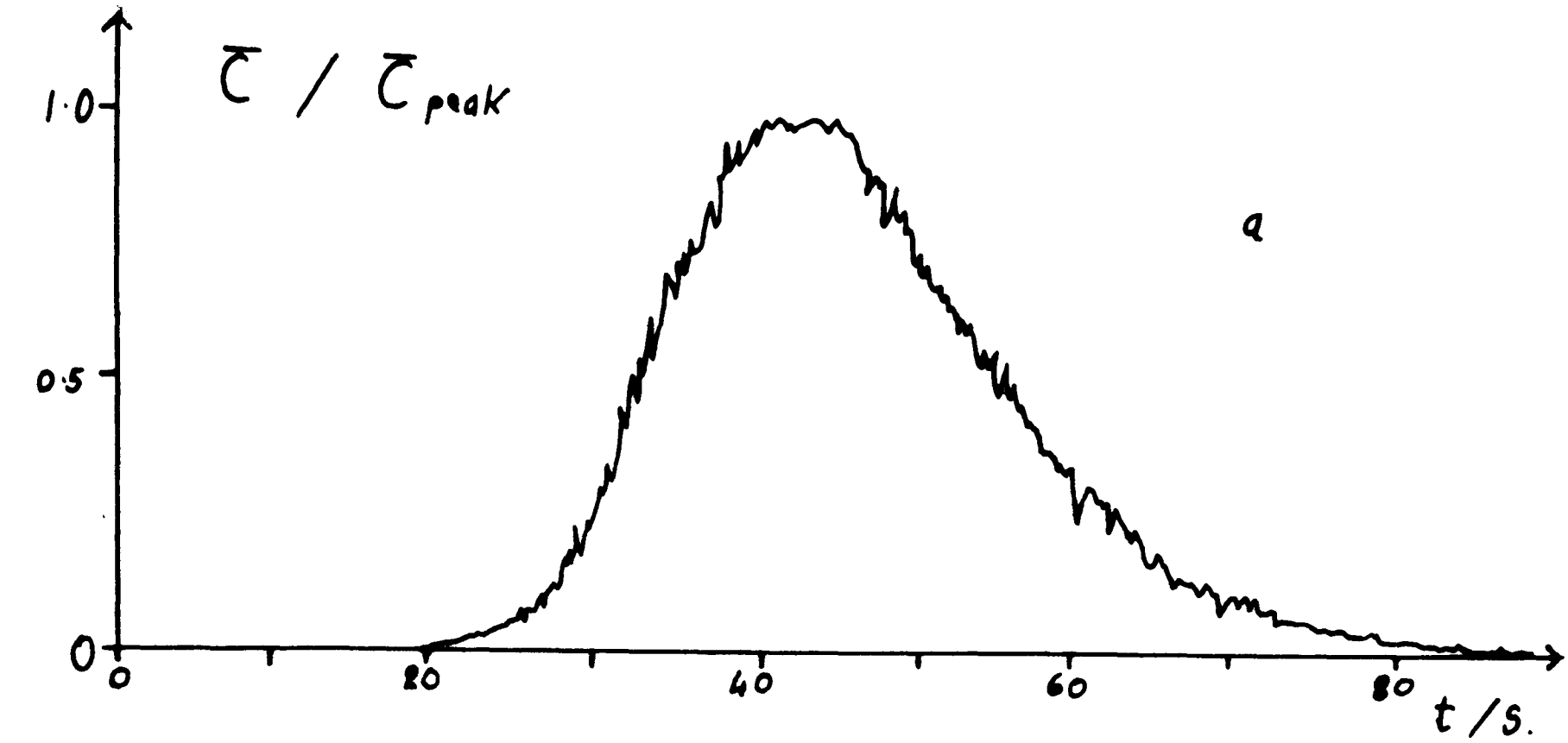

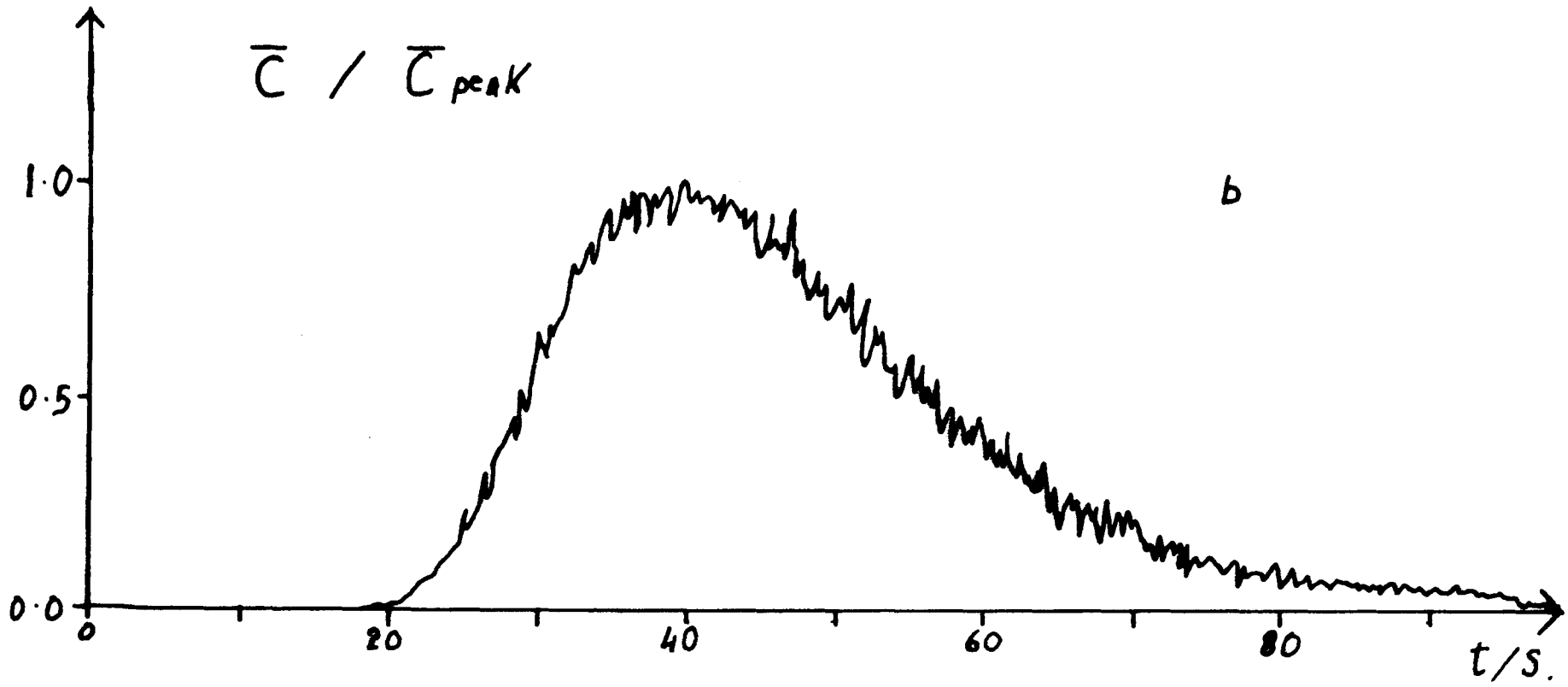

Examples of concentration readings against time as a slug of Duranol Blue leaves the furrowed channel blood oxygenator.

a/ a = 7.5 mm f = 2 Hz Q = 424 ml/min.

b/ a = 7.5 mm f = 3 Hz Q = 424 ml/min.

Figure 7.1

We may obtain a quantitative summary of the rate at which axial spreading of the contaminant is taking place by measuring the time for which the concentration reading is greater than half its peak value for that particular set of run conditions. This is effectively a time bandwidth of the pulse response curve. If we assume that half of this quantity ($\hat{t}$) is approximately equal to the standard deviation of the concentration versus time curve then, following Levenspiel (273), we relate $\hat{t}$ to the dispersion coefficient D, by the expression

$$\hat{t}^2 = \bar{t}^2 \frac{2D}{UL}, \qquad (7\text{-}1)$$

where we use the following notation:

$\bar{t}$ = time (after injection) taken for the $\bar{C}$ reading to reach a maximum,

U = bulk speed of channel fluid,

D = effective dispersion coefficient,

L = distance of gauge from the injection point.

The experimental results obtained for $\hat{t}$ are shown in table 7.1 These values correlate very well with the equation

$$\hat{t} = B' Q^{-1.05} s^{0.19} f^{0.23}, \qquad (7\text{-}2)$$

where B' is some constant.

Alternatively we may replace this expression by one which is approximately equivalent,

$$\hat{t} = B Q^{-1} Re^{0.2}, \qquad (7\text{-}3)$$

where $B = 1.7 \times 10^{-4}$ for $\hat{t}$ in seconds and Q in ml/min.

We may relate U to parameters we know by using the expression,

$$U = \frac{LQ}{V}, \qquad (7\text{-}4)$$

where V is the volume of liquid between the injection point and the measurement point (in the case of the readings given in table 7.1 this was 472 ml).

We may eliminate U from equation (7-1) using (7-4) and substitute in the empirical expression for $\hat{t}$ given by equation (7-3) to obtain the following empirical expression for the dispersion coefficient,

$$D = \frac{Q}{2} (L\ B)^2\ Re^{0.4}\ V^{-3}. \qquad (7\text{-}5)$$

This equation indicates that the dispersion coefficient is very large. At a forward flow Reynolds number of order 100 and a mean flow rate of 300 ml/min (values typical of those used in an oxygenator), the dispersion coefficient predicted by the empirical relation given in (7-5) is 1.9×10^{-3}, i.e. a factor of four million times as large as the diffusion coefficient. As Sobey (221) has pointed out, it is the Peclet number $\frac{UL}{D}$ † which determines how large a deleterious effect the presence of dispersion has upon the transverse mass transfer efficiency. Thus, to predict the effect on dispersion of changing the various flow parameters, we should consider the value of $\frac{D}{Q}$. Equation (7-5) indicates that this parameter is independent of Q, the mean flow rate down the channel, at least for the range of flows normally used. The large oscillatory flows therefore cause a very significant spreading of a contaminating slug. These are features of flows which are well mixed laterally, since a poorly mixed flow (for example one with a parabolic velocity distribution) would be

† here U is the steady flow bulk velocity and is proportional to Q.

quite critically affected by the steady flows which cause a long term distortion of the slug down the channel. This expectation is confirmed by the results of Aris (10) who used a method of moments to calculate the effect of flow oscillations upon his basic steady flow work; he concluded that the effect was usually small. The important difference between Aris's study and the experimental model we consider here is the large effect of secondary flows (due to the oscillations and the furrows) upon the mass transfer processes. It may be that, under certain circumstances, the very large dispersion coefficients associated with the vortex mixing principle provide a more critical limit upon the outlet concentrations than does the transverse transfer efficiency. It is certainly not the case that dispersion is only important when the stroke is larger than the device length.

The dye measurement technique has therefore given us an inexpensive set of apparatus which is easy to use and from which useful empirical predictions may be obtained.

S (mm)	f (Hz)	Q (ml/min)	$\hat{t}$ (s)
-	-	122	32.8
-	-	270	15.2
-	-	440	8.4
4.0	1.0	270	16.1
4.0	2.0	270	16.6
4.0	3.0	270	18.4
4.0	4.0	270	20.9
4.0	5.0	270	22.6
4.0	6.0	270	23.9
7.5	1.0	424	10.2
7.5	2.0	424	11.4
7.5	4.0	424	13.2
7.5	5.0	424	13.9
7.5	4.0	280	25.8
7.5	4.0	122	51.8
15.0	1.0	270	21.1
15.0	2.0	270	24.8
15.0	3.0	270	25.6
15.0	4.0	270	25.7

Table showing the outlet concentration pulse half-width (secs) variation for different strokes, frequencies and flows through a furrowed channel blood oxygenator.

Table 7.1

7.3 EXPERIMENTAL RESULTS OF FLAT CHANNEL DISPERSION

7.3.1 Treatment Of Data

The general form of the breakthrough curves measured from the oscillatory flow flat channel dispersion experiments described in chapter 6 are in agreement with the summary of the numerical predictions described in section 5.3. The responses of the gauges closest to the injection site have been found to be the most useful. This is because sensors which are far from the injection mechanism do not detect high concentration levels until the experiment has been run for a long enough time for the slug to have been well dispersed along the channel. At this stage, the interesting peaks in the concentration readings due to movement of the slug along the channel have been very nearly damped out. For this reason, the observations made in this section will concentrate upon conclusions drawn from the ±25 and 40 mm gauge positions.

For all the experiments, slugs of 22 mm length were injected and, on account of the layout of the apparatus, the slug would ideally initially lie such that the ends were at 0 and -22 mm. This means that there may effectively be an 11 mm shift of the gauge positions, so that the -25 mm gauge could be -14 mm from the slug centre. The -25mm gauge therefore lies 3mm from the ideal upstream end of the slug. In reality, the slug diffuses as it is injected and eddying during the injection process also causes a premature spreading. The level of the initial concentrations which the -25 mm gauge detects therefore gave an indication of how poorly one end of the slug is formed. Typically (see figure 7.2) the initial reading of the gauge lay between 0.2 and 0.5. Since we are measuring a mere 3 mm from where we would ideally wish for an

infinite concentration gradient, this is a very reasonable result. However, we cannot be certain how far the slug has spread towards the pump end of the channel.

The main aim of the experiments is to determine the dispersion coefficient. One possible method would be to compare the concentration readings from the gauges at a particular instant and so obtain a description of the axial dependence of the concentration. From this information one could calculate the variance and so $\frac{\partial}{\partial t}(\sigma^2)$ could be evaluated and the dispersion coefficient obtained. For this treatment to be accurate, one would need a large number of accurate gauges spaced very close together otherwise gauges a long way downstream would measure small (and therefore inaccurate) concentrations. Note that since 'x' would be large, the contribution to the variance would, however, be significant. It is therefore likely that large errors would be incured using this treatment. The technique that has been adopted for the conversion of the experimental data into values of the dispersion coefficient was initially suggested by Smith (277). If we suppose that the concentration is a Gaussian function of distance then the mean cross channel concentration eventually obeys the equation

$$\bar{C} = \frac{M}{\Lambda\sqrt{2\pi}} \, EXP\left[-\frac{1}{2\Lambda^2} \, (x-\int U dt)^2 \right] \qquad (7\text{-}6)$$

where $\Lambda^2 = \sigma^2 \frac{4}{h^2}$

and M is the total amount of contaminant given by

$$M = 2 x_0 = 22 \times 10^{-3} m.$$

Once sufficient time has elapsed for the Gaussian equation given in (7-6) to hold, it is in principle possible to calculate the axial

concentration variance from just one reading of $\bar{C}$ for any time. However the equation is not easily solved even by simple iterative numerical techniques. Instead, we confine attention to the case when the term in the exponential of equation (7-6) is zero. When this is true, Λ^2 is simply given by,

$$\Lambda^2 = (M / \bar{C})^2 \frac{1}{2\pi}. \qquad (7\text{-}7)$$

This is effectively a statement of the conservation of mass within the channel. Equation (7-7) holds when the slug centroid lies in front of the gauge and the concentration reading is at a maximum for that period; i.e. when

$$x = \int U \, dt. \qquad (7\text{-}8)$$

This scheme can therefore give values for Λ^2 after only a small amount of manipulation of the data. The restrictions however are that:

1/ the gauge should be sited within the slug excursion distance i.e. $x < 2s$

2/ only peak concentration readings should be considered.

There is therefore much useful information which we are not actually using and in this respect, the scheme is somewhat limited. Ideally, a method of treatment for oscillatory flow dispersion data based upon that described by Chatwin (271) for steady flows should be developed if the results are to be fully exploited.

7.3.2 Results

The values of the dispersion coefficient obtained using the assumptions described in section 7.3.1 have been found to show little variation with frequency to the limits of experimental accuracy. This is not an unexpected result since the flow profile was predominantly parabolic (see chapter 2). The stroke dependence on the other hand is large and in agreement with the values obtained numerically. In order to compare the average experimentally measured dispersion coefficient at a particular stroke with the value predicted numerically at the same stroke, an account had to be taken of the different Schmidt numbers. It was assumed that the dispersion coefficient was proportional to κ; this is true if Po is large. In this way the numerical data (which were evaluated at $\kappa = 1.0 \times 10^{-9}\ m^2s^{-1}$) were scaled to give a prediction for the experimental value (for which $\kappa = 0.5 \times 10^{-9}\ m^2s^{-1}$). The experimental data presented in table 7.2 are for the lowest frequency of oscillation (the numerical data was evaluated for a frequency of about 1Hz). This is because the low frequency work is likely to give more accurate values for the dispersion coefficient since the experiments were allowed to run for a longer time. The storage capability of the computer imposed a restriction upon the number of cycles that could be studied with a reasonable resolution of each cycle; this implied a maximum number of cycles that could be observed and hence long period oscillations lead to longer experimental run times.

St	Experimental	Numerical
0.0500	9.26×10^2	5.95×10^2
0.0250	2.14×10^3	2.41×10^3
0.0200	3.33×10^3	3.73×10^3
0.0166	8.96×10^3	5.35×10^3
0.0125	1.49×10^4	9.53×10^3
0.0100	2.04×10^4	1.49×10^4

Table comparing experimentally measured values of $\frac{D}{\kappa}$ with the numerical predictions for various Strouhal numbers.

Table 7.2

We may use a simple least squares fitting technique to find the optimum value of A and B to fit the numerical and experimental data to the equation

$$\frac{D}{\kappa} = A\, St^{-B}. \qquad (7\text{-}9)$$

Table 7.3 gives the least squares fit values for A and B and figure 7.2 plots out the experimental, numerical and fitted curves.

	A	B
experimental value	1.54	2.055
numerical value	1.50	1.999

Table giving the values of the least sqares fit parameters A and B from equation (7-9) for the numerical and experimental dispersion coefficient data.

Table 7.3

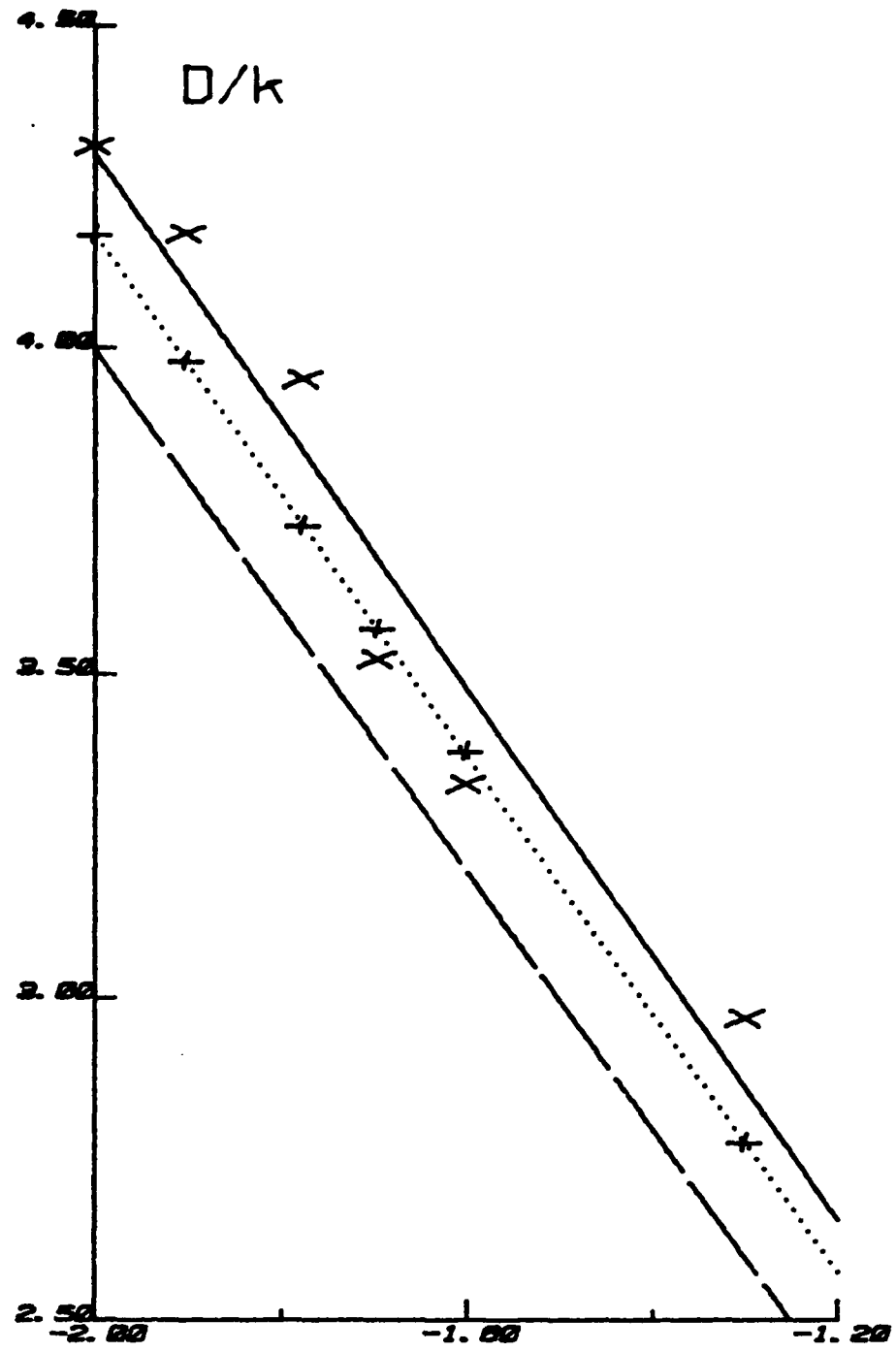

x = experimental points ..... = best fit of numerical data.

\+ = numerical points _____ = best fit of experimental data.

\- - - = analytical prediction.

Note: figures on axes are logs to base 10 of co-ordinates.

Plot on logarithmic axes showing experimental, numerical and analytical data for the variation of the dispersion coefficient with Strouhal number and the best fit straight lines.

Figure 7.2

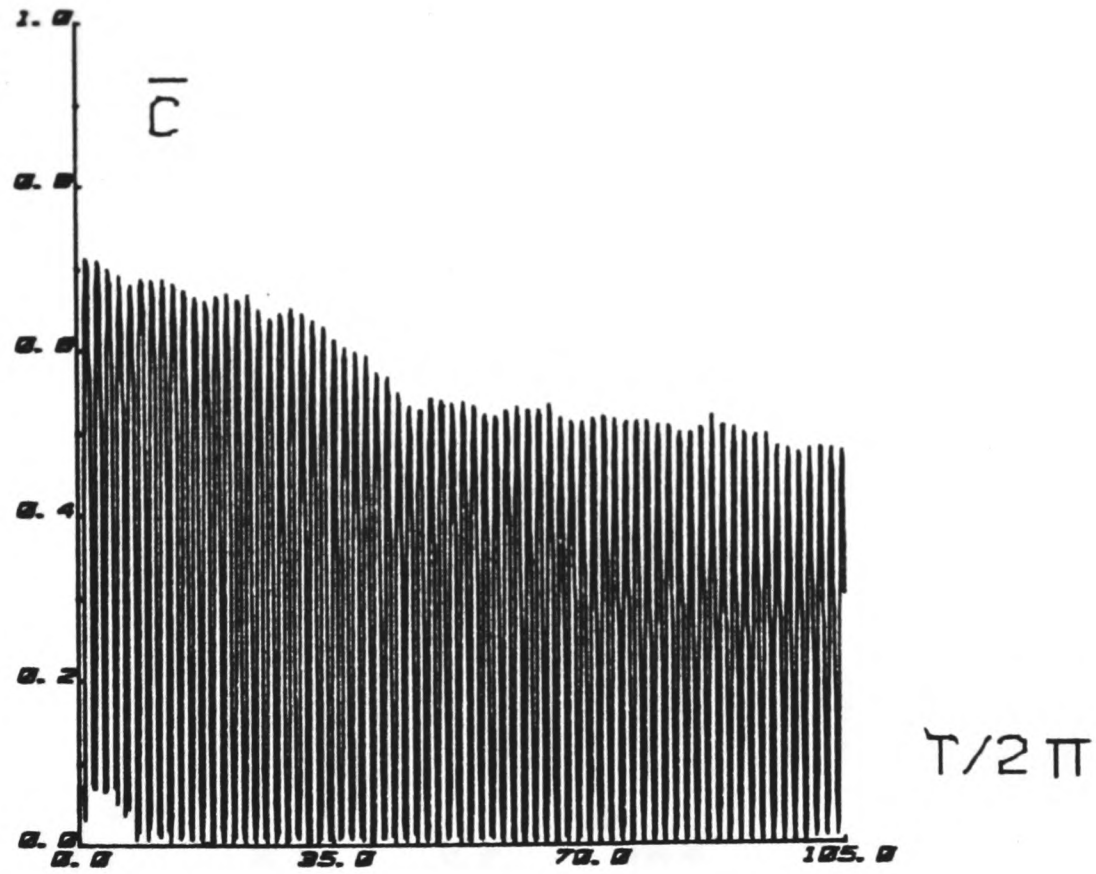

Plot of experimentally measured mean cross-channel concentration versus $\frac{T}{2\pi}$ with s = 40mm, f = 0.75 Hz, at the -25mm position.

Figure 7.3

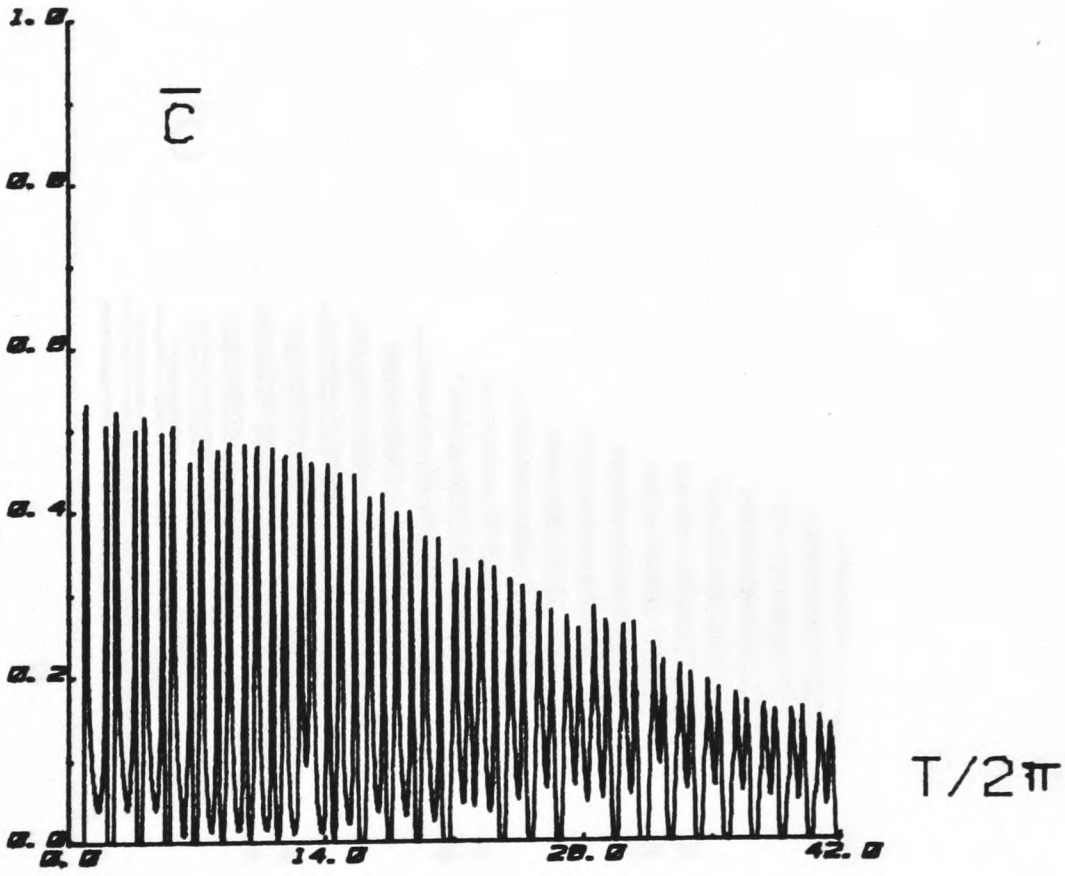

Plot of experimentally measured mean cross-channel concentration versus $\frac{T}{2\pi}$ with s = 40mm, f = 0.75 Hz, at the 40mm position.

Figure 7.4

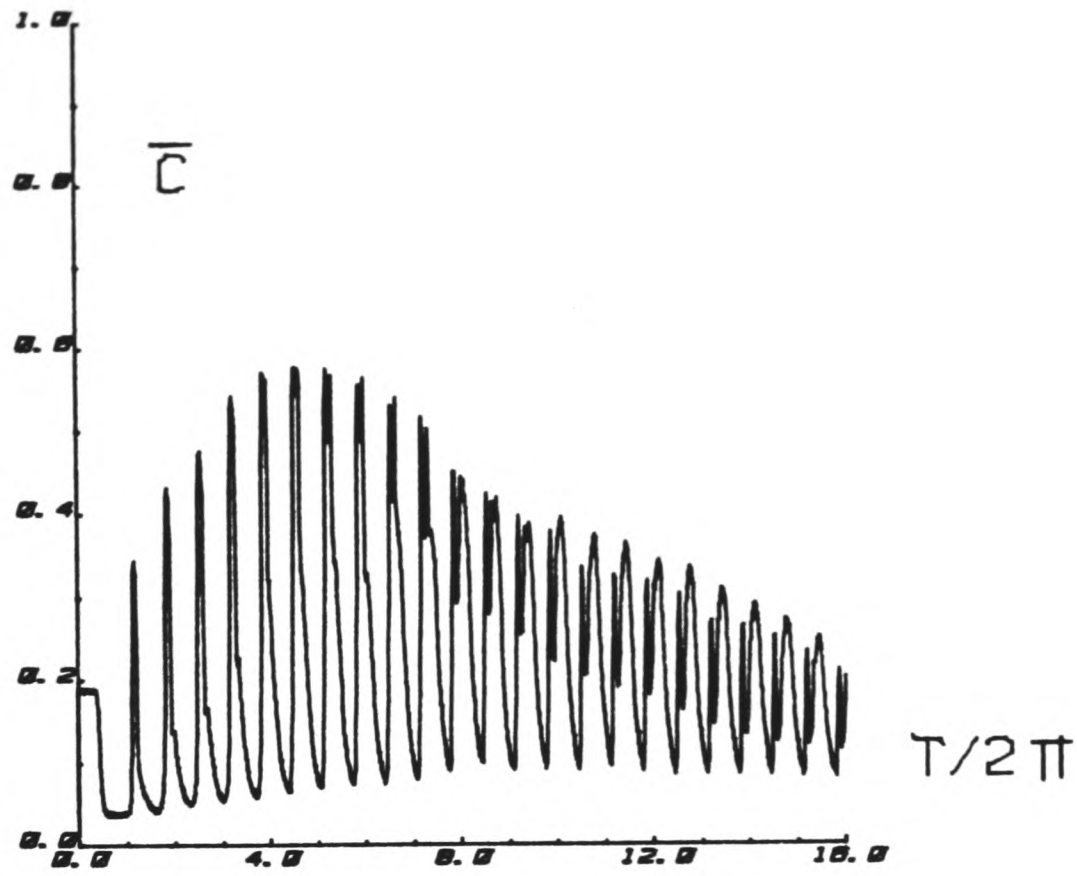

Plot of experimentally measured mean cross-channel concentration versus $\frac{T}{2\pi}$ with s = 10mm, f = 0.5 Hz, at the 25mm position.

Figure 7.5

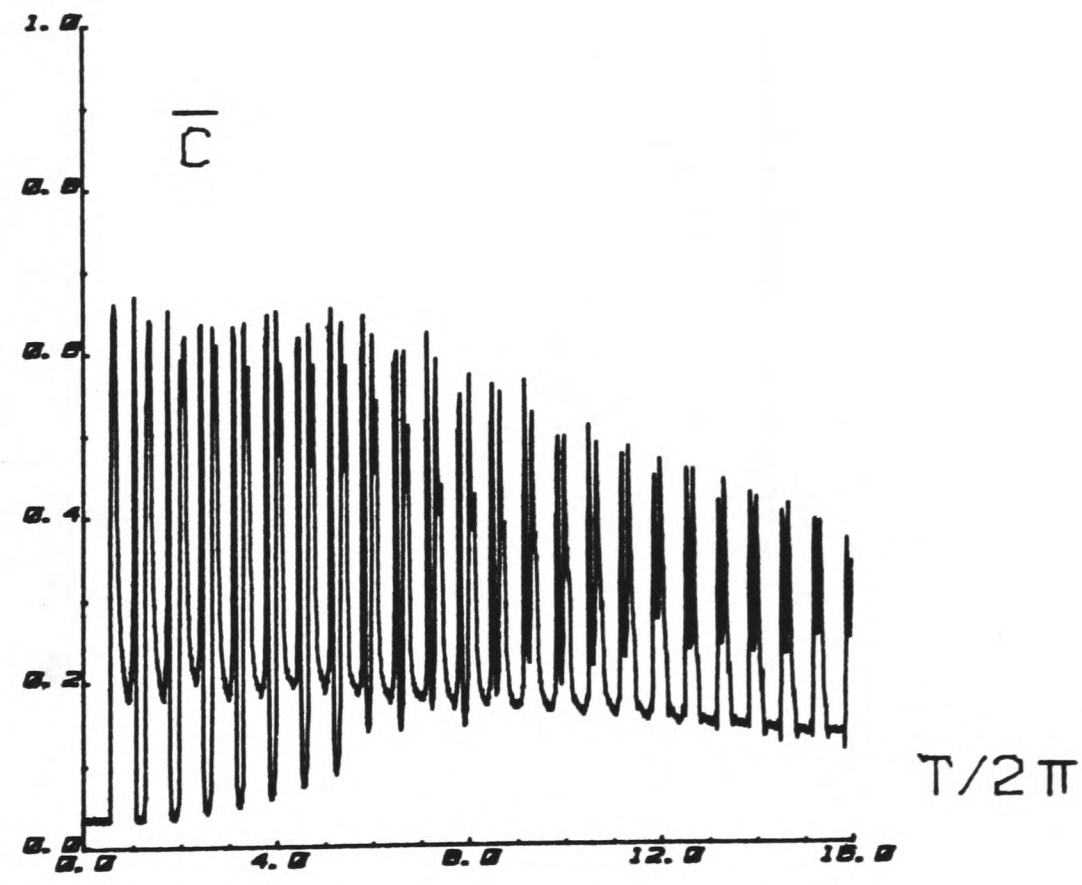

Plot of experimentally measured mean cross-channel concentration versus $\frac{T}{2\pi}$ with s = 40mm, f = 0.5 Hz, at the 25mm position.

Figure 7.6

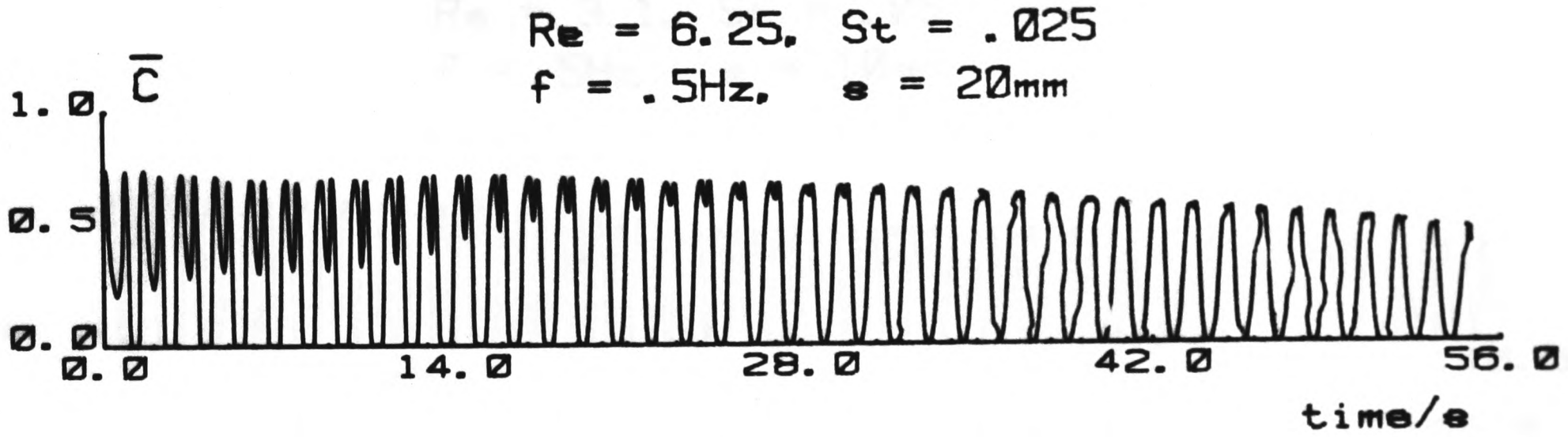

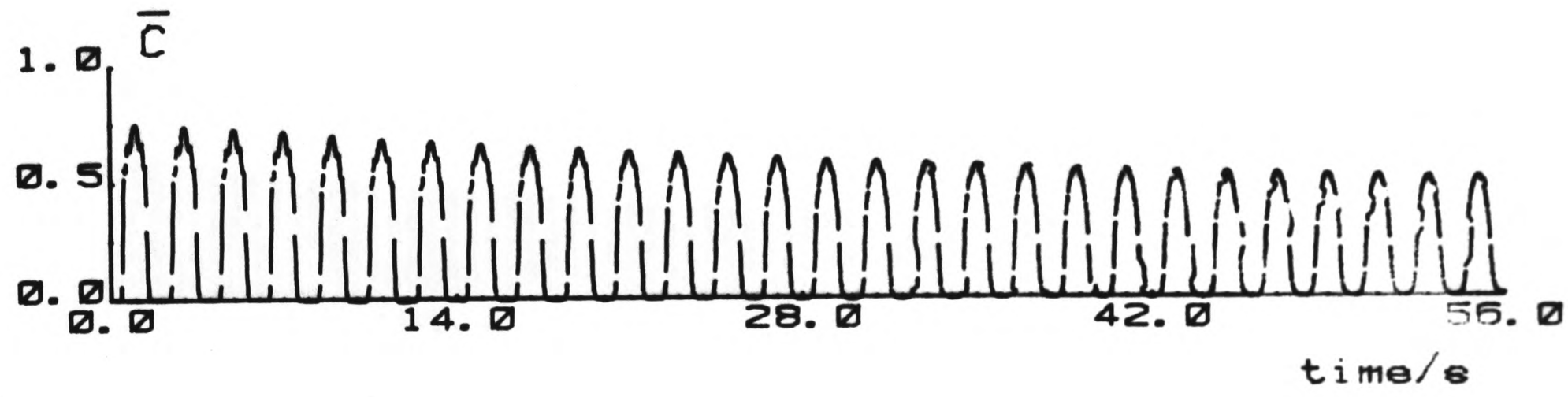

Plot of C — numerical
- - experimental
versus t at $\frac{x}{s}$ = 1.25.

Figure 7.8

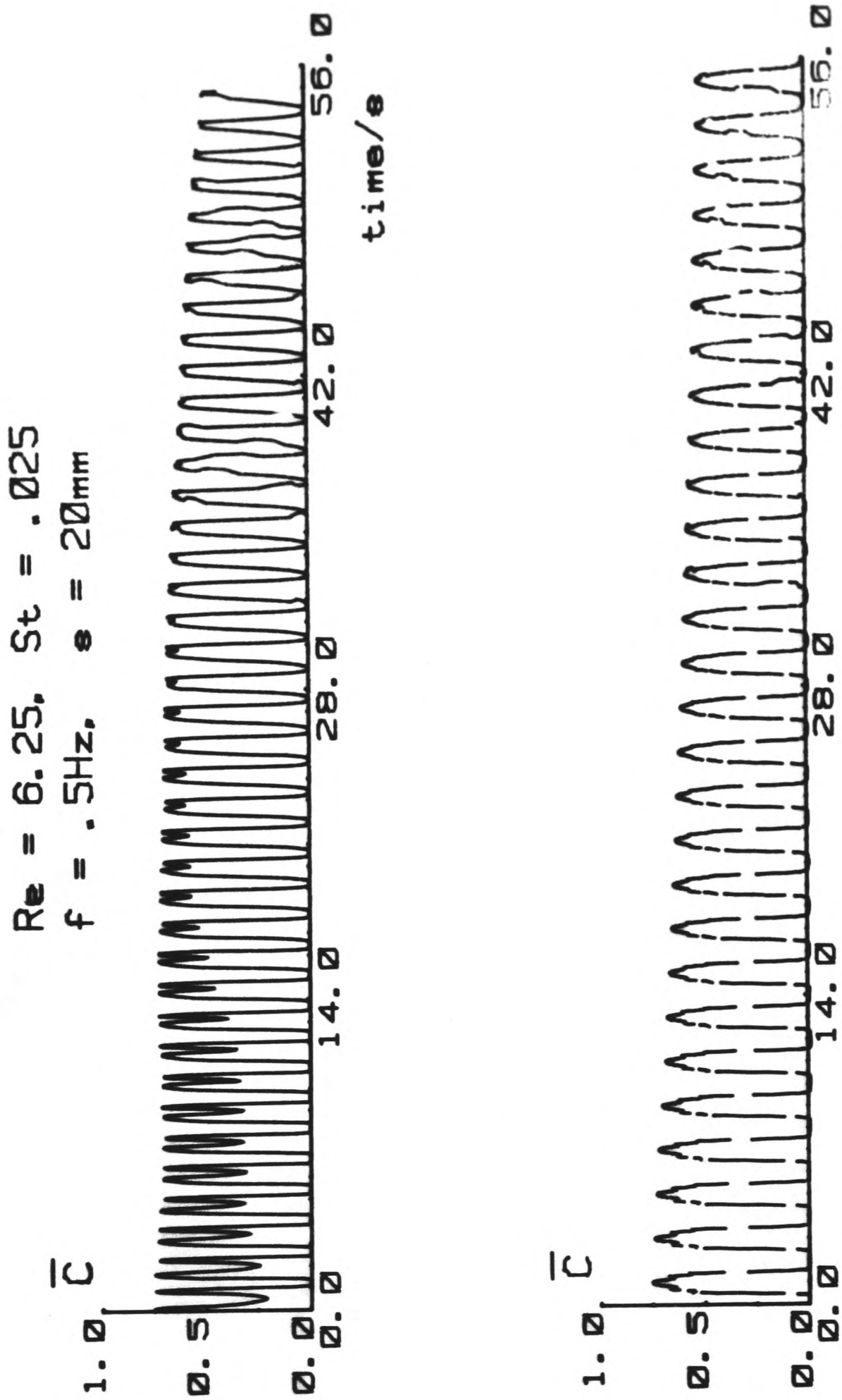

- - numerical

——— experimental

Plot of $\bar{C}$ versus t at $\frac{x}{s} = 1.25$.

Figure 7.8

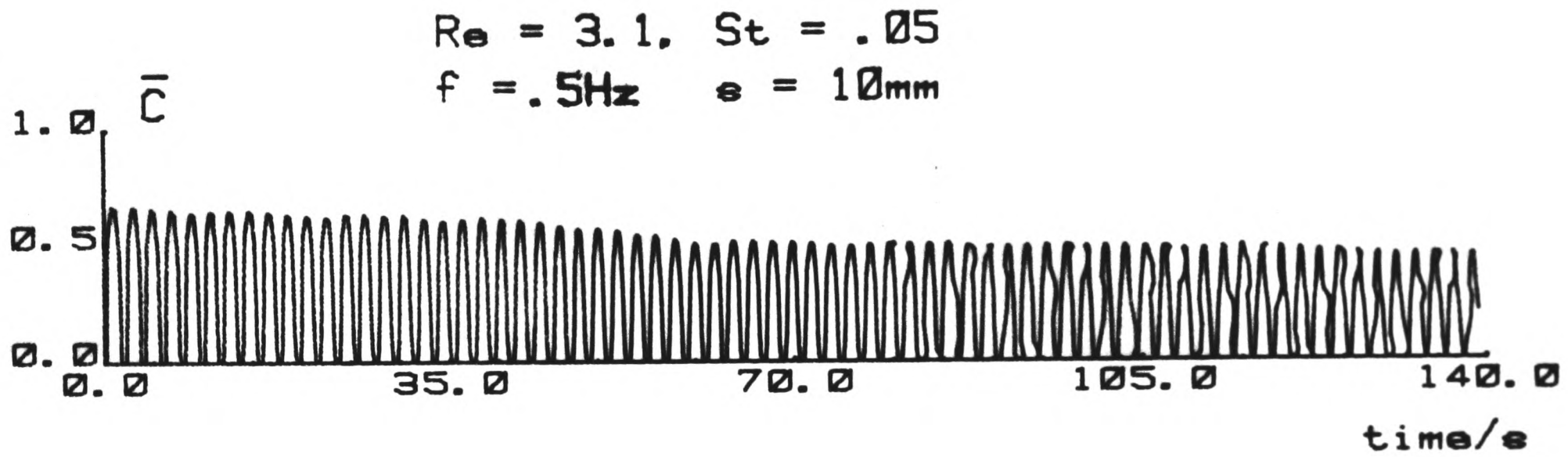

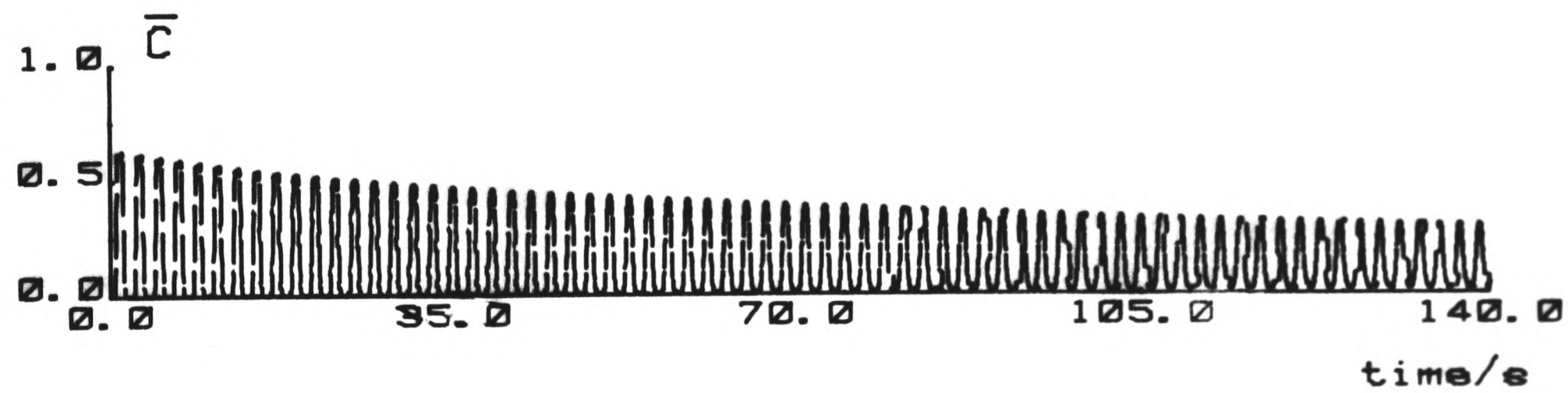

Plot of C — numerical

- - experimental

versus t at $\frac{x}{s}$ = 2.5.

Figure 7.9

The analytical line which is shown in figure 7.2 has been derived using the moments analysis of chapter 3 and assuming a parabolic velocity profile. This under-estimates the dispersion coefficient mainly because the analysis was only approximate. The slopes of the two best fit lines agree quite closely and the difference in intercept may well be due to an error in the value taken for the molecular diffusivity. Owing to the imperfect formation of the slug in the dispersion experiments, a direct comparison of the experimental readings of $\bar{C}$ with the predictions of the numerical treatment described in chapter 5 does not yield a fair assessment of the experiments. Three examples of such a comparison of the experimental and numerical breakthrough curves are shown in figures 7.7, 7.8 and 7.9 for $x/x_0 = \frac{25}{11}$. Generally, agreement between the curves is not particularly good during the early stages, since one is uncertain about the effective position of the centre of the slug of contaminant. In addition, initial slug malformations may have a critical effect upon the shape of the peaks on the plots (see figures 7.7, 7.8). However, for large strokes and for times which are not early, the breakthrough curves become very similar. These considerations need not have a deleterious effect upon our measurement of the dispersion coefficient since we only aim to measure the rate of spreading rather than the instantaneous concentration distribution.

7.4 SUMMARY OF OSCILLATORY FLOW DISPERSION EXPERIMENTS

The values of the dispersion coefficient calculated from the results of the experimental work have been in agreement with those of the numerical study presented in chapter 5. The numerical observation of the behaviour of the dispersion coefficient as the

inverse of Strouhal number squared has been verified by the experimental results. The less significant frequency dependence of the dispersion coefficient for quasi-steady velocity profiles has also been verified experimentally although the readings were not sufficiently accurate for the functional form of the dependence to be deduced.

Chapter 8

SUMMARY AND SCOPE FOR FUTURE WORK.

8.1 Summary.
- 8.1.1 Introduction.
- 8.1.2 Analytical work.
- 8.1.3 Numerical work.
- 8.1.4 Experimental work.
- 8.1.5 General summary of factors affecting oscillatory flow dispersion.

8.2 Future work related to the present study.
- 8.2.1 Analytical advances.
- 8.2.2 Numerical advances.
- 8.2.3 Experimental advances.

8.3 Scope for future advances in dispersion theory.

CHAPTER 8

SUMMARY AND SCOPE FOR FUTURE WORK

8.1 SUMMARY

8.1.1 Introduction

The investigations described in this document have been primarily concerned with an analytical, numerical and experimental investigation of axial dispersion in oscillatory flow down a flat channel. The velocity profile may be derived analytically as described in chapter 2. The velocity variation across the channel is parabolic for very small frequencies of oscillation and is uniform across the channel (plug-type) for very large frequencies. In the following subsections, summaries of the advances in dispersion made by the present investigation will be presented.

8.1.2 Analytical Work

By defining a transversely weighted mean cross-channel concentration $\bar{C}_m$ and then taking axial moments, approximate expressions for the variance and dispersion coefficient were obtained for cases when the velocity profile was parabolic. The

basic analysis was modified to account for a quartic velocity profile. The degree of approximation was reduced by including a third term in the Fourier series for the wall concentration. The predictions using these approaches have been in good agreement with the numerical work. The merit of this novel analytical scheme is its ability to yield reasonably accurate predictions which display all the trends of the exact solutions and yet the scheme is also simple to use.

8.1.3 Numerical Work

The concentration field in an oscillatory flow has been calculated numerically using the finite difference techniques described in chapter 4. Calculations of the dispersion coefficient from the data obtained by the numerical scheme have produced very good agreement with the work of Watson (256). The numerical work has also given valuable information about the transient behaviour of the dispersion process. The advantage of the finite difference approach over the results of a theoretical analysis is that the results are exact and can provide predictions of the concentrations over large temporal regimes.

8.1.4 Experimental Work

The experimental study of oscillatory flow dispersion described in chapters 6 and 7 has enabled values of $\bar{C}$ to be measured at a particular downstream location for the first O(50) seconds of the process. Assuming a Gaussian concentration profile, the results were used to predict the dispersion coefficient for both the flat and the furrowed channel geometries. The results for the flat channel case gave reasonable agreement with analytical and

numerical predictions.

8.1.5 General Summary Of Factors Affecting Oscillatory Dispersion

The nature of oscillatory flow dispersion in a flat channel is determined by two parameters when the velocity profile is quasi-steady. The Strouhal number has the greater influence on the dispersion coefficient and leads to a variation as St^{-2}. The origin of this behaviour lies in the effect of the pump stroke. The stroke may be considered to simply scale up the axial co-ordinate proportionately. The variance, on dimensional grounds, is therefore scaled as stroke squared or as inverse Strouhal number squared. The weaker effect on the dispersion process is that of the oscillatory Peclet number (Po) which gives the ratio of the time taken for cross-sectional diffusive mixing to the period of the pump. This ratio determines whether the concentration distribution is quasi-steady (for all the cases studied in this investigation, quasi-steady behaviour did not occur). In quasi-steady flows $\frac{D}{\kappa}$ varies as Po^2, but for the present large Po conditions $\frac{D}{\kappa}$ was virtually independent of Po.

This simple model was somewhat modified when the pulsatile Reynolds number exceeds order unity and the velocity profile deviated from the quasi-steady form to approach the plug limit. This behaviour caused an increase in the dispersion coefficient over what one would obtain at the same oscillatory Peclet number but with a parabolic velocity distribution.

8.2 FUTURE WORK RELATED TO THE PRESENT STUDY

8.2.1 Analytical Advances

The weighted moments approach may be extended to produce predictions which are applicable to a wider range of velocity profiles. In chapter 3 we only considered the improvement to the scheme when three terms were used in the approximate expression for the wall concentration c_w. Inclusion of more terms would make for more tedious algebra, but the analysis is still tractable and would be more accurate. Similarly, the general Taylor series expression for the velocity profile was truncated at the term in ψ^4 thus limiting the results to small pulsatile Reynolds numbers (and hence small frequencies). By truncating the series at higher order terms one would produce a more intimate coupling between the moments equations. Nevertheless the equations would still be soluble and the analysis could be extended to account for dispersion in oscillatory plug-type flows.

A useful improvement to the scheme would be provided if one could remove the approximation invoked by the expression for the wall concentration in terms of the transversely weighted mean cross-channel concentrations. One possible way of achieving this goal would be to consider $\bar{c}_m$ in the limit of $m \to \infty$. Consider the defining integral for $\bar{c}_m$:

$$\bar{c}_m = \int_0^1 \psi^m \, c \, d\psi. \qquad (8\text{-}1)$$

In the limit of large m, the greatest contributions to the particular value of $\bar{c}_m$ are given by the concentrations close to the wall since the values of ψ^m are small everywhere except at $\psi \approx 1$. One might therefore obtain a better approximation by relating

c_w not to the weighted concentrations of level 0, 2 and 4 but to perhaps level 100 alone. Indeed in the limit of $m \to \infty$, one might aim to express the wall concentration exactly as a function of $\bar{c}_m$. Letting $m \to \infty$ in equation (3-14) might then yield an exact analysis.

8.2.2 Numerical Advances

The numerical work could be extended by investigating the influence of the Schmidt number upon the predictions which were presented in chapter 5. For small values of Sc, the concentration distribution would ultimately become quasi-steady since the oscillatory Peclet number (defined in chapter 5) would be small implying that the cross-section mixing time was small compared to the period of the velocity reversals. For the most part the values of Po chosen in the present study have lead to only a weak frequency dependence of the dispersion coefficient when the velocity profile is quasi-steady. In the limit of small Po, D would be expected to vary as Po^2; a more detailed study of how the gradual disappearance of a frequency dependence is manifested would be useful. A more detailed consideration of the effect of slug length would be interesting as would an investigation of non-uniform slugs. Both of these deviations from the boundary conditions set out in equations [3-1]→[3-5] have been studied briefly, but a more detailed set of results would be required if a comprehensive set of predictions were to be produced. Similarly, the permeable wall condition has been set up but a detailed investigation has not been undertaken. It would be possible to study the oscillatory flow dispersion problem in a circular tube since the velocity profile may be derived by similar means to those described in chapter 2. The resulting formulation would contain

Bessel functions rather than hyperbolic functions and would therefore be more difficult to evaluate. In addition, the finite difference scheme might have to be modified to take account of the new geometry of boundary conditions, but in principle the techniques would be the same. This numerical study would have the advantage that if one assumed an axisymmetric concentration distribution, then the use of a two dimensional difference mesh would not involve the approximation that was necessary for the flat channel study (see appendix 2). A further study of mass transfer in an entry length carrying steady or oscillatory flow would be easily undertaken and would probably provide interesting results.

The possible application of the numerical scheme to the problem of flat channel dispersion in three dimensions must be considered to be unlikely unless a very powerful computer were to be used. The extra memory required to store the concentrations at each of the nodes on the three-dimensional mesh would be a limitation. In addition, the time of a simulation to run through say twenty periods would also increase tremendously since far more calculations would have to be undertaken per step in the t-mesh. If one were simulating a channel of large aspect ratio and it were important to let the calculation persist until the Chatwin-Sullivan asymptotic form (see appendix 2) had been reached, then the necessary number of cycles for which the simulation would have to be run would lead to a prohibitively large run-time. A possible way of side-stepping these limitations is to restrict oneself to calculating the dispersion coefficient. By doing this one could develop some approximate theoretical model which predicted the concentrations. This information would then be used to calculate a "starting" condition for a numerical scheme which would then tend

towards the correct solution.

8.2.3 Experimental Advances

The experimental study of dispersion could be improved so as to provide more accurate results which might make it possible to observe the frequency dependence of the dispersion coefficient. By building a channel with a larger gap one may increase the sensitivity of the gauges by supplying a larger optical path length. In addition, plug-like flows would be more easily imposed since lower frequencies of oscillation would be necessary in order to achieve a pulsatile Reynolds number which was greater than order unity. By using a bellows pump or a system with two pump bags (as described in chapter 6) one could ensure a reliable flow for a larger range of stroke-frequency combinations than has been possible using the present single pump bag system. By using a number of different dyes with different diffusion coefficients one could deduce the influence of Po upon the dispersion coefficient. A closer approach to the ideal of an initially uniform slug would be a great advantage. This might be achieved by creating the coloured region of fluid by a means other than injection. Flashing a broad beam of light across a channel in which the liquid underwent some irreversible colour change when so excited, could produce a better formed slug, although some small initial lateral concentration gradient might still be produced. Data might be more easily analyzed if a set of criteria describing the temporal moments were laid out for oscillatory flow in a similar mannner to that devised for steady flow by Østergaard and Michelsen (171) or by Chatwin (271). A more comprehensive set of measurements could be obtained by positioning the gauges much closer together. We

could extend the flat channel dispersion study to a furrowed channel by replacing the plane perspex sheets with a machined set of furrowed inserts. Recalibration of the gauges would then enable the dispersion coefficient to be determined in a manner similar to that used for the flat channel case. An alternative way of obtaining the same data would be to extend the in-line testing of a built blood oxygenator.

8.3 SCOPE FOR FUTURE ADVANCES IN DISPERSION THEORY

Until recently the process of averaging over the channel cross-section has been an almost unquestioned step in many theories which seek a solution to the dispersion equation. There are very good physical reasons for doing this (namely that this is how concentrations are usually measured) but the comments of Smith (219) lead one to question the effects of performing this integration. Since contaminant is continually being washed through each cross-section, the integration is bound to lead to effects which are not associated with the dispersive spreading in itself, but are merely artifacts of the way one is processing the data. In the case of the plots of the rate of growth of the variance versus time, the effect was so great that the more permanent and pertinent growth due to dispersive spreading was almost completely obscured. An alternative approach might be to continue to evaluate a mean cross-channel concentration but to redefine the term so as to eliminate this unwanted distortion of the data. Perhaps a better way of proceeding would be to evaluate the mean concentration, not over a line of constant χ, but along a curve which moved at the local fluid velocity (assumed to be parallel to the χ-axis) and was the locus of a line of non-diffusing particles which were initially

coincident with a line of constant χ. In the case of steady flow in a flat channel one would not evaluate the mean cross-channel concentration over a line

$$x = x_{offset}, \tag{8-2}$$

but instead one would evaluate the average concentration over a line

$$x = x_{offset} + 2Ut\ (1 - \psi^2). \tag{8-3}$$

In oscillatory flow the path of integration would be continually bowed out and warped by the non-uniformity of the velocity across the channel, but at least in the early stages, diffusion would occur in a direction perpendicular to this curve and this would certainly mean that the peaks on the moments plots, which were entirely due to a convective deformation of the slug, would no longer appear. The value of this $\bar{C}$ would represent a mean cross-channel concentration, albeit one with a somewhat different meaning. Naturally this newly defined average concentration would not correspond to anything one could measure experimentally, but analytical predictions of the behaviour of this quantity might give useful insights into the operation of the dispersion process. To date, no such analytical predictions have been devised.

APPENDIX 1

Description of the Mechanism for Dispersion in Oscillatory Flows

In this description we will, for simplicity, suppose that the velocity profile is a parabolic function of the cross channel co-ordinate (Ψ). There are two extremes of behaviour which will be used to illustrate the two mechanisms which interact:

1/ The case of negligible diffusion, which is applicable to the very early stages of the spreading,

2/ The case of neglible convection, which will be important in the limit of small pump stroke.

Consider the diffusionless case first. The non-uniformity of the velocity profile over the channel cross-section results in contaminant near the centre-line being moved further downstream than that near the walls. Thus a uniform slug of dye will initially lie symmetrically about the origin and will be bowed out by the velocity profile by a simple transportive mechanism. As long as the velocity is positive, the slug will continue to be sheared over in the direction of positive x. When the velocity reverses, the slug will retreat back up the channel until at the end of the period it lies exactly at its original position. This behaviour will repeat indefinitely, with the contaminant being continually bowed out and reconstituted. The convection itself does not spread the slug out along the channel permamently; the important effect that it does have however, is to shear the discontinuities in concentration at the edges of the slug around so that they do not continually lie perpendicular to the channel axis.

This may be visualized by considering a regular lattice of node points in the channel, rather like a finite difference mesh in which the intersections move with the local speed of the channel fluid. This movement will slide neighbouring nodes past one another so that the lattice is being continually moved and distorted by the velocity (see figure A1.1).

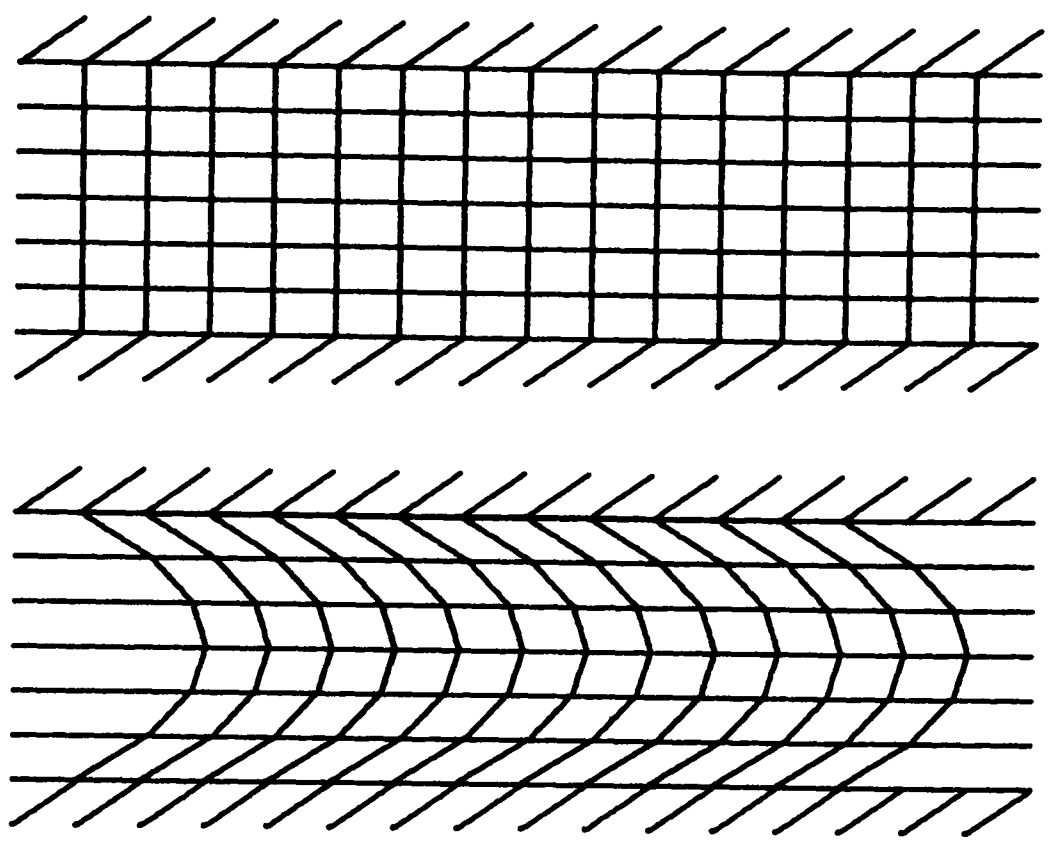

Illustration of how the shear associated with an oscillatory velocity bends lines which were initially perpendicular to the walls so that the forward facing normals are made to lie obliquely away from the centre-line.

Figure A1.1

Consider now, the case in which there is no channel velocity. The uniform slug will lie across the channel and will spread out very slowly by axial diffusion alone. This process may be described exactly and explicitly by the equation

$$\frac{c}{c_0} = \frac{1}{2}\left[\operatorname{erf}\left\{\frac{x-x_0}{2\sqrt{\kappa t}}\right\} + \operatorname{erf}\left\{\frac{x-x_0}{2\sqrt{\kappa t}}\right\} \right].$$

This solution is sketched schematically in figure A1.2.

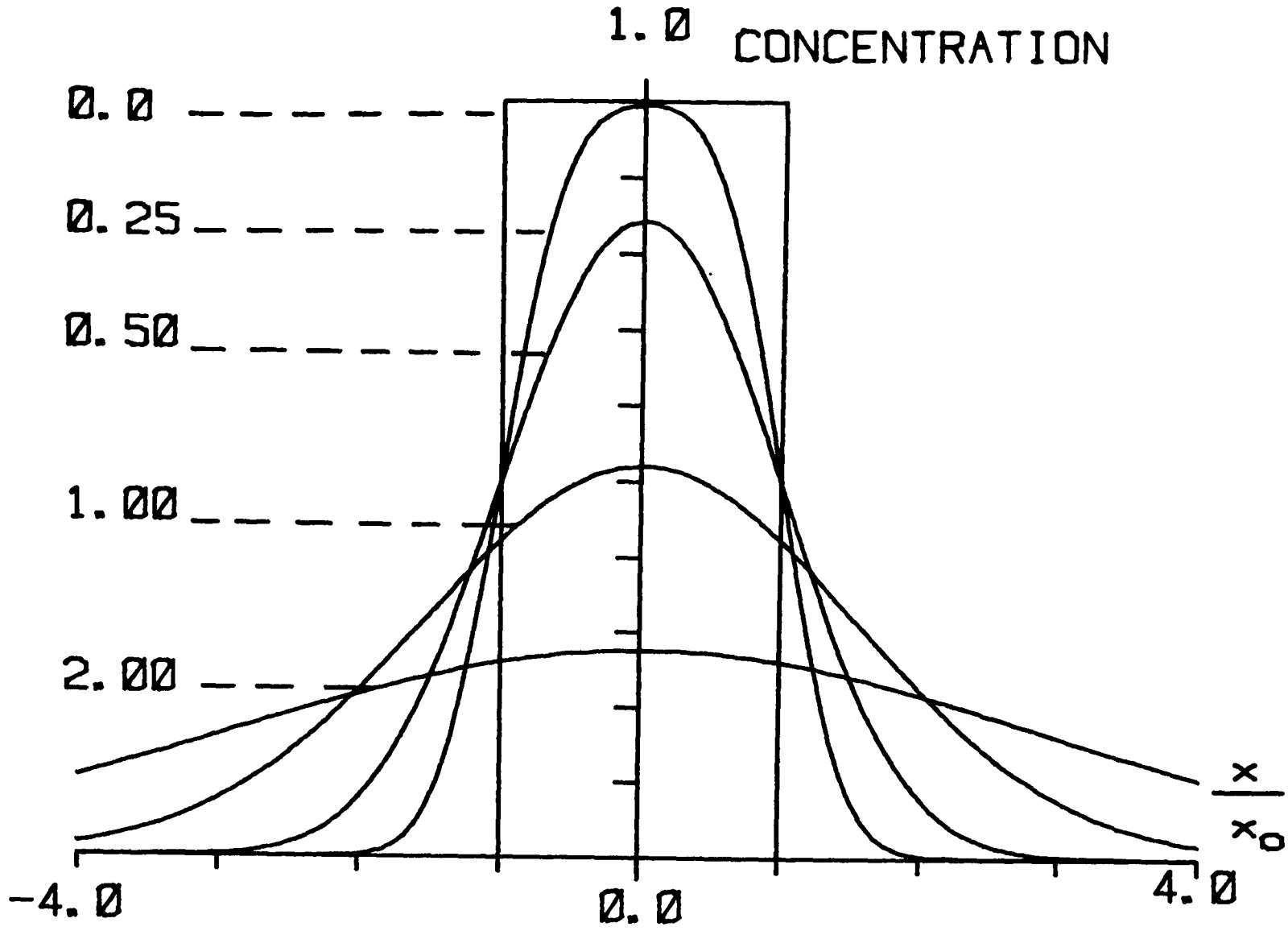

Plot of the axial concentration profile as a slug spreads as a result of diffusion alone. The numbers on the curves are values of Kt / x_0^2.

Figure A1.2

When we consider the two cases together (i.e. the diffusive effect which leads to a very slow spreading and the convective effect which leads to only transient distortions of the slug), it becomes apparent that there is a mechanism for vastly enhanced transport of the slug molecules: transverse diffusion may now also affect the concentration distribution. The leading (convex) edge of the slug is bowed out to face the channel walls obliquely so that any diffusion which occurs out of the front of the slug takes the contaminant towards the wall and into an area of lower

velocity. Similarly, diffusion out of the rear (concave) end of the slug takes the tracer into the centre of the channel where the fluid velocity is greater. Figure A1.3 demonstrates this process by illustrating the slug shape at the start of, in the middle of and at the end of the first cycle.

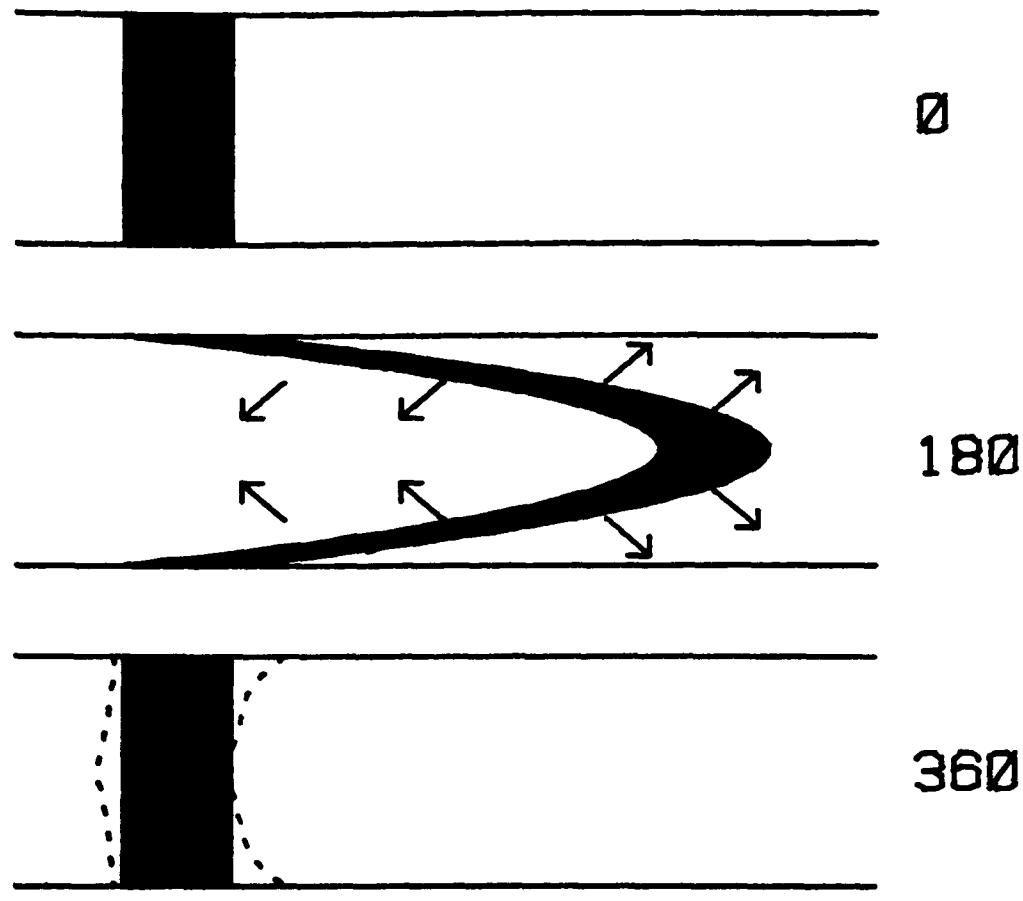

Exaggerated illustration of the slug form at the 0, 180, 360 degree positions in the dispersion evolution. The arrows illustrate the direction in which the local mass diffusion from the slug occurs.

Figure A1.3

The mechanism by which dispersion spreads out a tracer slug in oscillatory flow is very different from that which acts in steady flow. For steady flow, the slug is being continually extended down the channel by convection and indeed transverse diffusion actually limits the rate of spreading. The final mode of spreading is an equilibrium between this warping of the concentration field (which does in itself lead to an increase in concentration variance) and the lateral diffusion which counteracts it. For oscillatory flow

on the other hand, although there are transient surges in the variance due to the temporary movement of the slug down the channel, on the long term the velocity field per se does not increase the variance.

APPENDIX 2

The Effect of the Side Walls on Dispersion in a Flat Channel

It seems justified, when considering dispersive behaviour in a flat channel, with one dimension (h) much less than the other (b), to suppose that variations in velocity and concentration over the small side (y-direction) so completely dominate the variations over the large side (z-direction) that one may ignore the effects of the z-direction velocity and concentration gradients. This will be referred to as the 2-D assumption. This assumption is not however justified in all circumstances. Doshi, Daiya and Gill (80) and Chatwin and Sullivan (62) have obtained theoretical predictions for the steady flow dispersion coefficient in channels of rectangular cross-section. Both theories calculate that in the steady state the dispersion coefficient for this 3-D case, even for an infinite aspect ratio, is a factor of 8 greater than the value one would calculate by completely ignoring side walls, the error becoming more significant for smaller aspect ratios. Throughout the present study of oscillatory dispersion it has been assumed that there are no concentration or velocity shears in the z-direction. In this appendix the use of this approach is justified and reasons are given why this is not only a tenable assumption but also one which is preferable in many applications.

Consider the case of the Taylor-Aris model; the predictions for the dispersion coefficient become more accurate when the variations in concentration over a particular cross-section become small. In other words, only when a molecule of contaminant has had time to wander across the channel can the steady state be

approached. For a 3-D flat channel there are therefore two steady states which may be attained. The first is reached when a molecule has had time to wander over the y-direction a distance h. This corresponds to the stage to which the 2-D assumption is justified. The ultimate steady state is approached much more slowly and occurs only when sufficient time has elapsed for a typical molecule to have wandered a distance b in the z-direction. The concept of a flat channel having an infinite aspect ratio ever actually reaching a steady state is somewhat ambiguous since for any time interval, one can realistically imagine a channel so wide that the steady state would not even be approached. In short, when we refer to a flat channel in which the concentration variations over the z-direction may be ignored, it should be understood that this is synonymous with an assumption that the range of times to which the results may be applied is limited by the lower and upper asymptotic bounds described above. The lower bound is determined by the time necessary for the first 'h-distance' asymptotic state to be reached and the upper limit is determined by the necessity that the 'b-distance' asymptotic state should not be approached. Clearly the size of this temporal range is determined by the dimensions of the channel cross-section. In the limit of infinite aspect ratio, the fact that the "ultimate" steady state will give a different value for the dispersion coefficient from the 2-D assumption value is somewhat irrelevant since the 3-D asymptotic state will never be attained. It is probably true to say, that for times which are relevant to many engineering applications, only the first asymptotic state may be reached for channels which can be ascribed an aspect ratio of greater than about 10. These considerations justify the use of the 2-D assumption if we understand that predictions for the concentration arising from this model may only

be accurate away from the (b) side walls. It is also necessary to define a somewhat modified 'mean cross-channel concentration' if we are to use the 2-D assumption. If we set out to compare experimentally measured values of $\bar{C}$ with those predicted by a theory which invokes the 2-D assumption, then we must be careful to place the concentration sensors along the centre-line of the channel or at least not so near to the side walls that the very slowly growing concentration boundary layer there significantly modifies the readings. Numerical and analytical descriptions which are two dimensional will only describe the time evolution during the first asymptotic state; if the values so obtained for the dispersion coefficient are applied, out of context, to large times (times which are frequently so large as to be of very limited interest) then large errors may be incurred.

The analyses of Doshi, Daiya and Gill (80) and of Chatwin and Sullivan (62) which have dealt with the case of dispersion in a rectangular duct have only studied the case of steady flow. In oscillatory flow we may expect the same trends to apply although the magnitude of the large time error incurred by the use of the 2-D assumption may not be the same. In fact for small values of α^2, the velocity variation in the y-direction may be essentially parabolic whilst that in the z-direction could be of the plug type. Since plug type flows usually imply a larger dispersion coefficient

NOTE

For a channel of aspect ratio 100 and height h = 1mm, carrying a species with a diffusion coefficient of 1.0×10^{-9} $m^2 s^{-1}$, the first asymptotic state is reached after a time of order 200 seconds (i.e. about 3 minutes). The second asymptotic state is reached after about 3 million seconds (i.e. about 23 days).

than parabolic flows, we might tentatively suppose that the contribution of the side walls in the oscillatory flow case is larger than that in the steady flow case. The time taken to reach the respective asymptotic states will not however be changed and the use of the 2-D assumption even in oscillatory flows is still valid.

APPENDIX 3

Optical Measurement of Mean Cross-Channel Concentration

In chapter 6 an experimental method for determining mean cross-channel concentrations was described. An implicit assumption in the use of this method is that the intensity of the transmitted beam is independent of the lateral concentration profile. Thus if the gauges produce a certain voltage (implying a particular value of $\bar{C}$) then we suppose that the concentration distribution across the channel at the meaurement site may take any form at all -- as long as the mean cross-channel concentration stays the same, all distributions will lead to the same voltage. In this appendix it will be demonstrated that this assumption is justified.

Suppose that the beam intensity $I_{(y)}$ after passage through a small distance δy of liquid, decays to an intensity $I_{(y+\delta y)}$. Solutions of Maxwell's equations indicate that

$$I_{(y)} - I_{(y+\delta y)} = -k_{(y)}\, I_{(y)}\, \delta y, \qquad \text{(A3-1)}$$

or

$$\frac{\partial I}{\partial y} = - k_{(y)}\, I, \qquad \text{(A3-2)}$$

where k is some decay constant.

Integrating equation (A3-2) over the channel cross-section (y = 0→h) yields,

$$I_e = I_o\, \mathrm{EXP}\left\{ -\int_0^h k\, dy \right\}, \qquad \text{(A3-3)}$$

where I_o and I_e are the beam intensities at y = 0 and y = h respectively. The calibration procedure described in chapter 6 has

given results which indicate that the beam intensity varies exponentially with concentration (see figure 6.4). This being the case, we may write

$$k_{(y)} = c_{(y)}\ \epsilon, \qquad \text{(A3-4)}$$

where ϵ is some constant.

Substituting (A3-4) into (A3-3) yields

$$I_e = I_o\ \mathrm{EXP}\left[-\epsilon \int_0^h c\ dy \right]. \qquad \text{(A3-5)}$$

We may identify the integral term in (A3-5) with the mean cross-channel concentration. It can now be seen that the intensity of the beam after passage through the channel liquid is determined only by the mean of the concentrations it has sampled and not in any way by the distribution of the concentrations about that mean. It should be noted that the exponential calibration curve is essential if the system is to possess this desirable property.

$$I_e = I_o\ \mathrm{EXP}\left[-\epsilon\ h\ \bar{C} \right]. \qquad \text{(A3-6)}$$

APPENDIX 4

Analytical Prediction for Variance-Time Curve

This appendix contains an expression for the variance versus time curve as predicted using the analysis described in chapter 3. We have assumed that the velocity profile is a quartic of the form

$$u = \bar{U}\left[\sin(\tau)(p + p'\psi^2 + p''\psi^4) + \cos(\tau)(q + q'\psi^2 + q''\psi^4)\right].$$

The variance is then given by

$$\sigma^2 = d_8 + \frac{2\tau}{Po} + \frac{2}{St^2}\left[d_1\tau + \frac{d_2}{2}\sin(2\tau) - \frac{d_3}{2}\cos(2\tau) + \frac{d_4}{2}\sin(\tau) - \frac{d_5}{2}\cos(\tau)\right.$$
$$\left. + e^{-\pi^2\tau/Po}\left[\frac{d_7}{2}\left\{\sin(\tau) - \frac{\pi^2}{Po}\cos(\tau)\right\} - \frac{d_6}{2}\left\{\cos(\tau) + \frac{\pi^2}{Po}\sin(\tau)\right\}\right]\left[1 + \frac{\pi^4}{Po^2}\right]^{-1}\right].$$

Where

$$d_1 = \frac{1}{2}\left[p'b_2' + q'b_1' - q''c_1 + p''c_2 - \left(\frac{p'}{3} + \frac{p''}{5}\right)\left(q + \frac{q'}{3} + \frac{q''}{5}\right) + \left(\frac{q'}{3} + \frac{q''}{5}\right)\left(p + \frac{p'}{3} + \frac{p''}{5}\right)\right]$$

$$d_2 = \frac{1}{2}\left[q'b_1' - p'b_2' - q''c_1 - p''c_2 + \left(\frac{p'}{3} + \frac{p''}{5}\right)\left(q + \frac{q'}{3} + \frac{q''}{5}\right) + \left(\frac{q'}{3} + \frac{q''}{5}\right)\left(p + \frac{p'}{3} + \frac{p''}{5}\right)\right]$$

$$d_3 = \frac{1}{2}\left[p'b_1' + q'b_2' - p''c_1 + q''c_2 - \left(\frac{q'}{3} + \frac{q''}{5}\right)\left(q + \frac{q'}{3} + \frac{q''}{5}\right) + \left(\frac{p'}{3} + \frac{p''}{5}\right)\left(p + \frac{p'}{3} + \frac{p''}{5}\right)\right]$$

$$d_4 = q'a_3\frac{Po}{\pi^2} + c_1q'' - c_3q'' - \left(\frac{q'}{3} + \frac{q''}{5}\right)\left(p + \frac{p'}{3} + \frac{p'}{5}\right)$$

$$d_5 = p'a_3\frac{Po}{\pi^2} + c_1p'' - c_3p'' - \left(\frac{p'}{3} + \frac{p''}{5}\right)\left(p + \frac{p'}{3} + \frac{p''}{5}\right)$$

$$d_6 = c_3p'' - b_1'p' - p'a_3\frac{Po}{\pi^2}$$

$$d_7 = c_3q'' - b_1'q' - q'a_3\frac{Po}{\pi^2}$$

$$d_8 = \text{a constant determined by the value of } \sigma^2\Big|_{\tau=0}$$

$$c_1 = \frac{p}{5} + \frac{p'}{7} + \frac{p''}{9} + \frac{1}{Po}(12-2\pi^2)\left(b_2' - \frac{1}{3}\left(q + \frac{q'}{3} + \frac{q''}{5}\right)\right)$$

$$c_2 = \frac{q}{5} + \frac{q'}{7} + \frac{q''}{9} + \frac{1}{Po}(12-2\pi^2)\left(b_1' - \frac{1}{3}\left(p + \frac{p'}{3} + \frac{p''}{5}\right)\right)$$

$$c_3 = \left(\frac{12}{\pi^2} - 2\right)\left(b_1' + \frac{1}{3}\left(p + \frac{p'}{3} + \frac{p''}{5}\right)\right)$$

$$b_1' = \left(\frac{\pi^2}{Po}a_2 - a_1\right)\left[1 + \frac{\pi^4}{Po^2}\right]^{-1}$$

$$b_2' = \left(\frac{\pi^2}{Po}a_1 + a_2\right)\left[1 + \frac{\pi^4}{Po^2}\right]^{-1}$$

$$a_1 = \frac{p}{3} + \frac{p'}{5} + \frac{p''}{7} + \frac{\pi^2}{3Po}\left(q + \frac{q'}{3} + \frac{q''}{5}\right)$$

$$a_2 = \frac{q}{3} + \frac{q''}{5} + \frac{q''}{7} - \frac{\pi^2}{3Po}\left(p + \frac{p'}{3} + \frac{p''}{5}\right)$$

$$a_3 = \frac{\pi^2}{3Po}\left(p + \frac{p'}{3} + \frac{p''}{5}\right).$$

For the case of $\alpha^2 < O(1)$, the velocity profile is parabolic and we may write

$$p = 1.5 \qquad p' = -1.5 \qquad p'' = 0.0$$

$$q = 0.0 \qquad q' = 0.0 \qquad q'' = 0.0$$

Examples of the results yielded by these equation are given in chapter 3.

REFERENCES

1/ ALLEN,C.M., TAYLOR,E.A., The salt velocity method of water measurement. Trans. Am. Soc. Mech. Eng., 45, 285-341. (1923).

2/ ALLEN,C.M. Numerical simulation of contaminant dispersion in estuary flows. Proc. Roy. Soc., 381A, 179-194. (1982).

3/ ALONSO,C.V., Electrical conductivity probe for the measurement of concentration fluctuations. Journal of Physics E, Scientific Instruments, 3, 658-660. (1970).

4/ ANANTHAKRISHNAN,V., GILL,W.N., BARDUHN,A.J., Laminar dispersion in capillaries I, mathematical analysis. A.I.Ch.E.J., 11, 1063-1072. (1965).

5/ ARIS,R., On the dispersion of a solute in a fluid flowing through a tube. Proc. Roy. Soc., 235A, 67-77. (1956).

6/ ARIS,R., Further comment on "Notes on the diffusion-type model for the longitudinal mixing in flow." Chem. Eng. Sci., 9, 266-267. (1959).

7/ ARIS,R., Diffusion in reaction in flow systems of Turner's structures. Chem. Eng. Sci., 10, 80-87. (1959).

8/ ARIS,R., The longitudinal diffusion coefficients in flow through a tube with stagnant pockets. Chem. Eng. Sci., 11, 194-198. (1959).

9/ ARIS,R., On the dispersion of a solute by diffusion, convection and exchange between phases. Proc. Roy. Soc., 252A, 538-550. (1959).

10/ ARIS,R., On the dispersion of a solute in pulsating flow through a tube. Proc. Roy. Soc., 259A, 370-376. (1960).

11/ AUNICKY,Z., The longitudinal mixing of liquids in bends. Can. J.Chem. Eng., 46, 27-31. (1968).

12/ BABCOCK,R.E., GREEN,D.W., PERRY,R.M., Longitudinal dispersion mechanisms in packed beds. A.I.Ch.E.J., 12(5), 922-927. (1966)

13/ BAILEY,H.R., GOGARTY,W.B., Numerical and experimental results on the dispersion of a solute in a fluid in laminar flow through a tube. Proc. Roy. Soc., 269A, 352-367. (1962).

14/ BARTON,N.G., The dispersion of a buoyant solute in laminar flow in a straight horizontal pipe . Part 1. Predictions from Erdogan and Chatwin's (1967) paper. J.Fluid Mech., 74, 84-89. (1976).

15/ BARTON,N.G., The dispersion of a buoyant solute in laminar flow in a straight horizontal pipe . Part 1. The approach to the asymptotic state. J.Fluid Mech., 74, 91-112. (1976).

16/ BARTON,N.G., The initial dispersion of soluble matter in three dimensional flow. J.Aust. Math. Soc., 20B, 265-279. (1978).

17/ BATCHELOR,G.K., Diffusion in a field of homogeneous turbulence I, Eulerian analysis. Aust. J.Sci. Res., 2, 437. (1949).

18/ BATCHELOR,G.K., The application of similarity theory of turbulence to atmospheric diffusion. Quart. J.Roy. Met. Soc., 76, 133-146. (1950).

19/ BATCHELOR,G.K., Diffusion in a field of homogeneous turbulence II, the relative motion of particles. Camb. Phil. Soc., 48, 345-362. (1952).

20/ BATCHELOR,G.K., BINNIE,A.M., PHILLIPS,O.M., The mean velocity of discrete particles in turbulent flow in a pipe. Proc. Phys. Soc. B, 68, 1095. (1955).

21/ BATCHELOR,G.K., TOWNSEND,A.A., 'Turbulent diffusion', in 'Surveys in mechanics', ed. Batchelor and Davies, C.U.P. (1956).

22/ BATCHELOR,G.K., Diffusion in free turbulent shear flows. J.Fluid Mech., 3, 67-80. (1958).

23/ BATCHELOR,G.K., An introduction to fluid dynamics, C.U.P. (1970).

24/ BECKER,H.A., ROSENWIEG,R.E., GWOZDZ,J.R., Turbulent dispersion in a pipe flow. A.I.Ch.E.J., 12, 964-972. (1966).

25/ BELLHOUSE,B.J., Reserch in dialysis. Oxford University Engineering Laboratory Report no. 1315/80. (1980).

26/ BELTAOS,S., Longitudinal dispersion in rivers. Proc. A.S.C.E.J. Hydraul. Div., 106(1), 151-172. (1980).

27/ BELTAOS,S., Transverse mixing tests in natural streams. Proc. A.S.C.E.J. Hydraul. Div., 106(10), 1607-1625. (1980).

28/ BELTAOS,S., Dispersion in tumbling flow. Proc. A.S.C.E.J. Hydraul. Div., 108(9), 591-612. (1982).

29/ BILLOUS,O., BLOCK,H.D., PIROT,E.L., Control of continuous flow chemical reactors. A.I.Ch.E.J., 3(2), 248-261. (1957).

30/ BISCHOFF,K.B., Accuracy of axial dispersion model for chemical reactors. Chem. Eng. Sci., 14(5), 820-821. (1968).

31/ BISCHOFF,K.B., Axial dispersion with time variable flow. Chem. Eng. Sci., 19, 989-990. (1964).

32/ BOERICKER,R.R., HALL,D.W., Hydraulics and thermal dispersion in an irregular estuary. Proc. A.S.C.E.J. Hydraul. Div., 100(1), 85-102. (1974).

33/ BOORAS,G.S., KRONTY,W.B., Dispersion in the laminar flow of power law fluids through straight tubes. Ind. Eng. Chem. Fund., 15(4), 249-254. (1976).

34/ BOSWORTH,R.C.L., Distribution of reaction times for laminar flow in circular reactors. Phil. Mag., 89, 847-862. (1948).

35/ BOURNIA,A., COULL,J., HOUGHTON,G., Dispersion in gases in laminar flow through a circular tube. Proc. Roy. Soc., 261A, 227-236. (1961).

36/ BOWDEN,K.F., Horizontal mixing in the sea due to a shearing current. J.Fluid Mech., 21, 84. (1965).

37/ BRIAN,P.L.T., Concentration polarization in reverse osmosis desalination with variable flux and incomplete salt rejection. Ind. Chem. Eng. Fund., 4, 439-445. (1965).

38/ BRIER,G.W., The statistical theory of turbulence and the problem of atmospheric diffusion. J.Met., 7, 283-290 (1950).

39/ BRITTAIN,.M.I, WOODBURN,E.T., The influence of axial dispersion on carbon dioxide absorption tower performance. A.I.Ch.E.J., 12(3), 541-548. (1966).

40/ BRITTAN,M.I., The simultaneous measurement of axial dispersion and mass transfer coefficients. Chem. Eng. Sci., 22, 1019-1023. (1967).

41/ CARO,C.G., The dispersion of indicator flowing through simplified models of the circulation and its relevance to the velocity profile in blood. J.Physiol., 185, 501. (1966).

42/ CARBERRY,J.J., BRETTON,R.H., Axial dispersion of mass in flow through fixed beds. A.I.Ch.E.J., 4(3), 367-375. (1958).

43/ CARRIER,G.F., On convective diffusion in tubes. Quart. Appl. Math., 14, 108-112. (1956).

44/ CARTER,D., BIR,W.G., Axial mixing in a turbulent high pressure reactor. Chem. Eng. Prog., 58(3), 40-43. (1962).

45/ CASSEL,E.J., PERONA,J.J., Axial dispersion in turbulent flow through standard 90° elbows. A.I.Ch.E.J., 15, 81-84. (1969).

46/ CHANG,H-K., MOCKROS,L.F., Convective dispersion of blood gases in curved channel exchangers. A.I.Ch.E.J., 17(3), 541-549. (1971).

47/ CHATWIN,P.C., The dispersion of a puff of passive contaminant in the constant stress region. Quart. J.Roy. Met. Soc., 94, 350-360. (1968).

48/ CHATWIN,P.C., The approach to normality of the concentration distribution of a solute in a solvent flowing along a straight pipe. J.Fluid Mech., 43, 321-352. (1970).

49/ CHATWIN,P.C., On the interpretation of some longitudinal dispersion experiments. J.Fluid Mech., 48, 689-702. (1971).

50/ CHATWIN,P.C., The cumulants of the distribution of concentration of a solute dispersing in a solvent flowing through a tube. J.Fluid Mech., 51, 63-67. (1972).

51/ CHATWIN,P.C., A calculation illustrating effects of the viscous sublayer on longitudinal dispersion. Quart. J.Appl. Math., 26, 427-439. (1972).

52/ CHATWIN,P.C., On the longitudinal dispersion of dye whose concentration varies harmonically with time. J.Fluid Mech., 58(4), 657-667. (1973).

53/ CHATWIN,P.C., The dispersion of contaminant released from instantaneous sources in laminar flow near stagnation points. J.Fluid Mech., 66, 753-766. (1974).

54/ CHATWIN,P.C., A statistical model of the longitudinal dispersion process in turbulent flows in a channel. J.Eng. Maths., 9, 127-134. (1975).

55/ CHATWIN,P.C., On the longitudinal dispersion of a passive contaminant in oscillatory flow in tubes. J.Fluid Mech., 71, 513-527. (1975).

56/ CHATWIN,P.C., The initial dispersion of contaminant in Poiseuille flow and smoothing of the snout. J.Fluid Mech., 77, 593-602. (1976).

57/ CHATWIN,P.C., The initial development of longitudinal dispersion in straight tubes. J.Fluid Mech., 80, 33-48. (1977).

58/ CHATWIN,P.C., Comments on "dispersion measurements in a turbulent boundary layer". Int. J.Heat Mass Transfer, 21, 367-368. (1978).

59/ CHATWIN,P.C., SULLIVAN,P.J., The relative diffusion of a cloud of passive contaminant in incompressible turbulent flow. J.Fluid Mech., 91, 337-355. (1979).

60/ CHATWIN,P.C., SULLIVAN,P.J., Measurements of concentration fluctuations in relative turbulent diffusion. J.Fluid Mech., 94, 83-101. (1979).

61/ CHATWIN,P.C., SULLIVAN,P.J., Some turbulent diffusion invariants. J.Fluid Mech., 97, 405-416. (1980).

62/ CHATWIN,P.C., SULLIVAN,P.J., The effect of aspect ratio on longitudinal diffusivity in rectangular channels. J.Fluid Mech., 120, 347-358. (1982).

63/ CHEN,B.H., DOUGLAS,W.J.M., Axial mixing of liquid in a turbulent bed contactor. Can. J.Chem. Eng., 47, 113-118. (1969).

64/ CHEN,M.S.K., Effect of dispersion on microbial growth. A.I.Ch.E.J., 18(4), 849-851. (1972).

65/ CHRISTODOULOU,G.C., CONNOR,J.J., Dispersion in two-layer stratified water bodies. Proc. A.S.C.E.J. Hydraul. Div., 106(4), 557-573. (1980).

66/ CHUNG,S.F., WEN,C.Y., Longitudinal dispersion of liquid flowing through fixed and fluidized beds. A.I.Ch.E.J., 14(6), 857-866. (1968).

67/ COLLINS,D.J., GORTON,C.W., An experimental study of diffusion from a line source in a turbulent boundary layer. A.I.Ch.E.J., 22(3), 610-612. (1976).

68/ COLTON,C.K., SMITH,K.A., STROEVE,P., MERRILL,E.W., Laminar flow mass transfer in a flat duct with permeable membrane walls. A.I.Ch.E.J., 17(4), 773-780. (1971).

69/ CRANK,J., The mathematics of diffusion, O.U.P. (1976).

70/ DAGAN,G., Dispersivity tensor for turbulent uniform channel flow. Proc. A.S.C.E.J. Hydraul. Div., 95(5), 1699-1712. (1969).

71/ DANCKWERTS,P.V., Continuous flow systems. Chem. Eng. Sci., 2, 1-13. (1953).

72/ DAVIDSON,J.F., FARQUHARSON,D.C., PICKEN,J.Q., TAYLOR,D.C., Gas mixing in long pipelines. Chem. Eng. Sci., 4(5), 201-205. (1955).

73/ DAYAN,J., LEVENSPIEL,O., Longitudinal dispersion on packed beds of porous absorbing solids. Chem. Eng. Sci., 23, 1327-1334. (1968).

74/ DAYAN,J., LEVENSPIEL,O., Dispersion in smooth pipes with absorbing walls. Ind. Eng. Chem. Fund., 8(4), 840-842. (1969).

75/ DE MARIA,F., LONGFIELD,J.E., BUTLER,G., Catalytic reactor design. Ind. Eng. Chem., 53, 259-266. (1961).

76/ DEISLER,P.F., WILHELM,R.H., Diffusion in beds of porous solids; measurement by frequency response techniques. Ind. Eng. Chem., 45, 1219-1227. (1953).

77/ DEWEY,R., SULLIVAN,P.J., The asymptotic stage of longitudinal turbulent diffusion within a tube. J.Fluid Mech., 80, 293-303. (1977).

78/ DEWEY,R., SULLIVAN,P.J., Longitudinal dispersion in flows that are homogeneous in the streamwise direction. Z.Agnew. Math. Phys., 30, 601-613. (1979).

79/ DOSHI,M.R., Particle diffusion in electrostatic precipitators. Chem. Eng. Sci., 32, 789-790. (1977).

80/ DOSHI,M.R., DAIYA,P.M., GILL,W.N., Three dimensional laminar dispersion in open and closed rectangular conduits. Chem. Eng. Sci., 33, 795-804. (1978).

81/ DUNCKHORST,F.T., HOUGHTON,G., Digital computer simulation of non-linear equilibrium chromatography with axial dispersion. Ind. Eng. Chem. Fund., 5(1), 93-98. (1966).

82/ ELDER,J.W., The dispersion of a marked fluid in turbulent shear flow. J.Fluid Mech., 5, 544-560. (1959).

83/ ELLISON,T.H., A note on the velocity profile and longitudinal mixing in a broad open channel. J.Fluid Mech., 8, 33-40. (1960).

84/ ERDOGAN,M.E., CHATWIN,P.C., The effects of curvature and buoyancy on the laminar dispersion of solute in a horizontal tube. J.Fluid Mech., 29, 465-484. (1967).

85/ ERTL,H., GHAI,R.K., DULLIEN,F.A.L., Liquid diffusion of nonelectrolytes part II (journal review). A.I.Ch.E.J., 20(1), 1-20. (1974).

86/ EVANS,E.V., KENNEY,C.N., Gaseous dispersion in laminar flow through a circular tube. Proc. Roy. Soc., 284A, 540-550. (1965).

87/ FAN,L.T., HWANG,W.S., Dispersion of Ostwald-de Waele fluid in laminar flow through a cylindrical tube. Proc. Roy. Soc., 327A, 576-582. (1965).

88/ FEDORS,R.F., A method of estimating self-diffusion coefficients in liquids. A.I.Ch.E.J., 25(1), 200-201. (1979).

89/ FEDORS,R.F., A method to estimate critical volumes. A.I.Ch.E.J., 25(1), 202. (1979).

90/ FIFE,P.C., NICHOLES,K.R.K., Dispersion in flow through small tubes. Proc. Roy. Soc., 344A, 131-145. (1975).

91/ FISCHER,H.B., The mechanics of dispersion in natural streams. Proc. A.S.C.E.J. Hydraul. Div., 93(6), 187-216. (1967).

92/ FISCHER,H.B., The effects of bends on dispersion in streams. Water Resources Research, 5(2), 496-506. (1969).

93/ FISCHER,H.B., Mass transport mechanisms in partially stratified estuaries. J.Fluid Mech., 53, 671-687. (1972).

94/ FISCHER,H.B., Longitudinal dispersion and turbulent mixing in open channel flow, Ann. Rev. Fluid Mech., 5, 59-78. (1973).

95/ FISCHER,H.B., Mixing and dispersion in estuaries, Ann. Rev. Fluid Mech., 8, 107-133. (1976).

96/ FLINT,D.L., KADA,H., HANRATTY,T.J., Point source turbulent diffusion in a pipe. A.I.Ch.E.J., 6(2), 325-331. (1960).

97/ FLINT,D.L., EISENKLAM,P., Longitudinal gas dispersion in transitional and turbulent flow through a straight tube. Can. J.Chem. Eng., 47, 101-106. (1969).

98/ FUKUOKA,S., SAYRE,W.W., Longitudinal dispersion in sinuous channels. Proc. A.S.C.E.J. Hydraul. Div., 99(1), 195-217. (1973).

99/ GER,A.M., HOLLEY,E.R., Comparison of single point injections in pipe flow. Proc. A.S.C.E.J. Hydraul. Div., 102(6), 731-746. (1976).

100/ GILL,W.N., CHI TIEN, ZEH,D.W., Concentration polarization effects in a reverse osmosis system. Ind. Chem. Eng. Fund., 4, 433-439. (1965).

101/ GILL,W.N., CHI TIEN, ZEH,D.W., Analysis of continuous reverse osmosis systems for desalination. Int. J.Heat Mass Transfer, 9, 907-923. (1966).

102/ GILL,W.N., ANANTHAKRISHNAN,V., Laminar dispersion in capillaries II, effect of inlet boundary conditions and Turner type of system capacitance. A.I.Ch.E.J., 12, 906-915. (1966).

103/ GILL,W.N., A note on the solution of transient dispersion problems, Proc. Roy. Soc, 295A, 335-339. (1966).

104/ GILL,W.N., A note on the solution of transient dispersion problems. Proc. Roy. Soc., 298A, 335-339. (1967).

105/ GILL,W.N., Analysis of axial dispersion with time variable flow. Chem. Eng. Sci., 22, 1013-1017. (1967).

106/ GILL,W.N., ANANTHAKRISHNAN,V., Laminar dispersion in capillaries IV, the slug stimulus. A.I.Ch.E.J., 13, 801-808. (1967).

107/ GILL,W.N., ANANTHAKRISHNAN,V., NUNGE,R.J., Dispersion in developing velocity fields. A.I.Ch.E.J., 14, 936-946. (1968).

108/ GILL,W.N., Axial dispersion with time variable flow in multiphase systems. A.I.Ch.E.J., 15, 745-749. (1969).

109/ GILL,W.N., SANKARASUBRAMANIAN,R., Exact analysis of unsteady convective diffusion. Proc. Roy. Soc., 316A, 341-350. (1970).

110/ GILL,W.N., GUCERI,U., Laminar dispersion in Jeffrey-Hamel flows I, diverging channels. A.I.Ch.E.J., 17, 207-214. (1971).

111/ GILL,W.N., SANKARASUBRAMANIAN,R., Dispersion of a non-uniform slug in time-dependent flow. Proc. Roy. Soc., 332A, 101-117. (1971).

112/ GILL,W.N., SANAKARASUBRAMANIAN,R., Dispersion of non-uniformly distributed time-variable continuous sources in time dependent flow. Proc. Roy. Soc., 327A, 191-208. (1972).

113/ GILL,W.N., Unsteady tubular reactors - time variable flow and inlet conditions. Chem. Eng. Sci., 30, 1123-1128. (1975).

114/ GOLDSTEIN,S., On diffusion by continuous movements and on the telegraph equation. Quart. Journ. Mech. and Applied Math., 4(2), 129-156. (1951).

115/ GOMEZPLATA,A., BROWN,R.W., Axial dispersion coefficient measurement in two phase flow. A.I.Ch.E.J., 14(4), 657-658. (1968).

116/ GRIFFITH,A., Movement of a coloured index along a capillary tube. Proc. Phys. Soc., 23, 190-197. (1911).

117/ GUPTA,P.S., GUPTA,A.S., Effect of homogeneous and heterogeneous reactions on the dispersion of a solute in the laminar flow between two plates. Proc. Roy. Soc., 330A, 59-63. (1972).

118/ HARLACHER,E.A., ENGEL,A.J., Diffusion in a power-law fluid: a mathematical study. Chem. Eng. Sci., 25, 717-721. (1970).

119/ HAWTHORN,R.D., Effect of radial temperature variation on axial mixing in pipes. A.I.Ch.E.J., 6(3), 443-445. (1960).

120/ HOLLEY,E.R., Unified view of diffusion and dispersion. Proc. A.S.C.E.J. Hydraul. Div., 95(2), 621-631. (1969).

121/ HOLLEY,E.R., HARLEMAN,D.R.F., FISCHER,H.B., Dispersion in homogeneous estuary flow. Proc. A.S.C.E.J. Hydraul. Div., 96(8), 1691-1709. (1970).

122/ HORN,J.F.M., PARISH,T.D., The influence of mixing on tubular reactor performance. Chem. Eng. Sci., 22, 1549-1560. (1967).

123/ HORN,J.F.M., Calculation of dispersion coefficients by means of moments. A.I.Ch.E.J., 17(3), 613-620. (1971)

124/ HORN,J.F.M., KIPP,R.L., Induced transport in pulsating flow. A.I.Ch.E.J., 17(3), 621-626. (1971).

125/ HSU,C-J., An exact anlysis of low Peclet number thermal entry region heat transfer in transversely nonuniform velocity fields. A.I.Ch.E.J., 17(3), 732-740. (1971).

126/ HULL,D.E., KENT,J.W., Radioactive tracers to mark interfaces and measure intermixing in pipelines. Ind. Eng. Chem., 44, 2745-2750. (1952).

127/ HUNT,B., Diffusion in laminar pipe flow. Int. J.Heat Mass Trans., 20, 393-401. (1977).

128/ HUNT,J.C.R, MULHEARN,P.J., Turbulent dispersion from sources near two-dimensional obstacles. J.Fluid Mech., 61, 245-274. (1973).

129/ JAYARAJ,K., SUBRAMANIAN,R.S.+, On relaxation phenomena in field flow fractionation. Sep. Sci. Tech., 13(9), 791-817. (1978).

130/ JIRKA,G., WOOD,D.W., HARLEMAN,D.R.F., Transient heat releases from offshore nuclear plants. Proc. A.S.C.E.J. Hydraul. Div., 103(2), 151-168. (1977).

131/ JOHNSON,E.R., LLOYD,K.H., Determination of diffusion coefficients from observations on grenade glow clouds. Aust. J.Phys, 16, 490-499. (1963).

132/ JOHNSON,H.E., SAYRE,W.W., Predicting concentration profiles in open channels. Proc. A.S.C.E.J. Hydraul. Div., 96(10), 1983-1996. (1970).

133/ JORDAN,D.W., A theoretical study of the diffusion of tracer gas in an airway. Quart. Journ. Mech. Applied Math., 14(2), 203-222. (1961).

134/ KING,G.W., Monte-Carlo method for solving diffusion problems. Ind. Eng. Chem., 43, 2475-2478. (1951).

135/ KLINKENBERG,A., KRAJENBRINK,H.J., LAUWERIER,H.A., Diffusion in a fluid moving at uniform velocity in a tube. Ind. Eng. Chem., 45, 1202-1298. (1953).

136/ KLINKENBERG,A., SJEMITZER,F., Holding-time distributions of the Gaussian type. Chem. Eng. Sci., B/5, 258-270. (1956).

137/ KOUTSKY,J.A., ADLER,R.J., Minimization of axial dispersion by use of secondary flow in helical tubes. Can. J.Chem. Eng., 42, 239-246. (1964).

138/ KRAMERS,H., ALBERDA,G., Frequency response analysis of continuous flow systems. Chem. Eng. Sci., 2, 173-180. (1953).

139/ KRISHNAMURTHY,S., SUBRAMANIAN,R.S.+, Exact analysis of field-flow fractionation. Sep. Sci. Tech., 12(4), 347-379. (1977).

140/ LAMB,D.E., MANNING,F.S., WILHELM,R.H., Measurement of concentration fluctuations with an electrical conductivity probe. A.I.Ch.E.J., 6(4), 682-685. (1960)

141/ LARSEN,L.H., Dispersion of a passive contaminant in oscillating fluid flows. J.Phys. Oceanog., 7(6), 928-931. (1977).

142/ LAU,Y-L., KRISHNAPPAN,B.G., Transverse dispersion in rectangular channels. Proc. A.S.C.E.J. Hydraul. Div., 103(10), 1173-1189. (1977).

143/ LEE,N., DUKLER,A.E., Lagrangian simulation of dispersion in turbulent shear flow with a hybrid computer. A.I.Ch.E.J., 22(3), 449-455. (1976).

144/ LEONARD,R.A., BERNSTEIN,G.J., PELTO,R.H., ZIEGLER,A.A., Liquid-liquid dispersion in turbulent Couette flow. A.I.Ch.E.J., 27(3), 495-504. (1981).

145/ LEVENSPIEL,O., SMITH,K.W., Notes on the diffusion-type model for the longitudinal mixing of fluids in flow. Chem. Eng. Sci., (1957).

146/ LEVENSPIEL,O., Longitudinal mixing of fluids flowing in circular pipes, Ind. Eng. Chem., 50, 343-346. (1958).

147/ LEVENSPIEL,O., BISCHOFF,K.B., Backmixing in the design of chemical reactors. Ind. Eng. Chem. 51, 1431-1434. (1959)

148/ LEVENSPIEL,O., BISCHOFF,K.B., Patterns of flow in chemical process vessels. Adv. Chem. Eng., 4, 95-198. (1963).

149/ LEVENSPIEL,O., SMITH,W.K., Notes on the diffusion-type model for longitudinal mixing of fluids in flow. Chem. Eng. Sci., 6, 227-233. (1957).

150/ LIGHTHILL,M.J., Initial development of diffusion in Poiseuille flow. J.Inst. Maths. Applics., 2, 97-108. (1966).

151/ LIU,H., CHENG,A.H.D., Modified Fickian model for predicting dispersion. Proc.A.S.C.E.J. Hydraul. Div., 106(6), 1021-1040. (1980).

152/ LONGWELL,J.P., WEISS,M.A., Mixing and distribution of liquids in high velocity air streams. Ind. Eng. Chem., 45, 667-680. (1953).

153/ LOU,S-Z., NUNGE,R.J., Dispersion with pulsating turbulent flow. A.I.Ch.E.J., 17(4), 1001-1003. (1971).

154/ McCONALOGUE,D.J., The effects of secondary flow on the laminar dispersion of an injected substance in a curved tube. Proc. Roy. Soc., 315A, 99-113. (1970).

155/ McDONALD,D.A., Blood flow in arteries. pub. Arnold. (1974).

156/ McQUIVEY,R.S., KEEFER,T.N., Convective model of longitudinal dispersion. Proc. A.S.C.E.J. Hydraul. Div., 102(10), 1409-1424. (1976).

157/ McQUIVEY,R.S., KEEFER,T.N., Dispersion - Mississippi river below Baton Rouge La. Proc. A.S.C.E.J. Hydraul Div., 102(10), 1425-1437. (1967).

158/ MARINO,M.A., Longitudinal dispersion in saturated porous media. Proc. A.S.C.E.J. Hydraul. Div., 100(1), 151-157. (1974).

159/ MARON,V.I., Longitudinal diffusion in flow through a tube. Int. J.Multiphase Flow, 4, 339-355. (1978).

160/ MAYCOCK,K.P., TARBELL,J.M., DUDE,J.L., Numerical simulation of solute dispersion in laminar tube flow. Sep. Sci. Technol., 15(6), 1285-1296. (1980.)

161/ MARIETTA,M.G., SWAN,G.W., Particle diffusion in electrostatic precipitators. Chem. Eng. Sci., 33, 795-801. (1976).

162/ MELLISH,W.G., Applicability of dispersion results to packed columns. A.I.Ch.E.J., 14(4), 668. (1968).

163/ MICHELSEN,W.R., Measurements of the effect of molecular diffusivity. J.Fluid Mech., 7, 397-400. (1960).

164/ MILLER,A.C., RICHARDSON,E.V., Diffusion and dispersion in open channel flow. Proc. A.S.C.E.J. Hydraul. Div., 100(1), 159-171. (1974).

165/ MIXON,F.O., WHITAKER,D.R., ORCUTT,J.C, Axial dispersion and heat transfer in liquid-liquid spray towers. A.I.Ch.E.J., 13(1), 21-28. (1967).

166/ MOFFATT,H.K., Some developments in the theory of turbulence. J. Fluid Mech., 106, 27-47. (1981).

167/ MYERS,M.M., CALDWELL,K.D., GIDDINGS,J.C., A study of retention in thermal field flow fractionation. Sep. Sci. Tec., 9(1), 47-70. (1974).

168/ NUNGE,R.J., GILL,W.N., Mechanisms affecting dispersion and miscible displacement. Ind. Eng. Chem., 61(9), 33-49. (1969).

169/ NUNGE,R.J., LIN,T.-S., GILL,W.N., Laminar dispersion in curved tubes and channels. J.Fluid Mech., 51, 363-383. (1972).

170/ OKUBO,A., The effect of shear in an oscillatory current on horizontal diffusion from an instantaneous source. Inst. J.Oceanol., 194, 194. (1967).

171/ ØSTERGAARD,K., MICHELSEN,M.L., On the use of the tracer pulse method for determination of hold-up and axial mixing. Can. J.Chem. Eng., 47, 107-112. (1969).

172/ PALMER,M.D., IZATT,J.B., Dispersion prediction from current meters. Proc. A.S.C.E.J. Hydraul. Div., 96(8), 1667-1680. (1970).

173/ PETERSEN,J.P., CASTRO,W.E., ZIELINSKI,P.B., BECKWITH,W.F., Enhanced dispersion in drag reducing flow. Proc. A.S.C.E.J. Hydraul. Div., 100(6), 773-785. (1974).

174/ PHILIP,J.R., The theory of dispersal during laminar flow in tubes I. Aust. J.Phys., 16, 287-299. (1963).

175/ PHILIP,J.R., The theory of dispersal during laminar flow in tubes II. Aust. J.Phys., 16, 300-310. (1963).

176/ PHILIP,J.R., The damping of fluctuating concentration by continuous sampling through a tube. Aust. J.Phys., 16, 454-463. (1963).

177/ PRITCHARD,D.W., Dispersion and flushing of pollutants in estuaries. Proc. A.S.C.E.J. Hydraul. Div., 95(1), 115-124. (1969).

178/ PURTELL,L.P., Molecular diffusion in oscillatory laminar flow in a pipe. Phys. of Fluids, 24, 789-793. (1981).

179/ RAMANADHAN,K., GILL,W.N., Combined forced and free convective diffusion in vertical semipermeable parallel plate ducts. A.I.Ch.E.J., 15, 872-884. (1969).

180/ REEJHSINGHANI,N.S., GILL,W.N., BARDUHN,A.J., Laminar dispersion in capillaries III, experiments in horizontal tubes including observations on natural convection effects. A.I.Ch.E.J., 12, 916-921. (1966).

181/ REEJHSINGHANI,N.S., BARDUHN,A.J., GILL,W.N., Laminar dispersion in capillaries V, experiments on combined natural and forced convection in tubes. A.I.Ch.E.J., 14, 100-109. (1968).

182/ REIS,J.F.G., RAMKRISHNA,D., LIGHTFOOT,E.N., Convective mass transfer in the presence of polarizing fluids: dispersion in hollow fiber electropolarization chromatography. A.I.Ch.E.J., 24(4), 679-686. (1978).

183/ REYNOLDS,O., An experimental investigation of the circumstances which determine whether the motion of water shall be direct or sinuous, and of the law of resistance in parallel channels. Phil. Trans. Roy. Soc., 174, 935-982. (1883).

184/ RICHARDSON,L.F., Atmospheric diffusion on a distance-neighbour graph. Proc. Roy. Soc., 110A, 709-737. (1926).

185/ RICHARDSON,L.F., A search for the law of atmospheric diffusion. Beitr. Phys. Frei. Atmos., 15, 24. (1929).

186/ RICKER, N.L., NAKASHIO,F., KING,C.J., An efficient general method for computation of countercurrent separation processes with axial dispersion. A.I.Ch.E.J., 25(2), 229-240, 1979.

187/ ROACHE,P.J., Computational fluid dynamics. pub. Hermosa. (1976).

188/ ROBINSON,C., The nature of the aqueous solutions of dyes. Trans. Faraday Soc., 31, 245-261. (1935).

189/ ROGERS,R.S.C, GARDNER,R.P., Use of a finite stage transport concept for analyzing residence time distributions of continuous processes. A.I.Ch.E.J., 25(2), 229-240. (1979).

190/ ROSENWEIG,R.E., GWOZDZ,J.R., Turbulent dispersion in pipe flow. A.I.Ch.E.J., 17(5), 964-972. (1966).

191/ SAFFMAN,P.G., A theory for dispersion in a porous medium. J.Fluid Mech., 6, 321-349. (1959).

192/ SAFFMAN,P.G., Dispersion due to molecular diffusion and macroscopic mixing in flow through a network of capillaries. J.Fluid Mech., 7, 194-208. (1960).

193/ SAFFMAN,P.G., On the effect of the molecular diffusivity in turbulent diffusion. J.Fluid. Mech., 8, 273. (1960).

194/ SANKARASUBRAMANIAN,R., GILL,W.N., Taylor diffusion in laminar flow in an eccentric annulus. Int. J.Heat Mass Transfer, 14, 905-919. (1971).

195/ SANKARASUBRAMANIAN,R., GILL,W.N., Dispersion from a prescribed concentration distribution in time variable flow. Proc. Roy. Soc., 329A, 479-492. (1972).

196/ SANKARASUBRAMANIAN,R., GILL,W.N., Unsteady convective diffusion with interphase mass transfer. Proc. Roy. Soc., 333A, 115-132. (1973).

197/ SANKARASUBRAMANIAN,R., GILL,W.N., Correction to "unsteady convective diffusion with interphase mass transfer". Proc. Roy. Soc., 341A, 407-408. (1974).

198/ SAYRE,W.W., Dispersion of silt particles in open channel flow. Proc. A.S.C.E.J. Hydraul. Div., 95(3), 1009-1038. (1969).

199/ SCHLINGER,W.G., SAGE,B.H., Material transfer in turbulent gas streams. Ind. Eng. Chem., 45, 657-661. (1953).

200/ SCHUSTER,J.C., Canal discharge measurements with radioisotopes. Proc. A.S.C.E.J. Hydraul. Div., 91(2), 101-124. (1965).

201/ SCHWARTZ,J.G., WEGER,E., DUDUKOVIC,M.P., Liquid holdup and dispersion in trickle bed reactors. A.I.Ch.E.J., 22(5), 953-956. (1976).

202/ SHAH,Y.T., Mass transport in reverse osmosis in the case of variable diffusivity. Int. J.Heat Mass Transfer, 14, 921-930. (1971).

203/ SHAUGHNESSY,E.J., MORTON,J.B., Laser light-scattering measurements of particle concentration in a turbulent jet. J.Fluid Mech., 80, 129-148. (1977).

204/ SHERWOOD,T.K., BRIAN,P.L.T., FISHER,R.E., DRESNER,L., Salt concentration at phase boundaries in desalination by reverse osmosis. Ind. Chem. Eng. Fund., 4, 113-118. (1965).

205/ SHLIEN,D.J., CORRSIN,S., Dispersion measurements in a turbulent boundary layer. Int. J.Heat Mass Transfer, 19, 285-295. (1976).

206/ SITTEL,L.N., THREADGILL,W.D., SCHNELLE,K.B., Longitudinal dispersion for turbulent flow in pipes. Ind. Eng. Chem. Fund., 7, 39-43. (1968).

207/ SMITH,R., Longitudinal dispersion of a buoyant contaminant in a shallow channel. J.Fluid Mech., 78, 677-678. (1976).

208/ SMITH,R., Long term dispersion of contaminants in small estuaries. J.Fluid Mech., 82, 129-146. (1977).

209/ SMITH,R., Asymptotic solutions to the Erdogan-Chatwin equation. J.Fluid Mech., 88, 323-337. (1978).

210/ SMITH,R., Buoyancy effects upon lateral dispersion in open channel flow. J.Fluid Mech., 90, 761-779. (1979).

211/ SMITH,R., Buoyancy effects upon longitudinal dispersion in wide well-mixed estuaries. Phil. Trans. Roy. Soc., 296A, 467-496. (1980).

212/ SMITH,R., A delay-diffusion description for contaminant dispersion. J.Fluid Mech., 105, 469-486. (1981).

213/ SMITH,R., The importance of discharge siting upon contaminant dispersion in narrow rivers and estuaries. J.Fluid Mech., 108, 54-63. (1981).

214/ SMITH,R., Effects of non-uniform currents and depth variations upon steady discharges in shallow water. J.Fluid Mech., 110, 373-380. (1981).

215/ SMITH,R., The early stages of contaminant dispersion in shear flows. J.Fluid Mech., 111, 107-122. (1981).

216/ SMITH,R., Contaminant dispersion in oscillatory flows. J.Fluid Mech., 114, 379-398. (1982).

217/ SMITH,R. Where to put a steady discharge in a river. J.Fluid Mech., 115, 1-11. (1982).

218/ SMITH,R., Non-uniform discharges of contaminants in shear flows. J.Fluid Mech., 120, 71-89. (1982).

219/ SMITH,R., Gaussian approximation for contaminant dispersion. Quart. J.Mech. Appl. Math., 35(3), 345-366. (1982).

220/ SOBEY,I.J., On flow through furrowed channels. Part 1. Calculated flow patterns. J.Fluid Mech., 96, 1-36. (1980).

221/ SOBEY,I.J., The effect of small dispersion on two phase operations. I.M.A. J.Appl. Math., 27, 237-249. (1981).

222/ SOOKY,S.A., Longitudinal dispersion in open channels. Proc. A.S.C.E.J. Hydraul. Div., 95(1), 1327-1346. (1969).

223/ STEPHANOFF,K.D., SOBEY,I.J., BELLHOUSE,B.J., On the flow through furrowed channels. Part 2. Observed flow patterns. J.Fluid Mech., 96, 27-32. (1980).

224/ SUBRAMANIAN,R.S.+, Unsteady convective diffusion in capillary chromatographs. J.Chromatogra., 101, 253-270. (1974).

225/ SUBRAMANIAN,R.S.+, GILL,W.N., MARRA,R.A., Dispersion models of unsteady tubular reactors. Can. J.Chem. Eng., 52, 563-568. (1974).

226/ SUBRAMANIAN,R.S.+, GILL,W.N., Unsteady convective diffusion in non-Newtonian flows. Can. J.Chem. Eng., 54, 115-117. (1976).

227/ SUBRAMANIAN,R.S., On generalized dispersion theory. Chem. Eng. Sci., 32, 788-789. (1977).

228/ SULLIVAN,P.J., Some data on the distance-neighbour function for relative diffusion. J.Fluid Mech., 47, 601-607. (1971).

229/ SULLIVAN,P.J., Longitudinal dispersion within a two-dimensional turbulent shear flow. J.Fluid Mech., 49, 551-576. (1971).

230/ SUMER,S.M., FISCHER,H.B., Transverse mixing in partially stratified flow. Proc. A.S.C.E.J. Hydraul. Div., 103(6), 587-600. (1977).

231/ SUTTON,O.C., Eddy diffusion in the atmosphere. Proc. Roy. Soc., 135A, 143-165. (1932).

232/ TAYLOR,G.I., Diffusion by continuous movements. Lond. Math. Soc., 20, 196-212. (1921).

233/ TAYLOR,G.I., Dispersion of soluble matter in a solvent flowing slowly through a tube. Proc. Roy. Soc., 219A, 186-203. (1953).

234/ TAYLOR,G.I., Dispersion of salts injected into large pipes or blood vessels of animals. Appl. Mech. Rev., 6, 265-267. (1953).

235/ TAYLOR,G.I., Diffusion and mass transport in tubes. Proc. Phys. Soc. B, 67, 857-869. (1954).

236/ TAYLOR,G.I., The dispersion of matter in turbulent flows through a pipe. Proc. Roy. Soc., 223A, 446-468. (1954).

237/ TAYLOR,G.I., Conditions under which dispersion of a solute in a stream of solvent can be used to measure molecular diffusion. Proc. Roy. Soc., 225A, 473-477. (1954).

238/ TAYLOR,G.I., Present position in the theory of turbulent diffusion. Adv. Geophysics, 6, 101-112. (1959).

239/ TAYLOR,H.M., LEONARD,H.F., Axial dispersion during pulsating pipe flow. A.I.Ch.E.J., 11, 686-689. (1965).

240/ THACKER,W.C., A solvable model of "shear dispersion". J.Phys. Oceanog., 6, 66-75. (1976).

241/ TICHACEK,L.J., BARKELEW,C.H., BARON,T., Axial mixing in pipes. A.I.Ch.E.J., 3, 439-442. (1957).

242/ TOWNSEND,A.A., The diffusion of heat spots in isotropic turbulence, Proc. Roy. Soc., 209A, 418-430. (1951).

243/ TOWNSEND,A.A., The diffusion of heat behind a line source in homogeneous turbulence. Proc. Roy. Soc., 224A, 487-512. (1954).

244/ TURNER,G.A., The flow structure in packed beds. Chem. Eng. Sci., 7, 156-165. (1958).

245/ TURNER,G.A., The frequency response of some illustrative models of porous media. Chem. Eng. Sci., 10, 14-21. (1959).

246/ UCHIDA,S., The pulsating viscous flow superposed on the steady laminar motion of incompressible fluid in a circular pipe. Z.Agnew. Math. Phys., 7 403-422. (1956).

247/ ULTMAN,J.S., BLATMAN,H.S., A compartmental model of the analysis of mixing in tube networks. A.I.Ch.E.J., 23(2), 169-176. (1977).

248/ VALENTINE,E.M., WOOD,I.R., Longitudinal dispersion with dead zones. 103(9), 975-990. (1977).

249/ VALKO,E., Measurements of the diffusion of dye-stuffs. Trans. Faraday Soc., 31, 230-244. (1935).

250/ VAN der LAAN,E.T., Comments on "Notes on the diffusion-type model for the longitudinal mixing in flow". Chem. Eng. Sci., 7, 187-191. (1958).

251/ VON ROSENBERG,D.U., Mechanisms of steady state single-phase fluid displacement from porous media. A.I.Ch.E.J., 2(1), 55-58. (1956).

252/ WAN,C.-G., ZIEGLER,E.N., On the axial dispersion approximation for laminar flow reactors. Chem. Eng. Sci., 25, 723-727. (1970).

253/ WANG,S.T., McMILLAN,A.F., CHEN,B.H., Analytical model of dispersion in tidal fjords. Proc. A.S.C.E.J. Hydraul. Div., 103(7), 737-751. (1977).

254/ WARD,P.R.B., Prediction of mixing lengths for river flow gauging. Proc. A.S.C.E.J. Hydraul. Div., 99(7), 1069-1081. (1973).

255/ WARD,P.R.B., Transverse dispersion in oscillatory channel flow. Proc. A.S.C.E.J. Hydraul. Div., 100(6), 755-772. (1974).

256/ WATSON,E.J., Diffusion in oscillatory pipe flow. To be published (private communication). (1982).

257/ WEHNER,J.F., WILHELM,R.H., Boundary conditions of a flow reactor. Chem. Eng. Sci., 6, 89-93. (1956).

258/ WESTHAVER,J.W., Theory of open tube distillation columns. Ind. Eng. Chem., 34, 126-130. (1942).

259/ WISSLER,E.H., On the applicability of the Taylor-Aris axial diffusion model to tubular reactor calculations. Chem. Eng. Sci., 24, 527-539. (1969).

260/ WOERNER,J.L., JONES,B.A., FENZL,R.N., Laminar flow in finitely wide rectangular channels. Proc. A.S.C.E.J. Hydraul. Div., 94(3), 691-704. (1968).

261/ YEH,G.S., Three-dimensional pollutant modelling in shear flow. Proc.A.S.C.E.J. Hydraul. Div., 102(3), 351-365. (1976).

262/ YOTSUKURA,N., SAYRE,W.W., Transverse mixing in natural channels. Water Resources Research, 12(4), 695-704. (1976).

263/ ZEH,D.W., GILL,W.N., Convective diffusion in stagnation flow with an imperfect semipermeable interface. A.I.Ch.E.J., 13, 1014-1017. (1967)

264/ ZEH,D.W., GILL,W.N., Heat transfer and binary diffusion in variable property free convection flows. Int. J.Heat Mass Transfer, 10, 1159-1170. (1967).

265/ ZIERLER,K.L., Circulation times and the theory of indicator-dilution methods for determining blood flow and volume. Handbook of Physiology, Sec.2, Vol.1, (1962).

formerly SANKARASUBRAMANIAN,R.

ADDITIONAL REFERENCES

266/ BARTON,N.G., On the method of moments for solute dispersion. J. Fluid Mech.,126, 205-218. (1983).

267/ BELLHOUSE,B.J., BELLHOUSE,F.H., CURL,C.M., MACMILLAN,T.I., GUNNING,A.J., SPRATT,E.M., MACMURRAY,S.B., and NELEMS,J.M. "A high efficiency membrane oxygenator and pulsatile pumping system, and its application to animal trials." Trans. Amer. Soc. Artif. Organs, 19, 72-79. (1973).

268/ BELLHOUSE,B.J., BELLHOUSE,F.H., SNUGGS,T.A., AGGARWAL,J.K., Fluid mechanics of the Oxford membrane oxygenator and its evaluation in animal experiments. In "Physiological and Clinical Aspects of Oxygenator Design", Elsevier/North-Holland Biomedical Press. (1976).

269/ BURROWS,E., Assessment of pollution effects by the use of algae. Proc. Roy. Soc., 177B, 295-306. (1971).

270/ CARO,C.G., FITZ-GERALD,J.M., SCHROTTER,R.C., Atheroma and arterial wall shear observation, correlation and proposal of a shear dependent mass transfer mechanism for atherogenesis. Proc. Roy. Soc., 177B, 109-159. (1971).

271/ CHATWIN,P.C., Presentation of longitudinal dispersion data. Proc. A.S.C.E.J. Hydraul. Div., 106(4), 71-83. (1980).

272/ DEWEY,R.J., SULLIVAN,P.J., Longitudinal-dispersion calculations in laminar flows by statistical analysis of molecular motions. J. Fluid Mech., 125, 203-218. (1982).

273/ HAWORTH,W.S., STAIRMAND,J.W., to be published. (1983).

274/ LEVENSPIEL,O., Chemical reaction engineering, pub. Wiley. (1972).

275/ MCLAUGHLIN,G.M., RUSHTON,J.H., Interfacial areas of liquid-liquid dispersion from light-transmission measurements. A.I.Ch.E.J., 19(4), 817-822. (1973).

276/ PEACOCK,J.A., STAIRMAND,J.W., Film gauge calibration in oscillatory pipe flow. J.Phys. E, to be published 1983.

277/ PERRY,R.M., CHILTON,C.H., Chemical engineers' handbook, pub. McGraw-Hill. (1973).

278/ SMITH, R., personal communication. (1982).

279/ SMITH,R., Dispersion of tracers in the deep ocean. J. Fluid Mech., 123, 131-142. (1982).

280/ SMITH,R., The contraction of contaminant distributions in reversing flows. to be published. (1983).

281/ SOBEY,I.J., Oscillatory flows at intermediate Strouhal number in asymmetric channels. J. Fluid Mech., 125, 259-374. (1982).

282/ STAIRMAND,J.W., Optical concentration measurements for mass transfer studies. To be published. (1983)

283/ STAIRMAND,J.W., Dispersion in oscillatory laminar flow in a flat channel. To be published. (1983)

284/ JOSHI,C.H., KAMM,R.D., DRAZEN,J.M., SLUTSKY,A.S., Gas exchange in laminar oscillatory flow, part II: experimental measurements. To be published in J.Fluid Mech. (1983/4).

285/ WEAST,R.C., Handbook of Chemistry and Physics, 56th edition, pub. CRC press. (1975-76).

286/ MOORE,F.K., Theory of Laminar Flows, O.U.P., 1964.

287/ MOHANTY,A.K., ASTHANA,S.B.L., Laminar flow in the entrance region of a smooth pipe. J.Fluid Mech., 90, 433-447. (1979).

288/ HOLMAN,J.R., Heat Transfer, pub. McGraw-Hill. (1981).

Acknowledgements

I would like to express my gratitude to the following people without whose collective help this work could not have been carried out. Dr. B.J.Bellhouse has supervised the project and has given encouragement and shown an interest throughout its duration. The idea for the study came from Dr. I.J.Sobey who supervised the work in the early stages and who continued to give suggestions even though he was no longer directly involved in the project. Much inspiration was due to prolonged discussions with Dr. W.S.Haworth who gave useful guidance on the physical aspects of dispersion. Additional thanks are also due to Drs. Bellhouse and Howarth for the time and effort they put into proof-reading this manuscript and for the helpful suggestions which they gave.

The apparatus used in the experimental investigations was constructed by Mr. M.A.L.Stevenson and I would like to thank him for his work on the equipment he designed and built for me. I would also like to thank Dr. J.E.Allen for his continued guidance of a former student. Dr. N.StJ.Braithwaite gave useful suggestions regarding the electrical circuitry. Mr. J.A.Peacock wrote a series of computer programmes which proved to be very useful for the experimental data-logging.

I would like to thank the Science and Engineering Research Council for providing funds, and the British Petroleum Venture Research scheme for sponsoring the experimental work. I also acknowledge the receipt of a Paul postgraduate scholarship from University College Oxford.